The University of Nottingham

Institute of Engineering Surveying
and Space Geodesy

BRIDGE DEFORMATION MONITORING WITH SINGLE FREQUENCY GPS AUGMENTED BY PSEUDOLITES

By
Emily Cosser BSc

Thesis submitted to the University of Nottingham for the degree of Doctor of Philosophy

December 2004

Abstract

Bridges are an important part of the infrastructure of both road and rail networks. As bridge stocks age it is becoming increasing important to monitor their health and predict their lifespan. Current health assessment methods of visual inspection have many drawbacks and so non-destructive evaluation methods such as GPS are becoming more important.

This study focuses on the use of single frequency GPS for bridge deformation monitoring. Previous studies have focussed on the use of more expensive dual frequency receivers. This thesis has resulted in the development of single frequency processing software that has enabled these receivers to be used in bridge deformation situations. Improvements in integer ambiguity resolution methods mean it is now possible to be resolve ambiguities instantly for small bridges and greatly reduces ambiguity time for long bridges. The development of this software is outlined along with results from bridge trials.

The thesis further looks at extensions to the use of single frequency GPS by outlining experiments conducted with Garmin handheld receivers and also with JNS100 receivers measuring at 50 Hz. The potential to use Garmin receivers in monitoring applications is demonstrated. The use of 50 Hz data enables the identification of higher frequency bridge dynamics than has ever been possible before.

The final investigation looks at using pseudolites to augment the current GPS constellation specifically for bridge monitoring applications. The introduction of pseudolites led to improvements in all three coordinate directions, with the most improvement being seen in the vertical direction.

Acknowledgements

This research undertaken for this thesis was conducted at the Institute of Engineering Surveying and Space Geodesy (IESSG) at the University of Nottingham and was funded by the Engineering and Physical Sciences Research Council (EPSRC). I would like to thank my supervisors Professor Alan Dodson, Dr Gethin Roberts and Dr Xiaolin Meng for all their time and invaluable advice during the course of my research.

Part of this research was undertaken at the University of New South Wales in Sydney, Australia. I would like to thank the Universitas 21 scheme and the Australian Research Council International Research Grant for funding my trip to Australia. While in Australia I was supervised by Dr Joel Barnes and Professor Chris Rizos, who I would like to thank for their expertise and advice which contributed greatly towards the pseudolite section of this thesis.

I am grateful to Dr Chris Hide and Dr Mike Pattinson for their help with the Kinpos software. I thank Dr Chris Hill for his expertise and advice throughout the work on this thesis, and particularly for guidance during the Garmin handheld GPS receivers work. Thanks are extended again to Dr Xiaolin Meng for the many Matlab scripts he has written and the guidance during Matlab processing.

Many people helped out during the bridge field trials carried out for this thesis and it is not possible to mention them all here, although my thanks are extended to each and every one. Special thanks are given to Theo Veneboer, Samantha Waugh and Sean Ince for their patience and expertise during field work.

I would like to thank Jock Souter for keeping me sane with cups of tea during the many years of work in the IESSG. Special thanks are extended to Mark Edwards, who always listened and kept me going when things seemed impossible.

Finally and most importantly, I would like to thank my wonderful parents, Jenny and Mike Cosser for their love and encouragement. Without their support this work would not have been possible.

Contents

List of Figures

Chapter 3

Chapter 4

Chapter 5

Chapter 6

Chapter 7

Chapter 8

Chapter 9

Chapter 10

Chapter 11

List of Tables

Chapter 4

Chapter 6

Chapter 7

Chapter 8

Chapter 9

Chapter 10

Chapter 11

Appendix D

Appendix E

1. Introduction

1.1. Bridge Monitoring Systems

Road and rail transport authorities have responsibility for maintaining the road and rail networks so that they are safe and efficient. Bridges form an important part of both these infrastructures and are crucial transportation links. Since bridge failures would greatly affect the national economy and could also involve loss of life, bridge monitoring and maintenance has become an important issue. In recent years the spans of newly built bridges have become longer and their importance in the transport infrastructure system has increased.

There is a limited amount of money to spend on bridge maintenance, rehabilitation and reconstruction, so it is important that it is spent in an optimal way. Bridge management systems have been developed which consider condition information about bridges and output decisions regarding their maintenance. The decisions made by these bridge management systems are only as good as the information they receive.

Traditionally bridges have been assessed using visual inspection methods, however they are time consuming and expensive, as well as highly subjective and non-visible degradation is likely to be missed. Structural health monitoring based on measurement of the bridge's response has been suggested as a way to overcome the shortcomings of visual inspection. The ideal structural health monitoring system would be inexpensive, non-invasive (no damage to the bridge), automated and not require bridge closures.

Data from structural health monitoring systems would be used to collect information about the bridge's performance. This will help predict bridge failures and also be used in future bridge design codes. It is important that timely and accurate data is collected to aid decision making by bridge agencies.

The displacement of bridges can be split into two categories. There is the long-term bridge deformation, which is caused by foundation settlement, bridge deck creep and stress relaxation. These deformations take place over months or years and are irrecoverable (i.e. the bridge will never recover its original shape). The second type of deformation is short term, caused by traffic loading, wind, temperature or earthquakes. This type of deformation is known as a deflection, since the bridge will recover its original shape once the loading has been removed.

The Global Positioning System (GPS) has been shown to have many merits for deformation monitoring. One of these is the ability to measure the long and short term deformations of a structure simultaneously. As the technology has improved, the accuracy and reliability of the system has also increased. GPS does have some defects when applied to precise engineering applications which include achievable accuracy, data rate and multipath errors.

GPS has been used to monitor the deformations of many of the long span suspension bridges around the world in recent years. Studies have included trials upon the Humber Bridge (Roberts et al. 1999), the Akashi Kaikyo Bridge (Fujino et al. 2000) and the Tsing Ma Bridge (Wong et al. 2001). This has demonstrated the ability of GPS to measure the large deflections of long slow moving structures. GPS has also been used to measure the smaller deflections of shorter faster moving bridges such as the Wilford Suspension Footbridge (Meng 2002).

The majority of early trials conducted with GPS on structures concentrated on the slow long term displacements, since the GPS data rate was too slow to measure dynamic deformations. As receiver technology as improved the data rate possible with GPS receivers has increased (recently this possible data rate has increased to 100 Hz). The measurement of the short term dynamic deflections of structures is now the main research aim.

A considerable amount of the previous research conducted into structural monitoring with GPS has used high quality survey grade dual frequency GPS receivers. The results achieved using these receivers are reliable and accurate, but the price of implementing them can be prohibitive for many monitoring applications. The implementation of single frequency receivers, which typically cost around half the price of dual frequency, has become an important research topic.

One of the current limitations of using GPS for structural health monitoring is the deficiencies caused by the satellite constellation, not least of which is the difference in

precision in the horizontal and vertical directions. The augmentation of GPS with pseudolites is not a new area of study, and the use of this technology has been extended to the application area of bridge deformation monitoring.

1.2. Research Aims and Objectives

The main objective of this thesis is to investigate the use of single frequency GPS receivers for bridge deformation monitoring. This will include the development of a system and processing software that will achieve comparable results with dual frequency receivers. The objective of this research will be achieved by completing the following aims.

- Assessment of the accuracies achievable with dual and single frequency receivers for bridge deformation monitoring. Investigation of the limitations of single frequency receivers for precise engineering applications.
- Development of single frequency processing software.
- Implementation of algorithms which accelerate the time to integer ambiguity resolution in the context of bridge monitoring for both short and long bridges. Analysis of the improvements achieved in ambiguity resolution with the new algorithms.
- Experimentation with the new single frequency processing software, using results from bridge trials for both short and long bridges. Comparisons of the results from dual frequency processing software and the new single frequency processing software.

The following extensions to this research will also be included to further investigate the use of single frequency receivers for bridge deformation monitoring.

- Investigation into the use of single frequency Garmin handheld receivers for deformation monitoring applications.
- Examination of the use of JNS100 100 Hz GPS receivers, which measure at the highest data rate ever possible by GPS receivers and are only available currently as single frequency. The higher data rate can be used to study the high frequency vibrations of short bridges.

- Research into the use of pseudolites as an augmentation to the current GPS constellation, particularly in the context of bridge monitoring. Performance of DOP simulations of expected improvements seen with the introduction of pseudolites, compared to actual bridge trial results.

There are many novelties about this research. The use of single frequency GPS receivers to measure the deflections of short bridges has been seen before. However, there has been no research on using single frequency receivers for monitoring bridges which move more than around 5cm.

All the extensions to the single frequency GPS work are original areas of research. The use of Garmin handheld receivers for deformation monitoring and kinematic applications has not been a research topic before. The JNS100 100 Hz GPS receivers have only been released during 2004 (Javad Navigation Systems 2004a) and this is the first time they have been used to measure the higher frequency vibrations of structures. The use of pseudolites for deformation monitoring is still a relatively new and unexplored research topic and the experiments discussed in this thesis are the first conducted on bridges.

1.3. Thesis Outline

Chapter 2 provides an overview of the fundamental principles of the Global Positioning System. The error sources which particularly affect the GPS signals are focussed upon. The advantages and issues associated with using single frequency GPS receivers rather than dual frequency receivers are discussed.

Chapter 3 provides a literature review of bridge deformation monitoring techniques. The reasons behind the implementation of bridge monitoring is discussed, as well as the short-comings of visual inspection methods, which is the most common current technique for bridge monitoring. Other surveying techniques are introduced, and their advantages and disadvantages compared to GPS are examined. Previous bridge deformation monitoring research using GPS is reviewed and how the author's research leads on from this is highlighted.

Chapter 4 introduces the first short bridge trial conducted on the Wilford Bridge in Nottingham. During this trial the accuracy of dual and single frequency receivers are compared in a bridge environment. Important shortcomings of 'off-the-shelf'

processing software packages are discovered for single frequency receivers, which leads to the development of Kinpos processing software for single frequency receivers which is discussed in the following chapters. The investigation of the use of a total station for dynamic monitoring of bridges is also introduced. Initial feasibility kinematic trials are presented, as well as a trial on the Wilford Bridge. The results from the total station are compared to those from a closely located GPS receiver.

The development of the single frequency version of the Kinpos processing software is described in Chapter 5. An outline of the original software for processing dual frequency data is given, followed by the modifications made by the author. The methods of cycle slip detection and integer ambiguity resolution are particularly focussed on, since these had to be updated for single frequency data. Two new methods to accelerate the integer ambiguity search in the context of bridge monitoring, are introduced.

In Chapter 6 the second trial on a short bridge, which was also conducted on the Wilford Bridge, is described. The results from the new single frequency version of Kinpos are compared to the dual frequency results from SKi-Pro and also to the dual frequency version of Kinpos. Comparisons are made between two days' time series for various bridge sites and the use of adaptive filtering in high multipath environments is investigated. A further bridge trial, at the bridge site with the highest multipath problem is conducted, to assess what difference using a choke ring antenna would make to multipath problems. Frequency identification of the GPS and accelerometer data is carried out to detect the natural vibration frequencies of the Wilford Bridge.

Chapter 7 introduces the long bridge trials that were conducted on the Humber Bridge in Hull. The data from two bridge trials has been processed and analysed, one from February 1998 and one from March 2004. The single frequency version of Kinpos is compared to dual frequency data processed in SKi-Pro. The new method of accelerating the integer ambiguity search in the context of long bridge monitoring is compared to the original ambiguity resolution method, to show the improvements achieved. The dynamic displacement of the bridge is linked in to traffic movements and the long term movement of the bridge is linked to changes in temperature.

The use of Garmin handheld receivers for deformation monitoring is investigated in Chapter 8. The software called Gringo developed at the University of Nottingham (Hill and Moore 2002), which extracts raw carrier phase and pseudorange data from Garmin handheld receivers is introduced. Additional processing issues associated with

processing Garmin data and further modifications to the single frequency version of Kinpos are explained. The data quality produced by the Garmin receivers is compared to Leica Geosystem's single frequency 510 survey grade receivers in zero baseline, short baseline and kinematic trials.

Chapter 9 is concerned with JNS100 100 Hz GPS receivers. The data quality possible with these high frequency receivers is compared to Leica Geosystem's single frequency 510 survey grade receivers in zero baseline and short baseline trials. Kinematic trials are conducted on a bungee test rig and also on a bridge to compare the JNS100 receivers to the Leica receivers and also to a closely located accelerometer measuring at the same data rate. Frequency identification of the JNS100 GPS data and the accelerometer data is conducted and higher frequency bridge dynamics than have ever been possible with GPS before are identified.

Chapter 10 introduces the use of pseudolites to augment current GPS monitoring systems. The need for augmentation of GPS with pseudolites due to the current satellite constellation is explained. Additional issues and error sources associated with using pseudolites are described. A literature review of previous deformation monitoring systems using pseudolites is conducted. The improvement seen with the introduction of pseudolites is demonstrated with the results from a static trial.

Chapter 11 concentrates on pseudolites used for bridge deformation monitoring. Two pseudolite bridge trials are introduced, one on the Wilford Bridge in Nottingham UK and one on the Parsley Bay Bridge in Sydney Australia. DOP simulations are conducted for each bridge trial, to analyse the potential improvement when pseudolites are added. The actual bridge trial results are examined and compared to the results predicted by the simulations. Two different ways of removing the pseudolite multipath bias are introduced, both of which eliminate the bias affectively and produce identical results. The use of LocataLites as an extension to the work on pseudolites is introduced. The fundamentals of the system are described and a literature review of the LocataNet tests is conducted.

Chapter 12 concludes this thesis with a summary of the results achieved during this research. Recommendations are made for further work in this area.

2. Single Frequency GPS

2.1. Introduction

GPS is a system which allows position and velocity estimates to be obtained from passive signals transmitted by satellites. This chapter introduces some basic GPS concepts and error sources. For a more detailed explanation of GPS positioning the reader is referred to some of the many books and papers written on GPS positioning, for example Bingley and Roberts (1998), Hofmann-Wellenhof, et al. (2001), Parkinson, et al. (1995) and Teunissen and Kleusberg (1998).

2.2. Global Positioning System

GPS is an acronym of the Global Positioning System, and was developed by the US military to provide continuous all weather instantaneous positioning, velocity and time measurements. There are various accuracies that are achievable with the GPS system depending on the receiver type, processing software and whether the receiver is static or kinematic.

Two frequencies are transmitted by the GPS satellites in the microwave band, these are termed L1 (1575.42 MHz) which has a wavelength of approximately 19cm and L2 (1227.60 MHz) with a wavelength of approximately 24cm. The fundamental GPS satellite frequency is 10.23 MHz, from which all other frequencies are derived. GPS consists of two timing codes transmitted by the satellites, the Coarse/Acquisition (C/A) code and the Precise (P) code. The C/A code, which is only modulated on the L1 carrier wave, has a chipping rate of 1.023 MHz which means it has a wavelength of 300m and a repeat period of 1ms. The P code, which is modulated on both L1 and L2, has a chipping rate of 10.23 MHz which means it has a wavelength of 30m and its

repeat period is 38 weeks. The P code is encrypted to the Y code to deny access to civilian users by Anti-Spoofing (A/S). The encrypted Y code also guards against fake transmissions of satellite data. Dual frequency receivers can 'crack' the Y code giving access to the timing codes and carrier phase on both carrier waves (Rizos 1999b; Hofmann-Wellenhof et al. 2001).

As part of the GPS modernisation program a new civilian code will be added to the L2 frequency, known as L2C, which will mean that civilian GPS users can access two clean GPS signals (Fosburgh and Peetz 2004). Block IIR-M satellites, which are due for launch in 2005, will contain this new L2C capability.

The satellites also transmit a navigation message which contains information about the satellite clock, satellite orbit, satellite health status and various correction data, including ionospheric corrections for models.

The constellation is designed to have 24 satellites to provide global coverage of a minimum of four visible satellites. The satellites are arranged on six equally spaced orbits inclined at 55° to the equator. Simultaneous measurements to at least four satellites mean that a GPS receiver can compute its three-dimensional position. GPS satellites contain very accurate atomic clocks and so are regarded to be in perfect synchronisation with GPS time, but receivers contain cheap oscillators. The fourth satellite is used to solve for the fourth unknown which is the receiver clock offset from GPS time.

The GPS control segment consists of ground based tracking stations, which monitor the orbits and clock offsets of the satellites. This information is uploaded to the satellites and included in the navigation message broadcast by the satellites to all receivers.

2.2.1. Pseudorange

The fundamental GPS observable is the pseudorange and all calculations are based on precise timing. A GPS receiver compares the received satellite code to a locally generated replica code. The difference in the two timing signals is the distance in seconds which can be converted to metres by multiplying by the speed of light. This distance measurement is, however, contaminated by various error sources, some of which are considered in the following sections.

The pseudorange observation equation can be written as

$$p_r^s = \rho_r^s + c(t_r - t^s) + T_r^s + I_r^s + E_r^s + v_r^s \quad \textbf{(2-1)}$$

where,

p_r^s is the measured pseudorange observation between satellite s and receiver r in metres

ρ_r^s is the true range in metres

c is the speed of light in metres per second

t_r is the receiver clock error in seconds

t^s is the satellite clock error in seconds

T_r^s is the error caused by the tropospheric delay in metres

I_r^s is the error caused by the ionospheric delay in metres

E_r^s is the satellite orbit error in metres

v_r^s is the combination of all the remaining un-modelled errors such as multipath and receiver noise in metres

The pseudorange observation can be used for initialising the ambiguity searches for carrier phase based positioning when there are no initial coordinates or they are of bad quality. The precision of the pseudorange is roughly 3m for the C/A code and 0.3m for the P code (Hofmann-Wellenhof et al. 2001).

2.2.2. Carrier Phase

The carrier phase is observed by stripping the pseudorange from the received signal (Langley 1997). It is possible for GPS receivers to measure the carrier to better than 0.01 cycles, which corresponds to millimetre measurement accuracy (Hide 2003).

When GPS receivers lock onto the carrier phase it is only possible to measure the fraction part of the wavelength, but it is not possible to measure how many full cycles there are between the satellite and receiver. This unknown number of cycles is called the integer ambiguity. The receiver is able to measure how many cycles have accumulated since lock on and the integer ambiguity unknown remains the same at

every epoch unless a cycle slip occurs (Section 2.6.2). Integer ambiguity resolution is discussed in Section 2.6.1 and Chapter 5.

The carrier phase observation equation in metres can be written as

$$\Phi_r^s = \rho_r^s + c(t_r - t^s) - \lambda N + T_r^s - I_r^s + E_r^s + v_r^s \qquad \textbf{(2-2)}$$

where,

Φ is the measured carrier phase observation in metres between satellite s and receiver r

λ is the carrier wavelength in metres

N is the unknown integer ambiguity in cycles

2.3. GPS Error Sources

The following section will examine some of the error sources that affect the accuracy of GPS positioning solutions. These errors are split into three sections, satellite, receiver and propagation error sources (Rizos 1999a). Many of the error sources described below are mitigated or removed using differential positioning which is introduced in Section 2.4.

2.3.1. Satellite Errors

2.3.1.1. Satellite Orbit Errors

GPS positioning depends heavily on knowing the orbit of the satellites. The ephemerides are calculated by the tracking stations of the control segment and uploaded to the satellites. An orbit bias is the difference between the true position and velocity of the satellite and those calculated. This is caused by both errors in the computation of the orbit and also errors due to the unpredictable orbital motion since upload from the control segment. For Block I GPS satellites (none of which are now operational) the broadcast ephemerides were accurate to about 5m, now for the Block II satellites the accuracy is about 1m (Hofmann-Wellenhof et al. 2001).

The International GPS Service (IGS) has, since January 1994, been providing GPS orbits, tracking data and other GPS products for high precision applications over the

world wide web (IGS 2004). The IGS provides three products which are the ultra-rapid, rapid and final ephemerides. The ultra-rapid ephemeris has an observed part and a predictive part. The observed part is available 3 hours after the observation and has a quoted accuracy of less than 5cm. The predictive part is available in real-time and has an accuracy of about 10cm. The rapid ephemeris is available 17 hours after the observation and is accurate to less than 5cm, while the most accurate final ephemeris is not available until 12 days after the observation and is more accurate than 5cm.

For single point positioning, the orbit error is propagated into the positioning results. For differential positioning most of the error is removed over short baselines, but increases with baseline length.

2.3.1.2. Satellite Clock Errors

Although the GPS satellites contain high quality, accurate caesium or rubidium clocks, there are still significant satellite clock errors which change with time (Rizos 1999a). These clock offsets are monitored by the ground stations of the control segment. Polynomial coefficients are uploaded to the satellites and then transmitted in the broadcast ephemeris for use in clock error models. For single receiver positioning these models must be used to mitigate the satellite clock error, but when observations are differenced this error is removed.

2.3.2. Receiver Errors

2.3.2.1. Receiver Clock Errors

The clock contained in a GPS receiver is an inexpensive quartz oscillator. This clock is always offset from GPS time and every satellite to receiver range is contaminated with this error. Usually the receiver clock error is treated as an additional unknown in the pseudorange solution, meaning that four satellites have to be available to compute a position. The single difference between two satellites and the same receiver can also be used to eliminate this error.

The stability of the receiver time is directly related to the quality of the oscillator used and how often the clock is synchronised to GPS time using the pseudorange measurements.

2.3.2.2. Receiver Measurement Noise

The antenna, receiver and cables contribute to signal loss and add unwanted disturbances to the GPS signals (Langley 1997). The noise in the receiver is caused by the electronics; the cables act as attenuators and cause a signal loss; and antennas pick up radiation from the surrounding environment as well as the GPS signals. One way of assessing the receiver measurement noise is by conducting a zero baseline trial. Two GPS receivers are connected via a splitter to the same antenna and processed as a baseline. This results in the combined noise for the receiver pair. This, however, could provide an overly optimistic calculation of receiver performance as even some of the receiver noise can be differenced away (Langley 1997); but the counteracting effect is that one antenna signal is split over two receivers resulting in a loss of signal strength (Bona and Tiberius 2000).

Bona and Tiberius (2000) conduct zero baseline trials for seven geodetic dual frequency receiver sets. For the Leica 530 receiver (which is the type of receiver used during most trials in this thesis) the measurement precision of the L1 un-differenced carrier phase was calculated as 0.6mm and for the L2 carrier phase as 1.5mm. The theoretical minimum precision achievable by a GPS receiver was calculated by Bona and Tiberius (2000) as 0.1mm. Baseline precisions (given in baseline root mean squares) for the Leica receivers are quoted as 10mm+1ppm for the dual frequency 530 receiver and 20mm+1ppm for the single frequency 510 receivers (Leica Geosystems 1999).

2.3.2.3. Antenna Phase Centre Variations

The antenna phase centre (APC) is the point at which the radio signal measurement is made, and it is not the same as the physical centre of the antenna. The APC depends on the elevation, azimuth and intensity of the signal and it is also different for L1 and L2 (Hofmann-Wellenhof et al. 2001). The observed carrier phase depends on the orientation of the antenna, so it is important to align the GPS antennas in the same direction for different set ups in the same experiment. The APC variations are differenced away if the same antenna types are used at both ends of a short baseline. APC models can be used to provide corrections over longer baselines or when different antenna types are used.

2.3.3. Propagation Errors

2.3.3.1. Ionosphere

The ionosphere is the band of the atmosphere that reaches from 50km to 1000km above the surface of the earth, where a large number of free electrons are present. This medium is dispersive with respect to GPS signals, meaning that it has different effects on the L1 and L2 frequencies and also on the pseudorange and carrier phase parts of the signals. The pseudorange is delayed by the ionosphere meaning that the observed range appear longer than the true range and the carrier phase is advanced so that the observed phase is shorter than the true range.

The amount of delay depends on the total electron content (TEC) along the path of the signal. TEC varies according to the sunspot activity (which varies with an 11 year cycle), seasonal and diurnal variations, the elevation and azimuth of the satellite and the position of the observation site. TEC can be estimated, computed by models or eliminated (Hofmann-Wellenhof et al. 2001).

Various models of the ionosphere can be used, the most common of which is the Klobuchar model (Klobuchar 1996). Coefficients which can be used in the Klobuchar model are uploaded to the satellites and included in the broadcast ephemeris. For single point positioning with single frequency receivers, models are the only way to remove the ionospheric errors and it is known that they will only remove up to about 50% of the delay (Rizos 1999a). However the ionosphere is spatially correlated up to tens of kilometres, so it is effectively eliminated in differential positioning.

Since the ionospheric delay is a function of the signal frequency, for dual frequency receivers the ionosphere-free combination can be formed from the L1 and L2 carrier phases (see Hofmann-Wellenhof et al. (2001) for information on how this combination is formed). The ionosphere-free combination eliminates most of the ionospheric noise and can be used to remove ionospheric errors over longer baselines.

2.3.3.2. Troposphere

The neutral atmosphere (which contains no electrons) reaches from the surface of the earth up to about 40km (Pattinson 2002). It is made up of the troposphere and the stratosphere, but since most of the propagation error comes from the troposphere the stratosphere is largely ignored. The troposphere extends to about 12 km above the earth's surface (Spilker Jr 1994). This medium is non-dispersive so it has the same

effect on both the pseudorange and carrier phase signals, and also on L1 and L2 frequencies. So the elimination of the troposphere delay using dual frequency receivers is not possible.

The delay is split into the wet and dry components. The dry part is present though out the whole 40km of the troposphere, is responsible for about 90% of the delay and is easy to model from measurements of surface pressure and temperature. The remaining 10% of the delay is caused by the wet component, which is only significant in the 10km nearest the earth's surface and is difficult to model. The wet part is hard to model since it depends on the water vapour content of the atmosphere which is only weakly related to surface measurements and which varies considerably spatially and temporally.

The effect of both the wet and dry components increases as the elevation angle of the satellite decreases, since the signal takes a longer path through the atmosphere. The tropospheric delay can be double differenced away over short baselines, but the effect becomes more significant over longer baselines or if there is a large difference in height at the reference and rover receivers. There are various tropospheric models which either use surface metrological measurements (e.g. Saastamoinen) or those where no surface measurements are required (e.g. Magnet). For more information about the mitigation of tropospheric delay the interested reader is referred to Meng (2002) and Pattinson (2002).

2.3.3.3. Multipath

Most GPS signals travel in a direct path from the satellites to the receiver. However, some signals are reflected by the ground or surrounding environment and reach the receiver by an indirect path, which causes what are known as multipath errors. Multipath is unique to each receiver location and so cannot be removed by differencing observations between receivers.

Mitigation can be achieved by the use of choke ring antennas, receiver signal processing techniques, antenna location strategies and long term observations at the same site (Weill 1997). Choke ring antennas eliminate multipath from below the antenna and also at the sides, but they are still vulnerable to multipath from above (for example from buildings). Choke rings are larger and heavier than other antennas and also more expensive.

The most promising methods for multipath mitigation use signal processing techniques within the receivers in real time. This work has mainly focused on

mitigation of pseudorange multipath and not the carrier phase multipath. For more information about these techniques the reader is referred to Weill (1997).

Locating the antenna away from any reflective surfaces such as water and buildings will help to reduce the multipath at that site. Of course location of the antenna at such a low multipath site may not always be possible.

For static or semi static receivers the multipath characteristics, which depend on the satellite geometry, repeat on a daily basis (minus 4 minutes). So over a day the pattern of multipath can be determined and used to mitigate the multipath signal on subsequent days at the same site. The principles of adaptive filtering to mitigate multipath are based on the repeating satellite geometry from day to day (see Chapter 4, Section 4.4.1 and Meng (2002)).

2.4. Differencing GPS Observations

It is possible to obtain positions from a single GPS receiver to a level of precision far higher than for navigation applications. This approach is known as precise point positioning and requires satellite clock and orbit information to be taken from an external source (e.g. the IGS (IGS 2004)). Single point positioning avoids the constraint of requiring simultaneous observations at reference stations. Kouba and Heroux (2000) achieve centimetre precision in a static environment with precise point positioning using IGS products. However, for high precision dynamic applications single point positioning is not suitable and so differencing GPS observations is required.

Differencing GPS observations is used to remove some of the error sources that affect the accuracy of the positioning solutions. For differential GPS (DGPS) two receivers are required making simultaneous measurements to the same satellites. The 'reference' receiver is stationary on a location whose coordinates are known.

Differencing removes or mitigates error sources that are spatially correlated; however it does also increase the noise of the resulting observable. GPS observations can be differenced between satellites, receivers and/or time forming single, double or triple differences.

2.4.1. Single Difference

A single difference can either be formed between two receivers, which mitigates the satellite dependent biases such as the satellite clocks and orbit biases; or between two satellites, which will mitigate the receiver dependent biases, the largest being the receiver clock error. Over short baselines atmospheric propagation errors are also reduced by single differencing, using the assumption that the signals travel through the same part of the atmosphere. Errors such as multipath and receiver measurement noise are unique to each receiver and so cannot be removed through differencing (Townsend and Fenton 1994; Langley 1997).

2.4.2. Double Difference

Double differencing involves taking the difference of the observations between both two satellites and two receivers. The advantage of this method is that it removes both the satellite and receiver dependent biases, as well as the propagation errors. However, it does increase the noise of the observations compared to single differences. A double difference pseudorange measurement has a noise level twice that of a single one way pseudorange observation (Rizos 1999a).

The double difference equations for the pseudorange and carrier phase are defined in equations (2-3) and (2-4) below.

$$\Delta\nabla p_{ij}^{ST} = \Delta\nabla\rho_{ij}^{ST} + \Delta\nabla T_{ij}^{ST} + \Delta\nabla I_{ij}^{ST} + \Delta\nabla E_{ij}^{ST} + \Delta\nabla v_{ij}^{ST} \qquad \textbf{(2-3)}$$

$$\Delta\nabla\Phi_{ij}^{ST} = \Delta\nabla\rho_{ij}^{ST} + \Delta\nabla\lambda N_{ij}^{ST} + \Delta\nabla T_{ij}^{ST} - \Delta\nabla I_{ij}^{ST} + \Delta\nabla E_{ij}^{ST} + \Delta\nabla v_{ij}^{ST} \qquad \textbf{(2-4)}$$

where,

$\Delta\nabla$ is the double difference operator between satellites S and T and receivers i and j

The double difference measurement is used extensively in this thesis since Kinpos processing software uses double differences to compute positioning solutions (see Chapter 5). In the single and double difference carrier phase equations the integer ambiguity term, λN, remains.

2.4.3. Triple Difference

The triple difference is the difference of two double differences between two epochs. In a triple difference solution the integer ambiguity term is removed (Hofmann-Wellenhof et al. 2001). Triple differencing is sometimes used as a pre-processing technique to get good approximate positions for the double difference solutions (Leick 1995). Differencing over time reduces the sampling frequency of the observations, which for bridge deformation monitoring applications is not ideal as higher sampling frequencies are required. Triple differencing also has the further disadvantage that geometric strength is lost because of the differencing over time.

2.5. Coordinate Systems

WGS84 (World Geodetic System 1984) is a global coordinate system utilised by GPS users. ITRS (International Terrestrial Reference System) is a higher accuracy version of WGS84. There is a problem with trying to use a global coordinate system for land based applications, since the continents are constantly moving in relation to each other. Great Britain is moving with respect to WGS84 at a rate of 2.5 centimetres a year (Ordnance Survey 2004). So ETRS89 (European Terrestrial Reference System 1989) is used as the standard GPS coordinate system in Europe. For this thesis, the GPS measurements are recorded in WGS84.

OSGB36 is the coordinate system used by the Ordnance Survey (OS) to map Great Britain. Coordinates are given in local easting, northing and height. In this thesis coordinates are transformed from the global WGS84 coordinates into local OSGB36 coordinates. For more information about coordinate systems, WGS84 and OSBG36 the interested reader is referred to Ordnance Survey (2004).

2.6. Advantages and Issues Associated with Using Single Frequency Receivers

One of the research aims of this study was to use less expensive single frequency receivers for the application of bridge monitoring. Dual frequency receivers had been used in many bridge trials conducted by The University of Nottingham with good results (Ashkenazi et al. 1996; Roberts et al. 1999; Roberts et al. 2001a).

Single frequency receivers typically cost around half the price of dual frequency. For the Leica Geosystems receivers used for many of the trials in this thesis, the dual frequency receivers cost £13,500 and the single frequency receivers cost £8,300. However for other receiver manufacturers the difference can be larger; from the company Javad, single frequency receivers cost between $2,500 (£1,365) and $3,100 (£1,690) whereas the dual frequency receivers start at $15,950 (£8,710) and go up to $38,450 (£20,990) (Javad Navigation Systems 2004b). For a number of deformation applications the price of dual frequency GPS receivers may be too high and so restrict their use, but this might be reduced by using single frequency receivers instead.

Once the software had been developed for the Leica single frequency GPS receivers, it was then possible to use it to process data from other receivers. 100 Hz data from the JNS100 receivers is only available for the single L1 frequency. So, for an application where high frequency data is required, like monitoring the movement of short span bridges, single frequency receivers were used. For more information on the use of JNS100 receivers to monitor the movement of bridges see Chapter 9 and Roberts et al. (2004a).

Trials have also been conducted for this thesis with Garmin handheld GPS receivers, which again are only available in single frequency. For applications where very cheap GPS receivers are required (a Garmin receiver typically costs between £100 and £400 (GPS Warehouse 2004)) only single frequency models are available.

The main issues associated with using single frequency GPS receivers are ambiguity resolution, cycle slip detection and errors caused by the ionosphere.

2.6.1. Kinematic Ambiguity Resolution

Single frequency receivers have the weakness that it takes longer to resolve the integer ambiguities at the beginning of the session and after a cycle slip, compared to dual frequency receivers. Typically for L1 only data it can take anything up to 30 minutes when the receiver is static (Sharpe 1999). In a completely dynamic environment single frequency ambiguities may not be able to be resolved at all. However, for dual frequency receivers, ambiguity resolution times are reduced to under a minute in most cases. If the integer ambiguities are not resolved, the pseudorange solution is only accurate at the metre level, which is no where near exact enough for

precise engineering applications such as bridge monitoring. Long ambiguity resolution time can seriously affect the reliability of the whole deformation monitoring system.

The first stage in the ambiguity resolution process is the generation of the potential ambiguity combinations. The approximate coordinate of the antenna is known either from the pseudorange solution or from input coordinates. A search space is constructed which surrounds this approximate coordinate. The size of this search space affects the efficiency of the search, as a large search space means there are more possible combinations to look through. However, the search space must be large enough to contain the correct ambiguity combination and so should not be made too small.

The reason that the dual frequency ambiguity search is so much quicker than the single frequency one is due to the wide lane observable. The wide lane is formed from a linear combination of the L1 and L2 phases. Denoting Φ_{L1} as the L1 phase observation, Φ_{L2} as the L2 phase observation and Φ_{L1-L2} as the wide lane observation, equation (2-5) below describes their relationship.

$$\Phi_{L1-L2} = \Phi_{L1} - \Phi_{L2} \qquad \textbf{(2-5)}$$

The frequency of the wide lane is 347.82 MHz and so the corresponding wavelength is 86.2cm. This is significantly bigger than 19.0cm and 24.4cm for the L1 and L2 wavelengths respectively. The larger wavelength increases the ambiguity spacing within the search space and reduces the number of possible integer ambiguity combinations, so considerably speeds up the search time.

So, methods of accelerating ambiguity resolution in the context of bridge monitoring were investigated for single frequency receivers and are introduced in Chapter 5, Section 5.4.2 (Cosser 2004; Cosser et al. 2004b).

2.6.2. Cycle Slip Detection

A cycle slip displays itself as an instantaneous jump in the carrier phase value for a particular satellite. It is brought about by the receiver briefly losing lock on the satellite signal which can either be caused by physical obstructions such as people and buildings, or by a low signal to noise ratio on the signal caused by multipath, bad ionospheric conditions or low satellite elevation.

An uncorrected cycle slip will mean that the integer ambiguity values have to be resolved again for a particular satellite, or if the slip goes completely undetected it may mean that the ambiguities will have to be re-resolved for all satellites. (An undetected slip can cause an error in the positioning solution and create large residuals errors. Kinpos processing software will detect this, but not be sure on which satellite the slip occurred and so it unfixes all of the ambiguities.) Since whether the ambiguities are resolved or not affects the accuracy of the positioning solution so profoundly, it is important to have a robust cycle slip detection and repair routine to avoid loosing ambiguity resolution.

For dual frequencies receivers linear combinations of the L1 and L2 phases are used to detect and correct cycle slips (Hofmann-Wellenhof et al. 2001). For single frequency receivers, there is no second frequency with which to form the linear combination, and so precise cycle slip detection is more of a challenge. For this thesis single frequency cycle slip detection was achieved by a triple order difference of the carrier phase, which is introduced in Chapter 5, Section 5.4.1. The interested reader is referred to Roberts (1997a) for discussion of dual frequency cycle slip detection.

2.6.3. Ionosphere

Single frequency receivers cannot form the ionosphere free linear combination to remove the effects of the ionosphere from the solution, which dual frequency receivers can do. However in Section 2.3.3.1, it is stated that the ionosphere is spatially correlated over tens of kilometres (Rizos 1999a). For the experiments conducted in this thesis the baselines are all less than 5km and in the case of the Wilford Bridge most of the baselines are as small as 50 metres, so the influence of the ionosphere should be removed in a double difference solution.

3. Bridge Deflection Monitoring with GPS

3.1. Introduction

This chapter is an overview of bridge monitoring techniques both with and without GPS. The current primary method of bridge monitoring in the US and UK is by visual inspection, which is both time consuming and expensive. Section 3.2 looks at why bridges need to be monitored as well as deficiencies in the current visual inspection methods. Section 3.3 focuses on some case studies of particular bridges which highlight the need for GPS monitoring techniques. Section 3.4 discusses traditional surveying techniques and their advantages and disadvantages for bridge deformation monitoring. Previous GPS bridge monitoring systems are introduced in Section 3.5 and some of the deficiencies with these systems are highlighted. Section 3.6 talks about previous research conducted at the University of Nottingham and how the author's research follows on from this.

3.2. The Need for Monitoring

"They were made for the days of the horse and buggies, but survive in an era of 40-tonne trucks"

(Nova Scotia Department of Transportation and Public Works 2003)

Bridges are designed and built to withstand certain forces such as wind, traffic, tidal loading and perhaps even extreme environmental effects such as earthquakes and typhoons. These forces will have been taken into account in the bridge's design and will govern in part its characteristics and its life expectancy. However, bridges are now often required to operate outside their design assumptions. For example over the last twenty years the maximum permitted heavy load has increased by 33% and traffic

densities in some parts of the UK have exceeded design forecasts by over 300% (EPSRC 2001). Most of the 1100 major bridges (those with spans greater than 100 metres) in the USA are over 50 years old, and several of the notable ones are over 100 years old (Aktan et al. 2001). The cost of maintenance now exceeds the cost of building a new bridge, so it is important that the maintenance is carried out in the most cost effective way (EPSRC 2001). Since 1988 expenditure on UK trunk road bridge maintenance has been in excess of £800 million, with 80% of the expenditure driven by the need to improve safety (Haynes 1997). Timely detection of faults and effective response to them can save lives, reduce closure time and therefore save money.

Czepiel (1995) discusses Bridge Management Systems (BMS) and the history of legislation concerning BMS in the USA. After the collapse of the Silver Bridge in 1967 between West Virginia and Ohio the need to monitor the condition of bridges became apparent. A National Bridge Inventory database was set up after 1968, which was used to decide which bridges to replace due to the highest danger of failure. Bridges were all given ratings based on structural condition, function and essentiality for public use. If this rating was below a certain threshold funding was given so the bridge could be replaced. Later funding was also given to repair bridges before they got into a critical state.

In 1995 all US states were informed that they must implement a BMS, the components of which are data storage, cost and deterioration models and optimisation models. The database stores all the data from inspections. The inspections consist of attaching a subjective rating from 0-9 to each of the bridge components to represent its physical condition. Deterioration models predict the condition of the bridge elements in the future, while optimisation models analyse the least cost maintenance strategies determining the impacts of deferring repairs or implementing them now. The optimisation models can be used across the network of bridges taking into account the money available, deterioration of all the bridge and the amount and type of traffic a bridge serves.

Czepiel (1995) points out that the implementation of a BMS is only as good as the data put in. The information needs to be accurate for there to be optimal results. For these BMS visual inspection is the primary data collection method, with the ratings describing the overall evaluation of the bridge not the condition that caused the rating. Data from non-destructive evaluation (NDE) methods (which includes GPS) could add

valuable information into a BMS resulting in a more accurate description of the bridge's condition.

The Highways Agency in UK implemented a 15 year Bridge Rehabilitation Program in 1988 to deal with the backlog of substandard bridges, but it is thought that the activities will continue beyond the current program (Das 1996). A BMS similar to that implemented in the USA was being considered, particularly the more advanced PONTIS BMS. Das (1996) agreed that NDE testing and monitoring techniques need to be included in a bridge management system. Failures in visual inspections were also discussed with the main one being that not all serious defects may be identified. The defects may be hidden below a road surface, waterproofing or in another way not accessible for inspection.

Visual inspections are also carried out by Network Rail (formerly known as Railtrack) annually with detailed inspections taking place every six years (Bell 2004). Inspection codes of practice produced by Network Rail state that inspections should take place at times when there is the heaviest possible rail traffic and any abnormal movements or vibrations should be noted (Railtrack 2001). Foundation deficiencies can appear as movements which may be large enough to cause tilting, cracking or excessive movement at joints. Identification of abnormal movements could be difficult with visual inspection alone and this is where GPS could be used. A number of inspection methods described in Railtrack (2001) involve inflicting damage to the structure, such as excavations of trial holes and removal of bolts or plates. It is warned that the stability of the structure must not be compromised, but further damage may be incurred. A method such as GPS would not cause any further damage to the structure while evaluating its health.

An investigation into the reliability of visual inspection methods was conducted by US Department of Transportation (2001). It was discovered that the condition ratings were generally not assigned in a systematic manner and that the inspectors were unlikely to identify many of the defects which the type of inspection was meant for. The recommendations at the end of the report suggested more training for the inspectors in the types of defects that should be identified. This report further demonstrates in the inadequacies of only using visual inspection for monitoring bridges.

It is clear that visual inspection has major deficiencies due to the subjective nature of the rating and the fact that faults may be missed. A study conducted by the Federal Highways Agency (FHWA) revealed that at least 56% of the average condition ratings

from visual inspections were wrong with a 95% probability (Aktan et al. 2001). It is also time consuming and expensive. The biannual visual inspection of the Brooklyn Bridge in New York is reported to take three months and cost $1 million (Aktan et al. 2001). Decision making based on optimisation models is put into question if the data is not accurate and the whole BMS can be compromised. Other monitoring techniques such as GPS could be used to overcome the deficiencies of the current methods.

On April 5th 1998 the Akashi Kaikyo Bridge in Japan was opened and became the world's longest suspension bridge with a record main span of 1,991 metres (Cooper 1998). By comparison it is 366 metres longer than the StoreBaelt Bridge in Denmark and 560 metres longer than the Humber Bridge in England. The bridge cost $3.6 billion (US) to build, taking ten years to complete. Japanese officials are investigating the feasibility of building bridges with longer main spans of up to 2,400 metres, which is clearly a daunting challenge for suspension bridge design and management. Due to the cost of construction, the longer spans and the vital role they play in transportation systems, the need for effective monitoring and management has increased.

3.3. Case Studies

The Kingston Bridge in Scotland, one of Europe's busiest river crossings, underwent major repair and retrofitting in 1999 to fix structural deficiencies (BBC 1999). In 1996 the Koror-Babeldaob Bridge, in Palau in the Caroline Islands group, crashed into the sea severing Koror from its sources of water and power (Anon 2002). These two examples show that the need for bridge monitoring transcends international boundaries. The following are two further case studies of particular bridges, the Tacoma Narrows Bridge and the Millennium Bridge, where the need for monitoring is highlighted.

3.3.1. Tacoma Narrows Bridge

The Tacoma Narrows in Washington State, USA famously collapsed due to aerodynamic instability on 7th November, 1940 (O'Connor and Shaw 2000). It was a suspension bridge with a main span of 854 metres, which was opened to traffic on 1st July 1940. There were problems with the bridge before and after it was opened. On numerous occasions before the collapse large vertical oscillations were observed by

travellers on the bridge, who reported that cars in front of them actually disappeared from view and reappeared a number of times during a crossing.

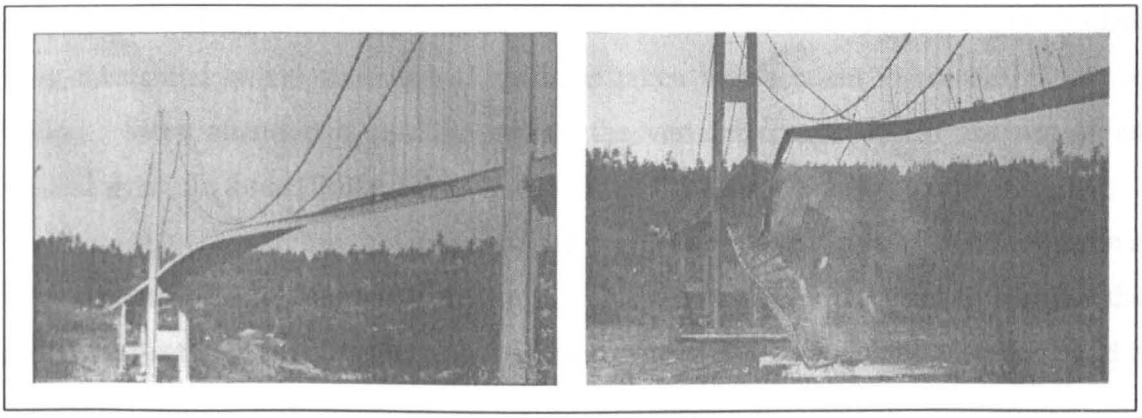

Figure 3-1 The Tacoma Narrows Bridge (Smith 1974). The left photo shows the torsional movement of the mid span just before failure. The right photo shows the bridge beginning to collapse.

On the day that the bridge collapsed it oscillated for hours at an unusual vertical mode. Suddenly the movement changed to a torsional motion (Figure 3-1) and became violent, which led quickly to visible damaged and then failure. The wind speed was measured at 68 kph. One of the factors that led to the collapse was the magnitude of the longitudinal movement between the deck and the main cables which was between 0.9 and 1.8 metres, causing damage to the main cables. This failure had a major effect on suspension bridge design so that aerodynamic stability was taken into account, which means that this type of failure is unlikely to occur again. However, it does demonstrate the need to monitor bridges for large movements which may cause damage or failure.

3.3.2. Millennium Bridge

The Millennium Bridge which crosses the River Thames in London was opened for three days, between Saturday 10th June and Monday 12th June 2000, before being closed for investigation into its unexpected movements. During the opening day there were up to 2000 people on the bridge at one time, with between 80,000 and 100,000 people crossing the bridge in the day (Dallard et al. 2001). The movement of the south and central spans became so large that people had to hold onto the handrails or stop to retain their balance. On the south side there were large horizontal and torsional movements reaching 50mm. On the central span the movement reached 70mm. After noon on 10th

June the rate that people were allowed on the bridge was limited, mainly to stop pedestrians feeling uncomfortable when the movements became large.

It is thought that the large lateral movement was caused by the high volume of pedestrians walking in synchronisation with each other and with the sway of the bridge. This substantial lateral loading had not been taken into account in the design of the bridge. More attention is usually paid to the vertical component of the pedestrian applied dynamic force (Dallard et al. 2001).

Investigations into the movement of the bridge were conducted by ARUP before a large amount of damping was added to it. This demonstrates the need to monitor the bridge to investigate movements outside the design specifications and therefore find a solution.

Roberts et al. (2004b) introduce trials conducted on the Millennium Bridge during its closure in November 2000. These trials were conducted as a viability test for GPS monitoring of bridges. It was known that the large lateral induced movements had caused difficulties upon the bridge and so the results from the lateral component were the most important. However, problems with the satellite geometry over the three days of the trial meant that the movement in the lateral direction appeared to be less than in the longitudinal direction. Due to these satellite geometry issues, the possible solution of using pseudolites were discussed by Roberts et al. (2004b) and are discussed and implemented in Chapters 10 and 11 of this thesis.

3.4. GPS Deflection Monitoring Versus Conventional Surveying Instruments

Recent advances in GPS receiver technology and processing techniques mean it is now a viable tool for deformation monitoring of manmade structures and natural processes. Traditionally, structural monitoring was carried out with surveying instruments such as levels and theodolites. The disadvantages of surveying instruments are the long intervals between observations which can be hours, days or weeks; the observations are not in real time as they usually batch processed after hours of observation; they have a poor level of automation; and the instruments may need a clear line of sight which may not always be possible especially in bad weather conditions. This section examines other techniques available to monitor the deformations of structures and gives the advantages and disadvantages of these techniques. It also

examines some of the advantages and error sources associated with GPS and how these can be mitigated.

Triaxial accelerometers measure displacements in the three component directions at a rate of up to 1,000 Hz. They are not dependent on electromagnetic waves and so have no refractivity and line of sight problems and do not have visibility problems in bad weather. However, they have instrumental biases and scale factor offsets which mean that the positions drift extremely rapidly, possibly reaching hundreds of metres after a few hours, even with high quality sensors (Meng 2002). Accelerometers need continuous updating to avoid error accumulation which can be achieved using GPS technology. Accelerometers are good at measuring high frequencies but have problems detecting low frequency vibrations, such as those experienced on long bridges (approximately 0.1-0.3 Hz). They are light and compact and so have a minimal affect on the properties of the structure they are monitoring. Wiring, that is required to link them to a central recording unit, can be easily damaged and adds noise to the signals especially if the wires are very long (Lovse et al. 1995).

Tilt meters and strain gauges are expensive, complex to install and maintain, require frequent calibration and are vulnerable to the environment.

Ground based laser scanners can be used to collect large clouds of data points about the 3 dimensional nature of the structure. This method is limited by the low sampling frequency (for a Leica Geosystems' Cyrax laser scanner used on the Wilford Bridge one measurement could take ten minutes); the fact that structure is required to be semi-static for each measurement; and the large amount of data which means that the image takes a long time to process. These factors mean that a laser scanner cannot be used for monitoring dynamic deformations of structures but could be used for long-term deformation monitoring.

Interferometric synthetic aperture radar (InSAR) can provide dense deformation measurements with sub-mm accuracy in a cost effective manner. However, since the repeat periods of the satellites are so long (35 days for ERS-1 and 44 days for JERS-1 (Meng 2002)), the temporal coverage is very limited. So, InSAR cannot be used for monitoring bridge deformations as temporally the data would be sparse.

Fibre-optic Bragg grating strain sensors demonstrate potential for long term bridge monitoring since they are exceptionally stable. The core of the fibre is exposed to an optical interference pattern and any strain is modulated as a wavelength shift (Li et al. 2004). A single axis strain and temperature sensor is created at the core of the fibre.

They have small physical size, are highly durable, have the potential to be inexpensive to mass produce and have immunity to electromagnetic interference (Maaskant et al. 1997). The most useful information about a structure can be gathered if the fibre optic sensor is embedded in the bridge structure before construction. Since this cannot occur in bridges which have already been built, they are most useful for future bridges. Concrete is highly alkaline, which attacks glass, which causes problems when locating fibres in bridges.

Electromagnetic distance measurement (EDM) instruments and total stations are used to measure the slow deformations of structures and natural processes with good results (Hill and Sippel 2002; Kuhlmann and Glaser 2002; Leica Geosystems 2002a). The advantages of using a total station include a high accuracy (Leica Geosystems (2002a) quote accuracies of better than 1mm for their bridge and tunnel surveys); the automatic target recognition (Hill and Sippel 2002); and the possibility of measuring indoors and in urban canyons (Radovanovic and Teskey 2001). The disadvantages include the low sampling rate (the total station, TCA2003, at The University of Nottingham will measure at a 1 Hz data rate in automatic target recognition mode, however Tsakiri, et al. (2003) use a total station that measures at 8 Hz), an uneven measurement rate; problems with measurements in adverse weather conditions; and the fact that a clear line of site is needed between the total station and the prism. Experiments were conducted by the author with a Leica TCA 2003 total station measuring in automatic target recognition mode at a 1 Hz data rate. The data rate of this machine proved to be too slow for measuring the small amplitude and high frequency vibrations of the Wilford Suspension Footbridge, but could possibly be used to measure deflections on larger bridges (See Chapter 4, Section 4.5).

GPS requires no line of sight between observation points and has no limitation on range. Automatic data collection at high sampling rates (10 Hz and now even 100 Hz with some receivers) is now possible and observations are linked to an absolute reference frame (WGS84) and have extremely accurate time tagging which allows synchronisation. From the work of Hyzak et al (see Meng (2002)p. 32) some of the advantages of GPS which have meant that it has found an application in structural monitoring are:

- All weather observations,
- The accuracies that can be achieved (at the mm level),

- The fact that the 3D positions are established in an absolute world reference frame (WGS84),
- Continuous monitoring at data rates up to 20 Hz (now 100 Hz),
- Automatic operation means there is less human intervention,
- The near real time capacity and no long term sensor drift.

GPS does have its disadvantages in the form of the error sources introduced in Chapter 2, Section 2.3. GPS is also dependent on the geometry of the satellite constellation through the mathematical quantity DOP (dilution of precision). A reliable solution is not always possible due to the geometry of the available satellites, specifically in urban canyons where there are obstructions due to the surrounding environment. One solution to the GPS geometry problem is pseudolites which are discussed in Chapters 10 and 11. The lack of data averaging in a kinematic GPS solution can mean that it is difficult to maintain a constant positioning accuracy.

In January 2001 29 GPS receivers were added to the 774 sensors already in operation on the Tsing Ma, Kap Shui Mun and Ting Kau Bridges in Hong Kong (Wong et al. 2001). The sensors already in operation included anemometers, temperature sensors, dynamic weigh-in-motion sensors, accelerometers, displacement transducers, level sensing stations and strain gauges. With so many sensors in place already, what advantages in monitoring could GPS add? The main sensors used to measure the bridge responses were level sensing stations and accelerometers. The level sensing stations measured at 2.56 Hz with an accuracy of 2 mm. The cost of installation of these sensors is high and they only measure vertical displacement, unlike GPS which measures in the three coordinate directions simultaneously.

Accelerometers can measure the acceleration of the bridge deck in the three coordinate directions, which is transformed into displacement by double integration. The natural frequencies of the Tsing Ma Bridge decks are low and so the double integration of the acceleration does not reflect the actual displacement. Accelerometers cannot detect continuous or steady displacements, only local vibrations, so temperature changes which raise or lower the bridge deck or strong wind pushing the bridge alignment to one side cannot be detected. Since GPS measurements are absolute it can measure these slow steady displacements well.

Even though GPS has many error sources, it has many advantages for structural monitoring over traditional surveying instruments.

3.5. GPS Bridge Monitoring Systems

Bridges experience two distinct types of deformation. The first is long term deformation which can exhibit itself over days, weeks or years, caused by settling of the foundations, stress relaxation and bridge deck creep. The second is the short term or dynamic deformation of structures which is caused by environmental factors such as temperature or wind, or loading by traffic. The bridge will usually recover from short term deformations, whereas long term deformations are mostly permanent. GPS can be used to measure both types of bridge deformation simultaneously.

Many studies have been carried out to assess how appropriate a tool GPS is for structural deformation monitoring both in the short and long term. The following is a review of some of the GPS bridge monitoring trials that have been conducted.

A study called "Dynamic displacement recording of large bridges with GPS" is summarised in Johns (2000). The aim of the study was to develop structural monitoring techniques using high frequency GPS to assess and mitigate the affects of hazards such as earthquakes and strong winds. At first the study looked at the possibility of using low cost single frequency GPS receivers which would provide a cost saving of $25,000 (£13,850) per site. Canadian Marconi (CMC) Allstar GPS receivers were chosen and two hours of data collection at a 10 Hz data rate was undertaken. It was found that the receivers did not provide real 10 Hz data and that approximately 30% of epochs were missed. It took between 10 and 20 minutes for the integer ambiguities to be resolved and even when they were resolved the precisions achieved (± 2cm horizontally and ± 2.5cm vertically) were below specification. It was concluded that single frequency receivers were not acceptable for structural monitoring applications and so the study changed to using dual frequency receivers.

Since this study was completed in 2000 advances in GPS technology have meant that single frequency receivers will record at a 10 Hz data rate and there are no missing readings. Cosser, et al. (2003) has shown that once integer ambiguities are resolved the results produced by single frequency GPS receivers are as good, if not better, than those produced by dual frequency GPS receivers. Investigations as part of this thesis have shown that the time to single frequency ambiguity resolution can be greatly reduced, by different methods applicable when monitoring the movement of a structure such as a bridge (see Chapters 5, 6 and 7).

Research in bridge deformation monitoring with GPS began as early as 1991 at the Applied Research Laboratory, the University of Texas (ARL:UT) (Hyzak and Leach 1995). In May 1991 experiments were conducted on the Luling, a cable-stayed suspension bridge in Louisiana where ten GPS receivers were employed on the bridge and two were used as reference receivers. Most data was only collected at 0.1 Hz, with a small amount being collected at 1 Hz data rate. From experience it is known that these data rates will only be good enough to measure the long term movement of the bridge, not the short term transient motion. Modal frequencies of the bridge movement were calculated and there was a dominant frequency of 0.002- 0.003 Hz, which was said to be a natural bridge frequency even though previous research showed that a similar bridge should have a frequency between 0.3 and 1.1 Hz. It is likely that the modal frequency which was calculated was not a bridge frequency at all, but more likely multipath. Multipath can appear in a GPS time series as low frequency fluctuations (Hofmann-Wellenhof et al. 2001), which was also seen by Roberts, et al. (2002) when a strong multipath frequency of 0.05 Hz was detected during experiments conducted on a footbridge.

Hyzak and Leach (1995) also introduce experiments conducted in 1994 also on the Luling Bridge. The same antenna sites were occupied as in the previous trial. During this experiment EDM and theodolite measurements were used to verify those collected from GPS and records were kept of the traffic crossing the bridge. Data was again collected mainly at 0.1 Hz and also some receivers recorded at 2 Hz, which was the maximum possible data rate at that time. Only data at 0.1 Hz are presented. Slow longitudinal displacements of the main span and towers were observed mainly due to temperature. These observations agreed well with EDM and tape measurements. Hyzak and Leach (1995) demonstrate that GPS can be used to measure slow deformations of bridges due to temperature changes, but the data rate used is not fast enough to demonstrate the possibility of dynamic deformation monitoring.

Duff, et al. (1997) concentrate on the error mitigation, system design and operational efficiency of a GPS-based structural monitoring system. Error mitigation strategies for GPS are discussed, particularly multipath which is mitigated by time averaging of the data or averaging data from multiple reference stations. Preliminary results of a trial in Scotland where controlled moving devices are used to simulate real bridge movement are presented. The actual movement of the controlled moving devices is known. The GPS results are averaged over two hour time intervals to get results

which agree to the truth to within 3 mm. GPS is used in the situation to measure the slow deformation of the controlled moving device with good results. The authors do not mention the frequency of observations or any attempt at measuring the dynamic deformation of the devices.

Duff and Nelson (1997) reviews the state of the current technology for GPS-based bridge deformation monitoring. When the first portable GPS receiver was introduced it weighed over 50 kg and cost $120,000 (£66,500). Since then there have been many improvements in GPS receiver size, weight, power consumption and cost; and more importantly GPS receivers are now more accurate due to the production of increasingly higher quality carrier phase data. All of these improvements have meant that GPS is now a viable tool for structural deformation monitoring.

Duff and Nelson (1997) also discuss integrating GPS with other measurements particularly GLONASS satellite measurements and accelerometers. Including GLONASS satellites into the processing of GPS data can produce better results, particularly in obstructed environments where extra satellite signals are especially important. Integration of GPS with accelerometers can overcome the deficiencies of both systems. A further method of augmenting the GPS signal especially in obstructed environments is by the use of pseudolites which are discussed in Chapters 9 and 10 of this thesis.

The world's longest single span suspension bridge, the Akashi Kaikyo Bridge was opened in April 1998 with a single span of 1,991 metres and a total bridge length of 3991 metres (Fujino et al. 2000). A system of three GPS receivers have been installed to measure the deformation of the bridge, along with many other measuring instruments including accelerometers, anemometers and seismometers. Three GPS receivers are insufficient to measure the global movement of such a long bridge. One of these receivers is used as a reference, even though it is located on the bridge itself. It is located at a reasonably stable point, but some bridge movement may permeate into the data and so affect the positioning solution at the other two sites.

Fujino, et al. (2000) compare temperature and vertical displacement data from GPS averaged every 10 minutes for a day and taken at the same time every day for six months. The results show a good correlation between the two. Averaging data every ten minutes will remove the multipath from the positioning solutions so that semi-static displacements caused by wind and temperature can be identified. However, it is far too slow to identify any dynamic bridge characteristics or response to loads. GPS data is

recorded at a 20 Hz data rate during earthquakes and high winds but no data is presented at this frequency.

No discussion of the errors associated with GPS is presented Fujino, et al. (2000) and there is no attempt to mitigate any of these errors. Issues such as tropospheric delay may have a great effect on the monitoring system, particularly as one of the rover receivers is located at the top of one of the towers. Erroneous conclusions may be drawn from data where GPS error sources have not been considered.

In January 2001 29 GPS receivers were added to the 774 sensors already in operation on the Tsing Ma, Kap Shui Mun and Ting Kau Bridges in Hong Kong (Wong et al. 2001). The Tsing Ma Bridge is the longest span suspension bridge in the world that carries both road and rail traffic, with a mid span length of 1,377m. Two reference receivers were used and 14 rovers were positioned along the deck, cables and towers of the Tsing Ma Bridge. The data is collected a 10 Hz data rate which is transferred via a network of fiberoptic cables to workstations. The resulting displacements of the deck are calculated with 2 seconds latency and displayed in the control room. Post-processing of the GPS data does occur, but results and analysis of this is not included. The paper is mainly concerned with the layout of the GPS receivers, the architecture of the system and the reasons for including them in the bridge monitoring system. There is no discussion of GPS error sources or ways of mitigating them to produce a more reliable system. The data rate used in the system is high enough for important bridge characteristics to be determined from the data, but no analysis of this is provided.

Lennartz-Johansen and Ellegaard (2002) conducted a 4 day measurement trial on the Great Belt Fixed Link (East) which is the longest single span suspension bridge in Europe and the second longest in the world with a mid span of length 1,624m . It was discovered that the use of GPS for the deflection monitoring meant that the survey cost about half as much compared to traditional surveying methods, mainly due to the reduction in man-power. Traditional survey techniques require surveyors to operate the equipment all the time the data is being collected, whereas GPS can be set up and left for the day with returns only to download the data.

The survey conducted by Lennartz-Johansen and Ellegaard (2002) recorded data every 15 seconds and processed a solution every 15 minutes over four days, during which 20,000 people walked across the bridge. Again this data rate is far too slow to be able to identify the dynamic displacement of the bridge and is only useful for slow deformations. Since the dynamic response to 20,000 pedestrians crossing the bridge

was one of the aims of the study, a higher data rate should have been chosen to fulfil this goal. The data was analysed in WGS84, not transformed into the local coordinate system. To fully analyse the bridge movement in the three coordinate directions, transformations of the WGS84 coordinates into bridge coordinates need to be conducted. This is especially important to be able to analyse the magnitude of the bridge displacement. Since the data has been averaged over many epochs during processing, the size of the bridge displacement may not be measurable anyway.

A real time deformation monitoring software has been developed by Hein and Riedl (1995) called DREAMS. Experiments were conducted where GPS receivers were installed on pillars where the coordinates were known. The pillars were located next to a building and trees and so the multipath was expected to be quite high. Static and kinematic trials were conducted in order to assess the accuracy of the system. Good results were obtained with sub-centimetre accuracies, although it was thought that due to the high multipath nature of the surrounding environment the results were degraded by about 2-3 times. It should be noted that as this software has been developed specifically for deformation monitoring, it is likely to be quite often in worse multipath environments than the one described, especially if GPS is to be used for bridge monitoring.

A low-pass filter was passed through the data to remove the multipath signature lower then 10^{-2} or 10^{-1} Hz. During the kinematic trials one of the pillars is moved up by a known amount at a recorded time. There is a time delay of a few seconds for the GPS positioning solution caused by the low-pass filter. This kind of positioning latency is unacceptable when measuring the displacements of structures that move quickly and would have to be removed before using the system on a bridge.

Further trials were conducted with DREAMS software, one of which is detailed in Hein and Riedl (2003). A GPS bridge trial was conducted on a motorway bridge between Würzburg and Frankfurt in Germany, where four GPS receivers were installed on the bridge, with the reference station being some distance away on top of a service station. The area surrounding the bridge did not allow the placement of the reference station near to it, which would have obviously been the ideal situation. Data were recorded at a 1 Hz data rate for most of the observation session, a data rate that could be considered to be too slow especially considering that the span that was being measured was only about 100 metres long. Dynamic movement of the bridge was shown to be about 4 centimetres at all the bridge sites and there was a coincidence of movement

shown by the three receivers that were on the same side of the bridge. The data were also processed every hour to show the overall bridge movement.

Wieser and Brunner (2002) suggest that monitoring the dynamic deformation of bridges using GPS receivers placed on the bridge deck is not possible. Two experiments are conducted on "Rosenbrücke" at Tulln in Austria, one where the GPS receiver is positioned on top of the tower and one where a GPS receiver is placed on the bridge deck. Results for the receiver placed on top of the tower are very good due to no obstructions or multipath. The receiver on the bridge deck is located very close to the steel cables at the mid span of the bridge. Cables cause diffraction effects which mean that the movement of the bridge is not distinguishable from the GPS noise. The problem is especially difficult since the dynamic movements of the bridge in question are very small and are swamped by the GPS noise. In this situation adaptive filtering of two days time series could be used to distinguish the multipath from the actual bridge movement. This method has been used with good results by Roberts, et al. (2002) and is discuss in Chapters 4 and 6. On a bridge with a small span (400 metres for the whole bridge) and small amplitude, the fundamental frequencies of bridge movement are likely to be high, whereas multipath will display itself as low frequency movement. This would also aid in the identification and separation of the two. Identification of bridge movement on a small bridge is more of a challenge in the presence of a high multipath signal, but it is by no means impossible.

This section has introduced and analysed a number of GPS-based bridge monitoring studies conducted around the world. Generally the studies have focussed on slow or long term movements of bridges using slow data rates and averaging of observations. Averaging means that multipath is removed but also means important information about the bridge's dynamic displacement is lost. Due to GPS error sources dynamic monitoring of bridge movement is more of a challenge and this monitoring is the focus of this thesis.

3.6. GPS Based Bridge Monitoring at The University of Nottingham; Previous Research

This section reviews some of the trials conducted by researchers at The University of Nottingham and how the authors work will lead on from this.

Research into the deformation of structures, specifically bridges, has been underway at The University of Nottingham for almost ten years. The first trial on the Humber Bridge was conducted in March 1996 (Ashkenazi et al. 1996). The results showed large vertical displacements of the bridge and demonstrated the possibility of monitoring the movement with dual frequency real time kinematic GPS.

The IESSG were joined by researchers from Brunel University and members of the Humber Bridge Board to conduct a controlled experiment on February 16th 1998 on the Humber Bridge (Roberts et al. 1999). Originally antennas were attached to poles which were clamped onto the handrails of the bridge. Results from earlier trials demonstrated that the data had been significantly affected by the vibration of the poles and so specialised clamps were designed to secure the antennas directly to the bridge's handrails. Five fully laden lorries weighing a total of almost 160 tons were hired in for the trial and made to cross the bridge in various configurations. Eight GPS receivers logged the data; one on a lorry, five on the bridge and two reference receivers. Three receivers on the bridge were located at the mid spans, two on the east and one on the west; one receiver was located at the quarter span on the east side and one was located on the mid span of the Barton side span on the west side. A diagram of the layout of the receivers for this trial can be found in Figure 7–1 in Chapter 7, where the results are further analysed.

An FE model of the Humber Bridge had been developed at Brunel University which could be used to predict the consequences of any damage incurred by the bridge. The model needed to be validated by real bridge movement data and the GPS data was used for this. During the trial the southbound side of the bridge was closed to traffic but it was not possible to close the northbound side, however traffic at the time the trial was conducted (1am) was very light.

Three lorry configurations were used. First all five lorries travelled southbound on the eastern side of the bridge at a constant speed of about 30 miles per hour. Second all five lorries travelled northbound on the western side of the bridge at the same constant speed. The final configuration had two lorries travel from the south end of the bridge and two lorries travel from the north end meeting in the middle and staying there for five minutes.

Results showed a maximum vertical displacement of 600 millimetres at the mid span of the bridge when the lorries were on that particular side. The side without lorries on showed a vertical displacement of 500 millimetres showing that the bridge was not

only displacing but also twisting at the same time. When the lorries were on the main span the Barton span was pulled upwards and vice versa showing a cantilever effect caused by the suspension cables. The displacements all agreed well with the FE model predictions and fast Fourier transforms of the data produced vibration frequencies that also agreed well with the model.

Young (1998) conducts preliminary investigations into the use of single frequency receivers for the application of bridge deformation monitoring. Results from the dual frequency trial on the Humber Bridge in February 1998 (discussed above) are compared to single frequency results from a further bridge trial conducted on 14th August 1998. During the August 1998 trial, long ambiguity resolution times were encountered for the single frequency receivers, which at some bridge sites meant no useful information about the bridge movement could be ascertained at all. When ambiguities were resolved, the single frequency receivers could track the movements as well as the dual frequency. However, due to the long ambiguity resolution times Young (1998) suggests that single frequency receivers cannot be used for 'critical' applications where a high reliability is needed.

One of the limiting factors for high accuracy GPS structural monitoring is multipath. Dodson, et al.(2001) introduce adaptive filtering for multipath mitigation. By comparing the time series from two consecutive days' data the common part and uncommon part of the two signals can be identified. This method can be used to remove multipath from the reference receiver time series, the rover receiver time series and also to remove receiver random noise from a solution if two GPS receivers are monitoring the same bridge movement. Adaptive filtering can be further used to remove tropospheric delay from a time series (Roberts et al. 2001b; Meng 2002) and to integrate data from GPS and accelerometers. The adaptive filtering algorithms developed at The University of Nottingham are used to remove multipath from two days time series in Chapters 4 and 6 of this thesis and more explanation of this technique is included there.

To overcome the deficiencies of both systems a hybrid GPS and accelerometer bridge monitoring system was proposed by researchers at The University of Nottingham (Meng 2002). For a discussion of the advantages and disadvantages of GPS and accelerometers see Section 3.4. Initial platform tests of the hybrid system produced good results (Roberts et al. 2000) before bridge trials were conducted. When GPS only data is compared to GPS and accelerometer data combined, the accelerometer can

bridge the gaps in the GPS data and removed outliers (Roberts et al. 2001a). The GPS data updates the accelerometer position and so removes the accelerometer drift.

To enable a bridge to be remotely monitored without the need for onsite inspection the possibility of real-time GPS correction transmission needs to be investigated. Most previous work on real time corrections has been conducted using radio modems, but they have many deficiencies which include slow information transmission speed, single directional data flow and the requirement of a line of sight between the reference and rover receivers. For a discussion of other disadvantages of radio modems for RTK corrections, the reader is referred to Omar and Rizos (2003).

Meng et al. (2004a) propose an internet-based RTK GPS correction transmission system, where both the corrections from the reference receiver to the rovers and the rover receivers' final coordinates are transmitted over the internet. The system consists of three parts, which are the reference station, the monitoring nodes and the control segment. The reference and rover receivers (monitoring nodes) are Leica Geosystems System 500 dual frequency GPS receivers. The reference transmits corrections to the rover, which using internal algorithms calculates the position solutions and transmits them to the control segment. The control segment receives the final coordinates and conducts real-time processing to remove multipath and cycle slips, detect missed data and also visualise the results. The data is streamed at a 10 Hz data rate with a maximum latency of 0.1s. There are no missing epochs for any of the trials conducted, but due to failures in positioning data transmission, there are occasions where the last epoch's data is retransmitted to fill in a data gap. More investigation into the success rate of RTK correction transmission will be conducted in the future.

For one of the trials introduced in Meng et al. (2004a) the results of the internet-based system are compared to a direct cable connected system and also to post-processed results. The findings show that the most precise results are achieved with the direct cable connected reference and rover, with the next best produced by the internet-based corrections and the worst results by the post-processed solutions. For a further trial undetected cycle slips in the internet-based correction system meant that the coordinate time series were very different when compared to the post-processed results. In the post-processing algorithms forwards and backwards processing is implemented and so cycle slips are more likely to be detected. The trials demonstrated that a positioning precision of several millimetres of the coordinates can be achieved by the internet-based transmission of corrections in real-time at a 10 Hz data rate.

3.6.1. Contributions Made by this Thesis

Previous research at The University of Nottingham into bridge deformation had predominately been conducted with dual frequency GPS receivers, apart from one study conducted by Young (1998). One of the research aims of this thesis is to use less expensive single frequency receivers for structural monitoring and obtain similar results to dual frequency. The limitations and challenges of using single frequency receivers have been discussed in Chapter 2, Section 2.5. The main disadvantage of single frequency receivers are the long ambiguity resolution times, which in some cases result can in no ambiguity resolution at all The implementation of single frequency GPS to monitor the movement of bridges is the main focus of this thesis and is discussed in more detail in Chapters 4-9. Chapter 5 focuses on the software development which will allow single frequency ambiguity resolution to be accelerated.

Meng, et al. (2002b) highlight the case of a bridge in London where the satellite geometry causes it to appear as though the longitudinal movement of the bridge is larger than the lateral in the GPS solution, when parallel observations by an accelerometer recorded opposite results. Solutions to satellite geometry problems by the integration of pseudolites into the GPS positioning solution is discussed by Meng et al. (2004b) and Barnes et al. (2003b) and further investigated in this thesis in Chapters 10 and 11.

It has long been known that many of the high frequency vibrations of structures could not be identified by relatively low frequency GPS. Until recently the maximum data rate that could be recorded by GPS was 20 Hz, but research in this thesis has used 100 Hz receivers measuring at a 50 Hz data rate to record bridge movement (see Chapter 9).

Geodetic receivers are very expensive even those that only record single frequency data. To investigate a more affordable monitoring system data from Garmin handheld receivers was collected and compared to geodetic receivers. The difference is price is massive but the difference in data quality after processing is quite small (Chapter 8).

3.7. Summary

The need for bridge deformation monitoring is examined and the advantages and disadvantages of GPS over traditional surveying methods are discussed. The

deficiencies of the current method of visual inspection are assessed. Previous work conducted on GPS for structural deformation monitoring is reviewed and deficiencies with the research are highlighted. Work conducted at the IESSG into bridge deformation monitoring is introduced and how this thesis leads on from this is presented.

4. Short Bridge Trial 1- Wilford Bridge

4.1. Introduction

The Wilford Bridge in Nottingham is a pedestrian footbridge, which crosses the River Trent. It is about 68 metres long and 4 metres wide. The main purpose of the bridge which is owned by Severn Trent, a water company, is to conduct water and gas via pipes laid underneath the footpath, to the other side of the river. This bridge has been used as a test bed for this project because of the large magnitude of movement for a bridge of its size and also because it is located quite close to The University of Nottingham campus. This bridge has been the focus for a number of trials carried out by the University of Nottingham (for more information on previous trials see for example Meng (2002) or Roberts, et al. (2001a)).

This chapter introduces the first bridge trial that was conducted on the Wilford Bridge. This trial was undertaken to test the equipment in a bridge environment and to test the feasibility of using GPS and a total station for dynamic monitoring. Interesting results were attained from the trial and short-comings of the current processing software were discovered. This chapter is split into two main sections. The first section looks at the comparison of single and dual frequency receivers both in static and bridge environments. The second section analyses the possibility of using a total station for dynamic monitoring of bridges.

The layout of equipment and procedure for the trial is explained in Section 4.2. Section 4.3 concentrates on comparisons between single and dual frequency receivers. Section 4.3.1 introduces zero baseline trials conducted to establish the accuracies of both single and dual frequency receivers in similar environments. The comparisons between single and dual frequency receivers in a bridge environment are presented in Section 4.4. This analysis is split into reference receivers on the riverside near the

bridge (Section 4.4.1) and reference receivers 3.6km away from the bridge (Section 4.4.2). The conclusions drawn from these comparisons are given in Section 4.4.3.

Section 4.5 introduces the work conducted into using a total station for dynamic monitoring. The initial feasibility trials conducted on the University campus are presented in Sections 4.5.2 and 4.5.3. The results from the bridge trial are given in Section 4.5.4 and conclusions drawn from this work in Section 4.5.5. No further work was conducted into using total stations for dynamic monitoring but some ideas of future work that could be undertaken are put forward in Section 4.5.6.

4.2. Wilford Bridge Trial 1 – June 2002

A GPS, accelerometer and total station bridge trial was conducted at the Wilford Suspension Footbridge, over the River Trent in Nottingham, on the 19th, 20th and 21st June 2002. The layout of the equipment can be seen in Figure 4-1 and Figure 4-2. A mixture of dual and single frequency receivers were used for this trial. At Ref1, Ref4, Bdg1 and Bdg2 there were Leica system 500 dual frequency GPS receivers. At the other sites there were Leica system 500 single frequency GPS receivers. Bdg2 had a single and dual frequency receiver connected via a splitter to the same antenna. The purpose of this set up was to compare the performance of the single and dual frequency receivers directly. All the reference receivers were connected to Leica AT503 (small choke ring) antennas and most of the rovers were connected to Leica AT504 (large choke ring) antennas, except Bdg1 which was connected to an AT502 (patch) antenna. The bridge was made to move by staff and students from the IESSG who passed across the bridge in different ways (marching, running etc.).

Five reference receivers were used in the trial. Ref1 and Ref2 were located on the riverside, only about 50 metres away from the bridge. Ref4 and Ref5 were located on the roof of the IESSG building which is about 3.6km away from the bridge. Ref3 was located on the top of the Tower building on the University campus. Analysis in this chapter only uses results from Ref1, Ref2, Ref4 and Ref5. The results from Ref3 were used for another research project about the effect of tropospheric delay on positioning results. The interested reader is referred to Clark (2003) for more information about the tropospheric delay estimation project.

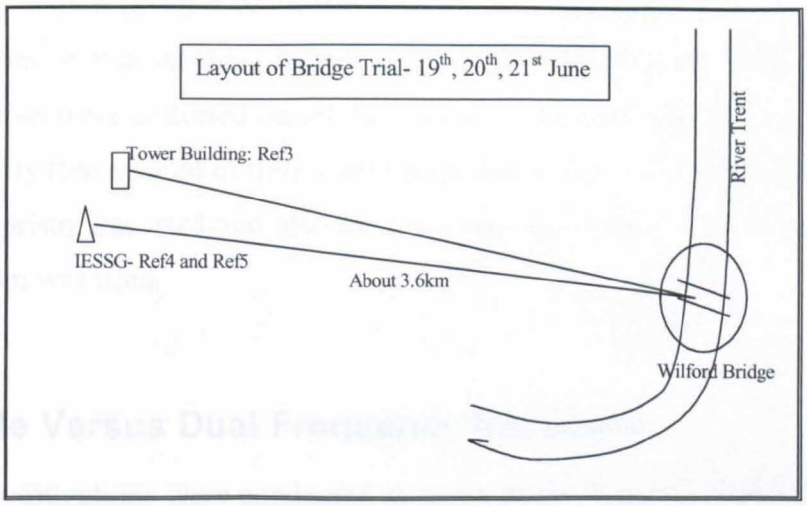

Figure 4-1 The layout of the three remote reference receivers in relation to the Wilford Bridge (not to scale)

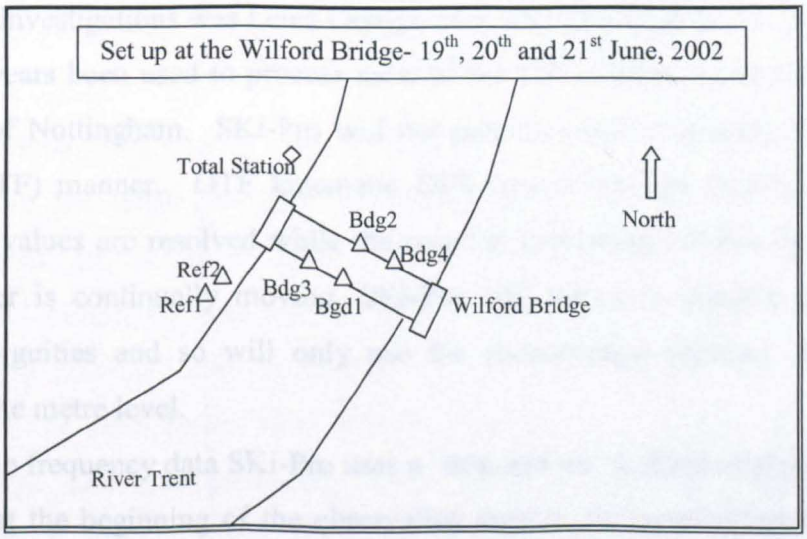

Figure 4-2 The layout of the receivers at the Wilford Bridge site (not to scale)

Figure 4-3 The two riverside reference receivers Ref1 on the right and Ref2 on the left with the Wilford Bridge in the background

Figure 4-4 The total station 360° prism located next to the GPS antenna and accelerometer

The total station prism was located next to the cage that housed the GPS antenna and accelerometer at point Bdg2, which can be seen in Figure 4-4. Measurements from the total station were collected on all three days of the trial only during the periods of highest activity (the amount of time varied from day to day). On the first day of the trial the circular prism was used and also the retro tape was tested. On the other two days the 360° prism was used.

4.3. Single Versus Dual Frequency Receivers

Initial investigations were conducted to compare the accuracy achievable with dual and single frequency receivers. For these trials Leica system 500 dual and single frequency geodetic receivers were used. The processing software used for these preliminary investigations was Leica Geosystems' SKi-Pro Version 2.5, which had for a number of years been used to process most of the GPS bridge monitoring data at The University of Nottingham. SKi-Pro will not process single frequency data in an On-The-Fly (OTF) manner. OTF kinematic GPS means that the carrier phase integer ambiguities values are resolved while the receiver is moving. If the single frequency GPS receiver is continually moving, SKi-Pro will not even attempt to resolve the integer ambiguities and so will only use the pseudorange solution, which is only accurate at the metre level.

For single frequency data SKi-Pro uses a 'stop and go' method of processing, which means that at the beginning of the observation session the receiver must be static for about ten minutes while the integer ambiguities are resolved. Receivers that are placed on the bridge are continuously moving, however on the Wilford Bridge this movement is small, usually only 1-2cm and about 5cm at maximum. Since this value is much less than an L1 wavelength, SKi-Pro can resolve the ambiguities by treating the data as static. This method works on short bridges with small amplitude movements, but for larger bridges with bigger amplitudes such as the Humber Bridge (Chapter 7), this method would not be appropriate. Section 4.3.1 compares results achieved with single and dual frequency receivers for a zero baseline trial. Then Section 4.4 compares the single and dual frequency receivers in the bridge trial conducted on the Wilford Bridge, which has been described in Section 4.2.

4.3.1. Zero Baseline Trials

A static zero baseline trial was conducted at the IESSG building over two consecutive days. On the first day, two single frequency Leica 510 receivers were connected via a splitter to a Leica AT503 choke ring antenna on the roof of the building. On the second day at the same time, two dual frequency Leica 530 receivers were connected via a splitter to the antenna in the same position. The aim was to compare the data from the dual and single frequency receivers under similar conditions. Due to the GPS constellation repeatability the receivers would see the same satellites on the two days. The dual frequency data was processed in an OTF manner and the single frequency data had a static initialisation of ten minutes before being processed as kinematic. Zero baseline tests mean that most of the errors associated with GPS are eliminated in the double difference solution i.e. multipath, ionosphere and tropospheric delays as they are exactly the same at both receivers. All that is left is the receiver noise (see Section 2.3.2.2).

The coordinate time series were calculated in WGS84 using SKi-Pro and then converted into the local OSGB36 coordinate system using Grid InQuest software (available from the Ordnance Survey). The mean value of each time series was calculated and subtracted from each coordinate in that time series. These coordinate values were plotted and can be seen in Figure 4-5 to Figure 4-7. The standard deviations of the time series were calculated using the standard formula (seen in equation (4-1)). This same procedure was followed for the results shown in the rest of this thesis.

$$\sqrt{\frac{n\sum x^2 - (\sum x)^2}{n(n-1)}} \qquad \textbf{(4-1)}$$

The results for the zero baseline trials for the east, north and vertical components can be seen in Figure 4-5 to Figure 4-7 and also in Table 4-1. It can be seen from these results that in every coordinate direction, the single frequency receivers have a more precise solution than the dual frequency. It is surprising that for both receivers the vertical component is more precise than the north. This was due to a decline in precision in the horizontal component that begins half way through the observation

period. This degradation was caused by an increase in the DOP values, due to the changing satellite constellation, which particularly affected the north component.

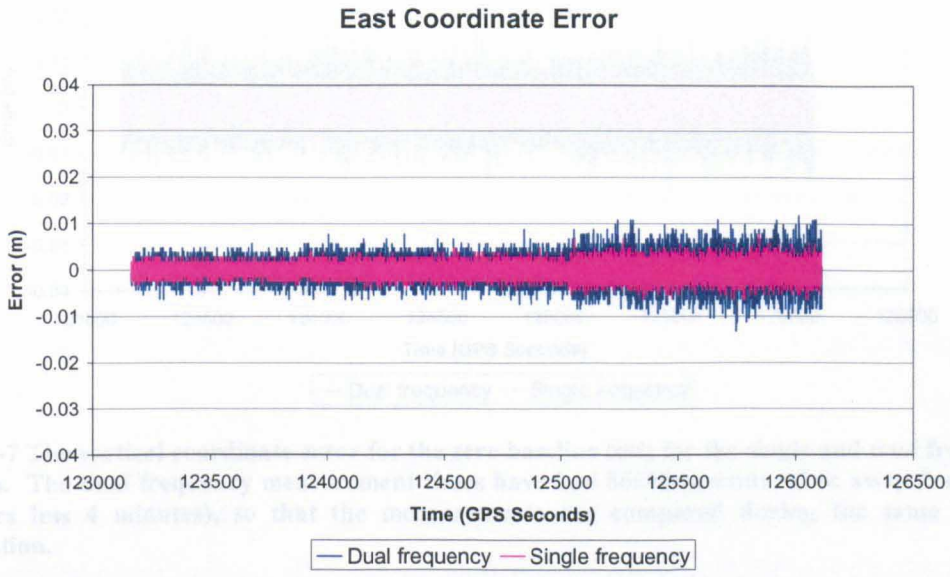

Figure 4-5 The east coordinate error for the zero baseline tests for the single and dual frequency receivers. The dual frequency measurement times have had 86160 seconds taken away from them (24 hours less 4 minutes), so that the measurements are compared during the same satellite constellation.

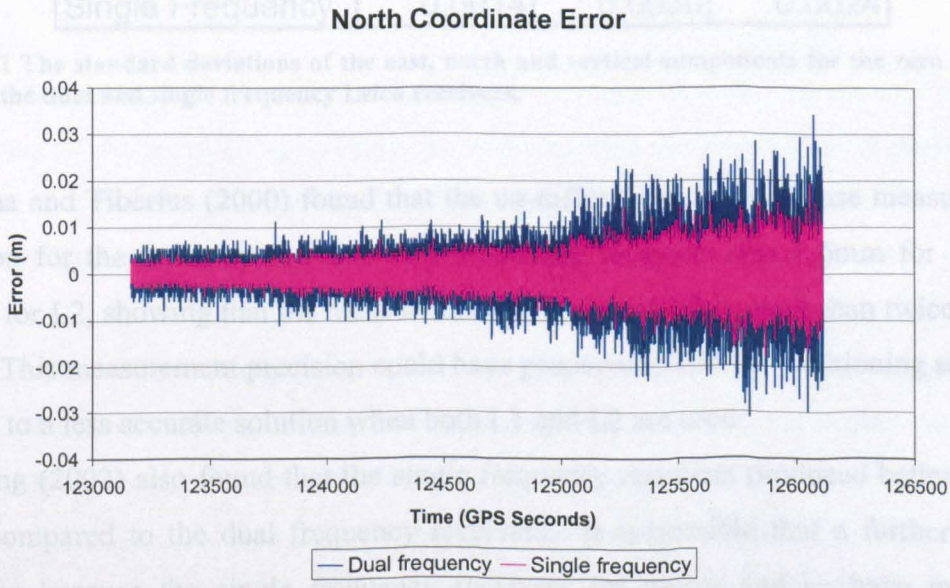

Figure 4-6 The north coordinate error for the zero baseline tests for the single and dual frequency receivers. The dual frequency measurement times have had 86160 seconds taken away from them (24 hours less 4 minutes), so that the measurements are compared during the same satellite constellation.

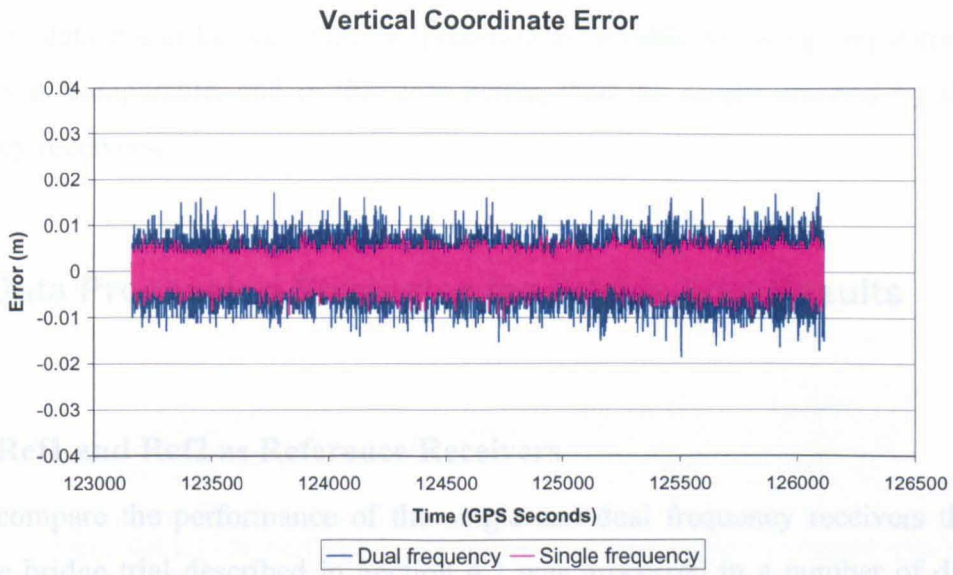

Figure 4-7 The vertical coordinate error for the zero baseline tests for the single and dual frequency receivers. The dual frequency measurement times have had 86160 seconds taken away from them (24 hours less 4 minutes), so that the measurements are compared during the same satellite constellation.

	Standard Deviations (m)		
Zero Baseline	East	North	Vertical
Dual Frequency	0.0024	0.0053	0.0042
Single Frequency	0.0014	0.0030	0.0024

Table 4-1 The standard deviations of the east, north and vertical components for the zero baseline trial for the dual and single frequency Leica receivers.

Bona and Tiberius (2000) found that the un-differenced carrier phase measurement precision for the Leica system 500 dual frequency receivers was 0.6mm for L1 and 1.5mm for L2, showing that the measurement precision of L2 is more than twice as bad as L1. This measurement precision could have propagated into the positioning solution, leading to a less accurate solution when both L1 and L2 are used.

Meng (2002) also found that the single frequency receivers produced better results when compared to the dual frequency receivers. It is possible that a further reason could be because the single frequency receivers are newer and so have upgraded hardware and firmware. The only error sources affecting this data are caused by the internal receiver noise and satellite constellation. By conducting the tests on two consecutive days at similar times, the receivers have been forced to see the same satellite constellation; any errors must be caused by the receiver noise. The benefits of dual frequency receivers, which are the modelling of ionospheric errors and faster

ambiguity resolution times, have not affected the solution in this zero baseline test. From this data it can be seen that the precision achievable by using single frequency receivers is comparable, and in this case better, than the results attained by the dual frequency receivers.

4.4. Data Processing Strategies for Bridge Trial Results

4.4.1. Refl and Ref2 as Reference Receivers

To compare the performance of the single and dual frequency receivers the data from the bridge trial described in Section 4.2 was processed in a number of different ways. At first the riverside reference stations Refl (dual) and Ref2 (single) (Figure 4-3) were used for the processing. These reference stations were only about 50 metres away from the rovers on the bridge. Processing was concentrated on Bdg2 as this was the site that had the dual (Bdg2d) and single (Bdg2s) frequency receivers connected via a splitter to the same antenna. Bdg2d was processed in an on-the-fly manner, while the single frequency rover had ten minute static initialisation before being processed as kinematic.

The data presented in the following sections analyse the east, north and vertical components of the positioning solution. In later chapters the bridge data is analysed in the bridge coordinate system of lateral, longitudinal and vertical. However, for this initial investigation it was decided to keep the coordinates in the east, north and vertical coordinate system.

The results of the initial processing can be seen in Table 4-2. It can be seen from this Table that the best result is found when the single frequency rover is processed with the single frequency reference. In this case the standard deviation is lower in every component with the most noticeable being in the vertical direction. It can also be seen that even with the dual frequency reference the single frequency rover is better. Figure 4-8 shows the vertical displacement for the single frequency rover processed with the dual and single frequency reference receivers. It can be seen from this Figure that with the dual frequency reference the coordinates are indeed nosier. There are two noticeable times within the observation period where the coordinates for Refl-Bdg2s (dual frequency reference) have a noticeable jump, meaning there is an offset from the

zero mean. It is conjectured that this is due to multipath or more likely a cycle slip. Plotting of the dual frequency rover with dual frequency reference reveals a similar pattern in the coordinates, implying that the cycle slip or multipath occurred at the dual frequency reference receiver.

	Standard Deviations (m)		
	East	North	Vertical
Ref1- Bdg2d	0.0035	0.0055	0.0109
Ref1- Bdg2s	0.0031	0.0053	0.0097
Ref2- Bdg2s	0.0027	0.0038	0.0067

Table 4-2 The standard deviation of the east, north and vertical components for the second day of the June bridge trial, for the dual and single frequency rover receivers processed with dual and single frequency reference receivers.

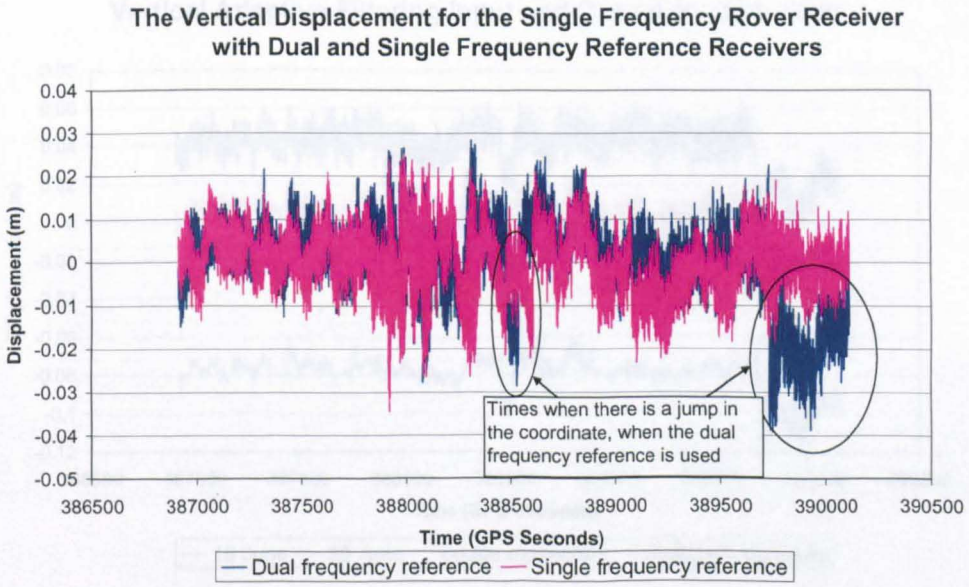

Figure 4-8 The vertical displacement for the single frequency rover processed with dual and single frequency references

Data from the first day of the bridge trial (19th June) are processed for the same sites as for the second day. The purpose is to use adaptive filtering to remove the multipath by comparison of two days' data. A Matlab adaptive filtering script is used, the principles of which are introduced in Dodson, et al. (2001) and Meng (2002). The fundamental idea is that the GPS constellation repeats daily but shifted by four minutes due to the difference in sidereal time and Universal Time (Hofmann-Wellenhof et al. 2001). The satellites follow the same ground tracks from day to day, apart from the four minutes shift. Due to this repeatability, the multipath at static or semi-static sites should be the same on the two consecutive days. Using this information the multipath

can be extracted from the signal leaving behind the real bridge movement. The desired signal is the time series from the second day of the trial and the reference signal is the time series from the first day. These two signals are offset by four minutes.

The result of the adaptive filtering in the vertical component can be seen in Figure 4-9 for the single frequency rover with the dual frequency reference. The jump in the coordinates is obvious in both days' data and it can be seen that adaptive filtering removes this offset. Investigation into the cause of the jump revealed that a cycle slip was to blame. Cycle slips can repeat on a day to day basis if they caused by the same obstructions. So the use of adaptive filtering can remove cycle slips as well as multipath.

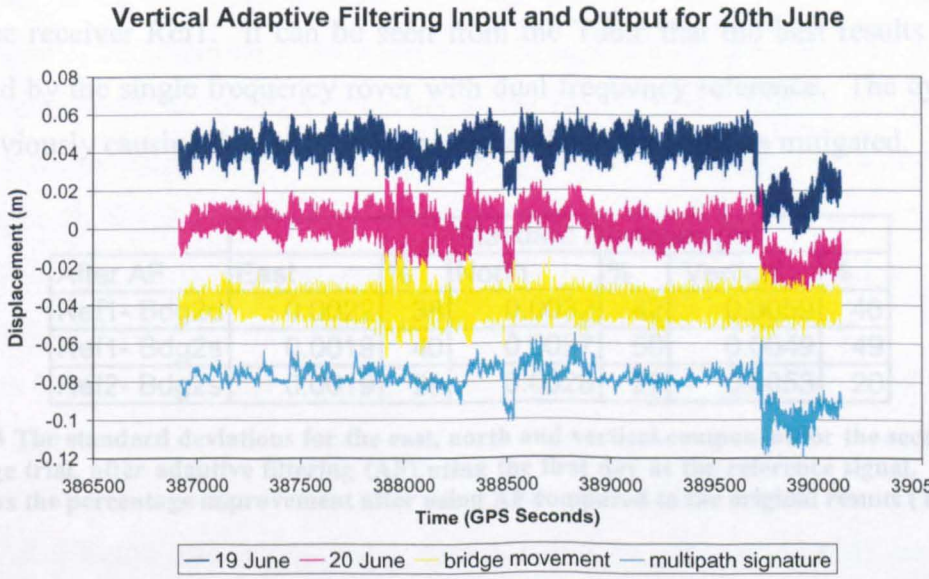

Figure 4-9 Vertical adaptive filtering for two days time series for the single frequency rover with dual frequency reference. Desired signal is the coordinates from 20th June, reference signal is the coordinates from 19th June, the output signal is the bridge movement and the common part is the multipath signature and cycle slips. (The time series from the 19th June, the bridge movement and the multipath signature are all offset from zero for clearness in the graph.)

To verify the success of adaptive filtering the correlation level of certain components were calculated. Of particular interest was the correlation between the output signal (bridge movement) and the common part (multipath signature) and also the output signal and the reference signal (19th June), as both of these correlations should be close to zero for successful adaptive filtering. It was found that the correlation between the reference signal and the output signal was -0.0243 and between the output signal and the common part was 1e-5. Both of these values were very small

and showed there was little correlation between these components. The correlation between the desired (20th June) and reference signals was found to be 0.6659, as they shared a common part which was the multipath but the bridge movement in each case should be different. The desired signal's correlation with the output signal was 0.5328 and with the common part was 0.8339, which showed that more of the desired signal was made up of multipath than bridge movement. All these results showed that adaptive filtering was successful in this case and similar results were found for the other components and receiver combinations.

Table 4-3 shows the standard deviations of the east, north and vertical components after adaptive filtering and also the percentage improvement seen after adaptive filtering compared to the original results (Table 4-2). The adaptive filtering has removed the multipath and also the jumps in the coordinates caused by two cycle slips at the reference receiver Ref1. It can be seen from the Table that the best results are now produced by the single frequency rover with dual frequency reference. The cycle slips were obviously causing degradation in the signal that has now been mitigated.

	Standard Deviation (m)					
After AF	East	%	North	%	Vertical	%
Ref1- Bdg2d	0.0022	38	0.0032	42	0.0059	46
Ref1- Bdg2s	0.0019	40	0.0027	50	0.0049	49
Ref2- Bdg2s	0.0019	29	0.0028	27	0.0053	20

Table 4-3 The standard deviations for the east, north and vertical component for the second day of the bridge trial, after adaptive filtering (AF) using the first day as the reference signal. The table also shows the percentage improvement after using AF compared to the original results (Table 4-2).

4.4.1.1. Removing Satellites

Removing the cycle slips that caused the degradation in the Ref1 signal could also improve the positioning solution when using this receiver as the reference. Since the cycle slips has only been caused at Ref1 and not at Ref2, it was thought that some trees west of the reference station could have caused an obstruction. A sky plot revealed that satellite 4 was most likely to be the satellite causing the problems. The results when satellite 4 was removed from the solution can be seen in Table 4-4. As it can be seen from this Table the removal of this satellite greatly improves the solution for both cases where Ref1 is the reference receiver. The cycle slips on satellite 4 were both L2 cycle slips. Table 4-4 shows that for the north and vertical components the single frequency rover with the dual frequency reference has the smallest standard deviation; while for

the east component the single frequency rover with the single frequency reference has the smallest standard deviation.

	Standard Deviations (m)		
Satellite 4 removed	East	North	Vertical
Ref1- Bdg2d	0.0027	0.0041	0.0069
Ref1- Bdg2s	0.0028	0.0037	0.0062
Ref2- Bdg2s	0.0026	0.0039	0.0063

Table 4-4 The standard deviations for the east, north and vertical components for the second day of the bridge trial, with satellite 4 removed.

It is known that the indirect method of calculating the carrier phase for L2 results in weaker signal strength (Pratt et al. 1997; Satellite Positioning and Navigation Group 2001), and means that it is more prone to cycle slips than L1. This in turn means that dual frequency receivers are more prone to cycle slips than single frequency, which has been demonstrated in the data collected at the bridge trial. Before the removal of satellites and/or adaptive filtering, cycle slips and/or multipath had caused severe degradation in the dual frequency reference receiver, which had in turn affected the accuracy of all solutions computed in relation to it. By adaptive filtering and/or removing satellites this degradation was removed.

It can be concluded that before adaptive filtering and/or the removal of satellites, using single frequency receivers as reference and rover produced a more precise solution. Since cycle slips on L2 occur more often, this is likely to be the case in future trials. After further processing has occurred and cycle slips have been removed, the dual frequency reference produces improved results. It is now the case that the most precise results are found when a dual frequency reference is used with a single frequency rover.

There is now very little difference between the standard deviations for each coordinate component shown in Table 4-3 and Table 4-4. After further processing, all three receiver combinations have produced very similar results.

Section 4.3.1 introduces zero baseline trials where the results for the single frequency receivers were better than for the dual frequency receivers. The use of single frequency receivers in the bridge trial has also resulted in slightly improved results, which could be attributable to the upgraded firmware in the single frequency receivers.

Another explanation is that the inclusion of the L2 data on such a short baseline adds more noise to the solution with very little benefit.

4.4.1.2. Coordinates for Static Initialisation

In SKi-Pro there is a function called init(track) which allows the user to input the coordinates of the static initialisation for the single frequency rover receiver. This allows a shorter static initialisation to be used, as the ambiguity values are resolved more quickly due to this known coordinate. The subsequent coordinates are only as accurate as the initial coordinate entered. This function was investigated for the data from the bridge trial. The data from Bdg2s was processed as static and the average coordinate from the whole session was used as the input coordinate for static initialisation.

The minimum static initialisation that is allowed is one minute. So, using this amount of initialisation and the coordinates from the static processing, the single frequency rovers were processed with both the dual and single frequency references receivers. When using only one minute static initialisation, the average coordinates and standard deviations were the same as the results when ten minutes of static initialisation had occurred. So, this method could be used to reduce the amount of static initialisation that is needed.

4.4.2. Ref4 and Ref5 as Reference Receivers

The next stage of the processing was to use the reference stations which were located at the IESSG building, on The University of Nottingham campus, which was approximately 3.6km from the bridge. Ref4 was a dual frequency receiver and Ref5 was a single frequency receiver. The same processing took place of the dual frequency rover with the dual frequency reference, and the single frequency rover with both dual and single frequency references. When the dual frequency reference was used, ambiguity resolution was possible with the dual frequency rover. At first ambiguity resolution was not possible at all for the single frequency rover.

To allow ambiguity resolution to occur the single frequency receiver had to be given a known coordinate for static initialisation as described in Section 4.4.1.2 above. When this coordinate was given ambiguity resolution was possible, but only when the dual frequency reference was used. For the single frequency reference no ambiguity

resolution was possible at all, and so obviously the solution produced was not nearly as precise. Table 4-5 shows the standard deviations of the components when the reference stations at the IESSG were used. It can be seen from this Table that the most accurate results were found when the dual frequency reference and rover were used. When the single frequency rover was used with dual frequency reference the results are slightly worse but the difference is quite small in each case.

	Standard Deviations (m)		
From IESSG Refs	East	North	Vertical
Ref4- Bdg2d	0.0070	0.0115	0.0171
Ref4- Bdg2s	0.0072	0.0123	0.0177
Ref5- Bdg2s (no ambiguity resolution)	0.6120	0.0194	0.4788

Table 4-5 The standard deviations of the east , north and vertical components for the second day of the bridge trial, with the IESSG points used as the reference receivers

It was thought that the amount of static initialisation may not be enough for single frequency ambiguity resolution over this distance, so an initialisation of 20 minutes was used. After this amount of time the ambiguities were resolved even for the single frequency reference. However a loss of lock occurred on one of the satellites during the observation period, only for one epoch, but this caused the ambiguities to be lost on all of the satellites. For the single frequency data no further attempt was made to resolve the ambiguities. This is a fundamental flaw in the processing method that is undertaken for single frequency receivers by SKi-Pro; if there is a cycle slip or temporary loss of lock no further ambiguity resolution is possible. The only option would be to have another static initialisation. Since ambiguities can be resolved in a minute when the riverside reference stations are used, this could be a possibility. However, when reference stations further away are used, a longer static initialisation is needed and so this would produce a longer 'outage' of coordinates.

4.4.3. Conclusions

When using the riverside reference stations in the bridge trials, cycle slips on L2 caused the data processed with the dual frequency reference to be of poorer quality than the data processed with the single frequency reference. Since cycle slips are more likely on L2, this is a problem when using dual frequency receivers. After using adaptive

filtering, multipath and cycle slips were removed. The most accurate results were then found with a dual frequency reference and single frequency rover. With the riverside reference stations the worst results were found when using two dual frequency receivers.

For the reference stations that were 3.6km away from the bridge different results were found. The best results were with two dual frequency receivers. For two single frequency receivers a longer static initialisation was needed for ambiguity resolution to be possible. Ambiguities were resolved but then they were lost due to a temporary loss of lock to one of the satellites. For the single frequency receivers, no further ambiguity resolution was attempted. This is the main flaw of processing single frequency data in this manner; if ambiguities resolution is lost another static initialisation must take place for ambiguity resolution to be possible.

This initial comparison of data from dual and single frequency receivers has shown that bridge monitoring with single frequency receivers is a possibility. The accuracies achievable by single frequency GPS, once the ambiguities have been resolved, are comparable with dual frequency solutions. However the current method of resolving single frequency ambiguities used by SKi-Pro results in coordinate 'outages' while a static initialisation takes place. If ambiguities are lost then there is no attempt to re-resolve them unless a further static initialisation is undertaken.

For the results introduced in this chapter only the reference stations 3.6km from the bridge suffer from ambiguity loss problems. The rover station Bdg2 is located on the mid span of the bridge with a clear view of the sky and so does not suffer from many cycle slips or losses of lock to the satellites. Rovers that are located closer to the bridge's towers and cables suffer more from the loss of ambiguity resolution. For a number of trials conducted, even when the riverside reference stations are used, loss of ambiguities part way through a session can be a problem.

One way initially implemented to stop the ambiguities being lost was to remove the satellite on which the cycle slip or loss of lock occurred from the SKi-Pro solution, as mentioned in Section 4.4.1.1. However, in a lot of cases removing satellites from a solution can increase the DOP values and compromise the accuracy of the resulting solution.

It is clear that this is limiting the usefulness of single frequency receivers for dynamic monitoring and software needs to be developed to resolve these problems. Chapter 5 explains the development of single frequency processing software undertaken

by the author for this thesis and Chapter 6 introduces improved results from a second Wilford Bridge trial using the new processing software, Kinpos.

4.5. Total Station for Dynamic Bridge Monitoring

Chapter 3, Section 3.4 mentions that total stations have been used to measure the slow deformations of structures with good results (Hill and Sippel 2002; Kuhlmann and Glaser 2002; Leica Geosystems 2002b). The advantages of using a total station include the high accuracy, automatic target recognition and the possibility of measuring indoors and in urban canyons. The disadvantages are the slow sampling rate (1 Hz for the total station owned by the University of Nottingham), problems measuring in adverse weather conditions and the fact that a clear line of sight is needed between the total station and the prism. For a total station used in bridge deformation monitoring, refraction can be a problem when the line of sight has to pass over a body of water.

Radovanovic and Teskey (2001) conducted experiments to compare the performance of a robotic total station with GPS. These experiments were conducted because GPS is not an option in many application areas such as indoors. The total station was run in automatic target recognition mode, which means the total station tracks the prism taking automatic measurements of angles and distances once lock has been established manually. When compared to GPS it was found that the total station performed better in a stop and go situation, where measurements were taken of a moving object only when it was stationary. In a completely kinematic situation GPS performed the best. It was found that there were two main problems with the total station in kinematic mode. These were a low EDM accuracy caused by a ranging error that was linearly dependent upon the line of sight velocity; and an uneven sampling rate over time worsened by no time tagging.

This Section outlines some of the preliminary trials conducted with the total station on The University of Nottingham campus, which included a trial with a moving monument and a metronome. The total station was used in the bridge trial introduced in Section 4.2. The results were compared to those from a GPS antenna located close to the prism (Figure 4-4).

4.5.1. Technical Specifications and Software

The University of Nottingham own a Leica TCA 2003 total station. The technical specifications for this instrument are angle measurements are accurate to 0.5", rapid tracking distance measurements are accurate to 10mm+2ppm (parts per million), automatic target recognition up to 200m away adds an error of 1mm and the 360° prism adds errors of 5mm in distance and 5mm for the angles (Leica Geosystems 2000).

A piece of software called Geocom provided by Leica Geosystems allows the angle and distance measurements from the total station to be displayed on a laptop screen. When Geocom mode is selected on the total station, all readings go directly to the laptop. This software was tested and modified by the author so that the angles and distances, in rapid tracking mode, were output to a file along with a time tag. This time tag was accurate to a second and taken directly from the laptop. Sub-second time tagging was investigated, but there was no success with this for the Visual Basic program. When the total station was in rapid tracking mode it could measure angles and distances approximately every second, so at approximately a 1 Hz data rate. Since it was not possible to know the time more accurately than every second, the exact data rate could not be calculated. It is known from Radovanovic and Teskey (2001) and from the experience of the author that this data rate is probably not constant.

4.5.2. Initial Tests

Some initial tests were conducted on the University campus to test the software and the total station. The first took place on 6th June 2002. A prism was attached to a monument which was forced to move up and down. Figure 4-15 show a picture of a monument used in a subsequent trial. A monument is a similar to a tripod, however there is a plate on top of the monument that can be made to move up and down by a handle. The total amount that the monument could move up and down was measured as 0.09m in the vertical direction and no movement in the horizontal direction. The total station in Geocom mode was attached to the top of another monument. Four set ups were carried out with the distance between the two monuments changed at every setup (these distances were 12m, 22m, 40m and 60m). The prism was moved up and down a number of times at each set up and the results were recorded.

Figure 4-10 and Figure 4-11 show the vertical and horizontal movement of the prism as recorded by the total station. It can be seen that the vertical movement is about

0.09m as expected and the horizontal is about 0.004m. Since there was little or no movement in the horizontal direction, the measurement of 0.004m is attributed to the errors of the instrument. The results at all separation distances were similar, all showed a clear vertical movement of 0.09m in the vertical direction and the movement in the horizontal direction was always around 0.004m. So, at this slow speed the total station measured all the movements well.

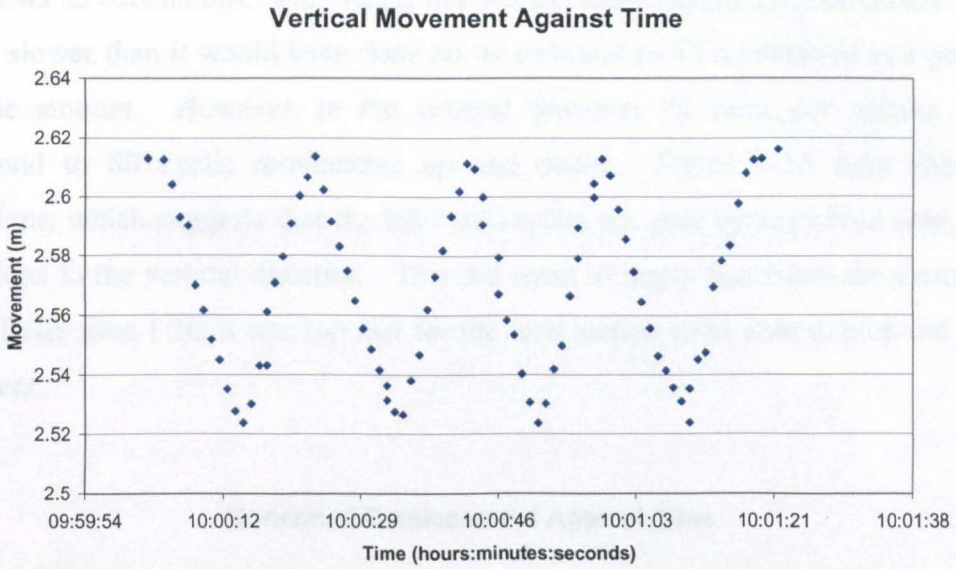

Figure 4-10 Vertical movement of the prism at a distance of 40m

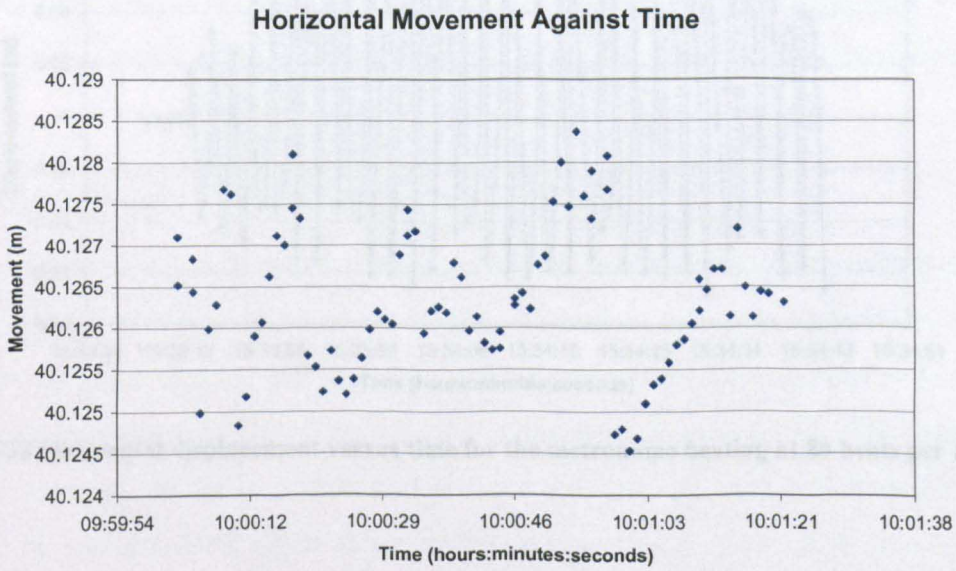

Figure 4-11 Horizontal movement of the prism at a distance of 40m

A second experiment occurred on campus, where a small sticky retro target was attached to the hand of a metronome. The metronome was made to beat at various

speeds, 120, 100, 80, 60 and 50 beats per minute. The total station was set up about 14 metres away from the target and about a minute of data was collected at each speed.

Figure 4-12 and Figure 4-13 show the horizontal and vertical displacements versus time for the metronome beating at 80 beats per minute. Figure 4-12 shows a period of approximately one minute when measurements were taken. The metronome is moving at approximately 80 beats per minute and so about 40 oscillations in the horizontal direction should be observed (as there are 2 beats per horizontal oscillation). Figure 4-12 shows 33 oscillations. The weight of the retro target caused the metronome to beat slightly slower than it would have done on its own and so 33 oscillations is a perfectly plausible amount. However, in the vertical direction 80 beats per minute should correspond to 80 cyclic movements up and down. Figure 4-13 only shows 26 oscillations, which suggests that the total station did not pick up anywhere near all the oscillations in the vertical direction. This did seem to imply that when the metronome moved faster then 1 Hz it was too fast for the total station to be able to pick out all the movement.

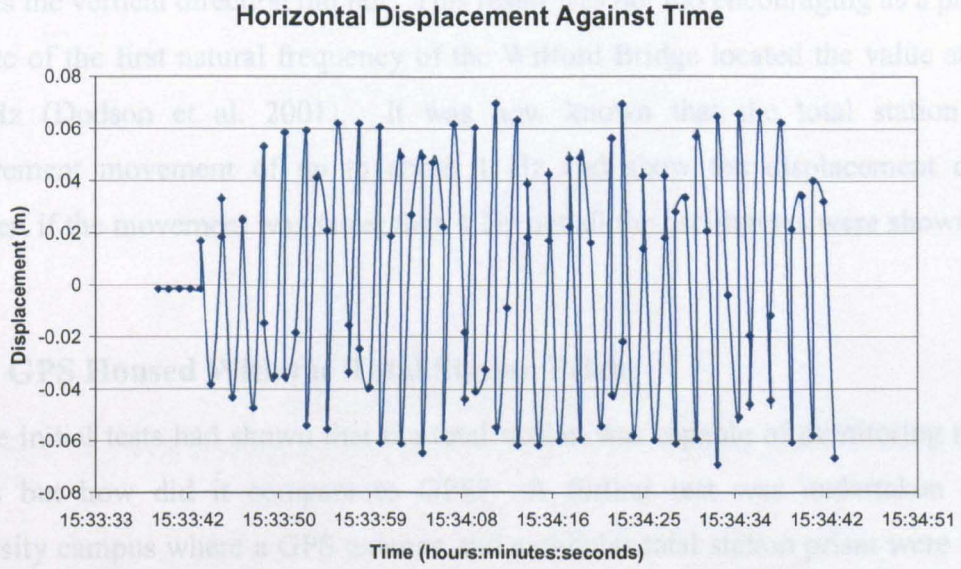

Figure 4-12 Horizontal displacement versus time for the metronome beating at 80 beats per minute

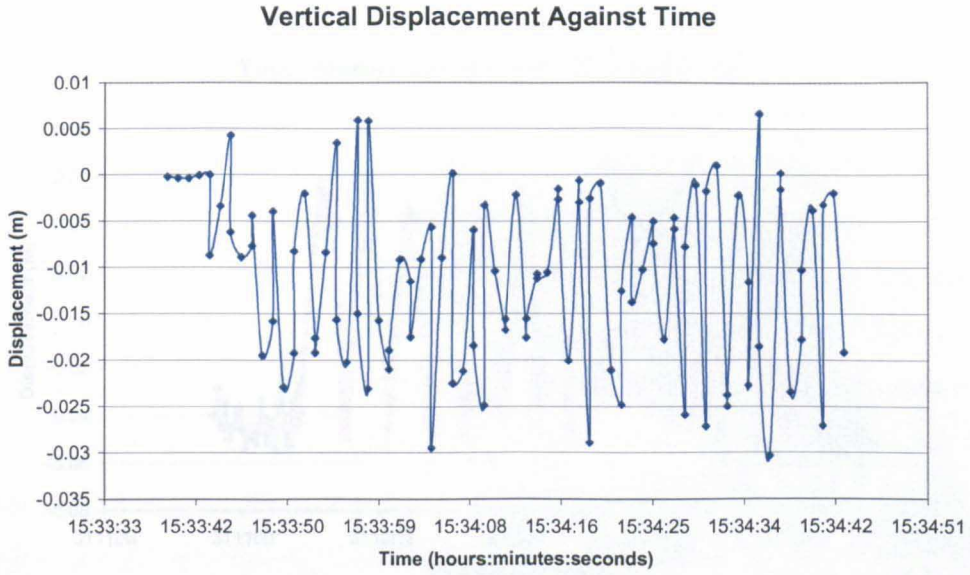

Figure 4-13 Vertical displacement versus time for the metronome beating at 80 beats per minute

The results for the metronome moving at other speeds were similar to those shown in Figure 4-12 and Figure 4-13. The horizontal displacement always showed clear oscillations of movement in line with those expected by the speed of the metronome, whereas the vertical direction did not. This result was not too encouraging as a previous estimate of the first natural frequency of the Wilford Bridge located the value at about 1.75 Hz (Dodson et al. 2001). It was now known that the total station could measurement movement of up to about 1 Hz and show the displacement clearly; however, if the movement was faster than 1 Hz not all the oscillations were shown.

4.5.3. GPS Housed With the Total Station Prism

The initial tests had shown that the total station was capable of monitoring moving objects but how did it compare to GPS? A further test was undertaken on the University campus where a GPS antenna and a circular total station prism were housed together as one unit and placed on top of a monument (Figure 4-15). The prism was made to move up and down a measured distance of 0.1m. A Leica dual frequency GPS receiver recording in RTK mode at a 1 Hz data rate was used as the rover with a similar receiver as reference transmitting corrections.

The results from this test can be seen in Figure 4-14 which shows that the agreement between GPS and the total station was good. They follow the same pattern of movement showing the expected displacement of approximately 0.1m.

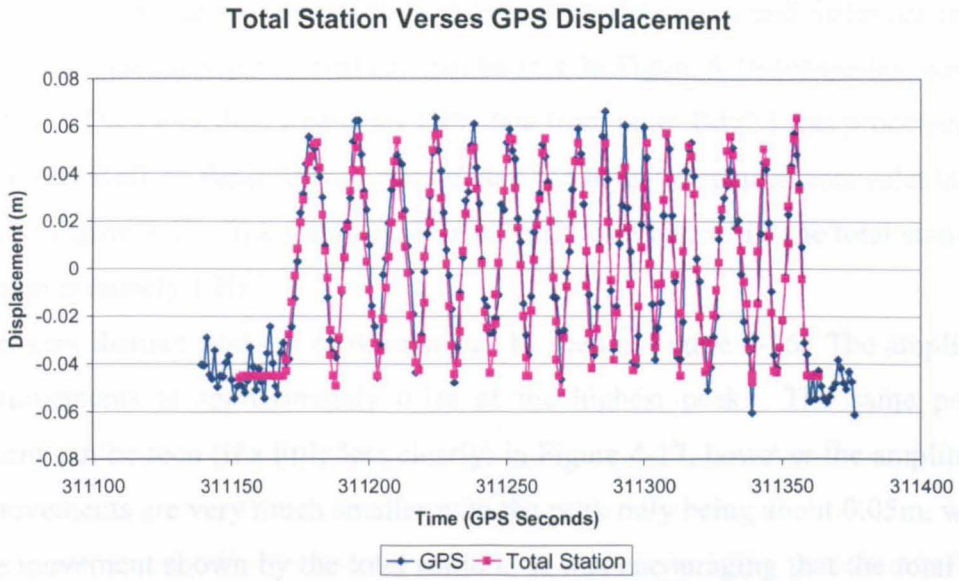

Figure 4-14 The comparison of the displacement shown by the total station and GPS

Figure 4-15 The GPS antenna and the total station prism housed together as one unit on a monument.

The initial tests had shown that the total station was a good tool for kinematic monitoring, but the metronome test had shown that the total station could not keep up if the frequency of movement was too high. The next test was to take the total station to the Wilford Bridge to see if it could pick out the movement. It was known that the total station could only be used to identify the bridge movement; it would not be able to be used for the calculation of natural frequencies as the data rate was far too slow.

4.5.4. Bridge Trial Results

Calculations of the movement of the prism, from the angles and distances recorded by the total station were performed and can be seen in Figure 4-16 for the last day of the bridge trial. The Leica dual frequency GPS data from point Bdg2d was processed using SKi-Pro with Ref1 as the reference station, and the height displacements calculated can be seen in Figure 4-17. The GPS data is at a 10 Hz data rate while the total station data rate is approximately 1 Hz.

Four very distinct peaks of movement can be seen in Figure 4-16. The amplitude of these movements is approximately 0.1m at the highest peak. The same peaks of movement can be seen (if a little less clearly) in Figure 4-17, however the amplitudes of these movements are very much smaller with the peak only being about 0.05m, which is half the movement shown by the total station. It was encouraging that the total station picked out the peaks of movement in this case, but why were the amplitudes so different?

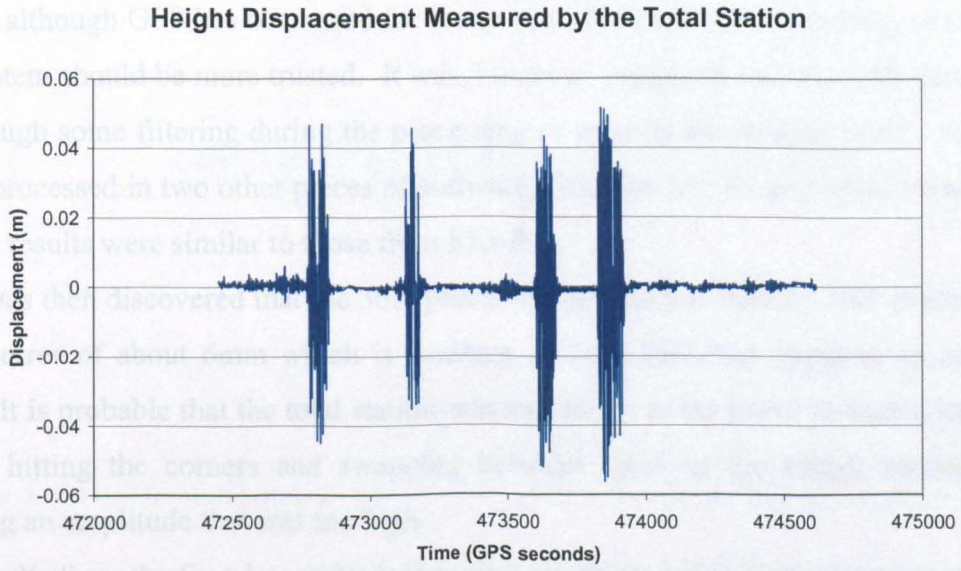

Figure 4-16 The height displacement measured by the total station at the Wilford Bridge trial on Friday 21st June, 2002

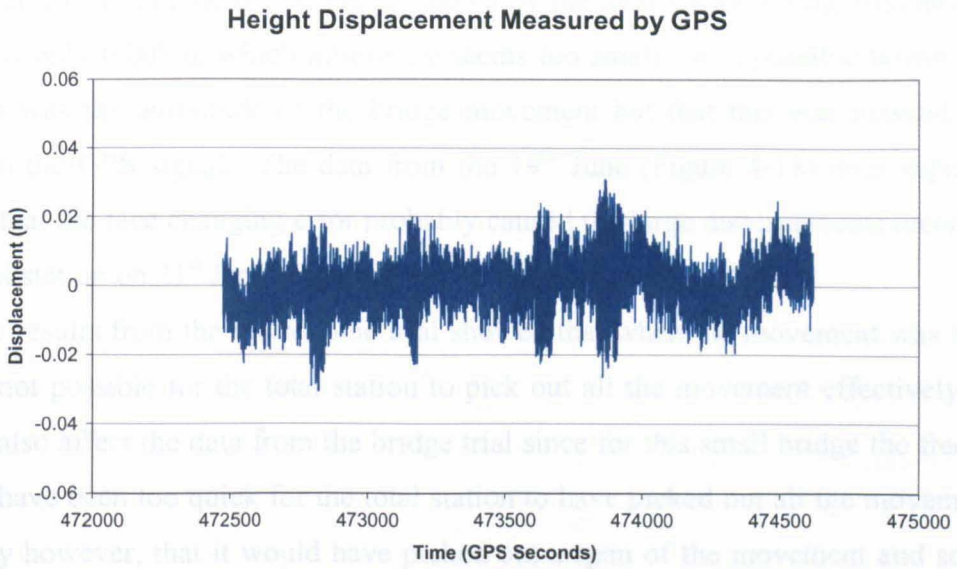

Figure 4-17 The height displacement measured by GPS at the Wilford Bridge trial on Friday 21st June, 2002

For a long time the reason for the difference in amplitude calculated from the two systems was not known. In this situation it was difficult to ascertain which showed the 'truth', although GPS has been used for many years for dynamic monitoring, so perhaps this system should be more trusted. It was, however, suggested that the GPS data could go through some filtering during the processing or even in the receiver itself. The data was reprocessed in two other pieces of software, GrafNav and Kinpos (dual frequency), and the results were similar to those from SKi-Pro.

It was then discovered that the 360° prism was probably to blame. 360° prisms have a face error of about 6mm which is constant on each face, but opposite on adjacent faces. It is probable that the total station was measuring to the prism in such a way that it was hitting the corners and swapping between faces as the bridge moved, thus showing an amplitude that was too high.

Results from the first day of the bridge trial, when the circular prism was used, were also processed and these can be seen in Figure 4-18. It can be seen from this Figure that there is a difference in the amplitude of movement calculated by each system here too. However, in this case the GPS shows a much higher displacement. The peaks of movement seen in Figure 4-19 correspond to periods when people on the bridge were jumping up and down 'forcing' the bridge to move at a certain frequency, which caused the large amplitude movement of the bridge. This 'forcing' did not take place on the first day of the trial and as a consequence the bridge movement was much smaller.

However, the amplitude of movement shown by the total station on the first day of the trial was only 0.008m, which intuitively seems too small. It is possible however, that 0.008m was the amplitude of the bridge movement but that this was masked by the noise in the GPS signal. The data from the 19th June (Figure 4-18) does support the theory that the face changing error probably caused the large displacements recorded by the total station on 21st June (Figure 4-19) by the total station.

The results from the metronome trial showed that when the movement was too fast it was not possible for the total station to pick out all the movement effectively. This would also affect the data from the bridge trial since for this small bridge the frequency would have been too quick for the total station to have picked out all the movement. It is likely however, that it would have picked out a span of the movement and so could give a representation of how the bridge moved.

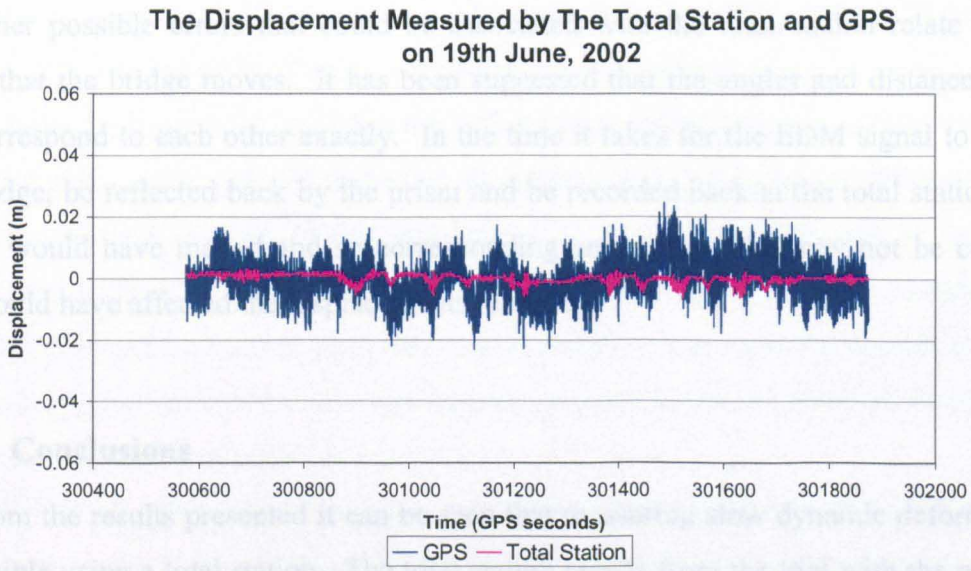

Figure 4-18 The displacement measured by GPS and total station on the first day of the bridge trial (19th June, 2002) when the circular prism was used.

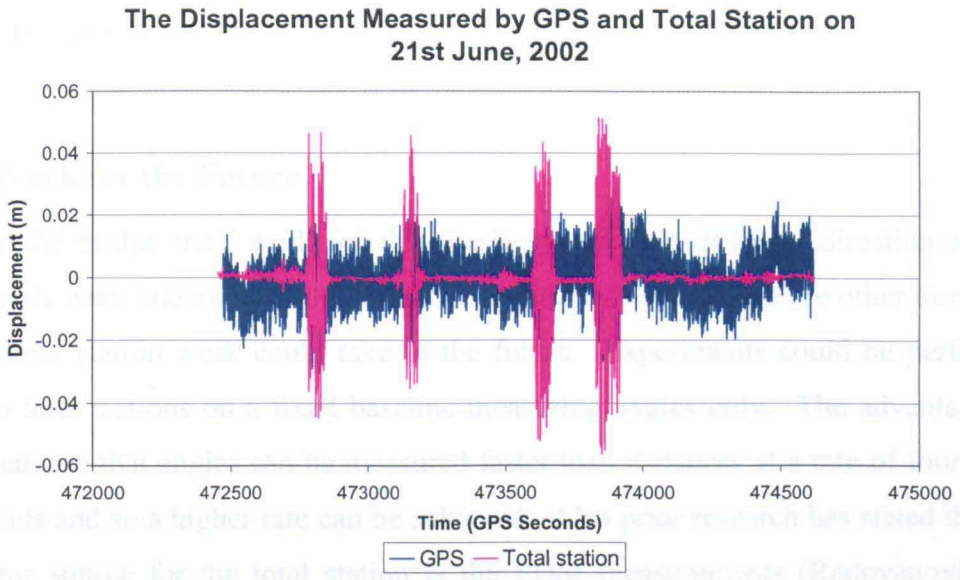

Figure 4-19 The displacement measured by GPS and total station on the third day of the bridge trial (21st June, 2002) when the 360° prism was used.

Other possible errors that could be associated with the total station relate to the speed that the bridge moves. It has been suggested that the angles and distances may not correspond to each other exactly. In the time it takes for the EDM signal to get to the bridge, be reflected back by the prism and be recorded back at the total station, the bridge would have moved and so corresponding angles recorded may not be correct. This could have affected the displacements recorded.

4.5.5. Conclusions

From the results presented it can be seen that measuring slow dynamic deformation is possible using a total station. The total station results from the trial with the moving monument matched well with the results obtained from GPS. However, the total station had difficulties measuring the dynamic movement of fast moving objects like the metronome and the bridge. Due to its slow data rate not all oscillations were recorded for the metronome trial. It can be concluded that for smaller bridges with small amplitudes and high frequency movement, at 1 Hz the total station is simply not fast enough to measure all the movement. For longer bridges that move at slower frequencies the total station could be a possibility for monitoring.

On the third day of the bridge trial the amplitude of the movement measured by the total station was very large. It is thought that this was caused by face changes on the

360° prism. When the circular prism was used no large amplitudes were seen which supports this theory.

4.5.6. Work for the Future

After the bridge trial, work for this thesis moved in a different direction and no further trials were undertaken with the total station. However, there are other directions that the total station work could take in the future. Experiments could be performed with two total stations on a fixed baseline measuring angles only. The advantages of this system are that angles can be measured faster than distances at a rate of four times per seconds and so a higher rate can be achieved. Also prior research has stated that the main error source for the total station is the EDM measurements (Radovanovic and Teskey 2001). This would mean that more accurate measurements could be made at higher data rates. This could also lead to the total station being able to measure all the movement on smaller bridges and would also remove the possible problem of whether the angle and distance measurements correspond to each other.

The main problem with the above method is ensuring that the total stations are both measuring at the same time. Connecting the laptops to an external oscillator or GPS receiver could be a solution to this problem. The uneven sampling rate of the total stations could cause problems for this method. Another problem is the accuracy to which the time can be known. At present it can only be known to the nearest second, which is not good enough for this application. If these issues are resolved interesting results could be achieved with this method.

Tsakiri, et al. (2003) use a total station measuring at a data rate of 8 Hz for their experiments on the Evripos cable-stayed bridge in Greece. At this high data rate much higher frequency movements can be recorded, which would mean that total stations could be used even for monitoring smaller bridges.

5. Software Development

5.1. Introduction

This chapter introduces the GPS processing software Kinpos that has been developed at the IESSG (Pattinson 2000) and further modified by the author. Section 5.2 gives an overview of the structure of the software. Section 5.3 describes the original dual frequency processing software focusing particularly on the cycle slip detection and ambiguity resolution methods employed. Then Section 5.4 explains the modifications to the software by the author which enabled single frequency GPS data to be processed. As part of this, Section 5.4.2 introduces the three different methods of single frequency ambiguity resolution that can be used in different situations, two of which were particularly developed for bridge monitoring applications. Section 5.4.3 discusses the process noise within the Kalman filter. The chapter is summarised in Section 5.5.

5.2. Kinpos

Kinpos was a dual frequency GPS post-processing software developed at the University of Nottingham by Dr Wu Chen and further modified by Dr Michael Pattinson (Pattinson 2000). The author modified the software so that it would process single frequency data and then added further modifications to accelerate the ambiguity search process in the context of bridge monitoring.

The software was originally developed to estimate position and tropospheric delay for a rover receiver relative to reference receiver for which position and tropospheric delay were already known. The author did not look further at the tropospheric delay element of the software.

All software development for this thesis took place on TOSHIBA Satellite Pro 6100 series notebook computer with an Intel Pentium 4 processor and with 256 MB RAM.

Kinpos has seven main stages which are depicted in Figure 5-1. The processing options set by the user are read in from a control file, an example of which can be seen in Appendix A. The data is read in from the reference and rover Rinex files one epoch at a time, at which point the cycle slip detection and repair plus the phase smoothing occurs. The single frequency version of Kinpos can only process with a single reference and single rover station. Then the double difference observables are formed for the pseudorange and carrier phase observations.

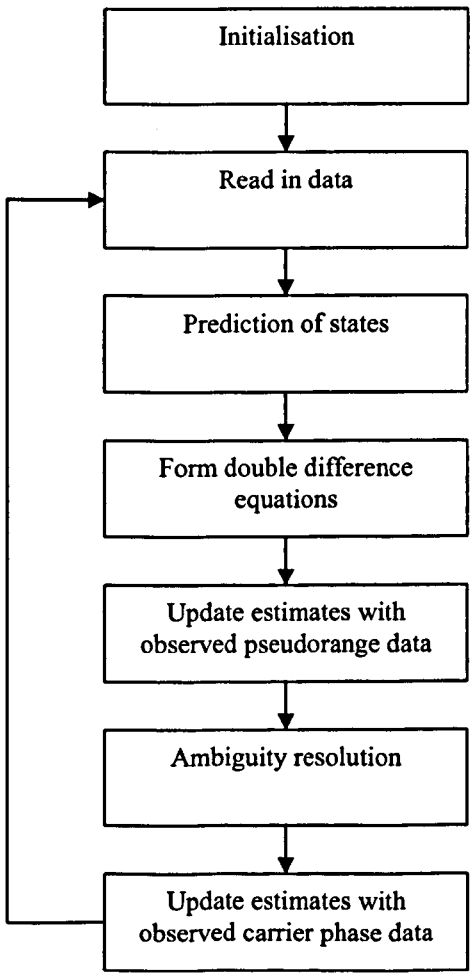

Figure 5-1 Overview of the process in Kinpos (Pattinson 2002)

In the Kalman filter the position, velocity and acceleration at the previous epoch are used to predict the unknown position, velocity and acceleration at the present epoch. The Kalman filter used in Kinpos is described in detail in Pattinson (2002). These

predicted values are first updated by the pseudorange measurements. The success of ambiguity resolution depends on the accuracy of the initial coordinate. Once the position has been updated by the pseudorange it is within a few metres of the true position.

Ambiguity resolution is attempted at this point of the data processing. If the ambiguities are resolved successfully the position, velocity and acceleration are updated with the carrier phase observations. If ambiguity resolution fails only the pseudorange positioning solution is available.

The basic framework of Kinpos has been left the same by the author; however a number of subroutines had to be changed to allow single frequency data to be processed. The main changes have occurred in the cycle slip detection and ambiguity resolution subroutines. An explanation of the original methods used for cycle slip detection and ambiguity resolution is contained in Section 5.3. The modifications to these parts of the software for single frequency data are introduced in Section 5.4.

5.3. Original Kinpos Software for Dual Frequency Data

5.3.1. Cycle Slip Detection and Repair

The cycle slips routine first checks there are no gaps in the data at a particular epoch, by checking the data interval between the current observation and the previous observation, before checking if there are any slips. There are three techniques used in Kinpos to detect cycle slips in dual frequency data. These are the ionospheric residual, the range residual and the four observables equation.

The ionospheric residual used to detect cycle slips in Kinpos is defined by equation (5-1) (Pattinson 2002).

$$\delta\Phi_{L1} = \Phi_{L1} - \frac{f_{L1}}{(f_{L1} - f_{L2})}(\Phi_{L1} - \Phi_{L2}) \qquad \textbf{(5-1)}$$

where,

Φ_{Li} is the carrier phase observation for the frequency *Li* in cycles

f_{Li} is the frequency of the *Li* carrier phase in Hz

Equation (5-1) is the ionospheric residual using the L1 and Lw (wide lane) observations rather than the L1 and L2 observations, since for dual frequency data it is easier to repair a cycle slip if the wide lane is used. From Chapter 2, Section 2.5.1 the wide lane is a linear combination of the L1 and L2 frequencies, creating an observable with a larger wavelength (86.2cm for Lw compared to 19.0cm for L1 and 24.4cm for L2), which aids in resolution of the integer ambiguities (Hofmann-Wellenhof et al. 2001).

Over time $\delta\Phi_{L1}$ will change due to the ionospheric activity but over just a few epochs the change should be very small. A large change in the ionospheric residual signifies the presence of a cycle slip and this is how cycle slips are first flagged in Kinpos.

Once a slip is flagged, an attempt at correction is made. Large slips (greater than 4 cycles) are corrected using the range residual method. Pseudorange observations show the absolute distance from the satellite to the receiver, but they are very noisy. Carrier phase observations are very precise, but do not show the absolute range. So at any epoch the observations from carrier phase and pseudorange cannot be compared. However, the difference in range from one epoch to the next, to the same satellite on the same frequency, should be the same for the pseudorange and carrier phase observations. The pseudorange is not affected by cycle slips, so the change in pseudorange can be compared to the change in carrier phase to detect cycle slips. The range residual calculation is described in equation (5-2) below (Roberts 1997b).

$$RR^{s}{}_{Li} = \frac{(\rho_{Li}{}^{s}(t_k) - \rho_{Li}{}^{s}(t_{k-1}))}{\lambda_{Li}} - (\Phi_{Li}{}^{s}(t_k) - \Phi_{Li}{}^{s}(t_{k-1})) \qquad \textbf{(5-2)}$$

where,

$RR^{s}{}_{Li}$ is the range residual on frequency *Li* to satellite s in cycles

$\rho_{Li}{}^{s}(t_k)$ is the pseudorange observation on frequency *Li* to satellite *s* made at time t_k in metres

$\Phi_{Li}{}^{s}(t_k)$ is the carrier phase observation on frequency *Li* to satellite *s* made at time t_k in cycles

λ_{Li} is the wavelength of frequency *Li* in metres

The reason that the range residual method can only be used for cycle slips of 4 cycles or more is due to the size of the measurement noise on the pseudorange observation.

For any small cycle slips (less than 4 cycles) that have not been corrected by the range residual method, the ionospheric residual method is used. From equation (5-1) it can be seen that there are two unknowns, one for L1 and one for L2. Different combinations of L1 and L2 cycle slips create different values for $\delta\Phi_{L1}$, the ionospheric residual. The ionospheric residual values produced for cycle slips of ±4 L1 or L2 cycles are unique and from well established tables it is easy to identify the slip values for both L1 and L2 (Pattinson 2002). The L1/Lw ionospheric residual is used, rather than the L1/L2, as it is easier to distinguish between ionospheric residual values when the wide lane is used.

Once the slips have been repaired using the range residual and ionospheric residual methods, the four observables equation is used to check that this has been done correctly. The four observables equation directly estimates the wide lane observable using the carrier phase and pseudorange observations on both L1 and L2 frequencies. For the definition of the four observables, please see Pattinson (2002). Any sudden jumps in the four observables value, which should be smooth between epochs, indicate that a cycle slip has occurred. If a slip is identified this method cannot distinguish whether the cycle slip has occurred on L1 or L2 and so it is just used as a check of the other two methods. If no slip is found with the four observables equation it is assumed that the slips have been repaired correctly. If a slip is still found in the data then the range residual and ionospheric residual have not been successful in repairing the slip and so the correction is not applied.

5.3.2. Ambiguity Resolution

Before carrier phase positioning can be carried out the integer ambiguities must be solved. Firstly float values are formed, which are real-valued estimates of the integer ambiguity values. Once the floats are formed a search is performed around these values to fix the ambiguities to integers.

When the carrier phase double difference equation is formed (equation (2–4)), the unknowns can be split into two parts, which are the positioning unknowns and the integer ambiguity term. The positioning unknowns change from epoch to epoch; whereas as long as there are no cycle slips the ambiguity term stays the same from one epoch to the next for each satellite pair.

The Helmert-Wolf method (Cross 1983) divides the unknowns into the two sets, of common parameters at every epoch and local parameters which change between epochs. A set of 'reduced normal equations' is formed, which take into account only the common parameters at each epoch (i.e. the ambiguity values). As the epochs are accumulated the system will be over-determined, as there will be more equations than unknowns. This will continue as long as the ambiguity terms remain the same. If there is a cycle slip or the base satellite changes, the ambiguity term will change and so the accumulation process must begin again.

Solving the Helmert-Wolf reduced normal equations will yield a set of real-value float ambiguities. The equations used to form and solve the Helmert-Wolf reduced normal equations can be found in Cross (1983) and Pattinson (2002). The float values are passed to a LAMBDA (Least squares AMBiguity Decorrelation Adjustment) subroutine. The Fortran 77 code of this subroutine was obtained from Delft University of Technology in the Netherlands. For a full derivation of the LAMBDA method see De Jonge and Tiberius (1996).

The basis of the method is the transformation of the float ambiguities, by the so-called z transformation, to decorrelate them. The search space is transformed from an elongated ellipsoid into a sphere, making the ambiguity search more efficient. The inputs into the LAMBDA subroutine are the float ambiguities and the covariance matrix, which are previously calculated by the Helmert-Wolf method.

A sequential conditional least squares estimation is used to search the ambiguity space for possible combinations. Any possible ambiguity sets and their corresponding squared norms are recorded and once the whole ellipsoid has been examined, the search ends. The possible ambiguities sets are transformed back by the reverse z transformation. There are three possible outcomes to the search. The first is that no possible ambiguity sets are found, which means that the ambiguities cannot be fixed at that epoch. The second possibility is that one ambiguity set is found, so this set is fixed as the integer ambiguity set. The final possibility is that more than one ambiguity set may be found. If this occurs, Kinpos performs a test to see if the best ambiguity set is

significantly better than the next best ambiguity set by calculating the ratio between the squared norms. If this ratio is greater than 3 then the best ambiguity set is significantly better than the next best one and so the ambiguities are fixed. If the ratio is less than three then the ambiguities cannot be fixed.

Once the ambiguities have been fixed they are held fixed for all subsequent epochs unless a cycle slip occurs. If a new satellite enters the solution it is not used in the positioning calculation until its ambiguities are fixed. The double difference residuals (which are defined in Pattinson (2002)) are monitored for jumps which could be caused by undetected cycle slips or steady increases which would mean that the incorrect ambiguities have been fixed. If residuals display either of these two characteristics, the ambiguities are unfixed and only a pseudorange solution is used at that epoch.

The basic ambiguity search used in Kinpos, described above uses an L1 and Lw search rather than an L1 and L2 search. Kinpos takes advantage of the presence of dual frequency data by performing a separate wide lane search before searching for the L1 and Lw ambiguities. As mentioned in Section 5.3.1, the wide lane observable has a longer wavelength than either the L1 or L2, which means there is an increase in the ambiguity spacing leading to quicker and easier resolution of the wide lane ambiguities.

The wide lane search is performed in the same way as the search described above. If the wide lane ambiguities are resolved then they are held fixed for the subsequent L1 and Lw search, which reduces the number of possible ambiguity combinations and makes it easier to resolve the L1 ambiguities.

5.4. Modifications to Kinpos for Single Frequency Data

5.4.1. Cycle Slip Detection and Repair

Section 5.3.1 describes the method of cycle slip detection and repair used in Kinpos before modifications by the author. Similar to the method described there, the single frequency cycle slip detection routine also first identifies gaps in the data by checking the data interval.

Both the ionospheric residual method and the four observables equation use data from both the L1 and L2 frequencies for cycle slip detection and repair, and so cannot be used for single frequency data. The range residual method can be used for data on

only one frequency, but as mentioned previously it can only be used for cycle slips of greater than ±4 cycles. A new method of cycle slip detection needed to be implemented for detecting small cycle slips.

In the context of bridge monitoring and also other dynamic deformation monitoring applications, the receivers are not completely kinematic. The receivers are continually moving, but never by more than a set amount. This is typically in the order of a few centimetres for short bridges and possibly up to a metre for larger suspension bridges. Due to this fact, it can be assumed that any large jumps in the carrier phase from epoch to epoch are likely to be caused by cycle slips and not receiver movement. In a completely kinematic situation these assumptions could not be made and so this method of cycle slip detection could not be used.

In Kinpos a method of single frequency cycle slip detection based on the triple order difference of the carrier phase, $\delta\Phi_{Li}^{s}(t_k)$, was implemented based on equation (5-3) below. This is a well-known algorithm used for GPS processing, but the source of the algorithm is unknown (Unknown source).

$$\begin{aligned}\delta\Phi_{Li}^{s}(t_k) = &[\Phi_{Li}^{s}(t_k)+\Delta\Phi_{Li}^{s}(t_{k-1})]-3[\Phi_{Li}^{s}(t_{k-1})+\Delta\Phi_{Li}^{s}(t_{k-1})] \\ &+3[\Phi_{Li}^{s}(t_{k-2})+\Delta\Phi_{Li}^{s}(t_{k-2})]-[\Phi_{Li}^{s}(t_{k-3})+\Delta\Phi_{Li}^{s}(t_{k-3})]\end{aligned} \qquad \textbf{(5-3)}$$

where,

$\Delta\Phi_{Li}^{s}(t_k)$ is the carrier phase correction for satellite *s* on frequency *Li* at time t_k. The carrier correction is the accumulation of all the slips on frequency *Li* that have occurred since the beginning of the observation session (or since the accumulation has been reset).

If the triple order difference, $\delta\Phi_{Li}^{s}(t_k)$, is larger than a specified threshold *T*, i.e. $\left|\delta\Phi_{Li}^{s}(t_k)\right| > T$, then a cycle slip is detected. For most receivers this threshold is set to 1, so this method will detect cycle slips as small as 1 cycle (for Garmin receivers *T* had to be set to 0.5, this is explained in Chapter 8, Section 8.3). If no cycle slip is detected at time t_k then the current cycle slip correction is set to the previous one, i.e. $\Delta\Phi_{Li}^{s}(t_k) = \Delta\Phi_{Li}^{s}(t_{k-1})$ and no further calculations are made for this satellite at frequency *Li*. If a cycle slip is detected then it is corrected using equation (5-4) below.

$$\Delta\Phi_{Li}^{s}(t_k) = \Delta\Phi_{Li}^{s}(t_{k-1}) + \lfloor \delta\Phi_{Li}^{s}(t_k) \rfloor \quad (5\text{-}4)$$

where $\lfloor\ \rfloor$ denotes rounding the value to the nearest integer. A repair is performed only if $S(t_{k-1}) < \lambda_{Li}/2$, where $S(t_k)$ is the square root of the sample variance at time t_k computed by equation (5-5) below.

$$S(t_k)^2 = 1/n\,\delta\Phi_{Li}^{s}(t_k)^2 + (n-1)/n\; S(t_{k-1})^2 \quad (5\text{-}5)$$

where n is the number of observations. If the condition is true, then a repair is performed. However if it is not true then no repair can be performed; the carrier phase correction $\Delta\Phi_{Li}^{s}(t_k)$ is set to 0, a cycle slip is flagged, the integer ambiguity for that satellite is reset and a further ambiguity search is conducted.

This method requires that four epochs of data for each satellite have accumulated before cycle slip detection can occur (three epochs for the triple-order time difference, equation (5-3), to be formed and one further epoch to compute the variance test in equation (5-5)). For the first three epochs coarse cycle slip detection occurs with the range residual method, which has been defined previously in equation (5-2). It has been mentioned previously that, due to the noise on the pseudorange observable, this method is only accurate enough to detect cycle slips larger than ±4 cycles. Although the range residual method can detect cycle slips, it is not precise enough to effectively correct them. So, during the first three epochs a cycle slip is simply flagged and no attempt at correction is made. At the fourth epoch a cycle slip is detected by equation (5-3), the triple time difference equation, but the slip is simply flagged and not corrected as there is no variance measure to test it against. At the fifth epoch and higher, flagged cycle slips that pass the variance test are also corrected.

5.4.1.1. Testing the New Cycle Slip Detection Routine

To test the new cycle slip detection routine, a simulated Rinex file that contained cycle slips at known epochs, which had been produced by the IESSG simulator (Farah 2003), was processed in Kinpos. Appendix B contains both the log file produced by the IESSG simulator of the cycle slips added to the Rinex file and the slip file produced by

Kinpos which contains information about the cycle slips detected and whether or not they were corrected. From both these files it can be seen that the single frequency cycle slip detection method flagged all of the simulated cycle slips. All but three of the slips were flagged by the triple order time difference method, which meant that exactly the right values of these cycle slips were calculated. Three slips were flagged and calculated using the range residual method; they were 4.1, 4.4 and 1.1 cycles away from their true cycle slip values.

Of the cycle slips that were flagged by the triple order time difference method 23 out of 44 slips were successfully corrected. For a further 20 of these cycle slips the variance was too high for correction to occur and the remaining cycle slip occurred at the satellite's fourth epoch and so no variance test was available to check against.

The Rinex file used for this simulation contained 16 minutes of data at a 1 second data rate and 47 cycle slips with magnitudes of hundreds of cycles, which were either positive or negative. When a cycle slip occurs and is flagged and corrected, the value of this cycle slip is used in the calculation of the variance test for the next epoch for that satellite (equation (5-5)). Therefore the more cycle slips that occur in the data for a particular satellite, the higher the variance test will be and the more likely the data is to fail the variance test. For this simulated data set there are a high number of cycle slips and they all have large values, so it is not surprising that on 20 out of 44 occasions the variance test is failed. For a 'real' data set it is likely that the number of cycle slips will be much lower.

This simulated data set had shown that the cycle slip detection routine worked well for cycle slips with large values of hundreds of cycles. The next test would be to see if it would detect cycle slips at the one cycle level.

A cycle slip simulator was developed by the author in Java to introduce small cycle slips into a Rinex file only on the L1 frequency. The program asks the user how many cycle slips to add to the Rinex file, then the times of the slips, the satellite numbers and the slip values. For ease of programming the cycle slip is only added to the L1 carrier phase at one epoch. This means that Kinpos should detect two cycle slips for every slip added. It should detect the cycle slip added and then at the next epoch the negative of that cycle slip.

Slips were added to the reference Ref2 and rover Bdg2 recorded at the Wilford Bridge trial conducted in June 2002 (Chapter 4, Section 4.2). Appendix C contains the log file produced by the Java simulator showing the slips added to the Rinex files and

also the output file produced by Kinpos showing the slips detected when the Rinex files were processed. It can be seen that all cycle slips were detected and corrected even the slips that were as small as one cycle. This showed that as well as being able to accurately detect and correct cycle slips of hundreds of cycles, the new cycle slip detection routine in Kinpos was capable of detecting and correcting cycle slips as small as one cycle. The cycle slip detection routine was working well and had shown that it could detect and correct cycle slips at the level of precision that was required.

5.4.2. Ambiguity Resolution

The first modification for single frequency ambiguity resolution simply used the same method of accumulating the normal equations by the Helmert-Wolf method to produce float solutions and passing these float values to the LAMBDA subroutine (as described for the dual frequency receivers in Section 5.3.2). This method of ambiguity resolution will be referred to as LAMBDA^{orig} (the original LAMBDA method). The only change made was to allow only L1 data to be used whereas previously both frequencies were needed. For dual frequency receivers LAMBDA^{orig} usually only took one epoch to resolve the integer ambiguities, however for single frequency receivers it normally took anywhere between 10 and 20 minutes for the ambiguities to be resolved (even if the same data set was used). If a cycle slip or loss of lock occurred it would take a further 10 to 20 minutes to re-resolve the ambiguities. For one the Wilford Bridge trials, there were periods of particular interest where there was a lot of movement on the bridge and during some of these times ambiguities were lost for the single frequency receivers. When the ambiguities are not resolved the coordinates of the solution are only accurate at the metre level and so no useful information about the bridge movement can be gained during these ambiguity 'outages'.

Reducing the amount of time it takes to resolve the integer ambiguities in the context of bridge monitoring was therefore a research aim, so that the ambiguity outages are lowered to a minimum amount of time. Two further methods of ambiguity resolution, for single frequency receivers in the context of bridge monitoring, were introduced into Kinpos. The first method, introduced in Section 5.4.2.1, can only be used for receivers on a short bridge with small amplitude movements of a few centimetres. The second method, presented in Section 5.4.2.2, was developed for longer bridges with amplitudes up to several tens of centimetres.

5.4.2.1. Deformation Monitoring Software for Small Bridges

This method was developed for short bridges with small amplitudes, specifically the Wilford Suspension Bridge in Nottingham which moves less than five centimetres at maximum.

Kinpos calculates the double difference between satellite S and T and receivers i and j forming the double difference observation equation at time t_k shown in equation (5-6) below:

$$\Delta\nabla\Phi_{ij}^{ST}(t_k) = \frac{1}{\lambda}\Delta\nabla\rho_{ij}^{ST}(t_k) + \Delta\nabla N_{ij}^{ST} + \Delta\nabla\varepsilon_{ij}^{ST}(t_k) \qquad (5\text{-}6)$$

where,

Φ	is the measured carrier phase observation in cycles
λ	is the wavelength in this case for $L1$ in metres
ρ	is the true range between satellite and receiver in metres
N	is the unknown integer ambiguity in cycles
ε	is the measurement noise, atmospheric influences and multipath in cycles
$\Delta\nabla$	is the double difference operator
ij	is the single difference between receivers i and j
ST	is the single difference between satellites S and T

Since the roving receiver does not move very much during an observation session, an average coordinate can be calculated for this receiver site. For real time applications this average coordinate would have to be established in advance. As the data in this research is post-processed this coordinate was established by processing the whole observation session as static in SKi-Pro. It is known from experiments that the average coordinate needs to be accurate to within about 3cm for this method to work. This average coordinate is used as the 'known' coordinate and is input into Kinpos. It is recognised that the roving receiver will not deviate more than 3-5cm from it.

This method of ambiguity resolution is based on the semi-kinematic initialisation technique where the rover is placed on a known location for a small amount of time so that the ambiguities can be resolved instantly. From equation (5-6), if the coordinates of the rover are known then equation (5-7) can be applied (assuming that the measurement noise is 0 or very close to it) to solve for the integer ambiguities.

$$\Delta\nabla N_{ij}^{ST} = \Delta\nabla\Phi_{ij}^{ST}(t_k) - \frac{1}{\lambda}\Delta\nabla\rho_{ij}^{ST}(t_k) \quad (5\text{-}7)$$

The solution to equation (5-7) is the observed minus computed double differences, which are set to the nearest integers to form the ambiguity values. This method resolves the ambiguities instantly at every epoch and so there are no times at all when there are ambiguity outages. Comparisons of the positioning solutions produced by this method and positions produced by the same data processed as dual frequency in SKi-Pro show that this method resolves the correct integer ambiguities (see Chapter 6, Section 6.3.1).

The assumption of a measurement noise of 0 only holds over short baselines up to a few tens of kilometres. For longer baselines the atmospheric errors will decorrelate and affect the ambiguity values. All baselines in this thesis which use this method are short, with most only being a few tens of metres.

5.4.2.2. LAMBDA Method for Large Bridges

As mentioned previously, the method described in Section 5.4.2.1 can only be used on bridges that move less than about 5cm. A method for longer bridges that moved more than 5cm needed to be developed, specifically for data from the Humber Bridge near Hull which moves up to several tens of centimetres.

The float ambiguities produced by the Helmert-Wolf method in Kinpos were investigated for data from the Wilford Bridge. By comparing these float values to the true integer ambiguities calculated by the method described in Section 5.4.2.1, it was discovered that they were very far away from the 'truth'. Since the float values were so far away from the true ambiguity values, it was taking 10 to 20 minutes for them to converge close to the actual ambiguities. So, a method of producing more precise float values was needed.

The maximum displacement of receivers on the Humber Bridge is likely to be in the order of 50-60cm (even though the bridge is designed to move up to a maximum of 4 metres). So, although the receivers do move more than an L1 wavelength, they do not move very much. So, for the receivers on the Humber Bridge an average coordinate of their positions was also calculated by processing the data as static in SKi-Pro for the whole observation session. Using this coordinate and equation (5-7), precise float values were calculated, which were then passed to the LAMBDA subroutine

(LAMBDA is introduced in Section 5.3.2). Having accurate float values meant that the time it took to converge to the actual ambiguity values was greatly decreased. This new method of accelerating the ambiguity search for large bridges will be referred to as $LAMBDA^{def}$.

As well as the accurate float values, a covariance matrix for the float values was also passed to the LAMBDA subroutine. Kinpos and the LAMBDA subroutine uses double difference observations. It is known that double difference observations are correlated due to the measurements being formed using the same GPS observations. The single differences are assumed to be uncorrelated as each range is measured independently and so the matrix of errors for the single differences would be diagonal with the diagonal elements formed from the sum of the variances from each range (Hide 2003). From Hide (2003), if the measurement errors for each range are considered equal, the double difference covariance matrix is simplified to one which has 4's on the diagonal and 2's off the diagonal. This is because each double difference measurement has two ranges in common with each other measurement. The diagonal elements have four measurements in common with themselves. So, a covariance matrix of 4's and 2's was formed and passed with the accurate float values to the LAMBDA subroutine. Normally the covariance matrix takes into account the geometry of the satellites in the solution through the least squares estimation. The covariance matrix described above does not take into account satellite geometry.

For data from the Humber Bridge on March 1st and March 4th (see Chapter 7) processed by the method $LAMBDA^{def}$, the average amount of time it took to resolve the integer ambiguities, either at the beginning of the session or after a cycle slip, was 8.4 seconds. The minimum amount of time was 0 seconds, or instantaneous resolution, and the maximum amount of time was 41.7 seconds. For the $LAMBDA^{orig}$ method of resolving ambiguities the average time to resolution was 7 minutes 24 seconds. The minimum amount of time was 2 seconds (which only occurred when the ambiguities were being resolved for a second time in any session) and the maximum amount of time was 28 minutes 5 seconds (some of the sites had no ambiguity resolution at all when using $LAMBDA^{orig}$). This shows that introducing more accurate float values before a LAMBDA search greatly reduces the amount of time that ambiguity resolution takes.

For the results shown in this thesis the data is post-processed and so the average coordinates are calculated by processing the whole session as static. For real time

applications this average coordinate would have to be established in advance. This is further discussed in Chapter 7.

Comparisons between the positions produced by this method and dual frequency data processed in SKi-Pro also show that this method produces the correct results (see Chapter 7, Sections 7.3.1 and 7.5.2).

5.4.2.3. Testing the New Ambiguity Resolution Routines

To initially test and compare the new ambiguity resolution routines, files from the Wilford Bridge trial conducted in June 2002 (Chapter 4, Section 4.2) were processed in Kinpos by each of the three methods. Ref2 was used as the reference receiver and Bdg1 was used as the rover. With LAMBDA^{orig} method it took 10 minutes and 45 seconds to resolve the integer ambiguities. With the ambiguity resolution method developed for small bridges, ambiguities were resolved instantly and also there was instantaneous resolution with LAMBDA^{def} method for longer bridges.

Further testing of Kinpos software was conducted and the results from processing can be seen in Chapters 6 and 7 of this thesis.

5.4.3. Process Noise within the Kalman Filter

The positions, velocity and accelerations within Kinpos are estimated in a Kalman Filter. Since Kalman filtering is not the subject of this thesis a detailed explanation of the process will not be included here. The interested reader is referred to Pattinson (2002) or Hide (2003) for a detailed explanation of how the Kalman filter in Kinpos operates.

Kalman filtering was developed by Kalman in 1960 and a way of finding the optimum estimates of quantities based on noisy observations. It uses a model to predict the unknown values from previous observations combined with the actual measurements at that epoch. A weight is given to the observations and the predicted model so that they are combined in the best way. If a high weight is given to the observations they will affect the final position produced by Kinpos to a far greater extent. However, if a higher weight is given to the model then the final positions will be much closer to those predicted by the model.

The model used in Kinpos for position updates is a constant acceleration model. This models the acceleration as a random walk and then calculates the predicted

velocity from the predicted acceleration and then the predicted position from the predicted velocity.

When Kinpos was first modified by the author, a low process noise was used, which meant that a high weight was given to the model and a lower weight to the observations. In many circumstances this would be ideal as it reduces the noise of the observations and produces more precise GPS solutions. However, smoothing of the output occurs, which means that the positioning solutions have a lower amplitude and the solution is less quick to respond to any movements in the observations. For bridge monitoring applications this is not ideal. When the original positions produced by Kinpos were compared to those produced by SKi-Pro, the Kinpos values showed a much lower amplitude and much smoother results. However, this smoothing was causing information about the bridge amplitude to be lost.

A bridge is continually moving and the size of the amplitude of movement is an important characteristic to measure. If the GPS data is smoothed too heavily in the Kalman filter, the amplitude of movement output by the processing software is lower than the true amplitude.

Different values of the process noise were used within Kinpos and the resulting amplitudes were compared to the output from SKi-Pro. By trial and error a suitable value of the process noise was decided upon. This empirical high value process noise was chosen so that most of the weight was put on the observations and a very small weighting on the model prediction. This does mean that the noise contained in the GPS solutions produced is higher when compared to some processing software (see Chapter 6), but it also means that true bridge movement is not smoothed out of the solution.

5.5. Conclusions

This chapter introduces the software Kinpos which has been developed at the University of Nottingham and further modified by the author to enable processing of single frequency data. An overview of the software is given before an introduction to the dual frequency methods of cycle slip detection and ambiguity resolution employed in Kinpos.

The modifications made by the author to enable single frequency data to be processed are introduced and discussed. The method of cycle slip detection which uses the triple order difference of the carrier phase is particularly focused on. It is shown

that, after accumulating data for four epochs, this method is accurate enough to detect cycle slips as small as one cycle.

Three different methods of single frequency ambiguity resolution were introduced into Kinpos. The first, LAMBDA^{orig}, simply uses the Helmert-Wolf method to accumulate the normal equations to produce float solutions. These float values are then passed to the LAMBDA subroutine to find the true ambiguity values. This method takes can take up to 30 minutes to resolve the integer ambiguities and in some instances there can be no ambiguity resolution at all (see Chapter 7). The second method of ambiguity resolution can only be used on small bridges with amplitudes of less than about five centimetres. It uses an average coordinate of the rover location to solve for the ambiguities instantly at every epoch. This method is based on the semi-kinematic initialisation technique and means that there are no times when ambiguities are not resolved. The third method, LAMBDA^{def}, is used on larger bridges where the movements are up to several tens of centimetres. The average coordinate is calculated in the same way as the second method and used to calculate precise float values, which are then passed to the LAMBDA subroutine. Since the floats are so precise, LAMBDA is much quicker at resolving the integer ambiguity values.

6. Short Bridge Trial 2 – Wilford Bridge

6.1. Introduction

The first Wilford Bridge trial was described and analysed in Chapter 4. This current chapter introduces the results from the second Wilford Bridge trial conducted in May 2003. Section 6.2 outlines the set up of the trial, explaining the location of the GPS receivers and accelerometers along the length of the bridge. The results are analysed in Section 6.3. The results are split into four main sections which are Kinpos compared to SKi-Pro (Section 6.3.1), Kinpos single frequency processing software compared to Kinpos dual frequency processing software (Section 6.3.2), comparison of two days time series (Section 6.3.3) and bridge component correlations (Section 6.3.4). A further bridge trial was conducted with receivers just on the point Bg06 and a reference point. This trial and the results from it are introduced in Section 6.4. Vibration frequency analysis of the bridge trial results from the GPS and accelerometers are examined and compared in Section 6.5. Finally the chapter is concluded in Section 6.6.

6.2. Wilford Bridge Trial 2 – May 2003

A second bridge trial was conducted on the Wilford Suspension Footbridge over the River Trent in Nottingham on 13th, 14th and 15th May 2003. Twelve Leica System 500 GPS receivers, a mixture of single and dual frequency, were secured to the handrails along the length of the bridge recording data at a 10 Hz data rate. The approximate layout of the receivers along the bridge can be seen in Figure 6-1, while the exact locations are described in Table 6-1, along with the receiver and antenna types used. It should be noted here that the location of the receivers along the length of the bridge was decided by the project partner, Cranfield University, based on algorithms for optimal

receiver location for structural vibration frequency and mode identification (Meng et al. 2003). Considerations were not made about the best receiver locations for multipath reduction or line of sight to satellites, which did affect the results from some of the receivers (see Section 6.3.3).

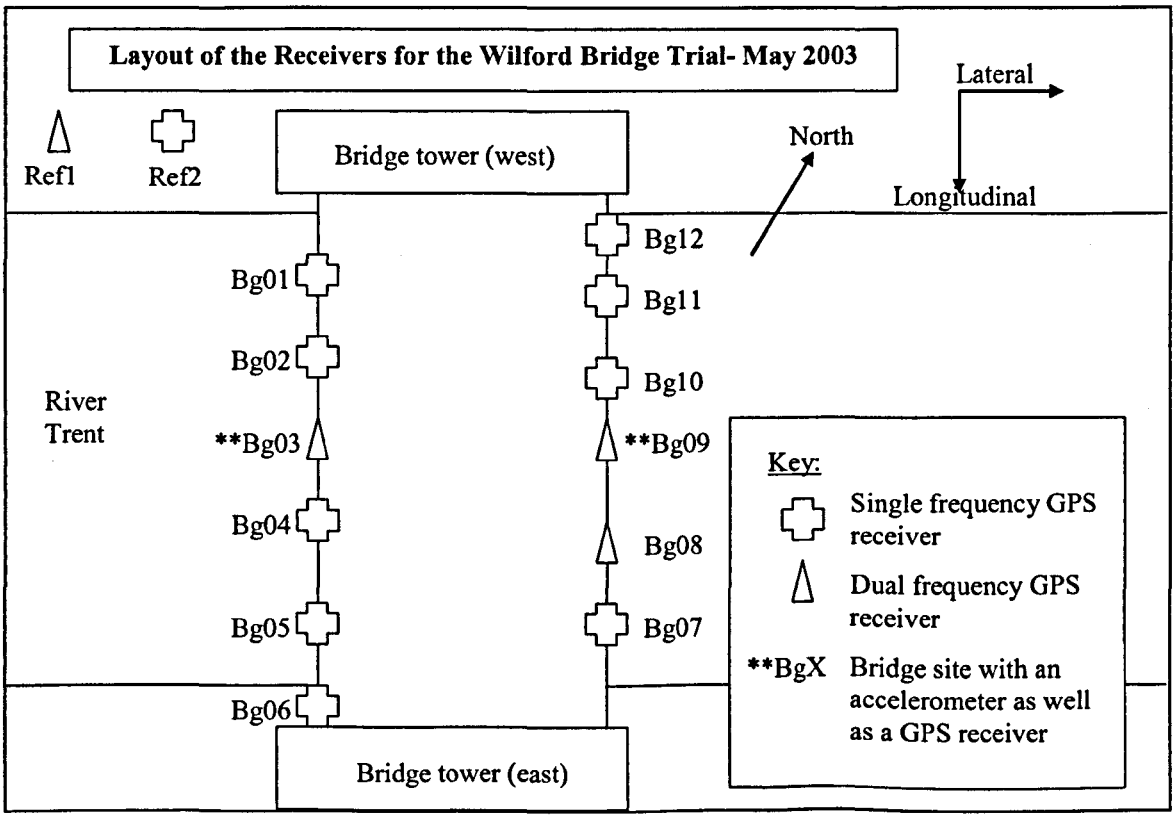

Figure 6-1 The layout of the receivers on the Wilford Bridge during the trial conducted in May 2003 (not to scale).

Bridge Site	Lateral	Longitudinal	Receiver Type	Antenna Type	Accelerometer
bg01	0	16.303	Single	AT503	
bg02	0	25.165	Single	AT503	
bg03	0	34.500	Dual	AT504	Accelerometer
bg04	0	41.671	Single	AT501	
bg05	0	50.871	Single	AT503	
bg06	0	59.935	Single	AT501	
bg07	3.8	52.765	Single	AT501	
bg08	3.8	43.768	Dual	AT504	
bg09	3.8	34.365	Dual	AT504	Accelerometer
bg10	3.8	27.329	Single	AT501	
bg11	3.8	18.129	Single	AT503	
bg12	3.8	8.929	Single	AT503	

Table 6-1 The location of the GPS receivers and accelerometers along the length of the Wilford Bridge. Lateral refers to the side of the bridge that the receivers are attached to and longitudinal is how far along the bridge. Point 0, 0, 0 is the northern corner of the bridge which is closest to the reference receivers (see Figure 6-1).

Two reference receivers were located on the riverside footpath next to the bridge, about 50 metres from the rover locations. Two triaxial accelerometers were located at the mid span sites (Bg03 and Bg09) in a specially designed cage that housed the accelerometers and the GPS antenna, so that they would sense the movement at the same time. At various periods on the three days, volunteers from the IESSG at The University of Nottingham jumped and ran across the bridge to force movement and vibration.

During the bridge trial there were periods that were of particular interest due to the amount of movement on the bridge. On the third day of the trial (May 15th) staff and students from the IESSG, were joined by workers from a local Nottingham City Council office on the bridge for a period of about ten minutes. The total combined weight of these thirty people was approximately 2,353 Kg. At two specific times all the people jumped up and down in unison to force vibration from the bridge. Following this the fourteen people from the council left, leaving sixteen people from the IESSG weighing 1,253 Kg. These people ran across the bridge and also jumped up and down on a further two occasions. Since this period was likely to exhibit the largest movements on the bridge, it was decided that processing and analysis of the bridge data should concentrate on the thirty minute interval surrounding these events.

6.3. Results

The procedure for post-processing the data was as follows:

1. Compute a static coordinate in SKi-Pro by processing the whole session of data at that site as static.
2. Input this coordinate into the control file of Kinpos (see Appendix A for an example of a control file used in Kinpos).
3. Process the data in kinematic mode as single frequency in Kinpos.
4. Transform the WGS84 x, y and z coordinates into easting, northing and height in OSGB36 with Grid InQuest. Grid InQuest is a piece of software which is available to download from the Ordnance Survey.
5. Convert the east and north coordinates in OSGB36 into bridge coordinates along the lateral and longitudinal axes of the bridge. The axis of the bridge is approximately 102° from the north. The transformation matrix seen in equation (6-1) is used for the OSGB36 to bridge coordinates transformation,

where α is the angle of the bridge axis. More information about bridge coordinate systems and transformations can be found in Meng (2002), including an explanation of equation (6-1).

$$\begin{bmatrix} Lateral \\ Longitudinal \\ Vertical \end{bmatrix} = \begin{bmatrix} \cos\alpha & \sin\alpha & 0 \\ -\sin\alpha & \cos\alpha & 0 \\ 0 & 0 & 1 \end{bmatrix} \begin{bmatrix} north \\ east \\ vertical \end{bmatrix} \quad (6\text{-}1)$$

Data from the third day of the bridge trial (May 15th) was processed from 11.45 (387900) to 12.15 (389700) GPS time and on May 14th from 11.49 (301740) to 12.19 (303540) for the purpose of adaptive filtering (see Chapter 4, Section 4.3.2.1 and also Section 6.3.3 of this Chapter). There were problems recording data at bridge sites Bg01 on all of the days and at Bg10 on May 15th, so results from these two locations will not be included. All other rover receivers recorded the data throughout all the sessions.

6.3.1. Kinpos Compared to SKi-Pro

Data from all the dual frequency rover receivers, which were located at positions Bg03, Bg08 and Bg09, were processed as dual frequency in SKi-Pro and as single frequency in Kinpos using the dual frequency receiver Ref1 as the reference. The purpose of this was to compare the positioning solutions output by both processing software. It is worth pointing out that SKi-Pro is post-processing software and so takes advantage of repeated search processes for more reliable ambiguity resolution (Kotthoff et al. 2004). The scripts used in Kinpos could all work in real time. No backwards processing or repeated searches takes place. So, it is expected that for the dual frequency data SKi-Pro will produce better results.

The vertical positioning results produced by Kinpos and SKi-Pro for Bg03, Bg08 and Bg09 can be seen in Figure 6-2 to Figure 6-4 below for 15th May. It can be seen from these graphs that the multipath patterns evident in the times series are similar when processed in either software. However, Table 6-2 reveals that even though the multipath patterns are similar there are differences in the precision of the results produced by each processing software. Table 6-2 displays the standard deviation of the displacement results for the three coordinate directions of lateral (across the bridge), longitudinal (along the length of the bridge) and vertical. It can be seen from this Table

that in each of the three components, and for all three bridge sites, the standard deviation is lower when processed in SKi-Pro than in Kinpos. The largest difference between the SKi-Pro and Kinpos results can be seen in the vertical direction and this difference is around 1.8-1.9mm.

There are several possible reasons for the difference in results produced by Kinpos and SKi-Pro. Chapter 5, Section 5.4.3 explains the processing noise value chosen for Kinpos, which places a higher emphasis on the observations rather than on the model. This results in noisier solutions since there is less smoothing, but also means that no important information about the bridge movement is smoothed away. Information about the models used in SKi-Pro for process noise is not readily available. It is possible that the data produced by SKi-Pro is more heavily smoothed than the output from Kinpos, which will produce a result with a lower standard deviation, but information about the bridge movement could be lost.

It is mentioned above that SKi-Pro takes advantage of forward and backward processing to produce its results. This will generally tend to result in a more precise solution, since the results from the forward and backward runs will be averaged. Any cycle slips or loss of ambiguity in the forward run may not occur in the backward run. So the smaller standard deviations produced by SKi-Pro could be due to this extra processing run. All the subroutines in Kinpos could run in real time and so if a real time bridge monitoring system is required then a slightly modified Kinpos could be used.

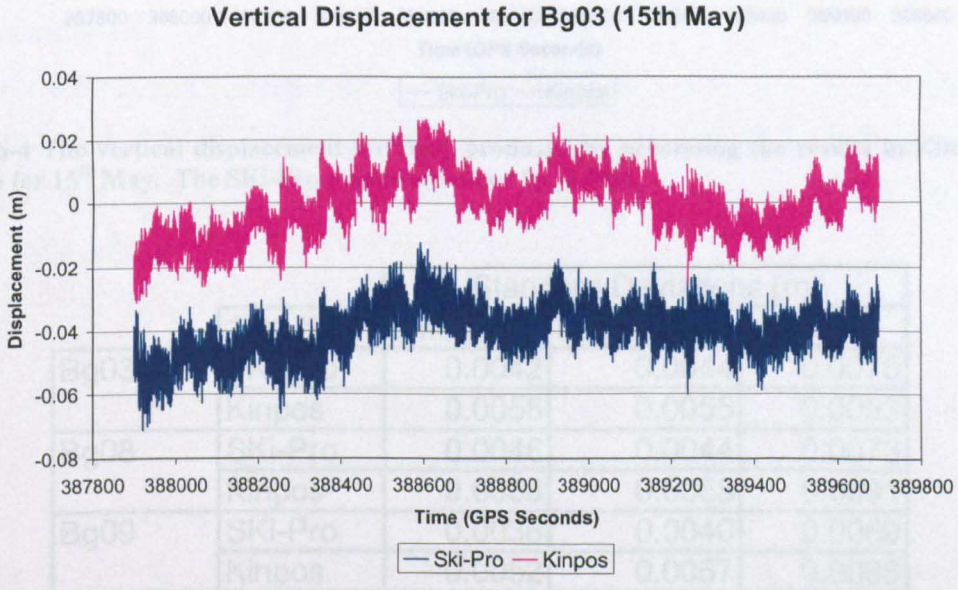

Figure 6-2 The vertical displacement for Bg03 produced by processing the results in Kinpos and SKi-Pro for 15th May. The SKi-Pro results are offset by -0.04m.

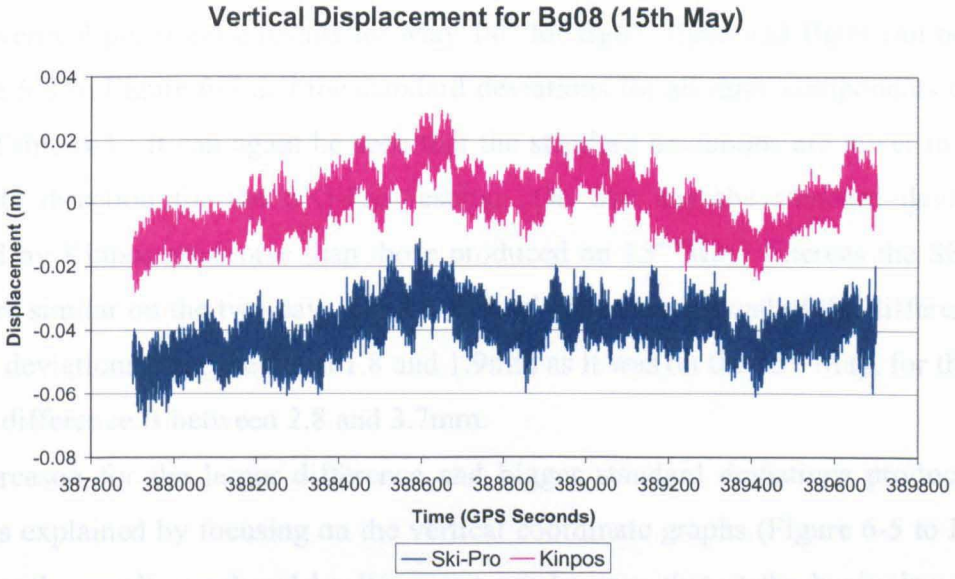

Figure 6-3 The vertical displacement for Bg08 produced by processing the results in Kinpos and SKi-Pro for 15th May. The SKi-Pro results are offset by -0.04m.

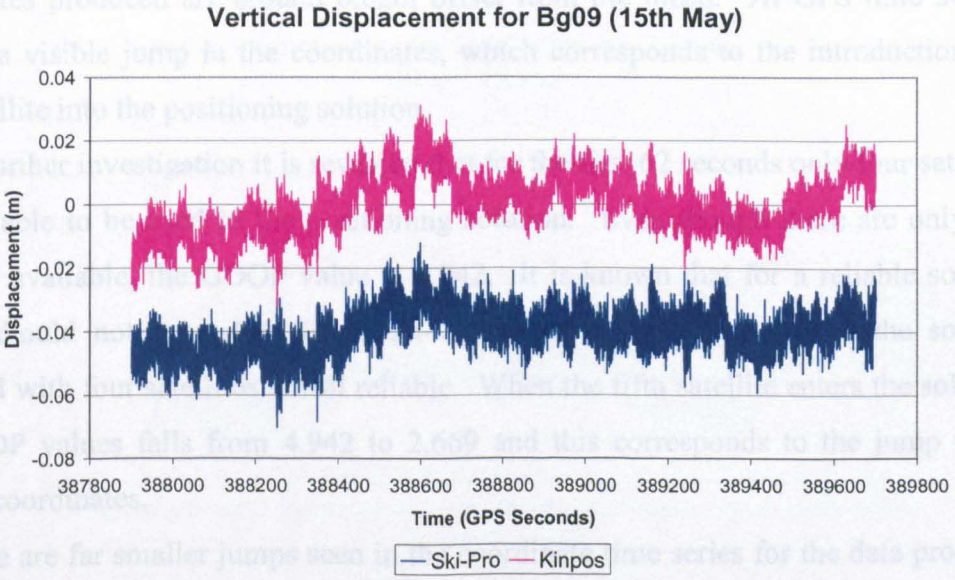

Figure 6-4 The vertical displacement for Bg09 produced by processing the results in Kinpos and SKi-Pro for 15th May. The SKi-Pro results are offset by -0.04m.

		Standard Deviations (m)		
	15th May	Lateral	Longitudinal	Vertical
Bg03	SKi-Pro	0.0042	0.0044	0.0075
	Kinpos	0.0055	0.0055	0.0093
Bg08	SKi-Pro	0.0046	0.0044	0.0073
	Kinpos	0.0058	0.0058	0.0091
Bg09	SKi-Pro	0.0038	0.0040	0.0069
	Kinpos	0.0052	0.0057	0.0088

Table 6-2 The standard deviations of the lateral, longitudinal and vertical components in a bridge coordinate system for Bg03, Bg08 and Bg09 for the results processed in Kinpos and SKi-Pro for 15th May.

The vertical positioning results for May 14th for Bg03, Bg08 and Bg09 can be seen in Figure 6-5 to Figure 6-7 and the standard deviations for all three components can be seen in Table 6-3. It can again be seen that the standard deviations are lower in every coordinate direction for the SKi-Pro results. On this day the standard deviations produced by Kinpos are worse than those produced on 15th May, whereas the SKi-Pro results are similar on the two days. In the vertical direction, instead of the difference in standard deviations being between 1.8 and 1.9mm as it was on the 15th May, for the 14th May the difference is between 2.8 and 3.7mm.

The reason for the larger difference and bigger standard deviations produced by Kinpos is explained by focusing on the vertical coordinate graphs (Figure 6-5 to Figure 6-7). For the results produced by Kinpos it can be seen that at the beginning of the observation session for each bridge site, there is a period of 62 seconds when the coordinates produced are around 0.02m offset from the mean. At GPS time 301802 there is a visible jump in the coordinates, which corresponds to the introduction of a new satellite into the positioning solution.

By further investigation it is revealed that for the first 62 seconds only four satellites are available to be used in the positioning solution. Even though there are only four satellites available, the GDOP value is 4.942. It is known that for a reliable solution GDOP should not exceed 6 (Hofmann-Wellenhof et al. 2001) and so the solution produced with four satellites is still reliable. When the fifth satellite enters the solution, the GDOP values falls from 4.942 to 2.669 and this corresponds to the jump in the vertical coordinates.

There are far smaller jumps seen in the coordinate time series for the data produced by SKi-Pro and this is again because of the forward and backwards processing algorithms. SKi-Pro is able to cope much better in this situation where only four satellites are available.

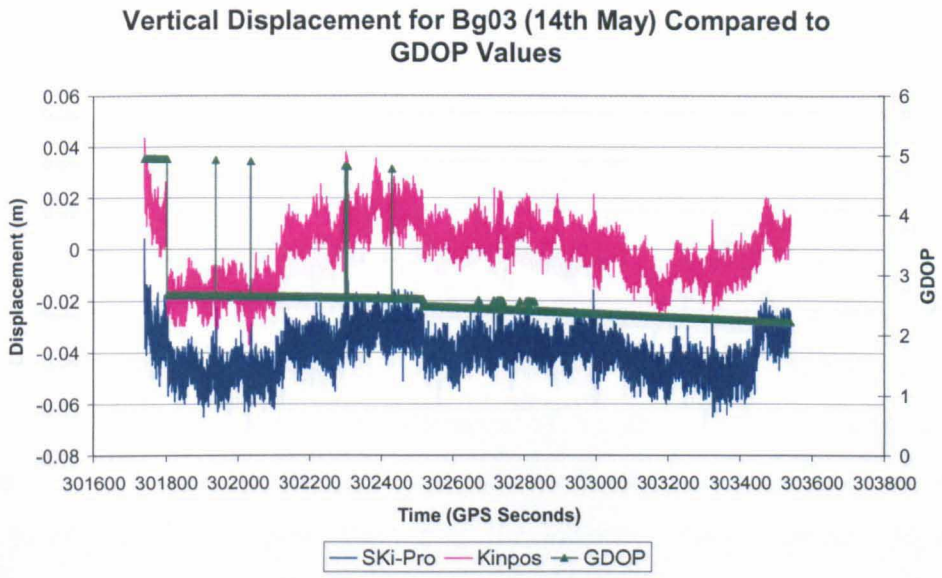

Figure 6-5 The vertical displacement for Bg03 produced by processing the results in Kinpos and SKi-Pro for 14th May. The SKi-Pro results are offset by -0.04m. GDOP values during the processing run are also shown in the graph.

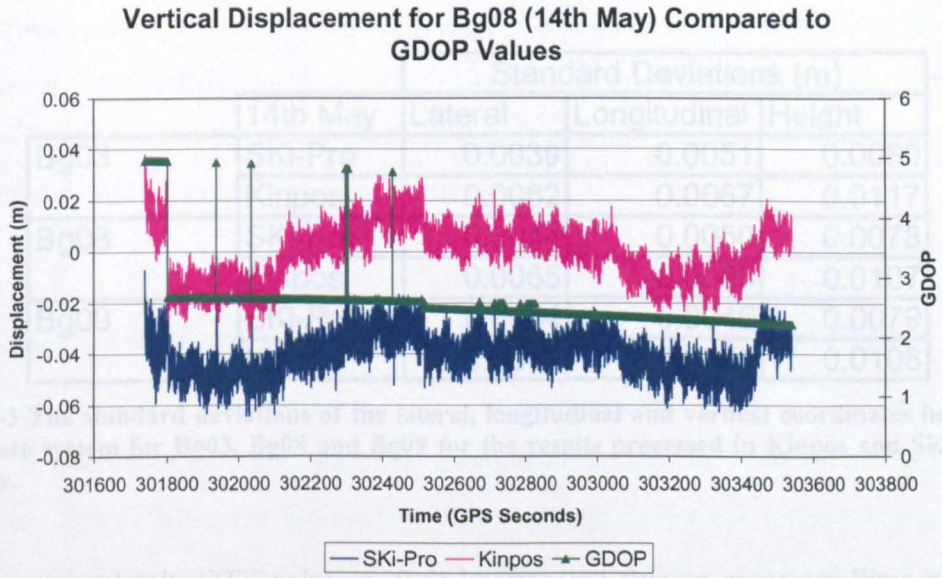

Figure 6-6 The vertical displacement for Bg08 produced by processing the results in Kinpos and SKi-Pro for 14th May. The SKi-Pro results are offset by -0.04m. GDOP values during the processing run are also shown in the graph.

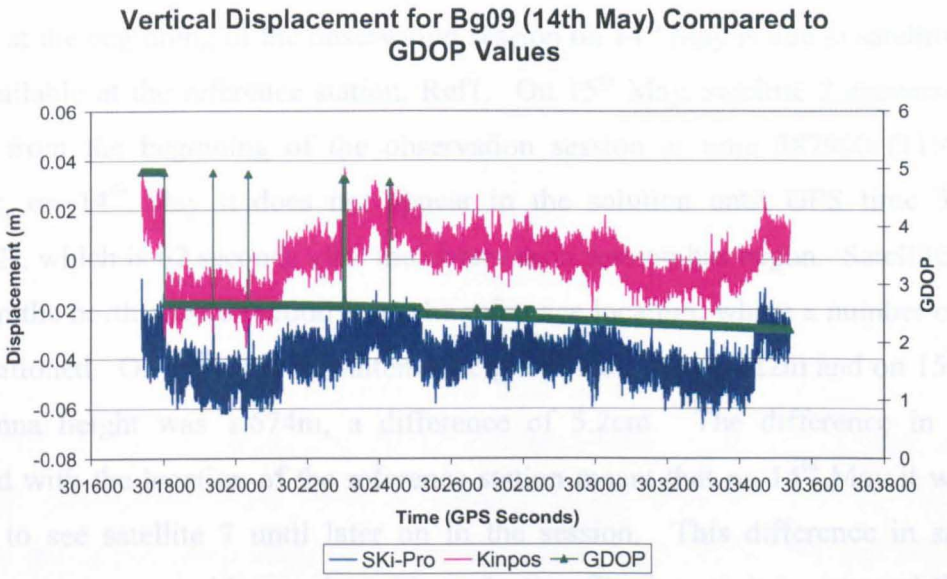

Figure 6-7 The vertical displacement for Bg09 produced by processing the results in Kinpos and SKi-Pro for 14th May. The SKi-Pro results are offset by -0.04m. GDOP values during the processing run are also shown in the graph.

		Standard Deviations (m)		
	14th May	Lateral	Longitudinal	Height
Bg03	SKi-Pro	0.0039	0.0051	0.0080
	Kinpos	0.0062	0.0067	0.0117
Bg08	SKi-Pro	0.0044	0.0050	0.0078
	Kinpos	0.0065	0.0065	0.0107
Bg09	SKi-Pro	0.0044	0.0046	0.0079
	Kinpos	0.0062	0.0065	0.0108

Table 6-3 The standard deviations of the lateral, longitudinal and vertical coordinates in a bridge coordinate system for Bg03, Bg08 and Bg09 for the results processed in Kinpos and SKi-Pro for 14th May.

For a completely OTF solution, it is known that five or more satellites would be needed (Roberts 1997b), and so in this situation the old version of Kinpos would not have been able to produce a positioning solution at all. The new single frequency version is still able to resolve the integer ambiguities even in this difficult situation with only four satellites.

There are four jumps in the GDOP during the observation session, where the number of satellites falls briefly to four, due to the loss of satellite 7. These satellite outages cause temporary jumps in the time series produced by both SKi-Pro and Kinpos.

On closer inspection of the Rinex files, it is evident that the reason there is only four satellites at the beginning of the observation session on 14th May is due to satellite 7 not being available at the reference station, Ref1. On 15th May, satellite 7 appears in the solution from the beginning of the observation session at time 387900 (11:45:00). However, on 14th May it does not appear in the solution until GPS time 301802 (11:50:02), which is 62 seconds after the observation session has begun. Satellite 7 was located in the north-west direction from the reference location, where a number of trees were positioned. On 14th May the antenna height of Ref1 was 1.622m and on 15th May the antenna height was 1.674m, a difference of 5.2cm. The difference in height combined with the location of the reference station meant that on 14th May it was not possible to see satellite 7 until later on in the session. This difference in satellite reception may cause problems when using adaptive filtering, as it is assumed that the same satellites are seen on both days.

As the reference receivers and tripods had to be taken down and set up again between subsequent days of the trial, differences in antenna height are unavoidable. For a permanent monitoring system, the reference receivers and rovers would be continuously located on the same positions and so the problems with satellite reception experienced in this trial would not be encountered.

6.3.2. Single Frequency Kinpos Compared to Dual Frequency Kinpos

Since SKi-Pro was specifically post-processing software and Kinpos could work in real time, it was decided to compare the results from Kinpos to software that could also work in real time. While the author had been developing Kinpos for processing single frequency receivers, in parallel the dual frequency version of Kinpos was being developed and extended further by Dr Chris Hide (Institute of Engineering Surveying and Space Geodesy 2004). The dual frequency version has been extended to also process inertial navigation data and the new name for the software is Kinpos^{i}. To avoid confusion during the following chapter the dual frequency version of the software will be called Kinpos^{i}(df) and the single frequency version of the software will be referred to as Kinpos(sf). This is the only chapter in which Kinpos^{i}(df) is used, so whenever Kinpos is referred to in the rest of the thesis it is the single frequency version that it referring to.

Kinpos^{i}(df) does a complete OTF ambiguity search either with L1 and the wide lane or with L1 and L2, taking full advantage of the dual frequency observations. Bg03, Bg08 and Bg09 were processed in Kinpos^{i}(df). This software will be provide a better comparison to Kinpos(sf) due to the real-time nature of both software and the post-processing nature of SKi-Pro.

The vertical coordinate displacements are compared for Kinpos(sf) and Kinpos^{i}(df) for Bg03 in Figure 6-8 and for Bg08 in Figure 6-9 for 15th May (Bg09 will be discussed separately below). When comparing the time series produced by Kinpos(sf) and Kinpos^{i}(df) the general shapes of the time series appear to be very similar, showing multipath patterns which are alike. However the time series produced by Kinpos^{i}(df) has two major problems areas which are circled in both Figure 6-8 and Figure 6-9. During the first section of the observation, there is a period where there is a jump in the coordinates which produces an offset value for about 225 seconds (3minutes, 45 seconds). Near to the end of the observation session there is a period where there are three small jumps in the coordinate time series. All these jumps are probably caused by erroneous ambiguity fixing by Kinpos^{i}(df). Kinpos(sf) does not suffer from this problem, due to the robust ambiguity routines in the context of bridge monitoring.

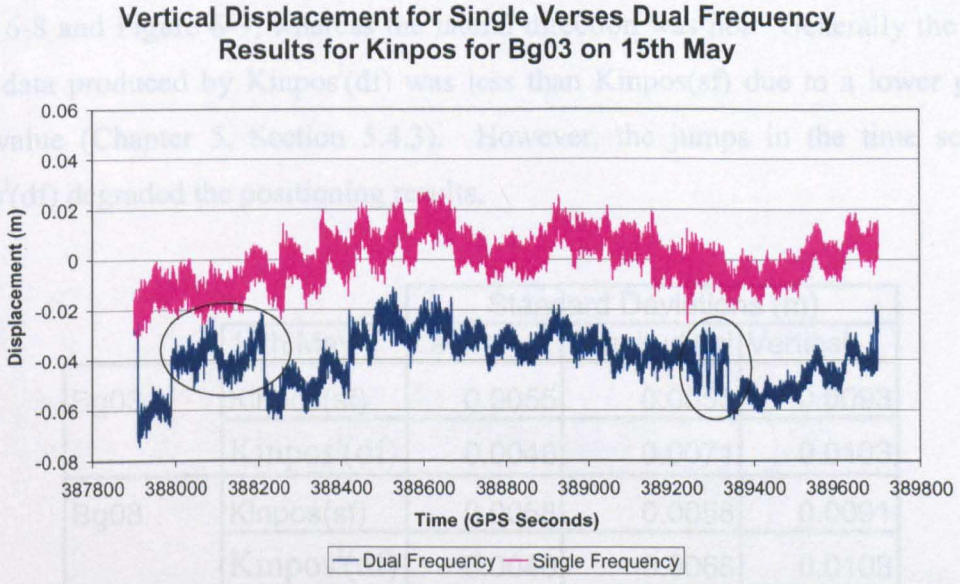

Figure 6-8 The vertical displacement for Bg03 produced by processing the results in Kinpos^{i}(df) and Kinpos(sf) for 15th May. The results from Kinpos^{i}(df) are offset by -0.04m.

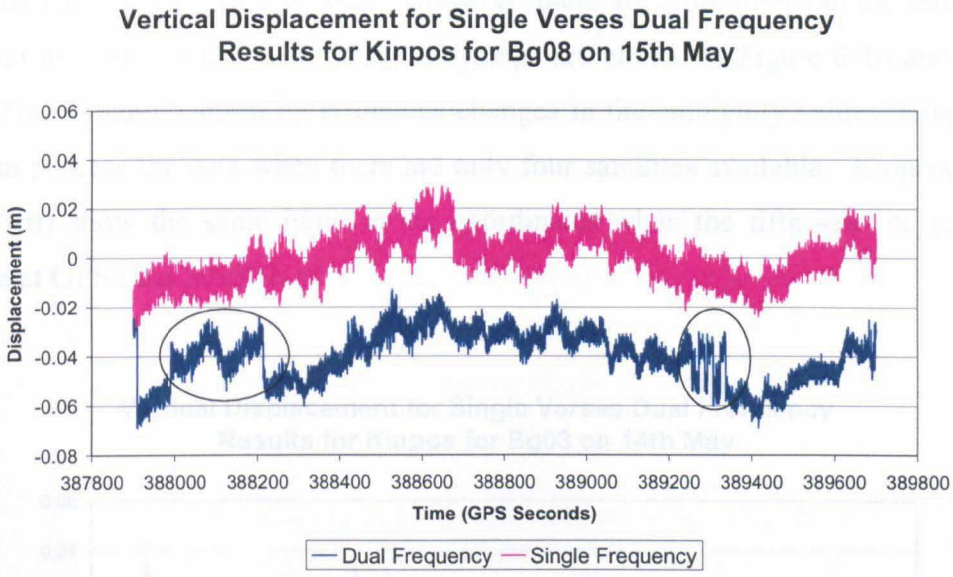

Figure 6-9 The vertical displacement for Bg08 produced by processing the results in Kinpos^{i}(df) and Kinpos(sf) for 15th May. The results from Kinpos^{i}(df) are offset by -0.04m.

Table 6-4 shows the standard deviations of the lateral, longitudinal and height components for Bg03 and Bg08 processed in Kinpos(sf) and Kinpos^{i}(df). In the lateral direction (across the bridge), the standard deviation is lower for Kinpos^{i}(df), but in the other two directions the standard deviation is lower for Kinpos(sf). The time series in the vertical and longitudinal directions were affected by the coordinate jumps seen in Figure 6-8 and Figure 6-9, whereas the lateral direction was not. Generally the spread of the data produced by Kinpos^{i}(df) was less than Kinpos(sf) due to a lower process noise value (Chapter 5, Section 5.4.3). However, the jumps in the time series of Kinpos^{i}(df) degraded the positioning results.

		Standard Deviations (m)		
	15th May	Lateral	Longitudinal	Vertical
Bg03	Kinpos(sf)	0.0055	0.0055	0.0093
	Kinpos^{i}(df)	0.0046	0.0071	0.0103
Bg08	Kinpos(sf)	0.0058	0.0058	0.0091
	Kinpos^{i}(df)	0.0048	0.0068	0.0103

Table 6-4 The standard deviations of the lateral, longitudinal and vertical coordinates in a bridge coordinate system for Bg03 and Bg08 for the results processed in Kinpos(sf) and Kinpos^{i}(df) for 15th May.

The results from 14th May processed in Kinpos(sf) and Kinpos^{i}(df) are shown in Figure 6-10 for Bg03 and in Figure 6-11 for Bg08. Similar results are seen in these

graphs as those shown for 15th May. However, there are more jumps in the time series produced by Kinpos^{i}(df). The main four jumps are circled in Figure 6-10 and Figure 6-11. This is again caused by erroneous changes in the ambiguity values. Kinpos^{i}(df) will also process the data when there are only four satellites available. Kinpos(sf) and Kinpos^{i}(df) show the same jump in the coordinates when the fifth satellite joins the solution at GPS time 301802.

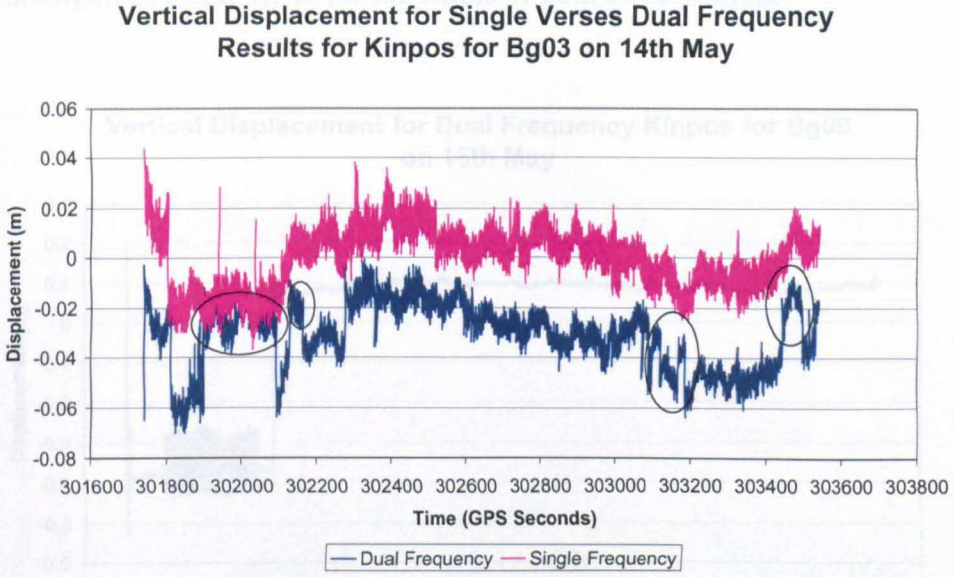

Figure 6-10 The vertical displacement for Bg03 produced by processing the results in Kinpos(sf) and Kinpos^{i}(df) for 14th May. The results from Kinpos^{i}(df) are offset by -0.04m.

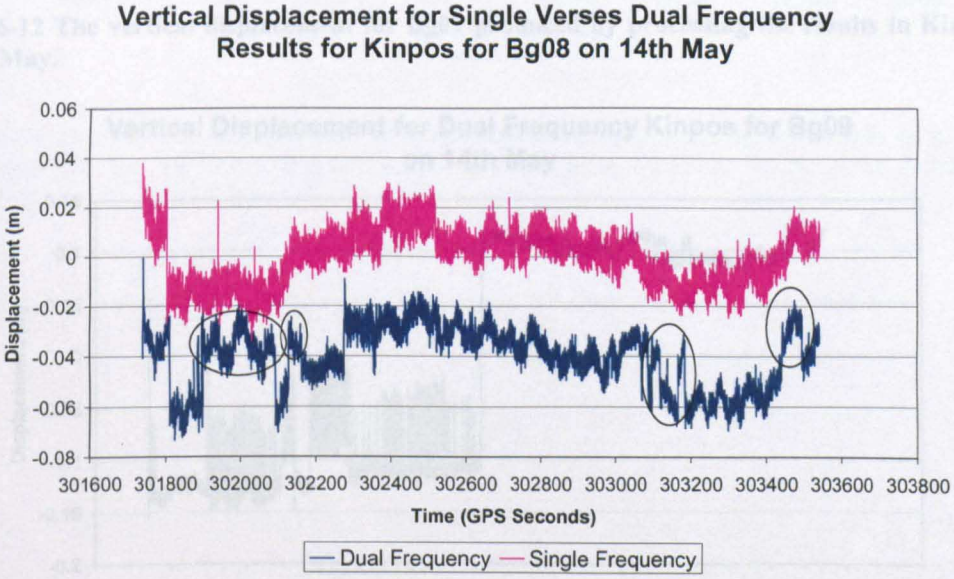

Figure 6-11 The vertical displacement for Bg08 produced by processing the results in Kinpos(sf) and Kinpos^{i}(df) for 14th May. The results from Kinpos^{i}(df) are offset by -0.04m.

The reason that Bg09 has been analysed separately from Bg03 and Bg08 is evident from Figure 6-12 and Figure 6-13 below, which show the vertical displacements results for Bg09 from Kinpos^{i}(df) for 15th and 14th May. On both days Kinpos^{i}(df) has fixed the wrong ambiguity values at the beginning of the session and kept them fixed at the these wrong values. Later on in the sessions the ambiguities have been fixed to the correct values. A weakness with a complete On-The-Fly search is that, even for dual frequency receivers, the wrong ambiguity values can be fixed. Kinpos(sf) fixed to the correct ambiguities at site Bg09 for the whole of both these sessions.

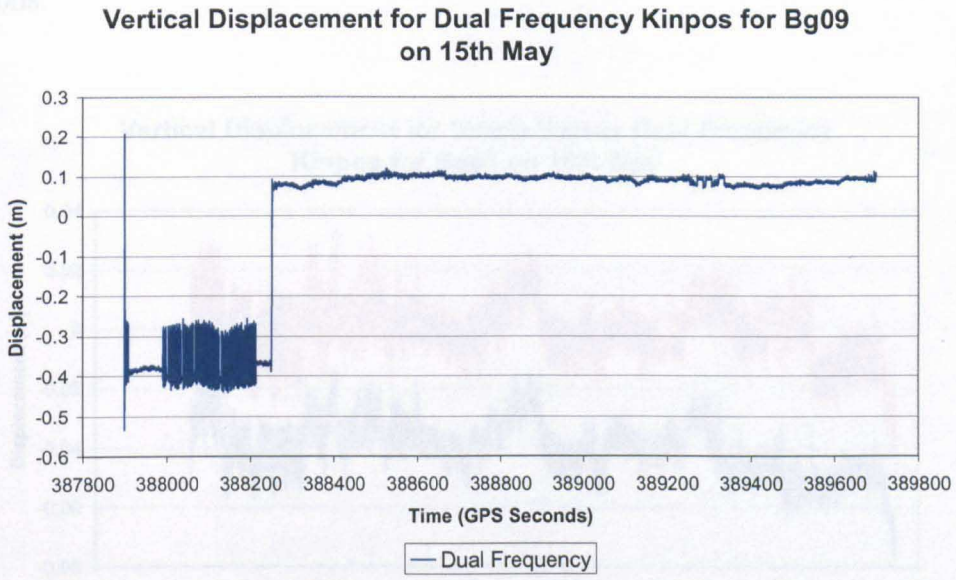

Figure 6-12 The vertical displacement for Bg09 produced by processing the results in Kinpos^{i}(df) for 15th May.

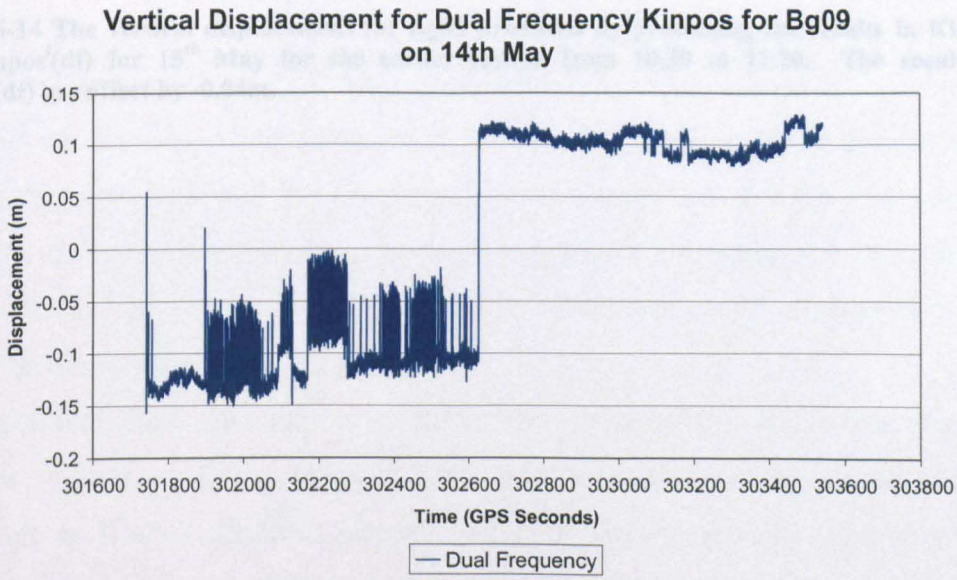

Figure 6-13 The vertical displacement for Bg09 produced by processing the results in Kinpos^{i}(df) for 14th May.

Data from 10.30 (GPS time 383400) to 11.20 (GPS time 386400) were processed in Kinpos(sf) and Kinpos^{i}(df) for Bg03 and Bg09 on 15th May. During this session the GDOP was at maximum 4.319 and the number of satellites never fell below 6. The results for Bg03 can be seen in Figure 6-14 and for Bg09 in Figure 6-15. It can be seen from these graphs that the results for Kinpos(sf) and Kinpos^{i}(df) have very similar multipath patterns and that the results produced are very alike. Table 6-5 also shows that in all three components the standard deviations produced by Kinpos(sf) and Kinpos^{i}(df) are very similar, with Kinpos^{i}(df) having marginally lower standard deviations.

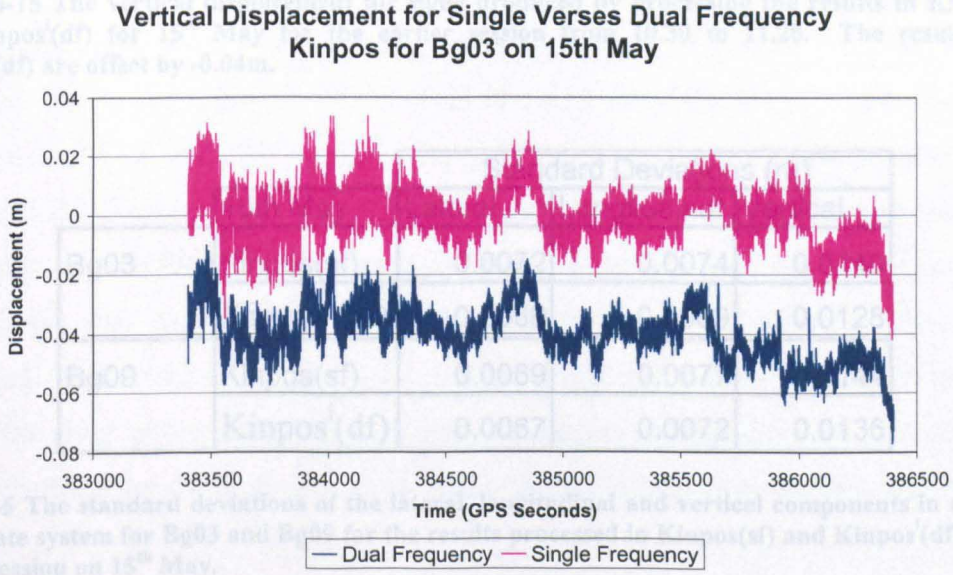

Figure 6-14 The vertical displacement for Bg03 produced by processing the results in Kinpos(sf) and Kinpos^{i}(df) for 15th May for the earlier session from 10.30 to 11.20. The results from Kinpos^{i}(df) are offset by -0.04m.

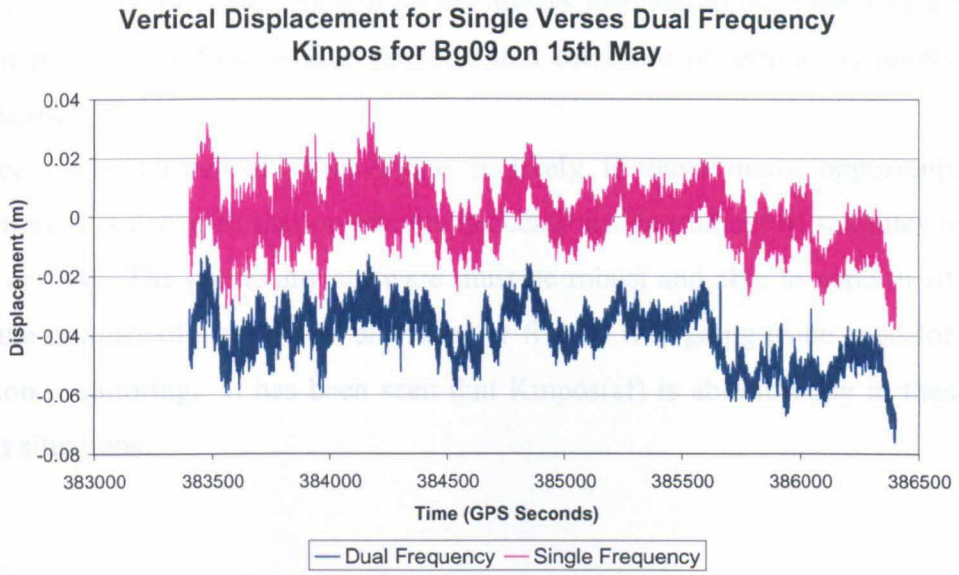

Figure 6-15 The vertical displacement for Bg09 produced by processing the results in Kinpos(sf) and Kinpos^{i}(df) for 15th May for the earlier session from 10.30 to 11.20. The results from Kinpos^{i}(df) are offset by -0.04m.

		Standard Deviations (m)		
	15th May	Lateral	Longitudinal	Vertical
Bg03	Kinpos(sf)	0.0072	0.0074	0.0140
	Kinpos^{i}(df)	0.0069	0.0069	0.0128
Bg09	Kinpos(sf)	0.0069	0.0077	0.0144
	Kinpos^{i}(df)	0.0067	0.0072	0.0136

Table 6-5 The standard deviations of the lateral, longitudinal and vertical components in a bridge coordinate system for Bg03 and Bg09 for the results processed in Kinpos(sf) and Kinpos^{i}(df) for the earlier session on 15th May.

The earlier session on 15th May, from 10.30 to 11.20, always had six or more satellites used in the positioning solution. In this situation both Kinpos(sf) and Kinpos^{i}(df) performed well and produced comparable results. For the later session on 15th May, from 11.45 to 12.15, the number of satellites is usually five and sometimes six. On the 14th May session, from 11.49 to 12.19, the number of satellites falls to four during the observation time.

Kinpos^{i}(df) does not seem to perform well in situations where the number of satellites is four or five. In these situations there are problems with ambiguity resolution, as Kinpos^{i}(df) fixes the ambiguities to the wrong values and so produces erroneous results. Kinpos^{i}(df) performs well only in situations where the number of satellites is continually above six or more. Kinpos(sf), however, performs well even in

the difficult situations. The ambiguities are always resolved to the correct values, even when there are only four or five satellites and there are no erroneous jumps in the coordinates.

Since the environment of a bridge is likely to have many opportunities for obstruction, it is expected that on numerous occasions the number of satellites may fall to four or five. The processing software must be robust and able to cope in situations where the number of satellites is only four or five, if it is going to be used for bridge deflection monitoring. It has been seen that Kinpos(sf) is able to cope in these more difficult situations.

6.3.3. Comparison of Two Days Time Series

The remaining rovers on the bridge were processed in Kinpos with Ref1 as the reference station for times 11.49 (301740) to 12.19 (303540) on 14th May and 11.45 (387900) to 12.15 (389700) on 15th May. As mentioned above, this did not include Bg01 and Bg10 which both had problems with data logging. The reason that these times were chosen for the two consecutive days was so that adaptive filtering could be used on the two days' time series. The basic principles of adaptive filtering are explained in Chapter 4, Section 4.4.1 and the interested reader is referred to Meng (2002) for more information. The adaptive filtering is used in this case to remove the multipath from the solution and leave behind only the bridge movement and receiver noise.

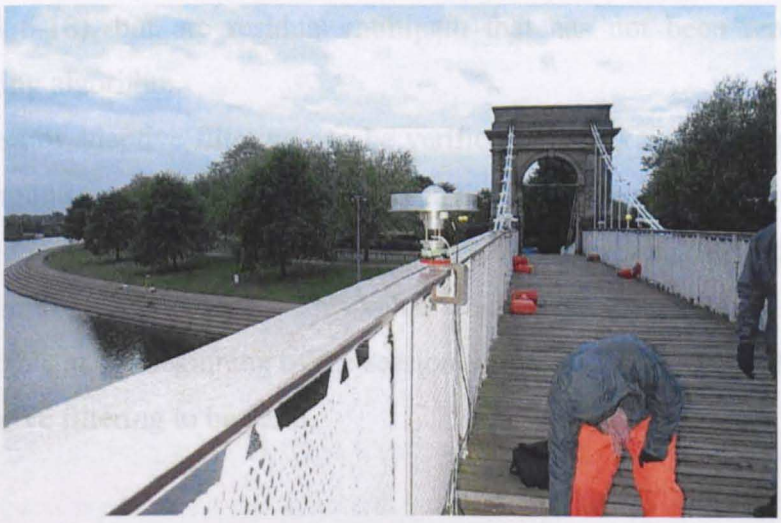

Figure 6-16 The location of Bg03 during the bridge trials, on the mid span of the bridge with a clear view of the sky.

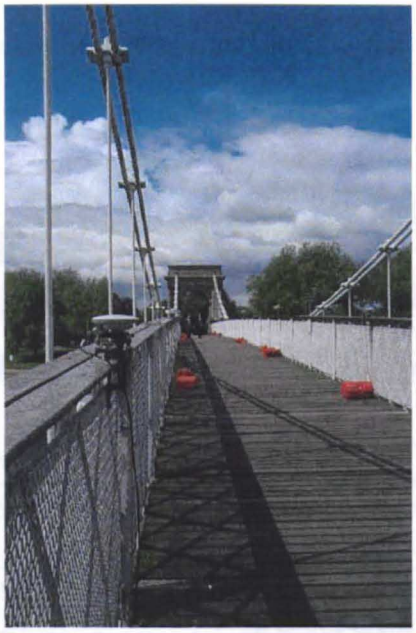

Figure 6-17 The location of Bg06 during the bridge trials. It was located very near to the bridge tower underneath some of the cables.

Figure 6-18 shows the input and output of adaptive filtering for Bg03 and Figure 6-19 shows the same but for Bg06. Bg03 was a bridge site that was located very close to the mid span of the bridge, which meant that it was far away from the cables and towers and so had a reasonably clear view of the sky (Figure 6-16). Bg06 was located very close to the south bridge tower which meant that it was very near to the bridge cables and so its view of the sky was obstructed (Figure 6-17).

Focusing on Figure 6-18, it can be seen that the output signal of bridge movement has most of the multipath removed. There are, however, periods within the data there is apparent motion which is not likely to be caused by bridge movement (these are circled within Figure 6-18), but are residual multipath that has not been removed by the adaptive filtering algorithm.

The success of adaptive filtering can be verified by checking the correlation levels of certain components. The correlation between the reference signal (14th May) and the desired signal (15th May) was found to be 0.5853, which meant that just over half the signal was common on both days. This value would have been affected by satellite 7 not been available at the beginning of the session on 14th May, but it is still a reasonable value for adaptive filtering to be valid.

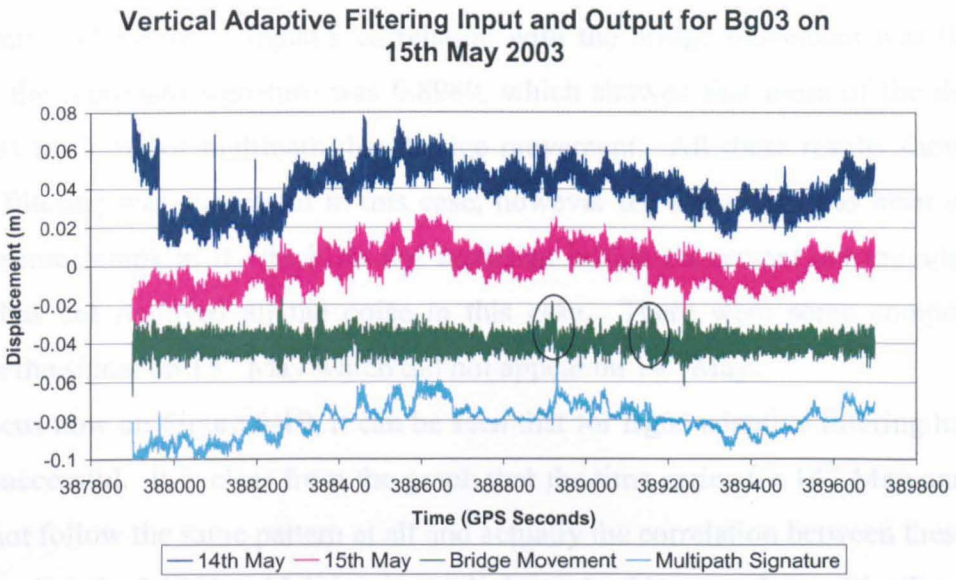

Figure 6-18 Vertical adaptive filtering for two days time series for Bg03. The desired signal is the coordinates from 15th May, the reference signal is the coordinates from 14th May, the output signal is the bridge movement and the common part if the multipath signature. The time series from 14th May, the bridge movement and the multipath signature have all been offset from 0 by 0.04m, -0.04m and -0.08m respectively.

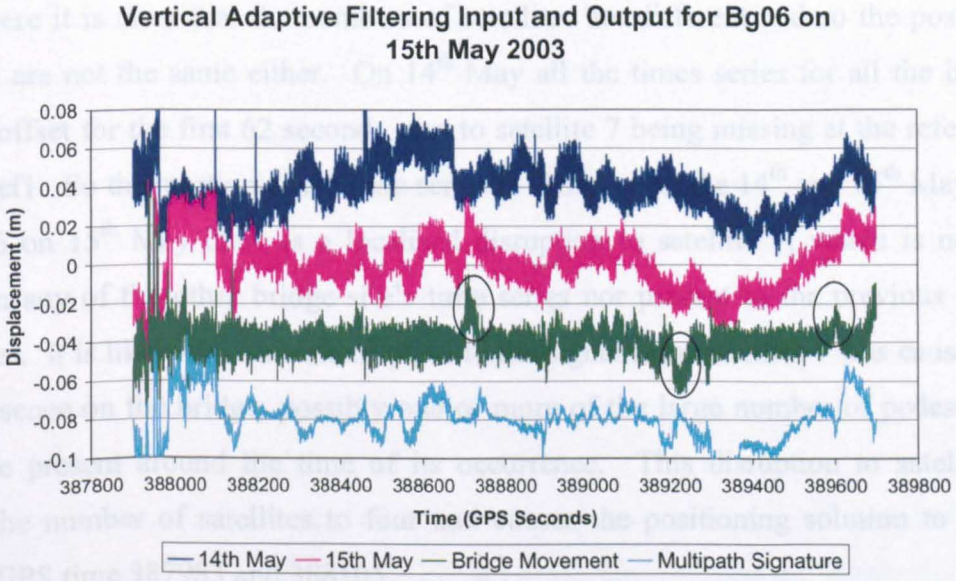

Figure 6-19 Vertical adaptive filtering for two days time series for Bg06. The desired signal is the coordinates from 15th May, the reference signal is the coordinates from 14th May, the output signal is the bridge movement and the common part if the multipath signature. The time series from 14th May, the bridge movement and the multipath signature have all been offset from 0 by 0.04m, -0.04m and -0.08m respectively.

Of particular interest is the correlation between the bridge movement and the multipath signature and also the bridge movement and the reference signal, as both of these should be close to zero for successful adaptive filtering. It was found that the correlation between the bridge movement and the multipath signature was -0.0206 and the correlation between the bridge movement and the reference signal was 0.0004. Both

these values were small and showed that there was little correlation between these components. The desired signal's correlation with the bridge movement was 0.4195 and with the multipath signature was 0.8989, which showed that more of the desired signal was made up of multipath than bridge movement. All these results show that adaptive filtering was successful in this case; however the signal that has been output still has some jumps in it which do not represent bridge movement, so the adaptive filtering has not removed all the noise in this case. There were some components present in the signal on 15th May which did not appear on 14th May.

To focus now on Figure 6-19, it can be seen that for Bg06 adaptive filtering has not been as successful. It is clear from the graph that the time series for 14th May and 15th May do not follow the same pattern at all and actually the correlation between these two time series is only 0.1241, which is extremely low. In this case, the multipath pattern has not repeated from day to day which has resulted in the bridge movement time series having a number of jumps in it, some of which are highlighted by circles in Figure 6-19.

There are two particular times within the two time series on 14th and 15th May for Bg06 where it is clear that the numbers of satellites are different and so the positions produced are not the same either. On 14th May all the times series for all the bridge sites are offset for the first 62 seconds, due to satellite 7 being missing at the reference station Ref1. So this portion of the time series is different on the 14th and 15th May. At site Bg06 on 15th May there is a localised disruption to satellite 7, which is neither present in any of the other bridge site's time series nor present in the previous day's time series. It is likely that this interruption to the signal from satellite 7 was caused by some presence on the bridge, possibly one or more of the large number of pedestrians who were present around the time of its occurrence. This disruption to satellite 7 reduces the number of satellites to four and causes the positioning solution to jump between GPS time 387983 and 388105.

For the rest of the time on the two days, the number of satellites at Bg06 is identical. However, the multipath patterns produced are not similar, even during these times when the satellite constellation is the same. Forward et al. (2003) investigated the use of GPS stacking techniques to remove multipath, under the assumption that the multipath signature will be well correlated from day to day. However, it was discovered that in the presence of an irregular signal reflecting surface, a strong daily correlation does not necessarily exist.

For Bg06 during this bridge trial, there does not appear to be a strong daily correlation between the multipath signatures. It is clear that the location of Bg06 means that it is in a high multipath environment as it is surrounded by cables (Figure 6-17). The amount of movement on the bridge was different on the two days of trial and this could have caused the differences in multipath signatures. When the bridge moved it would have caused the cables to be in different positions, which would have affected the signal dispersion.

All the receivers on the bridge and also the reference stations were removed and replaced between days of the trial. It is possible that the receiver was positioned in slightly different locations on each day; however the locations were all clearly marked and this should not have occurred. If the receiver locations were slightly different, the dispersion of the signals off the cables would have been different on the two days. It is unlikely that this problem was caused by the difference in antenna height at the reference receiver, as this would have affected all the rover locations but only two positions were affected (Bg05 and Bg06).

For other trials the correlation between two days time series for the Wilford Bridge has been around 0.77. For other larger bridges which move more, this correlation is lower. For the Millennium Bridge in London the day to day correlation was found on average to be around 0.3 and for the Humber Bridge in Hull it was around 0.18(Meng 2004). The reason that these correlations are lower is because a larger proportion of the GPS time series consists of bridge movement for these larger bridges. During this Wilford Bridge trial the movement on the bridge was relatively large, which meant that a lower day to day correlation was observed on all bridge sites, but particularly on some of those located near to the bridge cables.

Table 6-6 shows the day to day correlation of the time series on 14th and 15th May for all of the bridge sites. It is clear from this table that most of the correlations are between 0.50 and 0.62; however there are three bridge sites that have correlations below these values. Bg04, Bg05 and Bg06 were all located on the same side of the bridge in adjacent positions (Figure 6-1). Of the three sites, Bg04 had the clearest view of the sky being the furthest away from the towers and cables. It has a correlation of 0.4201 which is only just lower than the other bridge sites. Bg05 was located very near to one of the bridge cables, with the main part of the cable almost passing over the top of the antenna location (Figure 6-20). Bg05 also has a low day to day correlation, with a value of 0.1724. This demonstrates that it is likely to be the location of the cables that were

causing signal dispersion and producing these low correlations. However, Bg12 was also located very near to bridge cables but at the north end of the bridge (Figure 6-21), and this bridge site has the highest day to day correlation observed at 0.6115. So, just being close to the cables did not necessarily imply a low correlation. Most satellites appeared in the south direction and so at bridge sites Bg05 and Bg06 they would be blocked by the tower and the cables. Bg12 was only blocked in the north direction and was clear to the south and so would have still been able to pick up all the satellites without many obstructions.

Bridge Site	Bg02	Bg03	Bg04	Bg05	Bg06	Bg07	Bg08	Bg09	Bg11	Bg12
Correlation	0.5017	0.5835	0.4201	0.1724	0.1241	0.6025	0.5770	0.5611	0.584	0.618

Table 6-6 The day to day correlation for the time series on 14th and 15th May for all the bridge sites.

Figure 6-20 The location of Bg05 during the bridge trial. It was located very near to one of the bridge cables.

Figure 6-21 The location of Bg12 during the bridge trial. It was located near to the bridge cables at the north of the bridge.

It is clear that, for at least some of the bridge sites, adaptive filtering will not remove the entire multipath signature and so another method of mitigating the multipath and removing it from the signal had to be implemented. It is known that multipath has a long repeat period and therefore displays itself as a low frequency vibration within the GPS signal (Satalich 2004). By using a moving average filter of a specific length, all frequencies below a cut off will be removed from the data. As the data was recorded for this trial at a 10 Hz data rate, if a moving average filter of 10 samples is used, then this will remove all signals within the data that are 1 Hz or less. Results from previous trials have estimated the first natural frequency of the Wilford Bridge to be around 1.75 Hz (Dodson et al. 2001) and so removing all signals of 1 Hz or less will not remove any important information about the bridge characteristics.

Moving average filters of 10 samples were applied to all bridge sites. The results compared to the adaptive filtering output can be seen in Figure 6-22 for Bg03 and in Figure 6-23 for Bg06. Figure 6-22 shows that the signal produced when the moving

average filter is passed through the data is cleaner than the adaptive filtering signal, as there are no periodic movements that are caused by multipath. The four peaks of bridge movement around GPS times 388251, 388254, 389160 and 389249 can be much more clearly discerned within the moving average data.

For Bg06 a large improvement in the signal quality can be discerned when the moving average filter is used rather than adaptive filtering (Figure 6-23). This is as expected, since the day to day correlation value was very low for Bg06, meaning that affective adaptive filtering could not be performed. The data for Bg06 is noisiest for both time series at the beginning of the observation session. After this the moving average data shows no periodic signs of movement that could be attributed to multipath as these have been removed.

The four peaks of movement which are so clearly visible in Figure 6-22, cannot be distinguished in either time series in Figure 6-23. As Bg06 is located so close to the end of the bridge, the movement experienced at this bridge site would be considerably smaller than at the mid span location of Bg03. The movement of Bg06 cannot, in this case, be distinguished from the background GPS noise, even when the movement of the bridge is at its greatest.

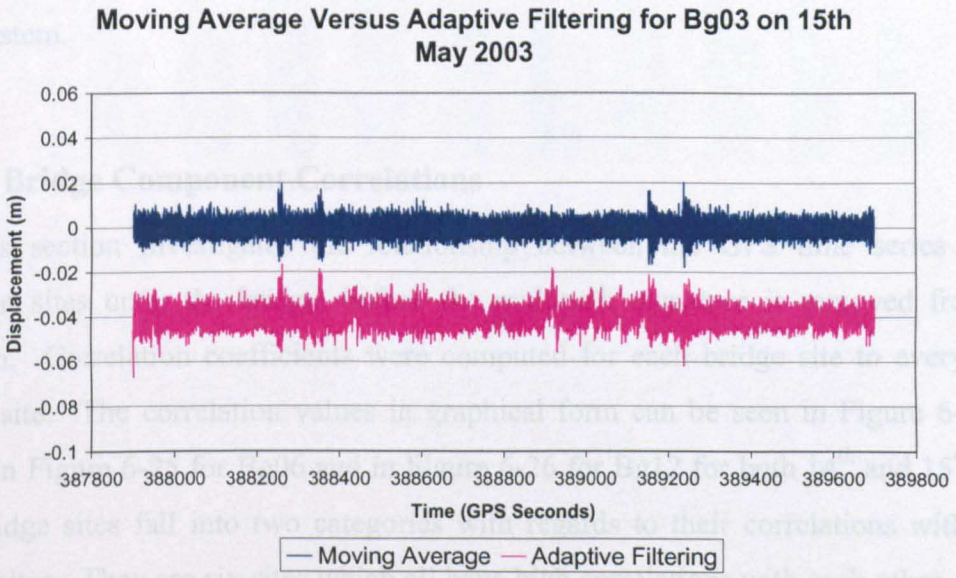

Figure 6-22 Moving Average filter of 10 samples compared to the results from adaptive filtering for Bg03 on 15th May. The adaptive filtering results are offset by -0.04m.

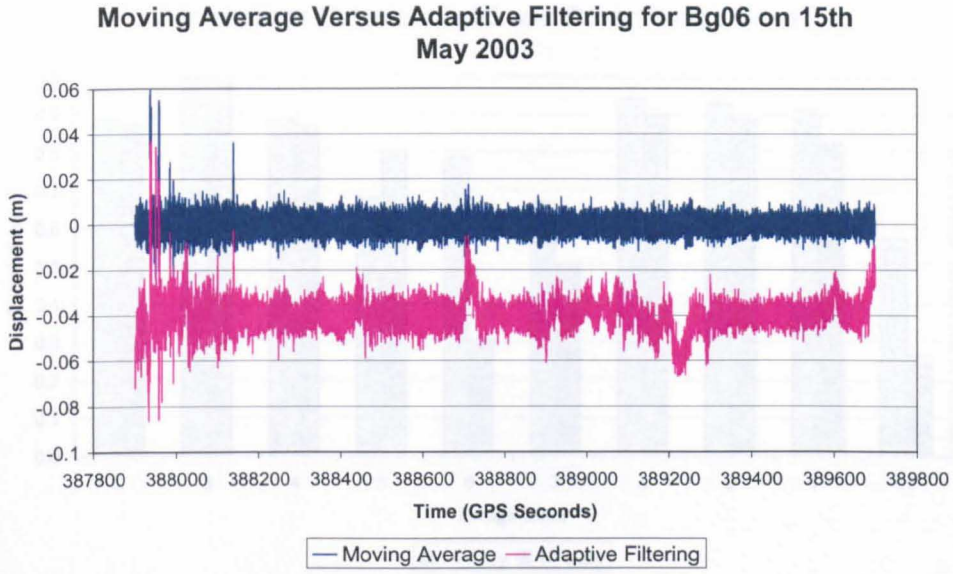

Figure 6-23 Moving Average filter of 10 samples compared to the results from adaptive filtering for Bg06 on 15th May. The adaptive filtering results are offset by -0.04m.

Since using a moving average filter provides a comparable and in most cases a better way of removing the multipath from the GPS time series, this method will be used throughout the rest of the thesis. Further investigation of adaptive filtering for multipath removal was not undertaken. It should be noted that a moving average filter can only be used in post-processing, so it would not be possible in a completely real-time system.

6.3.4. Bridge Component Correlations

This section investigates the relationship between the GPS time series at the different sites upon the bridge, before the multipath signature is removed from the solution. Correlation coefficients were computed for each bridge site to every other bridge site. The correlation values in graphical form can be seen in Figure 6-24 for Bg03, in Figure 6-25 for Bg06 and in Figure 6-26 for Bg12 for both 14th and 15th May. The bridge sites fall into two categories with regards to their correlations with other bridge sites. They are six sites which all have high correlations with each other. These are Bg02, Bg03, Bg04, Bg08, Bg09 and Bg11, which are the sites furthest away from the towers and cables, with the clearest view of the sky. The remaining four bridge sites Bg05, Bg06, Bg07 and Bg12, which are all very close to bridge cables, not only have a low correlation with the other six sites, but also with each other.

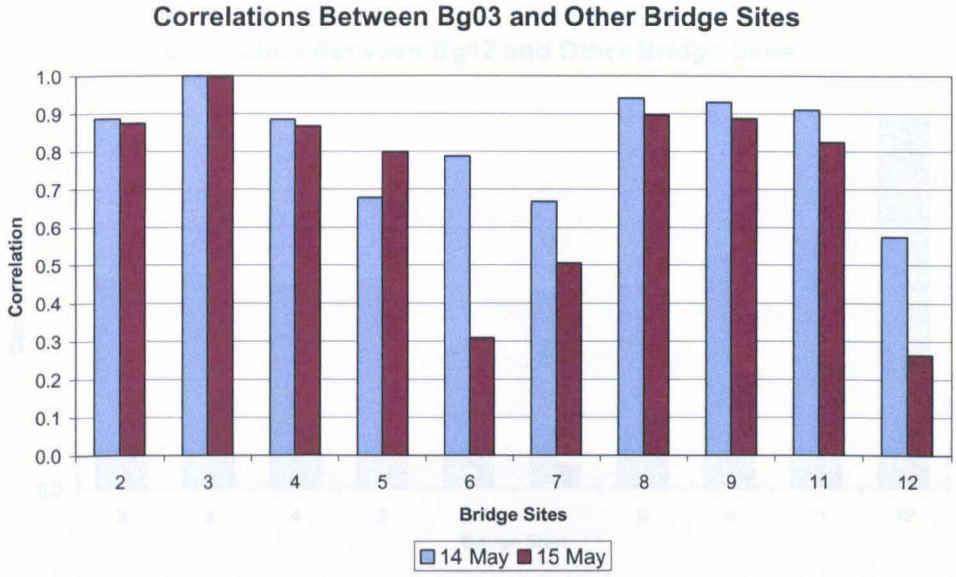

Figure 6-24 The correlation coefficients between Bg03 and all other bridge sites for 14th and 15th May.

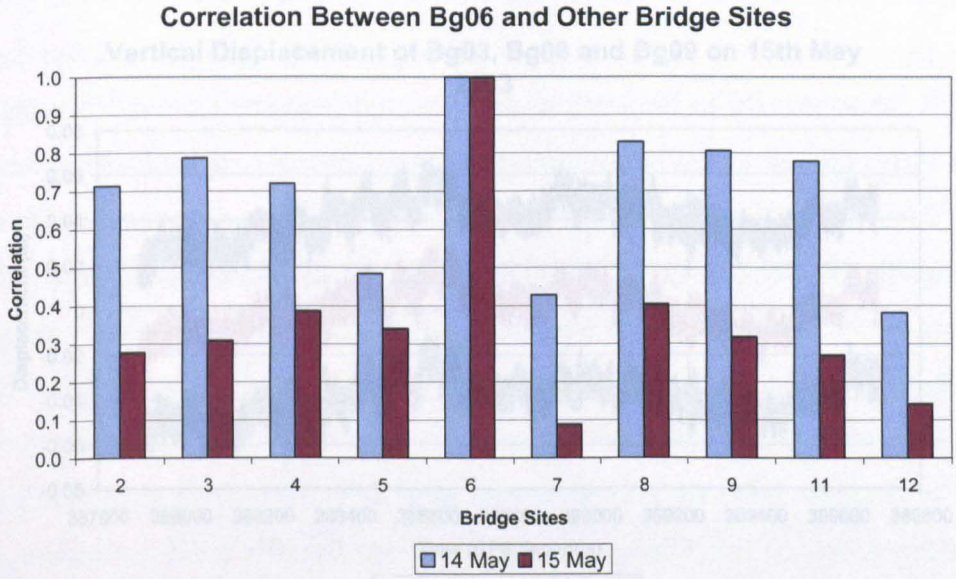

Figure 6-25 The correlation coefficients between Bg06 and all other bridge sites for 14th and 15th May.

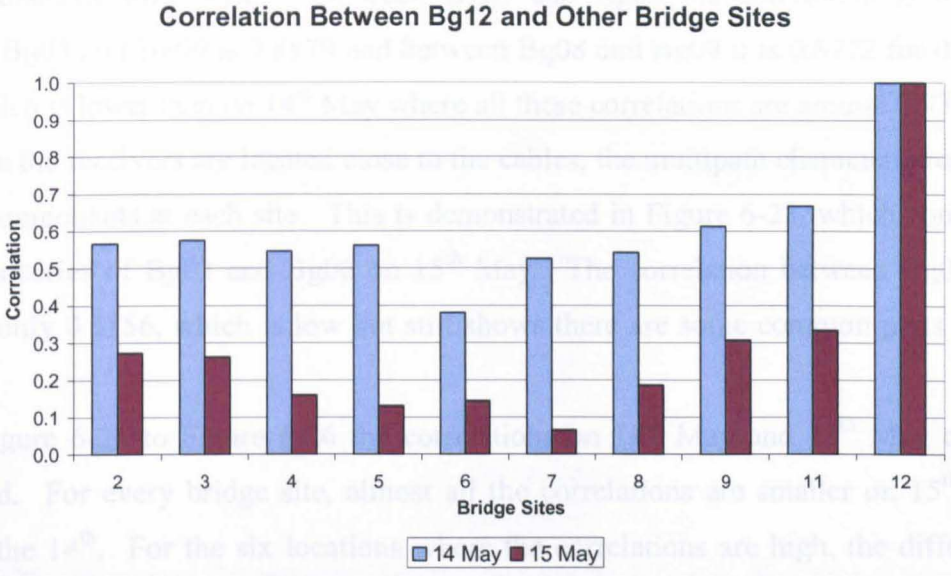

Figure 6-26 The correlation coefficients between Bg12 and all other bridge sites for 14th and 15th May.

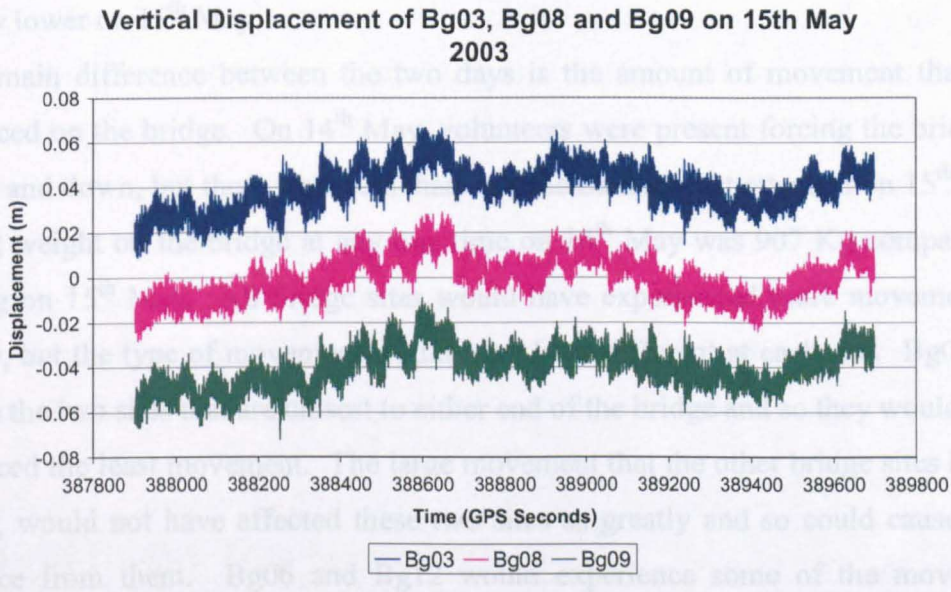

Figure 6-27 The vertical displacement of Bg03, Bg08 and Bg09 on 15th May, showing the similar multipath characteristics at the three sites. The time series of Bg03 is offset by 0.04m and for Bg09 the offset is -0.04m.

There are components within each GPS time series which are the same. Each bridge site is seeing the same satellites and using the same reference receiver's data. The reference receiver's multipath will be present in all the rover time series. The bridge movement is also a component in each of the times series, although the bridge will move differently at different points along its length. For the bridge sites that have a clear view of the sky, the multipath characteristics are almost identical, due to the similarities in the surrounding environment. This is demonstrated for Bg03, Bg08 and

Bg09 on 15th May in Figure 6-27, which shows that the three bridge sites have almost indistinguishable time series. Between Bg03 and Bg08 the correlation is 0.8978, between Bg03 and Bg09 is 0.8879 and between Bg08 and Bg09 it is 0.8772 for the 15th May, which is lower than on 14th May where all these correlations are around 0.93.

When the receivers are located close to the cables, the multipath characteristics have unique components at each site. This is demonstrated in Figure 6-28, which compares the times series of Bg03 and Bg06 on 15th May. The correlation between Bg03 and Bg06 is only 0.3156, which is low but still shows there are some common parts to the signals.

In Figure 6-24 to Figure 6-26 the correlations on 14th May and 15th May can be compared. For every bridge site, almost all the correlations are smaller on 15th May than on the 14th. For the six locations where the correlations are high, the difference between the two days is reasonably small. However, Figure 6-25 and Figure 6-26 particularly highlight, that for sites located near to the cables, the correlations are markedly lower on 15th May.

The main difference between the two days is the amount of movement that was experienced on the bridge. On 14th May, volunteers were present forcing the bridge to move up and down, but there were less than half the number that attended on 15th May. The total weight on the bridge at any one time on 14th May was 907 Kg compared to 2,353 Kg on 15th May. All bridge sites would have experienced more movement on 15th May, but the type of movement would have been different at each site. Bg06 and Bg12 are the two sites that are closest to either end of the bridge and so they would have experienced the least movement. The large movement that the other bridge sites had in common, would not have affected these two sites as greatly and so could cause their divergence from them. Bg06 and Bg12 would experience some of the movement though and this would cause a change in reflections from the cables, therefore changing the multipath characteristics experienced at these sites.

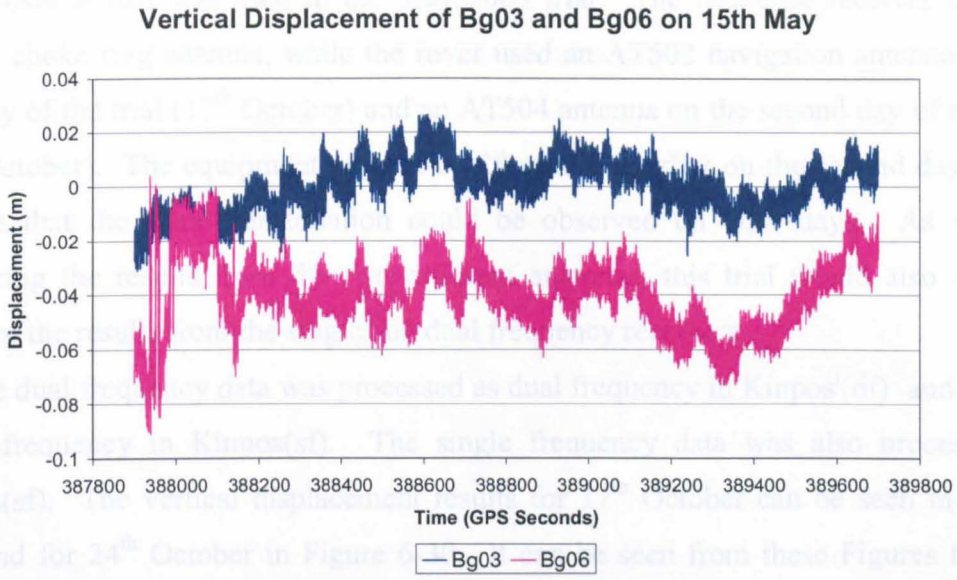

Figure 6-28 The vertical displacement of Bg03 and Bg06 on 15th May, highlighting the different multipath characteristics at these two sites. Bg06 is offset by -0.04m.

As mentioned above, the location of the bridge sites was not decided by the author, but by colleagues at Cranfield University based on algorithms for optimal sensor location. It is clear from this section and Section 6.3.3 how the multipath characteristics and results from GPS are affected by the choice of bridge location. Particularly sites such as Bg06 and Bg12 have problems with large amounts of multipath and different day to day signatures; however this can be removed by moving average algorithms. Since bridge cables will always cause problems on any cable-stayed bridge, knowing the effect of these cables on the GPS solution is important.

6.4. Bg06 Bridge Trial

During the May 2003 bridge trial, Bg06 was located in a position which had a large amount of multipath, which led to a small day to day correlation at this site. During this bridge trial a small navigation antenna (AT502) was used at Bg06. When initial processing of the results from Bg06 occurred it was suggested that the large multipath signatures could be reduced by using a choke ring antenna. In this high multipath environment a further trial was carried out to assess the improvement that could be achieved using a choke ring antenna.

On two days in October 2003, a single frequency and a dual frequency Leica system 500 GPS receiver were connected by a signal splitter to the same antenna located on position Bg06. A dual frequency reference receiver was located on the riverside on the

same position that was used in the May 2003 trial. The reference receiver used an AT504 choke ring antenna, while the rover used an AT502 navigation antenna on the first day of the trial (17th October) and an AT504 antenna on the second day of the trial (24th October). The equipment was set up 28 minutes earlier on the second day of the trial so that the same constellation could be observed on both days. As well as comparing the results from the two different antennas, this trial would also directly compare the results from the single and dual frequency receivers.

The dual frequency data was processed as dual frequency in Kinpos[i](df) and also as single frequency in Kinpos(sf). The single frequency data was also processed in Kinpos(sf). The vertical displacement results for 17th October can be seen in Figure 6-29 and for 24th October in Figure 6-30. It can be seen from these Figures that the single and dual frequency data have very similar multipath patterns on the same day; however the multipath pattern between days is very different. This is as expected since the results from the bridge trial analysed above showed a low day to day correlation at Bg06. Also for this trial, different antenna types were used at the rover on the two days and this will cause further decorrelation of the multipath.

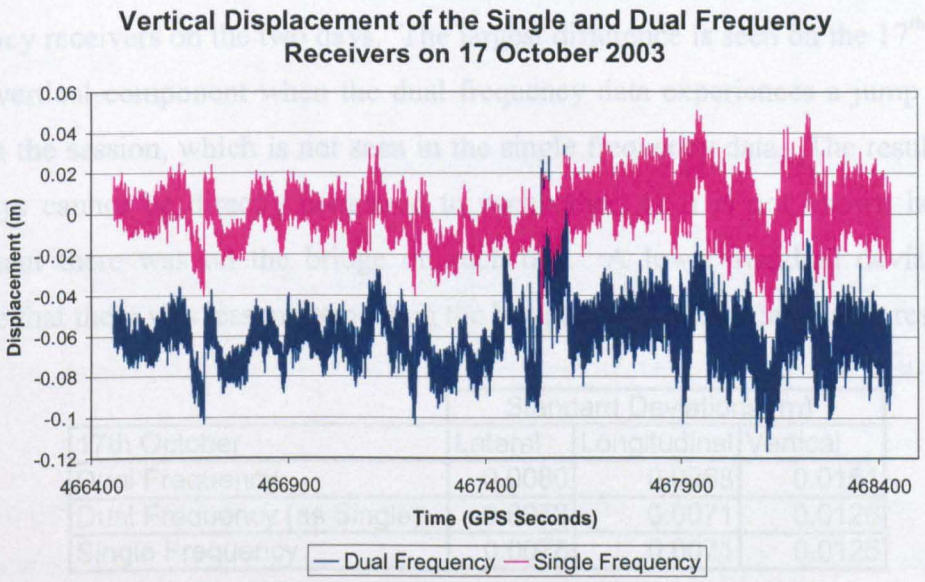

Figure 6-29 The vertical displacement for Bg06 on 17th October produced by processing the data with Kinpos(sf) and Kinpos[i](df). The dual frequency time series is offset by -0.06.

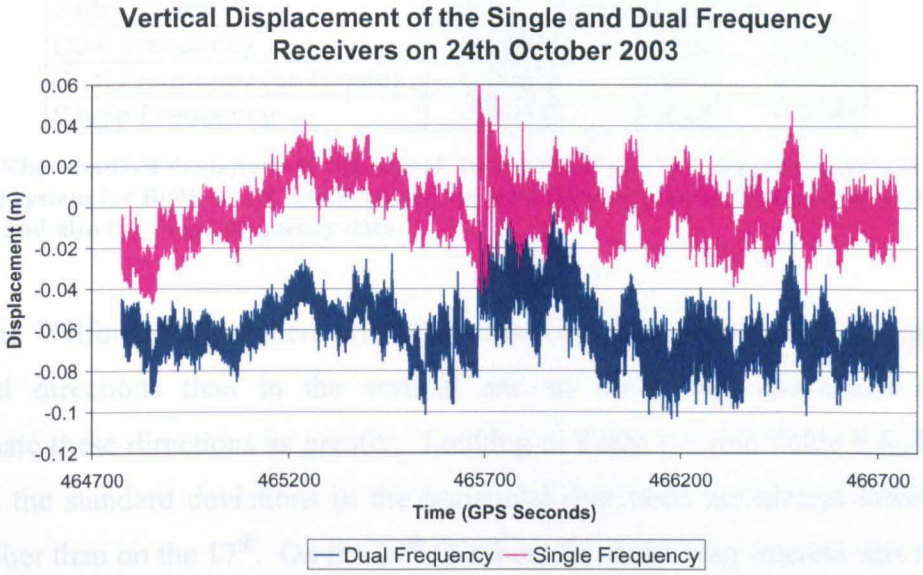

Figure 6-30 The vertical displacement for Bg06 on 24th October produced by processing the data in Kinpos(sf) and Kinpos(df). The dual frequency time series is offset by -0.06.

The standard deviations of the lateral, longitudinal and vertical components for the dual frequency data processed as both dual and single frequency and also for the single frequency data can be seen in Table 6-7 for 17th October and in Table 6-8 for 24th October. Both tables show that comparable results are recorded by the single and dual frequency receivers on the two days. The largest difference is seen on the 17th October, in the vertical component when the dual frequency data experiences a jump half way through the session, which is not seen in the single frequency data. The results for the two days cannot be directly compared to each other, as it is not known how much movement there was on the bridge on each day. A lower standard deviation may indicate that there was less movement on the bridge, rather than a less noisy result.

	Standard Deviations (m)		
17th October	Lateral	Longitudinal	Vertical
Dual Frequency	0.0080	0.0068	0.0151
Dual Frequency (as Single)	0.0078	0.0071	0.0126
Single Frequency	0.0078	0.0071	0.0125

Table 6-7 The standard deviations of the lateral, longitudinal and vertical components in a bridge coordinate system for Bg06 on 17th October, for the dual frequency processed as dual and as single frequency and also the single frequency data.

	Standard Deviations (m)		
24th October	Lateral	Longitudinal	Vertical
Dual Frequency	0.0061	0.0048	0.0148
Dual Frequency (as Single)	0.0062	0.0047	0.0142
Single Frequency	0.0063	0.0048	0.0141

Table 6-8 The standard deviations of the lateral, longitudinal and vertical components in a bridge coordinate system for Bg06 on 24th October, for the dual frequency processed as dual and as single frequency and also the single frequency data.

On the Wilford Bridge, there will always be less movement on the bridge in the horizontal directions than in the vertical and so the bridge movement will not contaminate these directions as greatly. Looking at Table 6-7 and Table 6-8, it can be seen that the standard deviations in the horizontal directions are always lower on the 24th October than on the 17th. On the 24th October, the choke ring antenna was used and so this is an initial indication that the multipath will be less with a choke ring.

To further investigate the comparison of the results on 17th and 24th October, the double difference carrier phase residuals were calculated for the dual and single frequency receivers. These residual can be seen in Table 6-9. It can be seen that for almost every satellite and each receiver, the standard deviation of the residuals are lower on 24th October than on 17th. The overall average of the standard deviations is lower on the 24th also. This indicates that the positioning solution was more precise on 24th October, when the choke ring antenna was used.

		Standard Deviations of the Double Difference Satellite Residuals (m)							
		8	10	17	21	26	27	28	Average
Dual Frequency	17th October	0.0082	0.0063	0.0033	0.0073	0.0047	0.0036	0.0073	0.0058
	24th October	0.0050	0.0051	0.0025	0.0055	0.0046	0.0016	0.0071	0.0045
Dual Frequency (as Single)	17th October	0.0081	0.0063	0.0047	0.0083	0.0047	0.0037	0.0082	0.0063
	24th October	0.0039	0.0045	0.0023	0.0053	0.0050	0.0020	0.0056	0.0041
Single Frequency	17th October	0.0080	0.0062	0.0047	0.0082	0.0047	0.0037	0.0082	0.0062
	24th October	0.0059	0.0055	0.0029	0.0068	0.0051	0.0021	0.0080	0.0052

Table 6-9 The standard deviations of the double difference satellite residuals for Bg06 on 17th and 24th October.

In this case, it appears that the choke ring antenna has produced results that are slightly better than the navigation antenna, as it would be expected. Due to the nature of the test, the results are by no means conclusive. This trial further highlights the similarity in the results produced by single and dual frequency receivers, even in difficult multipath conditions.

6.5. Frequency Identification

Frequency identification forms an important part of monitoring the health of structures. The fundamental bridge frequencies can reveal important information about the movement of the structure. Changes in the stiffness of the bridge, caused by damage, could lead to changes in modal parameters (Owen and Pearson 2004). A reduction in the stiffness of the bridge would cause a reduction in the natural frequency (Owen and Pearson 2004). Usually these changes in modal parameters are related to a Finite Element Model (FEM). The mode results are used to update the FEM and the location of the damage can be identified. Cranfield University developed a FEM of the Wilford Bridge which has been described in other papers (Meng et al. 2003). This section will only focus on the identification of the bridge's natural frequencies and not the updating of the FEM. The interested reader is referred to Meng et al. (2003) or Owen and Pearson (2004) for more information on FEM updating.

Identification of the bridge's natural frequencies is carried out in the following section using the GPS and accelerometer data, to compare the results from the two. It is important to note that there can be some problems with this method of damage identification, which includes the modal parameters not being sensitive enough to detect changes in the structure and difficulties of obtaining robust and reliable estimates of the modal parameters from experimental data (Owen and Pearson 2004). Despite these disadvantages it was decided that frequency analysis was the best way to proceed with the GPS and accelerometers data. Other more complex methods of analysing bridge vibration data are investigated by other authors (for example Owen and Pearson (2004)) but they are beyond the scope of this study and are not discussed here.

During the May Wilford Bridge trials, there were two triaxial accelerometers located at Bg03 and Bg09. There were problems with the data collected by the Entran accelerometer which was located at Bg03 and so the results that are included in the following section are only from the Kistler accelerometer which was located at Bg09. It was discovered that the data from the Entran accelerometer was very much noisier than the data from Kistler accelerometer even in static trials, and that is why the data is not analysed here. The GPS antenna and triaxial accelerometer were housed together as one unit (Figure 6-31), so that they could sense the same bridge movements.

Figure 6-31 The GPS antenna and triaxial accelerometer housed together as one unit, at Bg09.

The accelerometer data was recorded in volts directly to an attached laptop. The volts were converted into accelerations and then integrated twice to obtain the displacement values. For information on the processing algorithms used on the accelerometer data the interested reader is referred to Meng (2002). Results from the dual frequency GPS receiver located at Bg09 were processed as single frequency in Kinpos. The multipath signature was removed from the data with a moving average filter of 10 samples before comparing the results to the accelerometer.

The results for the GPS displacements compared to those calculated from the accelerometer can be seen in Figure 6-32. It can be seen from this Figure that there is a large amount of noise on the GPS signal compared to the accelerometer, meaning that it is hard to distinguish the movement of the bridge from this noise. The four main peaks of the movement, where volunteers from the IESSG and the local council offices jumped up and down on the bridge, can clearly be seen in the accelerometer time series. These four large peaks are the only movement that is visible in the GPS time series and they are not as clear as the accelerometer time series.

The amplitudes of the four peaks are different for the GPS and accelerometer data. The moving average filtering and other post-processing that was applied to the GPS data could have caused a loss of amplitude in these results. The accelerometer data could also be showing amplitudes that are too large during these periods of peak movement. (Problems also occurred in a bungee test rig trial where the accelerometer showed amplitudes that were too large compared to the GPS, see Chapter 9, Section 9.2.2.) As there is no way of knowing the 'true' amplitude of the bridge, it is unclear which system shows the correct amplitude.

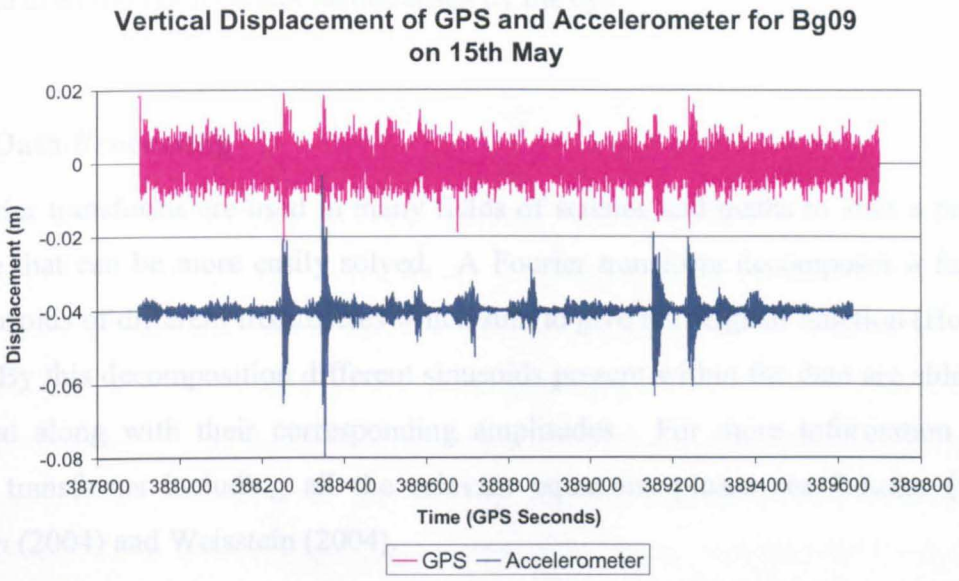

Figure 6-32 The vertical displacement shown by the GPS and accelerometer at Bg09 on 15th May. The accelerometer data is offset by -0.04m.

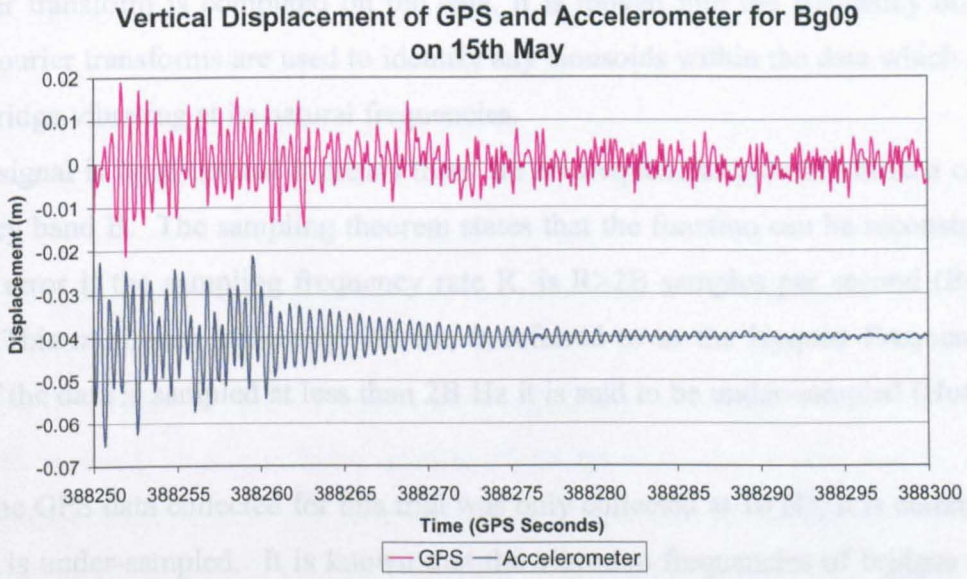

Figure 6-33 The vertical displacement shown by the GPS and accelerometer at Bg09 on 15th May. The graph focuses on a time where there was a large amount of movement on the bridge. The accelerometer data is offset by -0.04m.

Figure 6-33 focuses in the first peak of movement that can be seen in Figure 6-32. It can be seen from Figure 6-33 that both the GPS and the accelerometer data show the period of movement where people are jumping up and down on the bridge forcing it to vibrate. After the people have stopped jumping, the bridge was left to oscillate at its natural frequency, which is clearly visible in the accelerometer time series. This sinusoidal decay pattern is not clear in the GPS time series as it is masked by the noise.

However, frequency analysis reveals that this sinusoidal pattern is still present in the GPS data even though it cannot be discerned by the eye.

6.5.1. Data Processing

Fourier transforms are used in many fields of science and maths to alter a problem into one that can be more easily solved. A Fourier transform decomposes a function into sinusoids of different frequencies which sum to give the original function (Hoffman 2004). By this decomposition different sinusoids present within the data are able to be identified along with their corresponding amplitudes. For more information about Fourier transforms including all the relevant equations please see Bourke (1993), Hoffman (2004) and Weisstein (2004).

It is useful to think of the data as being in either the time or frequency domain. When the GPS and accelerometer data is originally collected it is in the time domain. If a Fourier transform is computed on the data, it is moved into the frequency domain. These Fourier transforms are used to identify any sinusoids within the data which could be the bridge vibrating at its natural frequencies.

If a signal is band-limited it means there are no frequencies present above a certain frequency band B. The sampling theorem states that the function can be reconstructed without error if the sampling frequency rate R, is R>2B samples per second (Bourke 1993). This minimum frequency, 2B Hz, is referred to as the Nyquist Frequency or Rate. If the data is sampled at less than 2B Hz it is said to be under-sampled (Hoffman 2004).

As the GPS data collected for this trial was only collected at 10 Hz, it is certain that the data is under-sampled. It is known that the vibration frequencies of bridges could span from under 0.1 Hz for a long span suspension bridge, to over 50 Hz for a short span bridge of only a few metres long (Meng et al. 2003). Due to the data being under-sampled, a phenomenon called aliasing may occur. When the data is under-sampled, the information about the spectrum is no longer complete. This causes the tailing end of the spectrum to fold back onto the apparent spectrum, which means that higher frequency modes are reflected back into the measured spectrum. This can cause false information about the mode values to be drawn from the data.

A Matlab (MATLAB® 2004) script was written to compute the discrete Fourier transform (DFT) of different sets of data and attempt to calculate the mode values from

this data. The results from the DFT of each data set are plotted as a frequency against amplitude graph. This method is often referred to as 'peak-picking' as the modes are chosen as the frequencies with the highest amplitude/peak on the graph. This method has been widely used to extract mode information from bridge deformation results. However, it is known that one of the disadvantages of this method is that it can become a quite subjective task, especially if the peaks are not clear (Peeters et al. 1998). From the experience of the author, it is true that it can become quite subjective and so only frequencies which are clearly repeated in a number of data sets can be trusted.

To aid in the identification of the frequencies from the GPS and accelerometer bridge displacement data, digital signal filtering of the data was carried out. Filters are signal conditioners, which take the original signal and instructions about which frequencies to block, before outputting a signal which is the original with the specified frequencies removed (Wagner and Barr 2002). There are many filter types, but the most common are lowpass, highpass, bandpass and bandstop. A lowpass filter only allows low frequencies, below a certain cut-off, to be output and so is used to remove high frequencies from a signal. A highpass filter is the opposite of the lowpass as it only allows high frequency components to be output. A bandpass filter only allows signals within a certain specified range to be output, while a bandstop filter allows high and low frequencies to be output but removes frequencies from a specified range in the middle. Using a bandpass filter, all frequencies outside the band of interest could be removed from the bridge displacement signal.

A filter has three different responses to frequencies which are passed through it, which are referred to as passband, stopband and transition band (Wagner and Barr 2002). Frequencies which are in a filter's passband are passed through (mostly) unchanged. If the frequency is within the filter's stopband it is highly attenuated. The transition band is the frequencies in the middle which will receive some attenuation but are not completely removed from the signal. The transition bandwidth is how quickly the filter makes the transition between passband and stopband and vice versa. In an ideal situation the filter will make an instantaneous transition from the passband to full attenuation, but most real world filters do not achieve this.

Filters come in two types which are Infinite Impulse Response (IIR) and Finite Impulse Response Filters (FIR) (MATLAB® 2004). The IIR filters have the advantage that they can usually meet a given set of requirements with a lower filter order and so require less computing power. The classical IIR filters, which are Butterworth,

Chebychev, elliptic and Bessel, all approximate the ideal 'brick wall' (no transition band) in different ways. The requirements of the filters used in this thesis were "loosely specified", as only the cut-off frequencies were stipulated and no strict requirements on the amount of stopband attenuation or transition band size were made. This meant it was sufficient to use a Butterworth filter (MATLAB® 2004). For a small portion of the data a Chebychev filter was compared to the Butterworth and the same results were achieved.

A Matlab script using a Butterworth bandpass filter was written to remove unwanted frequency information before a DFT was computed on the data. As the order of the Butterworth filter increases, the transition band become narrower (Hayes 1999). Through experimentation it was discovered that the optimal filter order for the GPS and accelerometer data was 8. Above this order the results were the same, but extra computation time was needed. Below this order the size of the transition band affected the results. For the equations associated with the Butterworth filter used for calculations in Matlab the interested reader is referred to MATLAB® (2004) and Mulgrew et al. (2003).

6.5.2. Results

Figure 6-33 shows a close up of the displacement recorded by the GPS receiver and accelerometer at Bg09 during a time when there was a lot of movement on the bridge. The people present on the bridge jumped up and down to force movement and then stopped leaving the bridge to oscillate at its natural frequency. When frequency identification occurs with a DFT, it is important that only the period where the bridge is left to swing is analysed and not the part where there was a forcing movement. If the forcing movement is analysed it is the frequency of this that will be identified and not the bridge's natural frequency.

Since there are four clearly visible peaks of movement in Figure 6-32, the frequency identification focussed on these four time periods. Care was taken only to include data from the natural decay of the bridge and not during the time when there was a forcing occurring on the bridge. These times periods shall be referred to as peak 1, peak 2, peak 3 and peak 4.

It has previously been stated that the GPS data for this trial was collected at a 10 Hz data, which was the highest data rate possible with the Leica System 500 receivers.

Using the Nyquist Theorem, it is known that only frequencies of 5 Hz or less can be identified within this data (Hayes 1999). In practise it will only be possible to identify frequencies up to about 3-4 Hz.

For the GPS and accelerometer data, three different bands were chosen for the bandpass filter to attempt to identify different frequencies within the data. It would have been possible to identify higher frequency bridge dynamics with the accelerometer data as it was recorded at an 80 Hz data rate. However, the accelerometer data is used here only for a comparison to GPS and so only the first three modes were considered.

It was known that the first natural frequency of the Wilford Bridge was around 1.75 Hz (Dodson et al. 2001). So, the first bandpass filter was chosen with the lower limit set to 1.5 Hz and the upper limit set to 2.5 Hz. The second bandpass was set so that the lower limit was 2 Hz and the upper limit was 3 Hz and the third bandpass filter had a lower limit of 2.5 Hz and an upper limit of 3.5 Hz. Since the first natural frequency is likely to be the strongest frequency present within the signal, it is useful to be able to remove it so that higher frequencies can be more easily identified.

When computing a DFT, the number of samples used can be very important. DFT will average the frequencies present within the data, and do not take into account when frequencies change over time (Li et al. 2004). However, the more samples that are used to compute a DFT, the more reliable the result will be. So, a compromise in the number of samples must be reached so that a reliable result is achieved, but a minimum of frequency averaging occurs. To overcome this problem, a number of different DFTs were computed for each peak, with a varying number of samples.

For the GPS data DFTs of 128, 256, 384 and 512 samples were computed for each peak, as well as DFTs of 100, 200, 300 and 400 samples. For the accelerometer data, since it was recorded at 80 Hz, which was eight times the data rate of the GPS data, the corresponding DFTs had lengths 1024, 2048, 3072 and 4096 and also 800, 1600, 2400 and 3200. 128 samples of GPS data corresponded to 12.8 seconds and also 1024 samples of the accelerometer data corresponded to the same amount of time, 12.8 seconds. The tables for all these DFTs for both the GPS and accelerometer data, for peak 1 to peak 4, can be seen in Appendix D (Table D–1 to Table D–16).

6.5.2.1. First Natural Frequency

The initial analysis will concentrate on the identification of the first natural frequency of the Wilford Bridge only. By studying Table D–1 to Table D–16 in Appendix D it may first be concluded that this mode could lie anywhere between 1.7 and 1.8 Hz, as the results take these values at different points and also many values in between. However, closer inspection of the results and the nature of the DFT calculations can lead to different conclusions.

One important feature of the DFT is that the values the mode frequencies can take are finite and are dependant on the number of sample points used to calculate the DFT. This is perhaps better explained by Table 6-10 and Table 6-11. Table 6-10 shows a summary of the values the GPS and accelerometer DFTs took for 12.8, 25.6, 38.4 and 51.2 seconds for all four peaks of movement, while in Table 6-11 the summary of the DFT results for 10, 20, 30 and 40 seconds are shown. When 12.8 seconds, which corresponds to 128 samples for the GPS data and 1024 samples for the accelerometer data, of data are used there are only two possible values between 1.7 and 1.8 Hz that the DFT can take which are 1.72 and 1.8 Hz. When 25.6 samples are used, the number of possible values increases to three at 1.72, 1.76 and 1.8 Hz. With 38.4 seconds of data the number of possible values is four and with 51.2 seconds of data the possibilities climb to six.

By looking at the data in Table 6-10, the 12.8 second data implies that the mode is between 1.72 and 1.8 Hz. The GPS data shows all the modes at 1.8 Hz, whereas the accelerometer data has half at 1.72 and half at 1.8 Hz. Using 25.6 seconds of data the mode is shown to be between 1.72 and 1.76 Hz, as half the data shows one mode and half the data the other. Using the 38.4 data, it can be seen that the mode is between 1.72 and 1.74 Hz, with more of the data favouring 1.72 Hz. Using 51.2 seconds of data produces very varied results for the value of the mode, which may mean that too much data is included and so other forces are present in this data. From this table it would be concluded that the mode is between 1.72 and 1.74 Hz, probably closer to 1.72 Hz.

Table 6-11, shows a far more clearly the convergence of the DFT results to the true mode value. For 10 seconds of data, all the results show the mode is at 1.8 Hz. For 20 seconds of data, the results show the mode is between 1.7 and 1.75 Hz with much more of the data favouring 1.75 Hz. For the 30 second data, the mode is between 1.7 and 1.73 Hz, again a lot more of the data favours 1.73 Hz. With the 40 second data, there is

again a divergence of values taken, but the accelerometer data still clearly favours 1.73 Hz as the mode value.

Combining the information from the two tables, it can be concluded that the most likely value of the mode of the Wilford Bridge is 1.73 Hz. This is the value that, when present in the possible DFT outcomes, appears the most frequently. It is interesting to note that the results from the GPS and accelerometer are very similar in each case, showing that even though there is much more noise on the GPS signal the correct bridge frequencies can be still be identified from the data.

Time (seconds)	Possible Modes	GPS	Accelerometer
12.8	1.72	0	2
	1.80	4	2
25.6	1.72	2	2
	1.76	2	2
	1.80	0	0
38.4	1.72	3	3
	1.74	1	1
	1.77	0	0
	1.80	0	0
51.2	1.70	1	1
	1.72	1	2
	1.74	1	1
	1.76	0	0
	1.78	1	0
	1.80	0	0

Table 6-10 Summary of the results for the first natural frequency for the GPS and accelerometer data for all four peaks of movement.

Time (seconds)	Possible Modes	GPS	Accelerometer
10	1.70	0	0
	1.80	4	4
20	1.70	1	0
	1.75	3	4
	1.80	0	0
30	1.70	1	0
	1.73	3	4
	1.77	0	0
	1.80	0	0
40	1.70	1	1
	1.73	1	3
	1.75	1	0
	1.78	1	0
	1.80	0	0

Table 6-11 Summary of the results for the first natural frequency for the GPS and accelerometer data for all four peaks of movement.

Table D–17 and Table D–18 in Appendix D contain data from time periods where there were small movements of the bridge due to cyclist or walkers. Table D–17 shows

a first vibration frequency of between 1.83 and 1.90 Hz, which is very different from the results seen in Table 6-10 and Table 6-11 above. This shows the importance of selecting data where only the natural decay of the bridge is present in the signal and no other forces are affecting the results from the DFT.

Table D–18 at point 6 does not contain a dominant part of the first natural frequency in its time series signal. The first frequency detected is over 2 Hz, which is likely to be the second natural frequency (see section 6.5.2.2). This shows that different frequencies are dominant at different times throughout the session and also that other frequencies are excited more by different movement on the bridge.

6.5.2.2. Second and Third Natural Frequencies

The second and third natural frequencies are harder to distinguish from the results shown in Appendix D. The graphs for 30 seconds of GPS and accelerometer data are shown in Figure 6-34 to Figure 6-41 below. The first thing that is immediately obvious from the graphs is the magnitude of the first natural frequency (which is at 1.73 Hz in all but one case), as these are very different for the GPS and accelerometer data. The graphs of the GPS data show the amplitude of the first frequency to be between 0.2 and 0.3, whereas the accelerometers graphs show the first frequency amplitude to be between 2.5 and 3.5. This shows that the magnitude of the first natural frequency is a lot higher in the accelerometer data than in the GPS. This will affect the identification of the second and third frequencies. In the GPS data, the magnitudes of the second and third DFTs are just smaller than the magnitude of the first DFT, whereas with the accelerometer, the magnitude of the first frequency is always considerably higher than the magnitudes of the other two DFTs.

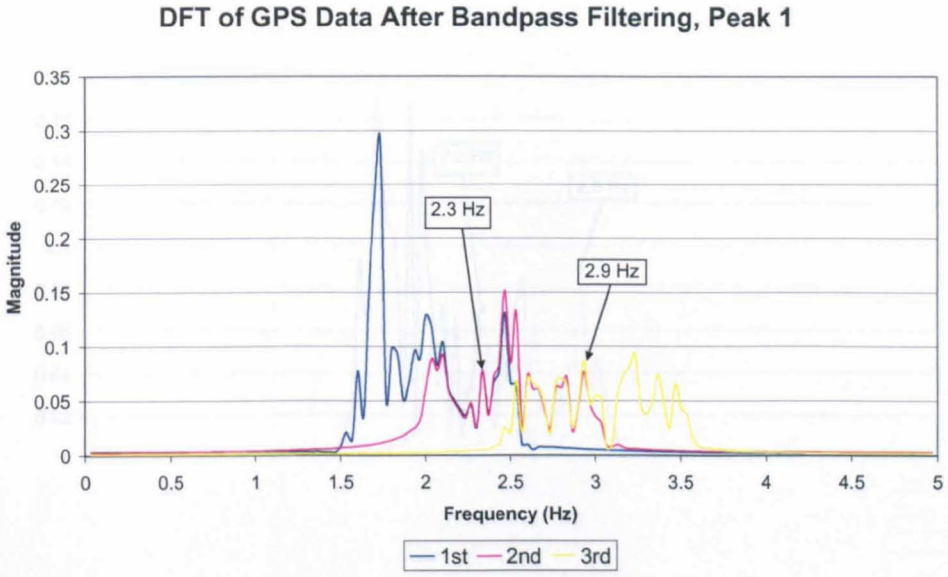

Figure 6-34 DFT of GPS data after bandpass filtering for peak 1. 30 seconds of data (300 samples) are used.

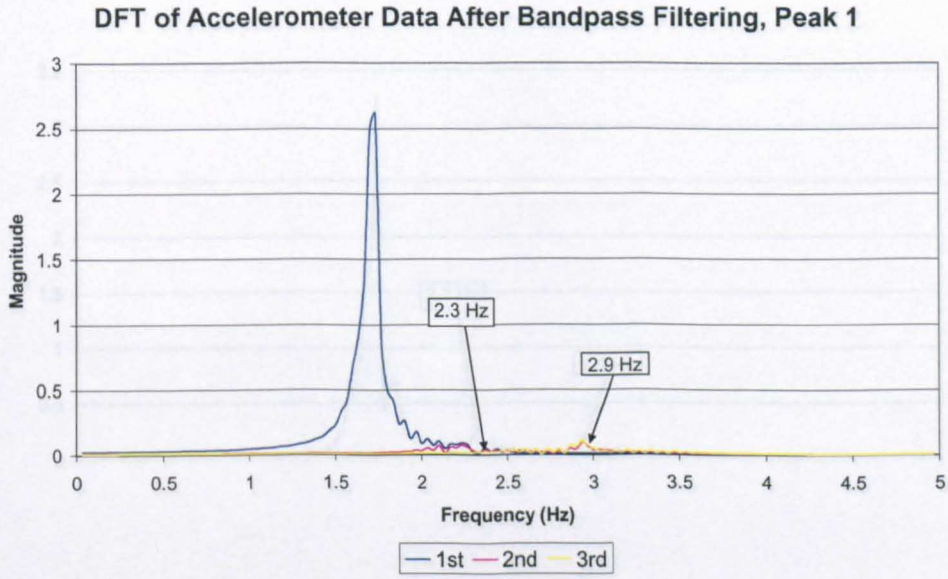

Figure 6-35 DFT of accelerometer data after bandpass filtering for peak 1. 30 seconds of data (2400 samples) are used.

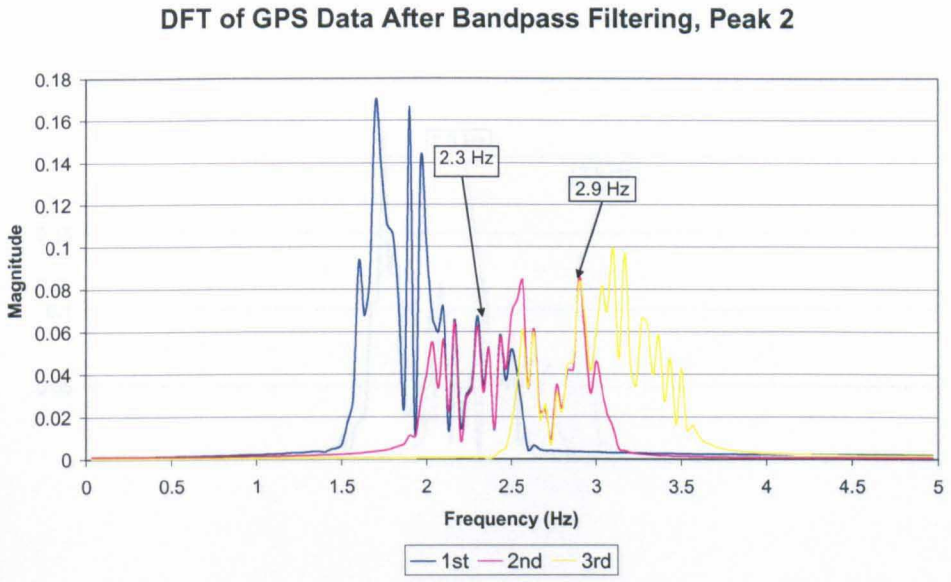

Figure 6-36 DFT of GPS data after bandpass filtering for peak 2. 30 seconds of data (300 samples) are used.

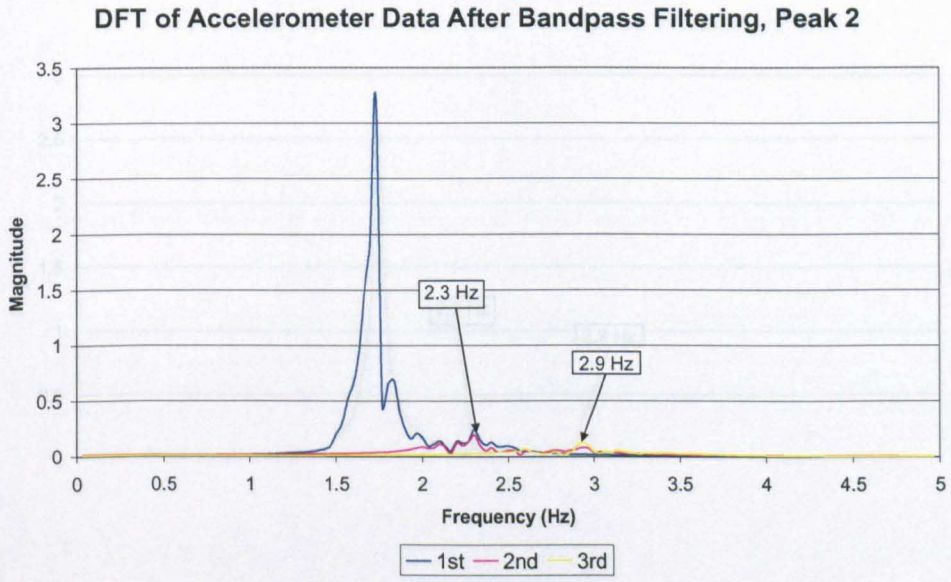

Figure 6-37 DFT of accelerometer data after bandpass filtering for peak 2. 30 seconds of data (2400 samples) are used.

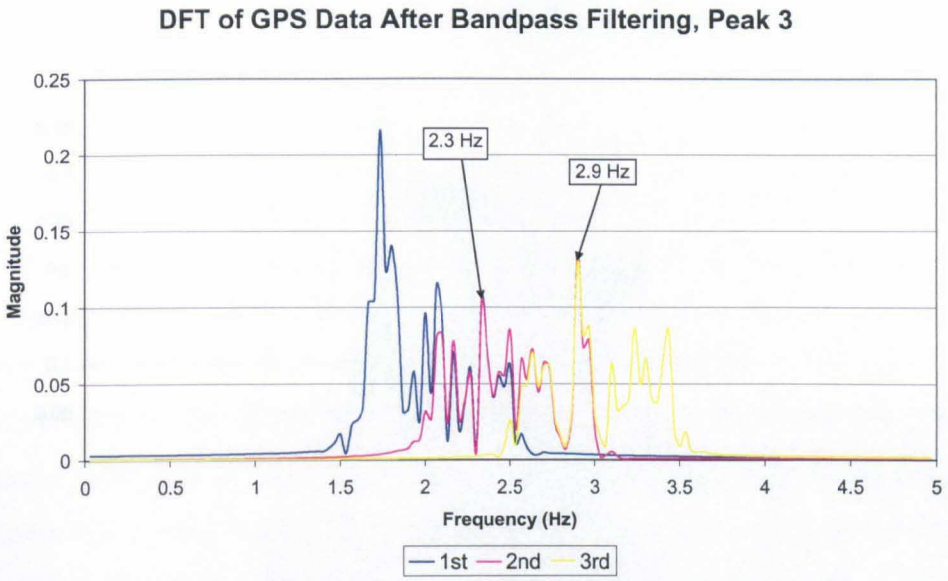

Figure 6-38 DFT of GPS data after bandpass filtering for peak 3. 30 seconds of data (300 samples) are used.

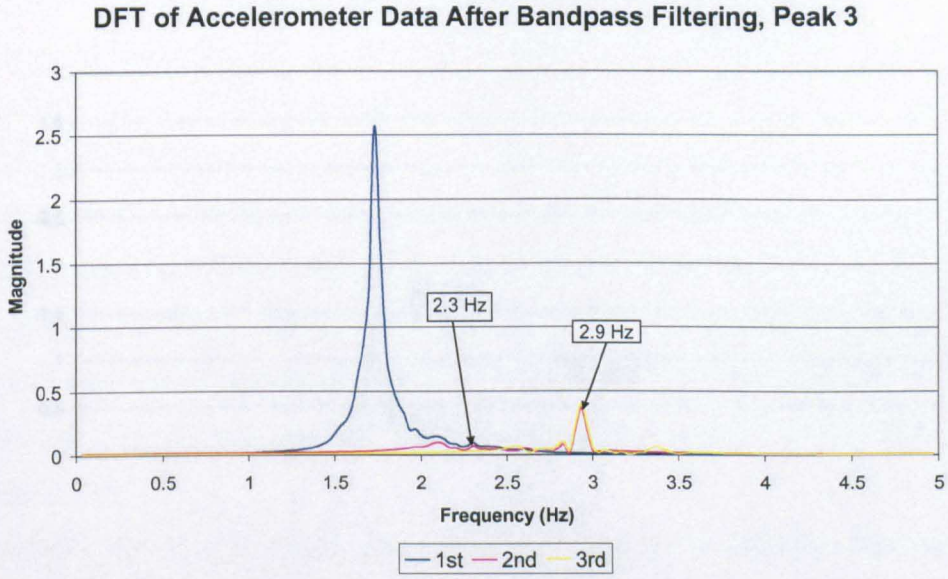

Figure 6-39 DFT of accelerometer data after bandpass filtering for peak 3. 30 seconds of data (2400 samples) are used.

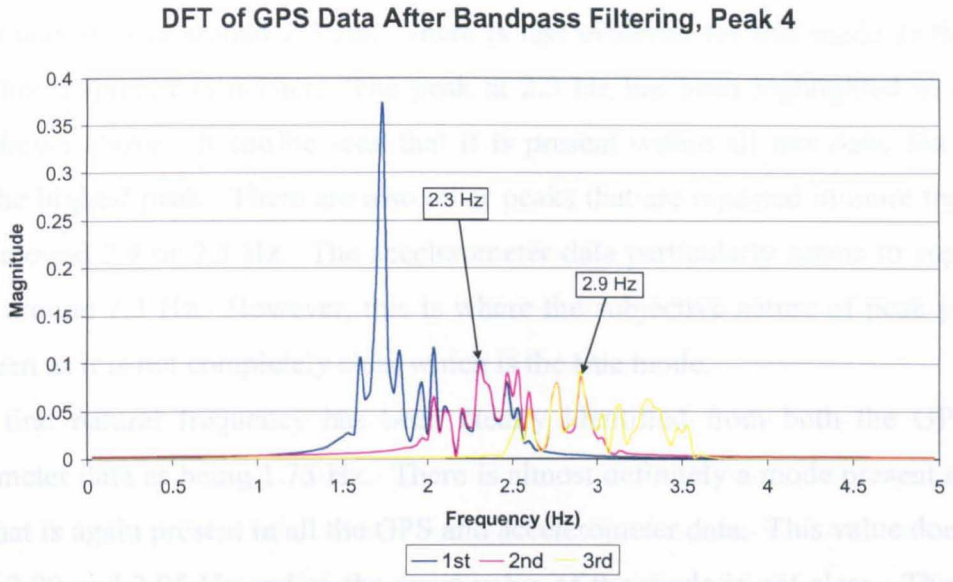

Figure 6-40 DFT of GPS data after bandpass filtering for peak 4. 30 seconds of data (300 samples) are used.

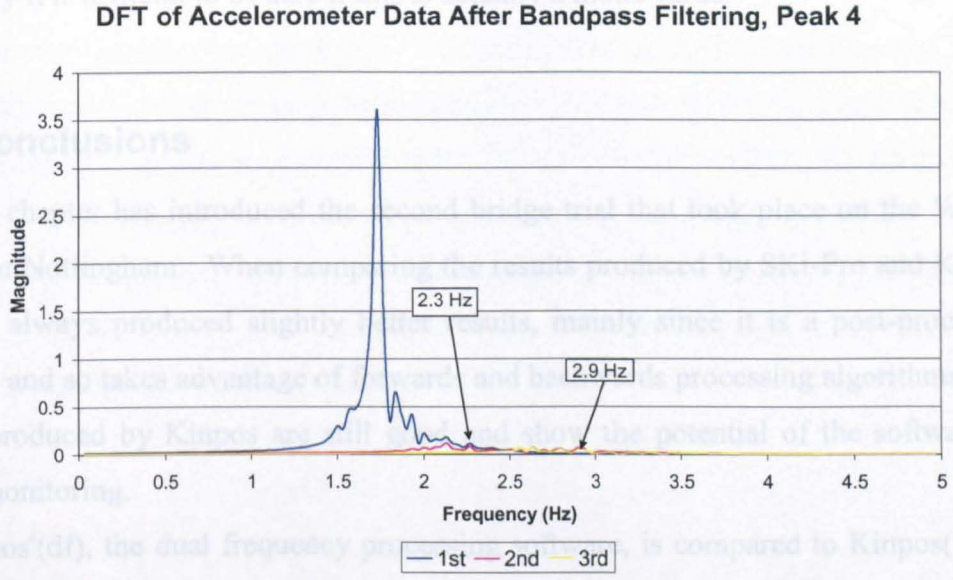

Figure 6-41 DFT of accelerometer data after bandpass filtering for peak 4. 30 seconds of data (2400 samples) are used.

By looking at Table D–1 to Table D–16 in Appendix D there is sufficient evidence to suggest that there is a mode located around 2.9 Hz. This number is repeated a lot of times in both the GPS and accelerometer data. The value does vary between 2.90 and 2.95 Hz, but could be considered to be the same mode that is being identified. In the graphs above, it can be seen that there is a peak around 2.9 Hz in all the graphs even if it is not the highest peak (as is the case in both Figure 6-34 and Figure 6-36). So although all the tables in Appendix D do not identify the highest peak being at 2.9 Hz, this peak is still present in the data.

It is also possible that there is a mode present within both the GPS and accelerometer data at around 2.3 Hz. There is less evidence for this mode as the data around this frequency is noisier. The peak at 2.3 Hz has been highlighted in all the graphs shown above. It can be seen that it is present within all this data, but is not always the highest peak. There are also other peaks that are repeated in more than one data set around 2.4 or 2.5 Hz. The accelerometer data particularly seems to support a mode at around 2.3 Hz. However, this is where the subjective nature of peak picking can be seen as it is not completely clear which is the true mode.

The first natural frequency has been clearly identified from both the GPS and accelerometer data as being 1.73 Hz. There is almost definitely a mode present around 2.9 Hz that is again present in all the GPS and accelerometer data. This value does vary between 2.90 and 2.95 Hz and so the exact value of the mode is not clear. There is a possible mode also present at 2.3 Hz, but since particularly the GPS is noisy around this frequency it is difficult to be sure if this is actually a mode value.

6.6. Conclusions

This chapter has introduced the second bridge trial that took place on the Wilford Bridge in Nottingham. When comparing the results produced by SKi-Pro and Kinpos, SKi-Pro always produced slightly better results, mainly since it is a post-processing software and so takes advantage of forwards and backwards processing algorithms. The results produced by Kinpos are still good and show the potential of the software for bridge monitoring.

Kinpos^{i}(df), the dual frequency processing software, is compared to Kinpos(sf) for the results from the May 2003 bridge trial. Kinpos^{i}(df) resolved the integer ambiguities to the wrong values, during some intervals, for all three dual frequency bridge sites, which leads to erroneous coordinates in the positioning solutions. Kinpos^{i}(df) produces good results only in situations where there are six or more satellites. Kinpos(sf) is able to produce the correct positioning solutions, even in cases where there are only four or five satellites. Due to obstructions in a bridge environment, the number of satellites is likely to fall to five or below on numerous occasions and Kinpos(sf) can cope in these situations.

When comparing the time series on two consecutive days from the same bridge sites, it was discovered that some bridge sites had very low day to day correlations.

Adaptive filtering could not be used to remove the multipath from these sites with the low correlation. It was discovered that even at bridge sites with high day to day correlations, the adaptive filtering algorithms did not remove the entire multipath signature. So, moving average filters of 10 samples were used to remove the multipath signatures from the data with good results.

The correlations between bridge sites on the same day, was also investigated. Bridge sites with an open view of the sky had high correlations with each other, while sites that were next to the cables had low correlations with all other bridge sites.

A further bridge trial, with just one rover receiver located at Bg06, was undertaken to see if results for this high multipath site could be improved by using a choke ring antenna. Horizontal positioning results and double difference residuals showed that a more precise solution could be achieved with a choke ring antenna. However the results were not conclusive since the movement of the bridge on the two separate days could not be taken into account.

Frequency identification using FFTs was undertaken on the May 2003 results for the GPS receiver and accelerometer located at bridge site Bg09. The first natural frequency of the Wilford Bridge has been identified as 1.73 Hz by both the GPS and accelerometer data. A further frequency is certainly present at 2.9 Hz and there is possibly another frequency around 2.3 Hz. It was not possible to identify higher frequency bridge modes with the 10 Hz GPS data. For the identification of higher frequency bridge modes of the Wilford Bridge see Chapter 9.

7. Long Bridge Trials – Humber Bridge

7.1. Introduction

The Humber Bridge in Hull crosses the Humber estuary and has the third largest span of any suspension bridge in the world (Virola 2003). It has four lanes of traffic crossing the 1,410m main span and the 280m and 530m side spans. It was opened to the public in 1981 and at the time was the world's longest single span suspension bridge (The Humber Bridge Board 2001). This long bridge provides many different challenges for monitoring compared to the short span Wilford Bridge, which has been the subject of Chapters 4 and 6.

This chapter focuses on two particular trials that were conducted on the Humber Bridge. Section 7.2 introduces the first trial conducted, which took place in February 1998 and Section 7.3 outlines the results for this trial. The second trial, which was conducted in March 2004, is introduced in Section 7.4, while the results for this trial are discussed in Section 7.5. Conclusions that can be drawn from this chapter are given in Section 7.6.

7.2. Humber Bridge Trial 1 – February 1998

The first trial discussed in this chapter, which has previously been discussed in Chapter 3, was conducted on the late evening/early morning of 15/16 February 1998. This trial took place before work on this thesis had begun, but data from the trial was made available to the author for analysis. Many papers have been written about this trial and the interested reader is directed to Brown et al. (1999) and Roberts et al. (1999) for more information. The data from this trial was used during the software

development stages of this research and is included here as an initial investigation into the precision achievable with the new single frequency processing software.

The approximate layout of the receivers along the bridge can be seen in Figure 7-1 below. There were four Ashtech ZXII dual frequency GPS receivers located on the bridge and one used as a reference station, all measuring at a 5 Hz data rate. Also two single frequency Ashtech GG24 GPS and GLONASS receivers were used in the trial, one as a reference and one as a rover at the mid span of the bridge. The reference receivers were both located on top of the Humber Bridge Board building, which is very near to the toll booths at the northern end of the bridge (Figure 7-9). This chapter will only be concerned with processing the data from the Ashtech ZXII dual frequency receivers. For more information about the processing of the data from the Ashtech GG24 GPS and GLONASS receivers, the interested reader is referred to Young (1998).

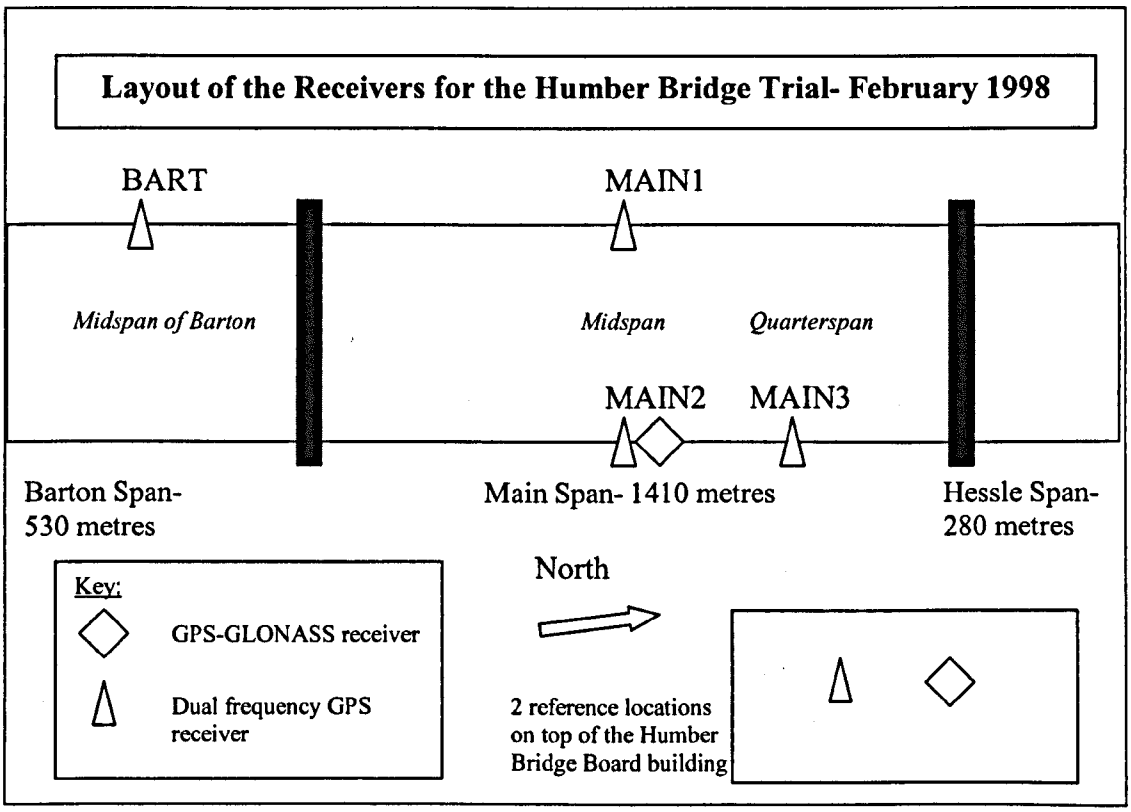

Figure 7-1 The layout of the receivers on the Humber Bridge during the trial conducted in February 1998 (not to scale).

The receivers were strategically placed so they could measure the largest bridge deflections and also compare the deflections on the main span and the Barton side span. During the trial the southbound bridge traffic was stopped completely, but it was not possible to stop the northbound traffic. However, the traffic flow in the northbound

direction was very light at the time the trial was conducted (1am). Five fully laden lorries each weighing around 32 tons, with a combined weight of around 160 ton, were hired in for the trial.

The lorries were made to cross the bridge in various configurations to force the bridge displacement. In the first configuration all the lorries travelled together southbound on the eastern side of the bridge at an approximate speed of 30 km/h. The second configuration consisted of all five lorries travelling together on the western side of the bridge in a northbound direction travelling at the same speed. For the third run, two lorries started at the Barton end of the bridge and another two lorries started at the Hessle end. The vehicles were then driven to the middle of the main span and they remained there for about five minutes as a static approximately symmetric load.

7.3. Results 1

7.3.1. Kinpos Compared to SKi-Pro and Ambiguity Resolution

Chapter 5 discusses the development of the single frequency processing software as part of Kinpos. Before the new ambiguity resolution routines for deformation applications were added, the original method of ambiguity resolution, which will be referred to as LAMBDA^{orig}, was taking on average been 10 and 20 minutes to resolve the ambiguities. In the section below, the time taken to resolve the integer ambiguities with the new deformation routines, referred to here as LAMBDA^{def}, will be compared to the old routines, to show how much improvement has been achieved.

The data from all four dual frequency bridge sites (MAIN1, MAIN 2, MAIN3 and BART) were processed as dual frequency in SKi-Pro and as single frequency in Kinpos. In Kinpos each site was processed twice, once using the LAMBDA^{orig} method of ambiguity resolution and once using the LAMBDA^{def} method, to investigate how much improvement had been achieved with the LAMBDA^{def} method. The results of the dual frequency data processed in SKi-Pro and the single frequency data processed in Kinpos using the LAMBDA^{def} method of ambiguity resolution can be seen in Figure 7-2 to Figure 7-5 below

Figure 7-2 shows the vertical displacement of BART, which was the GPS receiver located on the mid point of the Barton side span of the bridge. For the LAMBDA^{orig}

method of ambiguity resolution, it took 13 minutes and 35 seconds to resolve the ambiguities for the first time. After that the ambiguities stayed fixed for the whole of the observation session. For LAMBDA^{def}, ambiguity resolution took 0.4 seconds and then the ambiguities also remained fixed for the rest of the observation session. So, this is a large improvement of around 13 minutes and 35 seconds. It can be seen from Figure 7-2 that the results produced by the LAMBDA^{def} method in Kinpos match well with the results produced by SKi-Pro. The shape of the movement produced by both processing software is the same for BART; however the results produced for the other bridge sites are not as good.

Figure 7-3 shows the vertical displacement of MAIN1 which was the bridge site located on the western mid point of the main span. For LAMBDA^{orig}, initial ambiguity resolution of MAIN1 took 17 minutes and 29 seconds. The ambiguities then stayed resolved for 12 minutes and 42 seconds, before becoming unfixed. There was no further ambiguity resolution for the remaining 11 minutes and 49 seconds of the observation session. LAMBDA^{def} resolved the initial ambiguities in 2 minutes and 45 seconds. The ambiguities were then lost after 4 minutes and 16 seconds and then it took a further 6 minutes and 4 seconds to re-resolve the ambiguities for the second time. There was a brief session of 34 seconds where ambiguities were lost and resolved again. Apart from these times, the ambiguities were fixed for the whole of the observation session. From these time measurements it can be observed that there was a large improvement in the ambiguity resolution with LAMBDA^{def} compared to LAMBDA^{orig}.

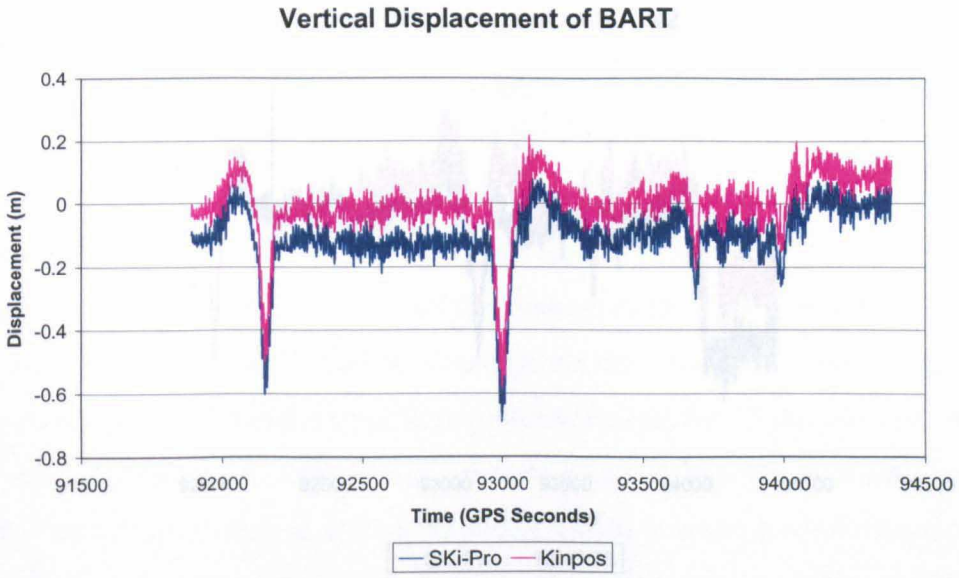

Figure 7-2 The vertical displacement for BART produced by processing the results as single frequency in Kinpos and as dual frequency in SKi-Pro for 16th February. The SKi-Pro results are offset from 0 by -0.1m.

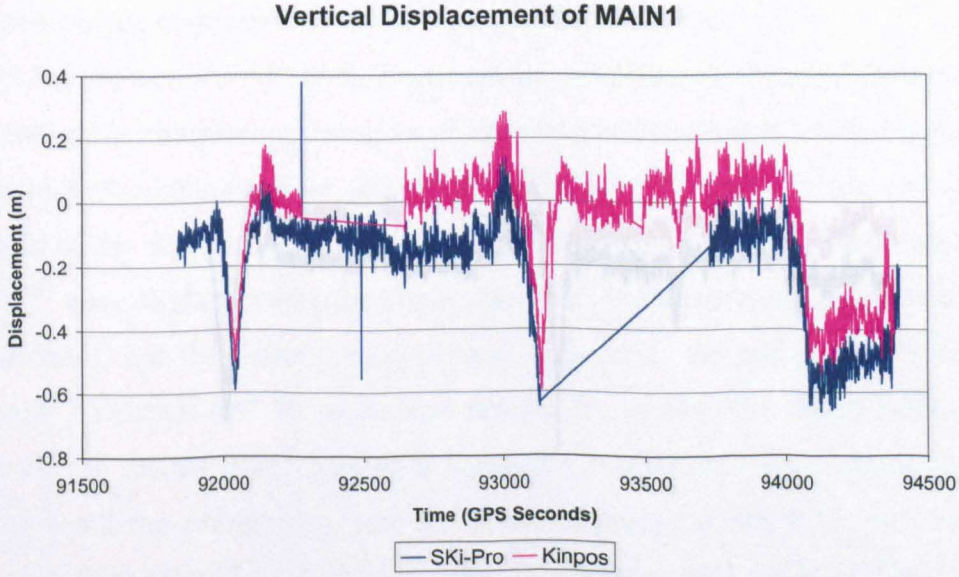

Figure 7-3 The vertical displacement for MAIN1 produced by processing the results as single frequency in Kinpos and as dual frequency in SKi-Pro for 16th February. The SKi-Pro results are offset from 0 by -0.1m.

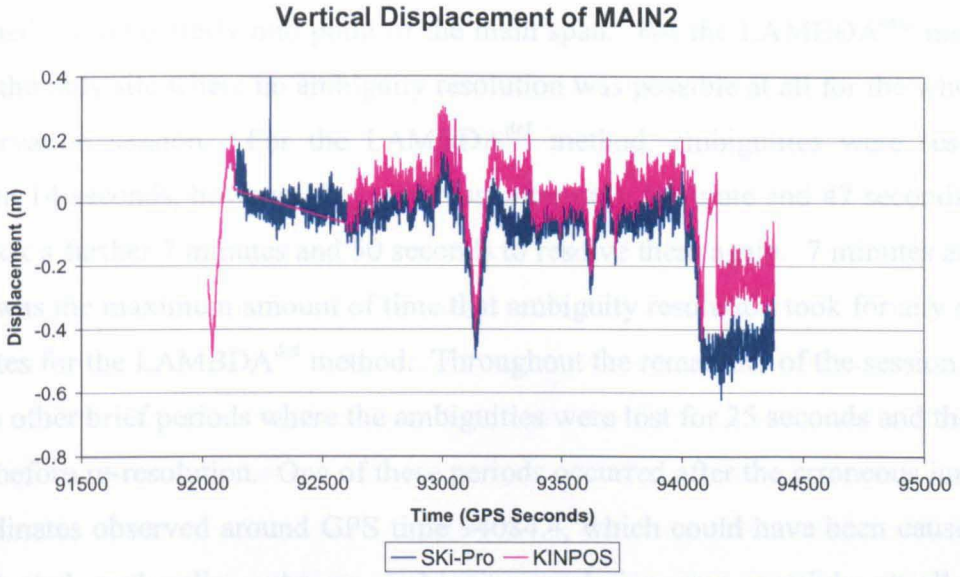

Figure 7-4 The vertical displacement for MAIN2 produced by processing the results as single frequency in Kinpos and as dual frequency in SKi-Pro for 16th February. The SKi-Pro results are offset from 0 by -0.1m.

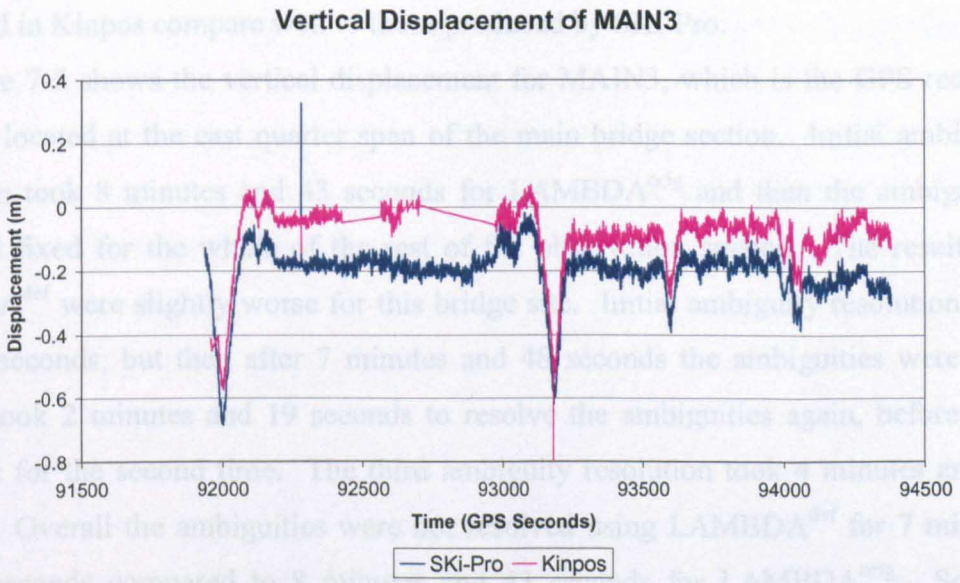

Figure 7-5 The vertical displacement for MAIN3 produced by processing the results as single frequency in Kinpos and as dual frequency in SKi-Pro for 16th February. The SKi-Pro results are offset from 0 by -0.1m.

The results produced by SKi-Pro for MAIN1 have a period of 9 minutes and 58 seconds, starting at GPS time 93131.8, where no ambiguity resolution was possible for the dual frequency data. Throughout this time the LAMBDA^{def} method has resolved ambiguities for the single frequency data and so is able to produce a precise carrier phase solution. This is one example of a situation where Kinpos actually produces better results that SKi-Pro.

The vertical displacement of MAIN2 can be seen in Figure 7-4. This GPS receiver was located on the easterly mid point of the main span. For the LAMBDA^{orig} method, this was the only site where no ambiguity resolution was possible at all for the whole of the observation session. For the LAMBDA^{def} method, ambiguities were resolved initially in 14 seconds, however they were lost after only 1 minute and 47 seconds, and then it took a further 7 minutes and 50 seconds to resolve them again. 7 minutes and 50 seconds was the maximum amount of time that ambiguity resolution took for any of the bridge sites for the LAMBDA^{def} method. Throughout the remainder of the session there were two other brief periods where the ambiguities were lost for 25 seconds and then 16 seconds before re-resolution. One of these periods occurred after the erroneous jump in the coordinates observed around GPS time 94084.4, which could have been caused by an undetected cycle slip. As no ambiguity resolution was possible at all with LAMBDA^{orig}, a great improvement has been observed by introducing the LAMBDA^{def} method for this bridge site. When ambiguities are resolved the results for MAIN2 processed in Kinpos compare well to those produced by SKi-Pro.

Figure 7-5 shows the vertical displacement for MAIN3, which is the GPS receiver that was located at the east quarter span of the main bridge section. Initial ambiguity resolution took 8 minutes and 43 seconds for LAMBDA^{orig} and then the ambiguities remained fixed for the whole of the rest of the observation session. The results for LAMBDA^{def} were slightly worse for this bridge site. Initial ambiguity resolution took only 30 seconds, but then after 7 minutes and 48 seconds the ambiguities were lost. Then it took 2 minutes and 19 seconds to resolve the ambiguities again, before they were lost for the second time. The third ambiguity resolution took 4 minutes and 32 seconds. Overall the ambiguities were not resolved using LAMBDA^{def} for 7 minutes and 21 seconds compared to 8 minutes and 43 seconds for LAMBDA^{orig}. So, for MAIN3 there is only a small improvement when the LAMBDA^{def} method is used. Again, when ambiguities are resolved the results produced by Kinpos compare well to those produced by SKi-Pro.

Overall the introduction of the LAMBDA^{def} method has improved the amount of single frequency ambiguity resolution for these four bridge sites during this trial. However, there are still some times where there are large ambiguity outages even with LAMBDA^{def}, the largest of these being at site MAIN2 for 7 minutes and 50 seconds. During these outages no positioning solutions can be extracted from the data and so no information about the bridge movement is possible. The dual frequency data processed

in SKi-Pro does have one large outage of coordinates due to no ambiguity resolution on bridge site MAIN1. However, generally the dual frequency data has much better solutions that the single frequency, due to considerably more ambiguity resolution.

In Chapter 3, Section 3.5 the work of Johns (2000) is discussed. Initial trials with single frequency receivers reveal that 10 Hz data collection was not possible, due to a high percentage (30%) of missing data epochs and the amount of time ambiguity resolution took was not acceptable. For the Humber Bridge trial conducted in 1998, similar findings about single frequency receivers may have been concluded.

The Ashtech ZXII dual frequency receivers used for this trial had a maximum data rate of 5 Hz. Most of the receivers did not have any problems with missing data epochs. However 6.4% of the epochs were missing at the reference receiver Ref1 and 1.1% of the epochs were missing at MAIN3. The missing data at Ref1 would have affected all the solutions, as it was used as a reference for all of them.

To overcome the problems of missing data at the stationary Ref1 a simple interpolation routine was written. The missing data was not caused by cycle slips and the receiver kept lock on all the satellites even though the data was not present at that epoch. Assuming that the increment in carrier phase and pseudorange values are the same between adjacent epochs, the carrier phase could be approximated by equation (7-1) below. The same equation could also be used to approximate the pseudorange values.

$$\Phi_k = \frac{\Phi_{k-1} + \Phi_{k+1}}{2} \qquad (7\text{-}1)$$

where,

Φ_k is the carrier phase value at time k

Interpolation of this nature could only be undertaken because Ref1 was stationary and so the increment in the pseudorange and the carrier phase values is expected to be the same between epochs. This interpolation was not carried out with the data from MAIN3. The missing epochs at MAIN3 could be one explanation of why the amount of ambiguity resolution does not improve very much when LAMBDA^{def} is used.

The results from the bridge trial in March 2004, discussed in Section 7.5, show obvious improvement in the GPS receivers in the six years from the 1998 Humber Bridge trial.

7.3.2. Traffic Induced Bridge Movement

Section 7.2 introduces the three configurations that the five fully laden lorries travelled in across the bridge. This section looks at how these configurations affected the bridge movement during the trial. Figure 7-6 shows the vertical displacement shown by the two GPS receivers located on the west side of the bridge at BART and MAIN1, while Figure 7-7 shows the vertical displacement of MAIN2 and MAIN3 on the east side of the bridge. A number of interesting bridge features can be deduced from these Figures.

In Figure 7-6, BART is located on the Barton side span, while MAIN1 is located at the mid point of the main span. It is interesting to see that the amplitude of the displacements of BART and MAIN1 are very similar for the first two displacements in each time series. The other interesting feature of the graph is the counterbalancing effect which seems to be produced between the main deck and the Barton side span. At the beginning of the graph when the lorries are on the main span, the Barton side span is pulled upwards and then when the lorries move onto the side span, the main span is pulled upwards. This occurs again when the lorries cross the bridge for the second time. When the lorries remain stationary at the mid span of the main deck, the Barton span is once again pulled upwards. This counterbalancing effect is caused by the cables which cross over the towers and connect the two bridge decks.

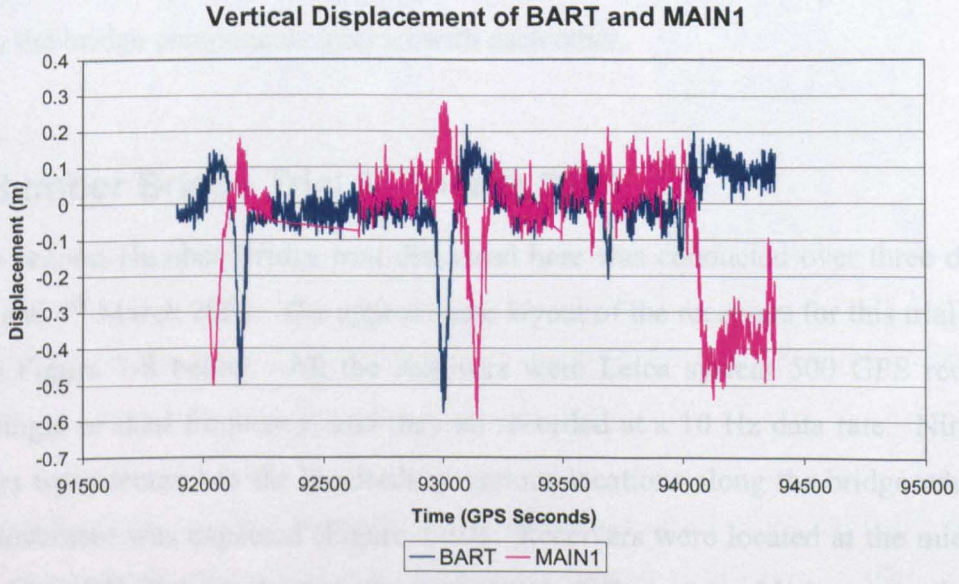

Figure 7-6 The vertical displacement of BART and MAIN1 during the February bridge trial. Both receivers were located on the west side of the bridge.

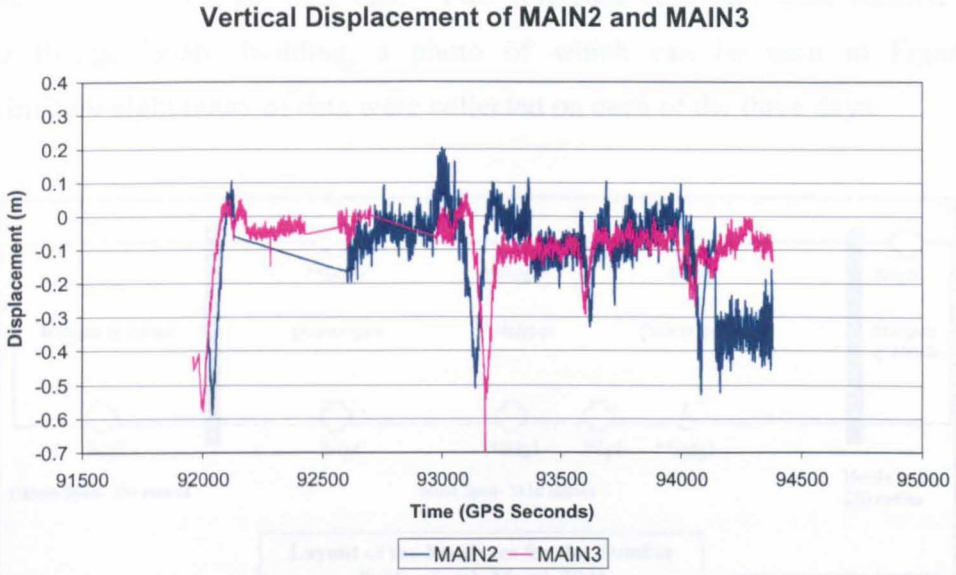

Figure 7-7 The vertical displacement of MAIN2 and MAIN3 during the February bridge trial. Both receivers were located on the east side of the bridge.

Looking at Figure 7-6 and Figure 7-7, it can be seen that the first time the lorries cross the bridge the west bridge sites displace by about 50cm, while the east bridge sites displace by about 60cm, since the lorries are on the eastern carriageway during this crossing. On the second crossing, the lorries are on the western carriageway and it is the western bridge sites that displace by about 60cm this time, while the eastern sites by only 50cm. As well as causing the bridge to displace, the movement of lorries is also causing the bridge to tilt.

So, although the single frequency data had problems with ambiguity resolution outages, it was still possible to gain useful information about the bridge movement and the way the bridge components interact with each other.

7.4. Humber Bridge Trial 2 – March 2004

The second Humber Bridge trial discussed here was conducted over three days on 1st, 2nd and 4th March 2004. The approximate layout of the receivers for this trial can be seen in Figure 7-8 below. All the receivers were Leica system 500 GPS receivers, either single or dual frequency, and they all recorded at a 10 Hz data rate. Nine GPS receivers were secured to the handrails at various locations along the bridge where the most movement was expected (Figure 7-10). Receivers were located at the mid spans of Hessle and Barton to compare the movement of these two side spans to the main span. Four triaxial accelerometers, located at the points marked with ** in Figure 7-8,

recorded data at a 100 Hz data rate. Two reference receivers were located on the Humber Bridge Board building, a photo of which can be seen in Figure 7-9. Approximately eight hours of data were collected on each of the three days.

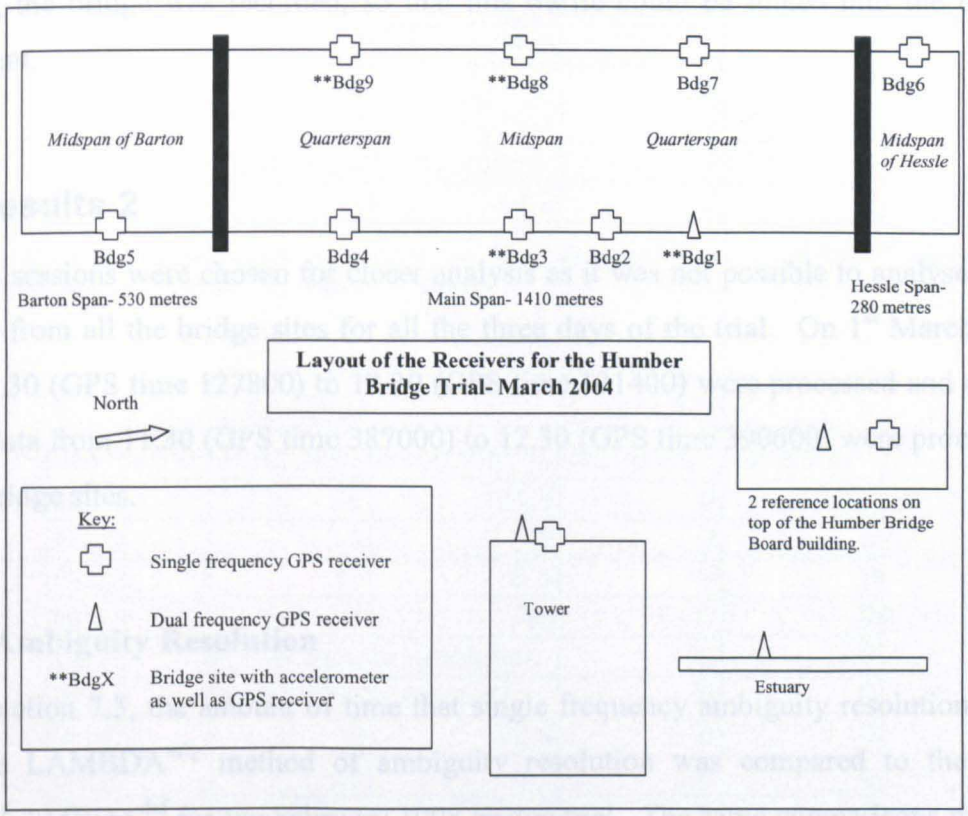

Figure 7-8 The layout of the receivers on the Humber Bridge during the trial conducted in March 2004 (not to scale).

Figure 7-9 The two reference receivers located on top of the Humber Bridge board building, with the Humber Bridge in the background.

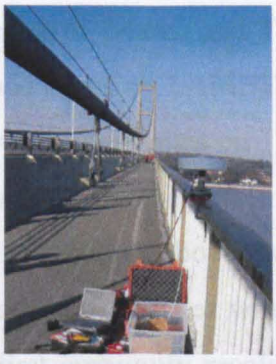

Figure 7-10 Antenna located at Bdg3, secured to the handrails of the bridge.

Another project at the IESSG was investigating the effect of tropospheric delay on GPS measurements, when the GPS receivers are located at different heights. For this project, receivers were located at the top of one of the 155.5m high towers and also

below the bridge in the estuary area. For more information about the tropospheric delay estimation project, the interested reader is referred to Clark (2003).

This trial measured the movement of the bridge under normal traffic loading. The bridge was left open and all normal traffic allowed across it. A video of the vehicles crossing the bridge was recorded, so that this traffic could be linked into the bridge movement.

7.5. Results 2

Two sessions were chosen for closer analysis as it was not possible to analyse fully the data from all the bridge sites for all the three days of the trial. On 1st March data from 11.30 (GPS time 127800) to 12.30 (GPS time 131400) were processed and on 4th March data from 11.30 (GPS time 387000) to 12.30 (GPS time 390600) were processed for all bridge sites.

7.5.1. Ambiguity Resolution

In Section 7.3, the amount of time that single frequency ambiguity resolution took with the LAMBDA^{orig} method of ambiguity resolution was compared to the new method LAMBDA^{def} for the February 1998 bridge trial. The same comparisons will be made for the March 2004 bridge trial for all nine bridge sites, on both 1st and 4th March. Table 7-1 shows the amount of time until the first ambiguity resolution using LAMBDA^{orig} and LAMBDA^{def} methods for all bridge sites on 1st March and Table 7-2 shows the same but for 4th March. The improvements made by using LAMBDA^{def} are evident from both Tables. Using LAMBDA^{orig} there are two bridges sites on 1st March and three on 4th March that have no ambiguity resolution at all for the whole session, which means it is not possible to discover any useful information about the bridge movement from any of these sites. Without taking into account the sites where there was no ambiguity resolution at all, the average time to first ambiguity resolution for LAMBDA^{orig} was 7 minutes 26.7 seconds for 1st March and 9 minutes 28.4 seconds for 4th March.

	LAMBDA^{orig}		LAMBDA^{def}	
1st March	Minutes	Seconds	Minutes	Seconds
Bdg1	5	36.3	0	28.1
Bdg2	no ambiguity resolution		0	40.8
Bdg3	3	54.6	0	0
Bdg4	8	22.8	0	0
Bdg5	17	37.8	0	2.4
Bdg6	2	11.3	0	0
Bdg7	9	39.1	0	31.1
Bdg8	no ambiguity resolution		0	0
Bdg9	4	44.9	0	0

Table 7-1 Time to first ambiguity resolution for the LAMBDA^{orig} and LAMBDA^{def} methods of ambiguity resolution for all bridge sites on 1st March.

	LAMBDA^{orig}		LAMBDA^{def}	
4th March	Minutes	Seconds	Minutes	Seconds
Bdg1	7	34.3	0	0.2
Bdg2	1	40	0	0
Bdg3	15	9.1	0	0
Bdg4	1	40	0	0
Bdg5	no ambiguity resolution		0	0
Bdg6	no ambiguity resolution		0	0
Bdg7	2	42.5	0	0
Bdg8	28	4.7	0	0
Bdg9	no ambiguity resolution		0	0

Table 7-2 Time to first ambiguity resolution for the LAMBDA^{orig} and LAMBDA^{def} methods of ambiguity resolution for all bridge sites on 4th March.

The results for LAMBDA^{def} show great improvements when compared to LAMBDA^{orig}. When using LAMBDA^{def}, there are no bridge sites on either day where ambiguity resolution was not possible. The average time to first ambiguity resolution is 7.5 seconds on 1st March and 0.02 seconds on 4th March.

Further investigations of the ambiguity resolution times after a cycle slip and/or loss of lock were also investigated. For the two days, the overall average time to ambiguity resolution for LAMBDA^{orig} was found to be 7 minutes 24.1 seconds and the maximum amount of time was 28 minutes 4.7 seconds (both results do not take into account the five bridge sites which had no ambiguity resolution at all). For LAMBDA^{def} the overall average time to ambiguity resolution was found to be 8.4 seconds and the maximum amount of time was 41.7 seconds. A huge improvement in the ambiguity resolution times has been achieved by the LAMBDA^{def} method.

These results are also a large improvement on the outcomes achieved in the first Humber Bridge trial in February 1998. For this trial, using LAMBDA[def], the average time to ambiguity resolution was 2 minutes 7.6 seconds and the longest time to ambiguity resolution was 7 minutes 50 seconds. The improvement in ambiguity resolution times for the second Humber Bridge trial in March 2004 cannot be explained by any difference in the processing algorithms used, since these were the same in both cases. Changes and developments in the receiver technology over the six year between trials are likely to be the cause.

Based on the first Humber Bridge trial results, seen in Section 7.3, it would have been concluded that even with the new ambiguity resolution routines, single frequency receivers still had too many coordinate outages when compared to dual frequency receivers. Outages of coordinates, where no ambiguity resolution was possible, of up to 7 minutes and 50 seconds during a bridge trial are not acceptable, especially as this could occur during a period of particular interest. However, with the greatly reduced ambiguity resolution times seen in the second bridge trial, it can now be concluded that using single frequency GPS receivers to measure the movement of large bridges is feasible.

7.5.2. Kinpos Compared to SKi-Pro

There was only one dual frequency receiver located on the bridge for this March 2004 trial, at Bdg1. So, it is only possible to compare the results from Bdg1 when processed in SKi-Pro as dual frequency and in Kinpos as single frequency. The results for Bdg1 on 1st March can be seen in Figure 7-11 and the results on 4th March can be seen in Figure 7-12. It can be seen from both these Figures that overall shape and amplitude of displacements are the same for each software package.

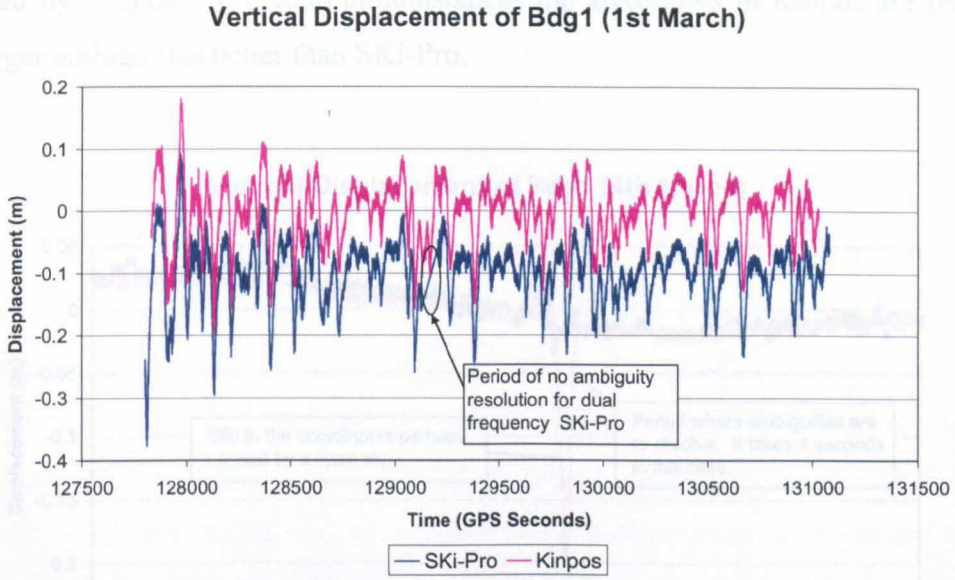

Figure 7-11 The vertical displacement for Bdg1 produced by processing the results in Kinpos and SKi-Pro for 1st March. The SKi-Pro results are offset by -0.1m. Highlighted is the period of 79.4 seconds where there is no ambiguity resolution for SKi-Pro.

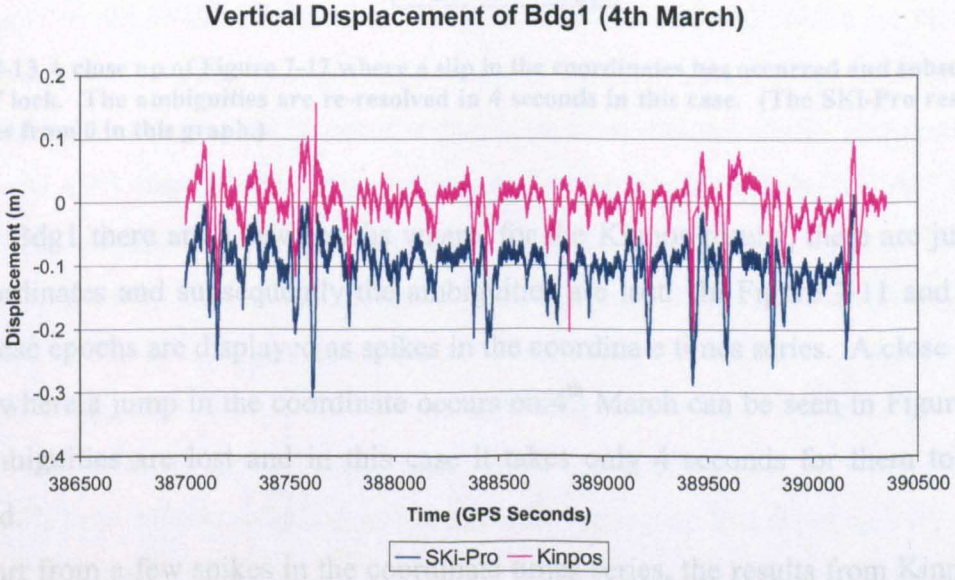

Figure 7-12 The vertical displacement for Bdg1 produced by processing the results in Kinpos and SKi-Pro for 4th March. The SKi-Pro results are offset by -0.1m.

The times series produced by SKi-Pro for Bdg1 on 1st March, which is shown in Figure 7-11, contains a period of 79.4 seconds where there is no ambiguity resolution, starting at GPS time 129125.8 and finishing at 129205.2 (this is highlighted in Figure 7-11). From Section 7.5.1 it has been shown that the longest amount of time it takes for Kinpos to resolve the integer ambiguities at any of the bridge sites is 41.7 seconds. So, this outage of coordinates produced by SKi-Pro is almost twice as long as the longest

produced by Kinpos. In certain circumstances the algorithms in Kinpos are resolving the integer ambiguities better than SKi-Pro.

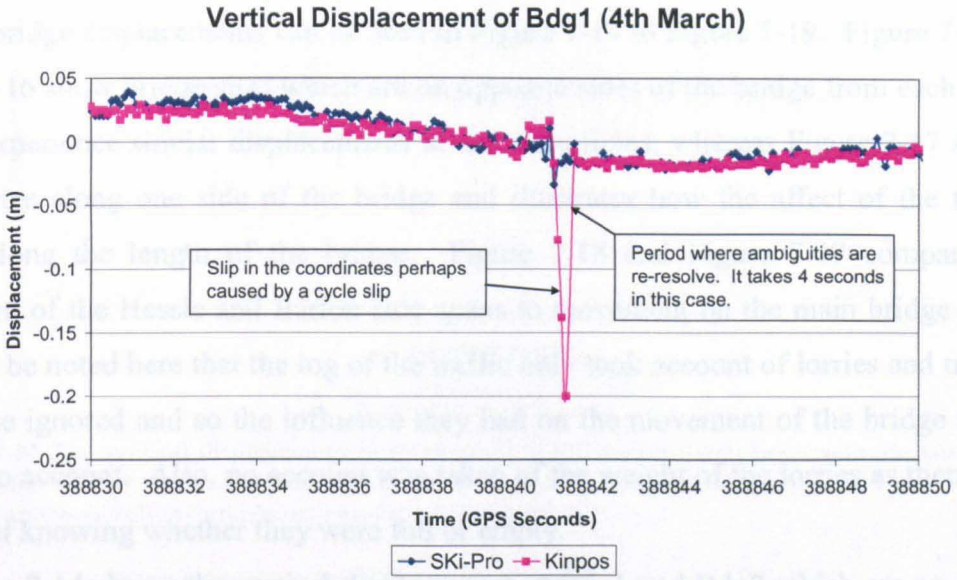

Figure 7-13 A close up of Figure 7-12 where a slip in the coordinates has occurred and subsequently a loss of lock. The ambiguities are re-resolved in 4 seconds in this case. (The SKi-Pro results are not offset from 0 in this graph.)

For Bdg1 there are a few epochs where, for the Kinpos results, there are jumps in the coordinates and subsequently the ambiguities are lost. In Figure 7-11 and Figure 7-12 these epochs are displayed as spikes in the coordinate times series. A close up of a period where a jump in the coordinate occurs on 4th March can be seen in Figure 7-13. The ambiguities are lost and in this case it takes only 4 seconds for them to be re-resolved.

Apart from a few spikes in the coordinate times series, the results from Kinpos and SKi-Pro are almost identical during both observation sessions analysed. This further demonstrates the capability of single frequency receivers to perform as well as dual, when measuring the movements of a long bridge.

7.5.3. Linking the Traffic to the Bridge Movements

In Section 7.3.2 the movement of a set of five lorries in different configurations was compared to the vertical displacements of the bridge. Since the lorries were the only traffic on the bridge and they moved in set arrangements that were recorded, it was easy to see how their movements had effected the Humber Bridge displacements. In this

section, an attempt is made to link the random traffic movement on the bridge, during the March 2004 trial, to the movement of the bridge.

On 4th March, as well as the video of the lorries crossing the bridge, a log of the crossing lorries was taken at Bdg1. The results from this log of the lorries as well as the vertical bridge displacements can be seen in Figure 7-14 to Figure 7-19. Figure 7-14 to Figure 7-16 show bridge sites which are on opposite sides of the bridge from each other and so experience similar displacements at the same times; whereas Figure 7-17 shows bridge sites along one side of the bridge and illustrates how the affect of the traffic moves along the length of the bridge. Figure 7-18 and Figure 7-19 compare the movement of the Hessle and Barton side spans to movement on the main bridge deck. It should be noted here that the log of the traffic only took account of lorries and trucks. Cars were ignored and so the influence they had on the movement of the bridge is not taken into account. Also, no account was taken of the weight of the lorries as there was no way of knowing whether they were full or empty.

Figure 7-14 shows the vertical displacement of Bdg1 and Bdg7 which are on either side of the northern quarter span of the main deck. The log of traffic was taken at Bdg1 and so the displacements should occur at the same time that the traffic was present at this site. At GPS time 389430 three lorries are on the bridge and the last one is just passing Bdg1 and Bdg7. This corresponds to a displacement of both Bdg1 and Bdg7 of about 15cm. At GPS time 389577 there are another three lorries on the bridge which corresponds to the next large displacement of both Bdg1 and Bdg7. A heavy lorry crosses the bridge at GPS time 389748 causing a displacement of similar size as when the three smaller lorries crossed the bridge. There is a displacement of both Bdg1 and Bdg7 at GPS time 389684, which does not seem to correspond to a crossing lorry at all; however a lorry does cross very soon after the displacement, so there could be a slight error when logging the time of the lorry crossing. It was possible that the lorries were miscounted sometimes due to how close they travelled together and how fast they were travelling.

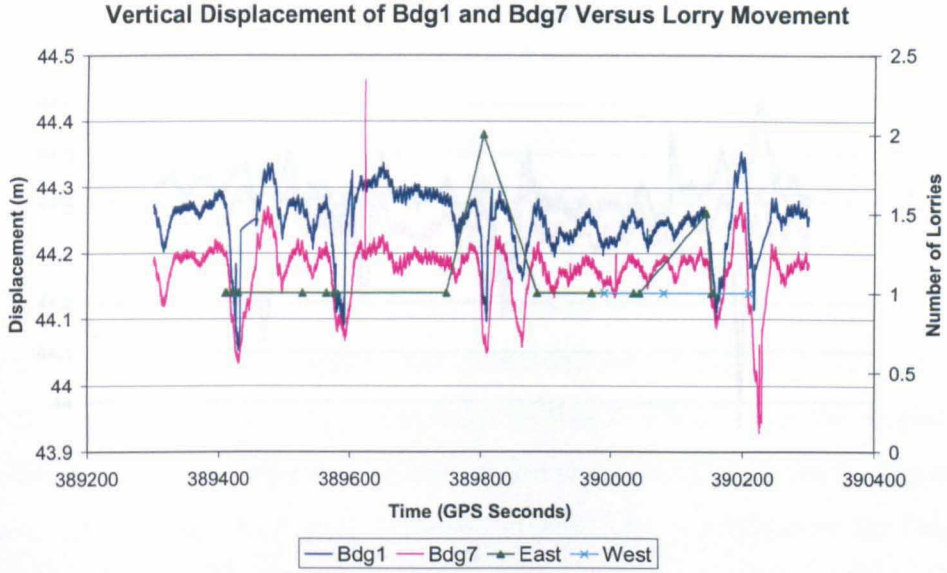

Figure 7-14 The vertical displacement of Bdg1 and Bdg7 linked in with the lorry movement along the Humber Bridge. East refers to the lorries moving along the east side of the bridge from north to south and west refers to the lorries moving from south to north.

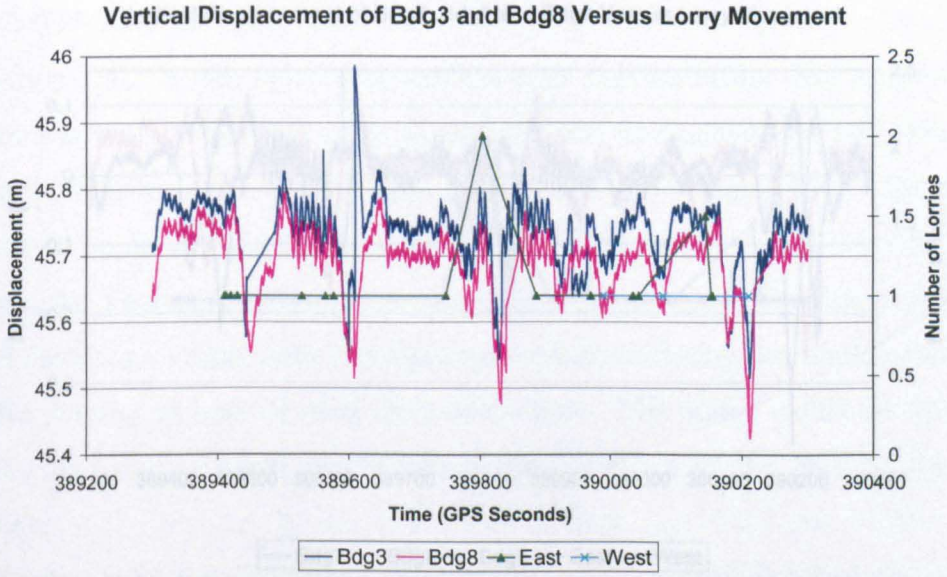

Figure 7-15 The vertical displacement of Bdg3 and Bdg8 linked in with the lorry movement along the Humber Bridge. East refers to the lorries moving along the east side of the bridge from north to south and west refers to the lorries moving from south to north.

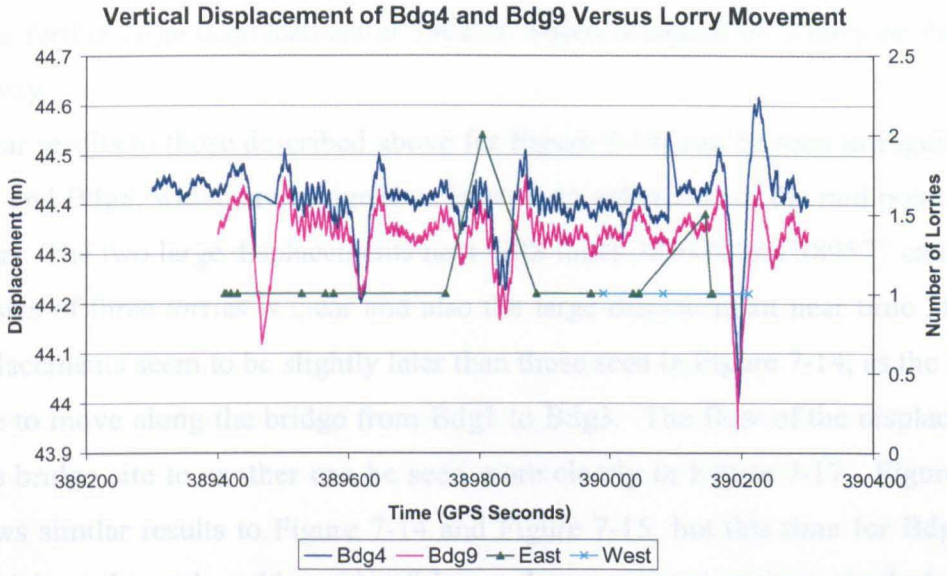

Figure 7-16 The vertical displacement of Bdg4 and Bdg9 linked in with the lorry movement along the Humber Bridge. East refers to the lorries moving along the east side of the bridge from north to south and west refers to the lorries moving from south to north.

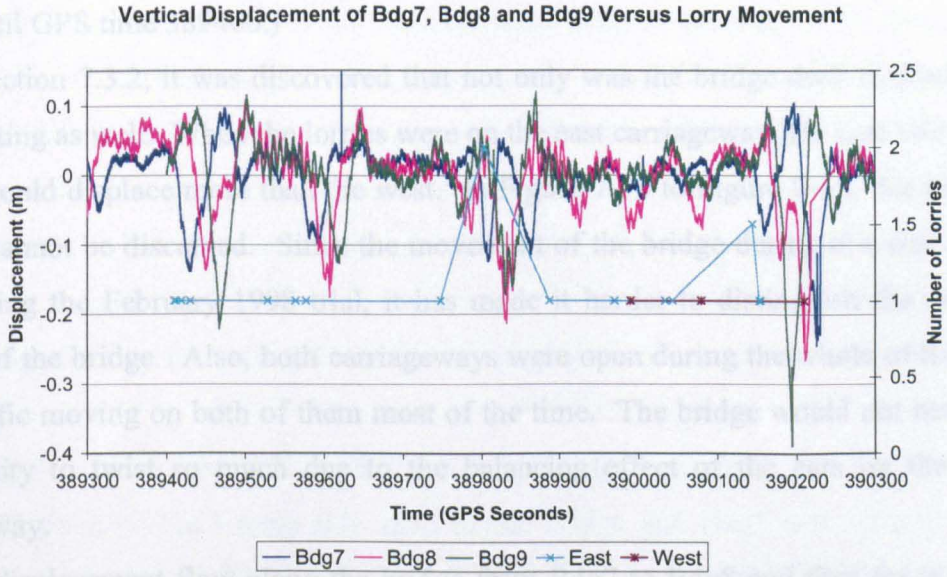

Figure 7-17 The vertical displacement of Bdg7, Bdg8 and Bdg9 linked in with the lorry movement along the Humber Bridge. East refers to the lorries moving along the east side of the bridge from north to south and west refers to the lorries moving from south to north.

Up until this point all lorries have been moving on the east side of the bridge from north to south, and so linking in the lorry movement to the bridge displacement has been relatively straight-forward. However, after GPS time 389866 lorries begin coming from the west as well and the movement of the bridge becomes a little harder to distinguish. It is clear that from GPS time 389866 to around 390150, the bridge displacements are smaller in amplitude, perhaps due to the balancing effects of lorries coming from both ends of the bridge. When the lorries come from both directions it is

much harder to link in the affect of the individual lorries on the movement of the bridge. There is a further large displacement at 390225, which is caused by a lorry on the west carriageway.

Similar results to those described above for Figure 7-14, can be seen in Figure 7-15 for Bdg3 and Bdg8, which are bridge sites located on either side of the mid point of the main span. The two large displacements near GPS times 389430 and 389577 caused by the two sets of three lorries is clear and also the large displacement near time 389748. The displacements seem to be slightly later than those seen in Figure 7-14, as the lorries take time to move along the bridge from Bdg1 to Bdg3. The flow of the displacement from one bridge site to another can be seen more clearly in Figure 7-17. Figure 7-16 also shows similar results to Figure 7-14 and Figure 7-15, but this time for Bdg4 and Bdg9, which are located at either side of the south quarter span of the main deck. (The time series for Bdg9 starts slightly later in Figure 7-16 and Figure 7-17 because an extra download had to be undertaken at this bridge site and the next recording phase did not begin until GPS time 389400.)

In Section 7.3.2, it was discovered that not only was the bridge deck displacing, it was twisting as well. When the lorries were on the east carriageway, the east side of the bridge would displace more than the west. In Figure 7-14 to Figure 7-16, this twisting motion cannot be discerned. Since the movement of the bridge during this trial is less than during the February 1998 trial, it has made it harder to distinguish the twisting motion of the bridge. Also, both carriageways were open during the whole of this trial with traffic moving on both of them most of the time. The bridge would not have had opportunity to twist so much due to the balancing effect of the cars on the other carriageway.

The displacement flow along the bridge from Bdg7 to Bdg8 and then on to Bdg9, can be seen in Figure 7-17. For the first part of the data all the lorries are on the east side of the bridge, moving from north to south. When the first three lorries cross the bridge at time 389430 the displacement is clearly seen at Bdg7, and then it moves along the bridge to Bdg8 and then onto Bdg9, as the lorries move south. It takes roughly 19 seconds for the displacement to move from Bdg7 to Bdg8 and about the same from Bdg8 to Bdg9. The distance between Bdg7 and Bdg8 is the same as the distance from Bdg8 to Bdg9 at 352.5 metres. This corresponds to a lorry speed of approximately 67 km per hour or about 42 miles per hour. The speed limit on the bridge is 50 miles per hour and so this speed is perfectly reasonable for a lorry.

The unusual thing about the movement of the bridge described above is that the displacement is the largest at Bdg9 which is one of the quarter span sites. It would be expected that the largest displacement would be seen at Bdg8, the mid span. However, as only the movement of the lorries is recorded it is uncertain how many other vehicles were on the bridge at the same time. There may have been a large amount of cars on the bridge near Bdg9 at this time causing the bigger displacement.

The displacements caused by the second set of three lorries, at time 389577, clearly moves along the bridge in a similar way to the displacement described above, from north to south. However, this time a slightly larger displacement is observed at Bdg8. At time 389748, a heavy lorry causes the displacement to move along the bridge once again.

From time 389866 to around 390150 there are lorries coming from both the east and west directions and the decrease in amplitude of the displacement is obvious from Figure 7-17 also. Around time 390210 a lone lorry moves on the west side of the bridge from south to north, and causes the displacements seen at the end of the observation period which moves from Bdg9, to Bdg8 and then on to Bdg7.

When the lorries are moving only in one direction, the way the displacements move along the bridge is clear. However, when the lorries are coming from both directions it is much harder to link in their travel to the displacement of the bridge deck, particularly on the main span. It is clear that when lorries are coming from either direction, there is a balancing effect on the main deck and so the displacements observed do not have such large amplitudes.

Figure 7-18 shows the vertical displacement of Bdg6 and Bdg7. Bdg6 was located at the mid point of the Hessle side span of the bridge and Bdg7 was located at the northern quarter span of the main deck; both were on the west side of the bridge. The first thing that is obvious from Figure 7-18 is the difference in amplitude experienced at each site. The usual displacement of Bdg6 is around the 3-5cm level, with the maximum displacement being about 10cm. The usual displacement of Bdg7 is around 10-15cm with the maximum displacement being 25cm. The movement of the first three lorries at time 389430 cause a displacement of Bdg6 which then moves on to Bdg7 and the same occurs for the next three lorries at time 389577. The large lorry at time 389748 seems to only have caused a small displacement at Bdg6.

During the time when there are lorries coming from both the east and west directions, there are still some large displacements visible at Bdg6, specifically at time

390032. This displacement could have been caused by the lorry on the west side of the bridge which passes Bdg1 at time 389990. It is far more likely on this small side span (only 280m), that only one lorry will be on in at any one time, even when the lorries are coming from either direction. The largest displacements of both Bdg6 and Bdg7 are seen at the end of the observation period and are caused by a lorry on the west side of the bridge.

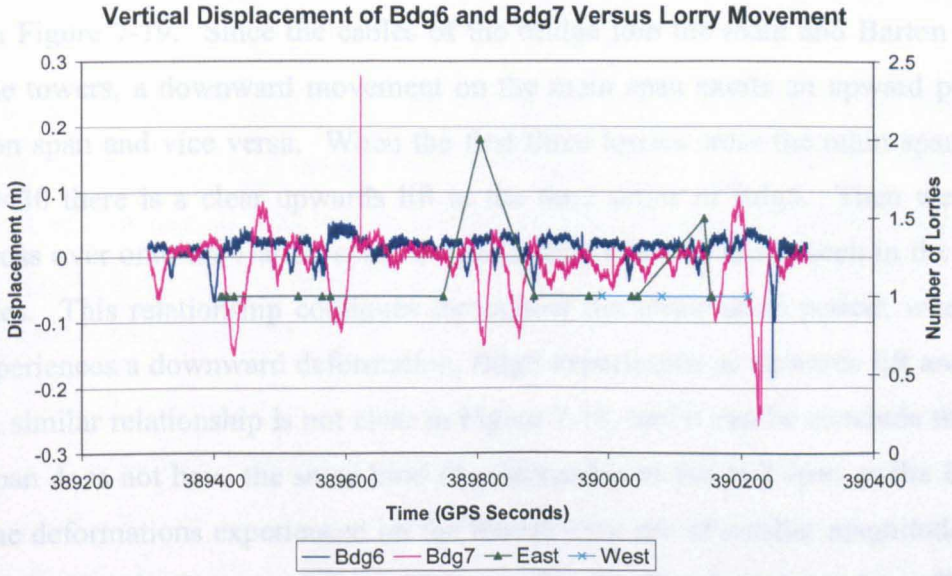

Figure 7-18 The vertical displacement of Bdg6 and Bdg7 linked in with the lorry movement along the Humber Bridge. East refers to the lorries moving along the east side of the bridge from north to south and west refers to the lorries moving from south to north.

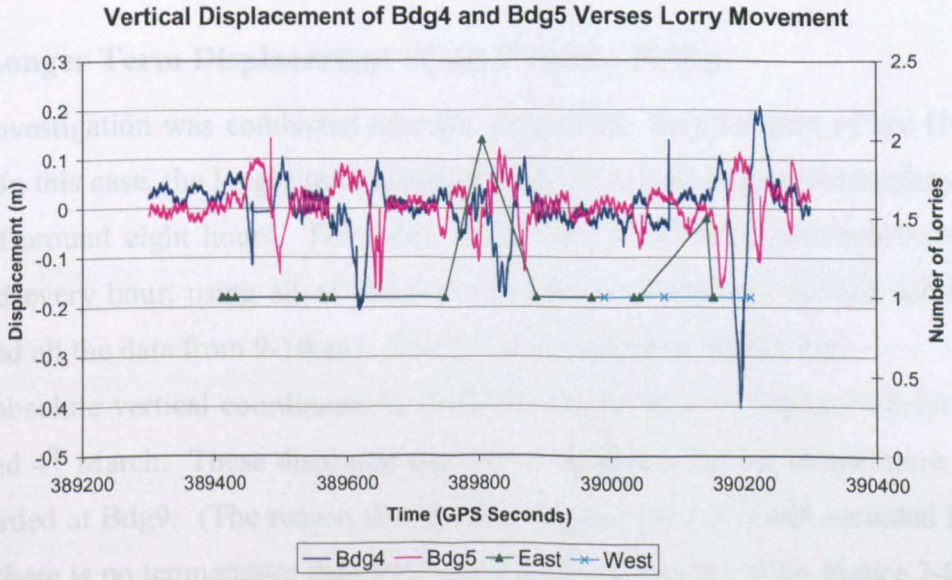

Figure 7-19 The vertical displacement of Bdg4 and Bdg5 linked in with the lorry movement along the Humber Bridge. East refers to the lorries moving along the east side of the bridge from north to south and west refers to the lorries moving from south to north.

Figure 7-19 shows the vertical displacement of Bdg4, which is located on the south quarter span of the main deck, and Bdg5 which is located on the mid point of the Barton side span; both on the east side of the bridge. Figure 7-18 showed that the displacements of the 280m Hessle side span were markedly different from those of the main span. It is clear from Figure 7-19 that the displacements of the 530m Barton side span are, in most cases, almost at the same level as the main span.

In Section 7.3.2 the counterbalancing relationship between the main span and Barton side span was demonstrated and discussed. This relationship is also clearly visible in Figure 7-19. Since the cables of the bridge join the main and Barton spans across the towers, a downward movement on the main span exerts an upward pull on the Barton span and vice versa. When the first three lorries cross the main span after time 389430 there is a clear upwards lift in the time series of Bdg5. Then went the lorries cross over onto the Barton span, the main span lifts and this is seen in the Bdg4 time series. This relationship continues throughout the observation period; whenever Bdg4 experiences a downward deformation, Bdg5 experiences an upwards lift and vice versa. A similar relationship is not clear in Figure 7-18, and it can be conclude that the Hessle span does not have the same kind of relationship to the mid span as the Barton does. The deformations experienced on the Hessle span are of smaller magnitude than either the main or the Barton spans, and this may be why they have less of an affect on the main span movement.

7.5.4. Longer Term Displacement of the Humber Bridge

An investigation was conducted into the longer term displacement of the Humber Bridge. In this case, the longer term displacement refers to average movement over the course of around eight hours. For Bdg1 on 2nd and 4th March, static solutions were computed every hour, using all of the data from the previous hour (so the solution at 10am used all the data from 9-10am). The data was processed in SKi-Pro.

The absolute vertical coordinates in OSGB36 can be seen in Figure 7-20 for Bdg1 on 2nd and 4th March. These displacements are compared to the air temperature which was recorded at Bdg9. (The reason that the data from 1st March is not included here is because there is no temperature data for this day.) It can be seen from Figure 7-20 that the level of the deck is considerably affected by the air temperature.

On 2nd March the air temperature at 9.15, when the session starts, is 4 °C. The temperature then decreases to its lowest point at 1.8 °C, and then slowly increases throughout the day to a maximum of 8°C. On this day, the first measurement of the bridge deck recorded a height of 44.45m. As the temperature increases throughout the day, the bridge deck gets lower and lower. On 4th March the air temperature starts at 14.5 °C, which is 10 °C higher than on the 2nd March. The bridge deck on 4th March starts at 44.34m, which is more than 10cm lower than on 2nd March. On the 4th March too, the bridge deck continues to get lower as the day progresses, but with a shallower gradient compared to 2nd March.

As a general rule, it appears that the higher the temperature, the lower the bridge deck. The decrease in deck height will not completely correspond to the temperature measured, as this was air temperature and the material temperature of the bridge is the most important thing. The temperature of the bridge deck will be rising throughout the day due to factors such as sun intensity and air temperature.

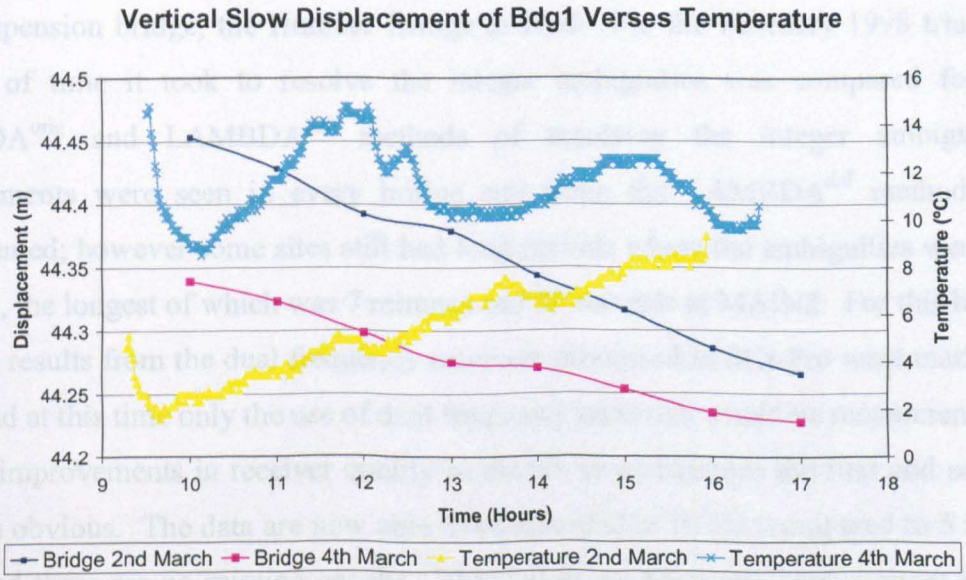

Figure 7-20 The vertical slow displacement of Bdg1 on 2nd and 4th March compared to the air temperature. Static GPS solutions were computed every hour.

On the 2nd March, the bridge deck sank by around 18.7cm during the eight hours of measurement and on 4th March it sank 11.1cm. Since the LAMBDA^{def} method of ambiguity resolution is based on reasonably accurate initial coordinates, this movement throughout the day could affect the results. For the results processing in Sections 7.5.1, 7.5.2 and 7.5.3, only an hour of data from each day was processed. In SKi-Pro the

average coordinate, just for the hour of interest, was processed and used as the initial coordinate. From the above results, it is known that this initial coordinate could change up to 18.7cm during an eight hour period.

This gradual displacement of the Humber Bridge will not cause any problems when the data is post-processed, but if the data was needed in real-time it could cause some difficulty. A way of solving this problem would be to continuously update the initial coordinate with an average of the output coordinates over the previous hour. Only coordinates where the ambiguities had been fixed would be used to calculate this average value. Or, the software could calculate a static coordinate every hour from all the stored observation data. This gradual drift of the coordinates only affects large structures such as the Humber Bridge and would not affect the results from smaller structures such as the Wilford Bridge discussed in Chapters 4 and 6.

7.6. Conclusions

This chapter has introduced results from two bridge trials conducted on the long span suspension bridge, the Humber Bridge in Hull. For the February 1998 trial, the amount of time it took to resolve the integer ambiguities was compared for the LAMBDA^{orig} and LAMBDA^{def} methods of resolving the integer ambiguities. Improvements were seen in every bridge site when the LAMBDA^{def} method was implemented; however some sites still had long periods where the ambiguities were not resolved, the longest of which was 7 minutes and 50 seconds at MAIN2. For this bridge trial, the results from the dual frequency receivers processed in SKi-Pro were markedly better and at this time only the use of dual frequency receivers would be recommended.

The improvements in receiver quality in the six years between the first and second trials are obvious. The data are now able to be recorded at 10 Hz (compared to 5 Hz in 1998) and there are no missing epochs. This led to an enormous improvement in the results produced with the single frequency receivers.

The LAMBDA^{orig} and LAMBDA^{def} methods of resolving the ambiguities are compared for the second trial, with the LAMBDA^{def} providing huge improvements in the amount of time to ambiguity resolution. The average time for ambiguities to be resolved with LAMBDA^{orig} was 7 minutes 24.1 seconds, compared to a tiny 8.4 seconds for LAMBDA^{def}. The longest time to ambiguity resolution was 28 minutes 4.7 seconds

for LAMBDA^{orig} and there were some sites where there was no ambiguity resolution at all, compared to only 41.7 seconds for LAMBDA^{def}.

There are still short periods within the time series where ambiguities are not resolved for the single frequency receivers even using the LAMBDA^{def} method, however this also occurs for the dual frequency data processed in SKi-Pro. The longest outage produced by SKi-Pro was 79.4 seconds, which is almost twice as long as the longest outage for the single frequency receivers, which was 41.7 seconds.

For both the February 1998 and March 2004 trials, the movement of the traffic across the bridge is linked in to the displacement of the bridge deck and interesting features of the deck movements are uncovered.

The long term displacement of the bridge over an eight hour period on two days of the March 2004 is introduced. This gradual bridge deck displacement is compared to the air temperature over the same period. The maximum long term displacement of the bridge deck was 18.7cm during this trial. The affect this gradual displacement may have on the success of the LAMBDA^{def} method of ambiguity resolution was discussed.

8. Garmin Handheld GPS Receivers

8.1. Introduction

The main aim of the work conducted for this thesis has been the use of single frequency GPS receivers instead of more expensive dual frequency ones. As an extension to the work conducted on single frequency receivers, experiments have been conducted with Garmin handheld GPS receivers.

Since the end of SA (Selective Availability) in 2000 (National Geodetic Survey 2000) the accuracies achievable by GPS in standalone mode have greatly increased. This has been coupled with the public awareness of GPS rising, so it is now possible to find handheld GPS receivers on sale in high street electronics shops, used by motorists and outdoor enthusiasts. This has led to a great improvement in positioning quality achievable by handheld GPS receivers and also led to reductions in price.

The receivers used for the results produced in Chapters 4, 6 and 7 are Leica system 500 dual and single frequency receivers. A Leica system 500 survey grade GPS dual frequency receiver costs £13,500, while a Leica single frequency receiver reduces the price to £8,300. While the data recorded by these receivers is very reliable, they can be too expensive for many monitoring applications. A Garmin handheld receiver can be purchased for between £100 and £400 (GPS Warehouse 2004). The Garmin model 76 receivers used for this experiment only cost £189 each.

This chapter introduces some initial trials conducted on The University of Nottingham campus, to assess whether it may be possible to use Garmin handheld receivers to monitor the movement of bridges. Section 8.2 outlines the software, called Gringo, which was developed at The University of Nottingham to extract raw pseudorange and carrier phase data from Garmin GPS receivers. The modifications to

the Kinpos software to enable the processing of Garmin data are explained in Section 8.3. Experiments are carried out to compare the accuracies achieved with Garmin receivers and Leica survey grade receivers. The static trials are introduced in Section 8.4.1, while the kinematic trials are described in Section 8.4.2. The chapter is concluded in Section 8.5.

8.2. Gringo

Gringo (GPS Rinex Generator) is a program developed at the IESSG, The University of Nottingham, to record the pseudorange and carrier phase output from a Garmin handheld receiver and convert it to Rinex format. Owners of Garmin 12 channel GPS receivers can use the software to enable extraction of raw data for post-processing. Post-processing is usually only available with expensive survey grade receivers.

Garmin Communications Protocols allow internal waypoints, tracks and other information to be exchanged with computers or other Garmin receivers. Some of these protocols are well documented, but others are not documented by Garmin at all. Gringo decodes one of the undocumented protocols which contains raw carrier phase and pseudorange data and logs this data in Rinex format. For more information about Gringo see Hill et al. (2000) and Hill and Moore (2002). The Garmin receiver must be connected to a laptop or data logger, by a serial port. The computer will then log the raw data in real time.

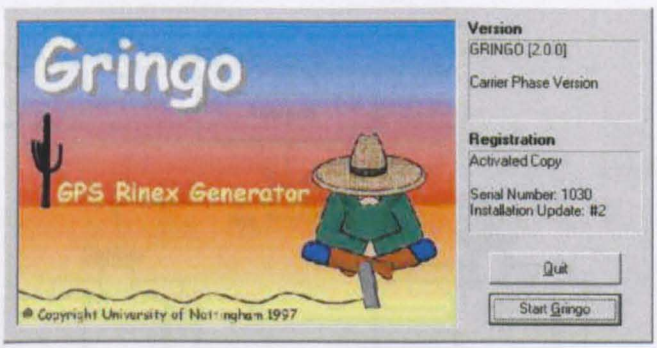

Figure 8-1 Gringo start up screen

Moore et al. (2002) conduct zero baseline trials with two Garmin receivers connected via a splitter to the same antenna. From Chapter 2, Section 2.3.2.2 it is known that zero baseline trials are a good way of assessing the receiver measurement

noise. They are useful as they remove a number of error sources associated with GPS such as atmospheric effects, satellite ephemeris errors and multipath because the effect of these error sources are the same at both receivers. The test was also carried out to analyse the ability of the decoding algorithms in Gringo, as an independent coding error at one receiver would not be found on the other receiver. The zero baseline trial was carried out over 10 minutes logging at a 1 Hz data rate. The data was processing using the ambiguity fixed carrier values in static mode and a distance of 0.0001m from the reference to the rover was recorded. Analysing the raw carrier phase residuals, the precision of the raw carrier phase measurement was calculated as approximately 0.0014m.

It was not possible to carry out a zero baseline trial for the results shown in this chapter. The newer generation of Garmin receivers use only 2 AA cells, and so provide only 3 volts to power an external antenna. Older Garmin receivers used 4 AA cells and so provided more than 5 volts, which enabled them to power an external survey grade antenna. The Garmin 76 receivers used for the experiments in this chapter do not have enough power to run an external antenna and so the Leica receivers connected via a signal splitter ran the antennas. It would be possible to have an external power source running the antenna so that the Garmin receivers could record data on their own. Connecting the Leica receivers to the 'hot' end of the splitter and the Garmin receivers to the 'cold' end allowed the antenna to be powered. By using a three splitter configuration, a four receiver splitter test was attempted but the signal power was insufficient to enable tracking by the receivers on the cold end of the first splitter (the configuration can be seen in Figure 8-2).

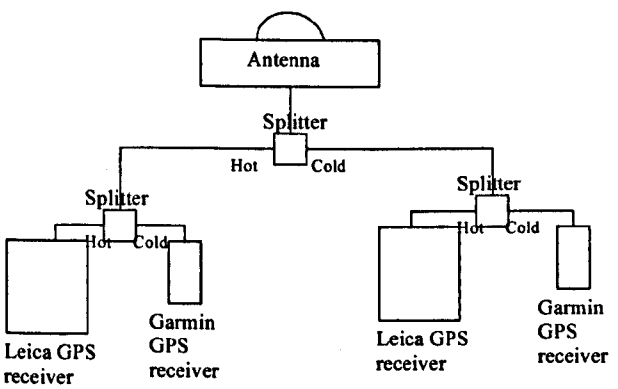

Figure 8-2 The zero baseline configuration

8.3. Additional Processing Issues

The modifications to Kinpos processing software undertaken by the author to enable processing of single frequency data are explained in Chapter 5. Section 5.4.1 introduces the new method of single frequency cycle slip detection. This method uses the triple order time difference of the carrier phase $\delta\Phi_{Li}^{s}(t_k)$, which is defined in equation (5–3). If the absolute value of $\delta\Phi_{Li}^{s}(t_k)$ is larger than a specified threshold then a cycle slip is detected. For most GPS receivers (certainly all those used so far in this thesis) this threshold will be set to 1, so cycle slips at the one cycle level will be detected.

However, for unknown reasons, the carrier phase from a Garmin receiver can slip by half cycle amounts. Conventional software packages will only detect full cycle slips and so do not cope well with Garmin data. P4 is static post-processing software that is provided with Gringo, which will cope with half cycle slips. However, so that the data could be processed in a kinematic mode, Kinpos had to be modified to be able to cope with Garmin data.

So, when Garmin data was processed in Kinpos the threshold for cycle slip detection was set to 0.5 cycles. Section 5.4.1.1 describes how the new cycle slip routine was tested, through simulations, before implementation in Kinpos. The java simulator developed by the author was used to induce cycle slips at the half cycle level in both Garmin and Leica data. As seen in Section 5.4.1.1 the cycle slip detection method was able to detect all slips at the 1 cycle level. However, when the threshold was set to 0.5 cycles, as well as detecting the true cycle slips, a large number of false cycle slips were detected by the software. These false cycle slips were corrected by the software and introduced into the processing solution.

It was concluded that the triple order time difference method could not be used to detect cycle slips as small as 0.5 cycles, so the threshold was set to 1 cycle for all receivers. However, when the Garmin data was being used, if the slips were bigger than 1 cycle they were corrected to the nearest half cycle (not to the nearest cycle as with other receivers). If the Garmin receiver does slip by just half a cycle, this will not be detected by the software and could affect the positioning solution.

Since the triple order time difference method can only be used after four epochs of data have been accumulated, the range residual method is used to detect cycle slips for the first four epochs. For the geodetic receivers, the range residual method can be used to detect cycle slips of ±4 cycles or larger due to the noise on the pseudorange. As it

will be seen in Section 8.4.1.1 the noise on the Garmin pseudorange is actually much higher than for a geodetic receiver, and so the range residual method is only used to detect cycle slips of ±15 cycles or larger. The range residual method is only used to flag cycle slips and not to correct them.

It is worth pointing out here that not only was the Garmin data processing made more difficult by the half cycle slips, but also by the sheer number of cycle slips that occurred. The Leica data usually only had one or two cycle slips during a session, whereas for the Garmin data, there could be hundreds of slips. For the short baseline trial discussed in Section 8.4.1.3, one cycle slip was detected in the Leica receivers' data. This compared to 75 cycle slips between both of the Garmin receivers. Some of the Garmin receivers' slips were detected using the range residual method which, due to the noisy pseudorange, may not have been slips at all. However, a good number were detected by the triple order time difference method and successfully corrected.

As well as detecting cycle slips to the nearest half cycle, the ambiguities had to be resolved to the nearest half cycle also. The formulas used to resolve integer ambiguities for small bridges are introduced in Section 5.4.2.1. Equation (5–7) defines how the integer ambiguities values are calculated from the observed minus computed double differences. For integer ambiguity values, $\Delta\nabla N_{ij}^{ST}$ (the double difference integer ambiguity in cycles between receivers i and j and satellites S and T), is set to the nearest integer. However for Garmin receivers $\Delta\nabla N_{ij}^{ST}$ is multiplied by 2 before being set to the nearest integer. Then this value is divided by 2, and the resulting ambiguity is accurate to the nearest half cycle. This method is used to resolve the ambiguities for the static data.

For the kinematic data, the method described in Section 5.4.2.2 for long bridges is used to resolve the ambiguities. In this case the float values are calculated and each multiplied by 2. The floats are then passed to the LAMBDA subroutine. When the ambiguities are fixed, each one is divided by 2 and this value is taken to be the ambiguity value for correction. These values are accurate to the nearest half cycle.

8.4. Results

8.4.1. Static Trials

Two static trials were conducted on The University of Nottingham campus in January 2004. For the first trial a Leica 510 single frequency GPS receiver and a Garmin 76 handheld GPS receiver were connected via a signal splitter to a Leica AT501 navigation antenna for a zero baseline trial. For the second trial the same receiver configuration of Leica and Garmin receivers was used at two different set-ups, one for the reference and one for the rover. The data from the first trial was processed as a zero baseline trial and also to investigate the raw data quality, the range residual variable was examined. For the second trial the short baseline was processed from Leica reference to Leica rover and from the Garmin reference to Garmin rover. Both trials were carried out a 1 Hz data rate (which is the maximum for the Garmin receivers).

8.4.1.1. Range Residual

The range residual variable was calculated for the Leica and Garmin data using equation (5–2) from Chapter 5. This variable is a good indicator of the quality of the pseudorange and carrier phase data from each receiver. The individual pseudorange and carrier phase values were split into different files for the different satellites and the range residual values for each individual satellite were calculated.

Figure 8-3 and Table 8-1 show that the range residual for the Leica data is about ±10cm at maximum, but it is usually around the 3cm mark. The standard deviation for the range residuals is 2.3cm. This value is normal compared to other results from the Leica receivers. Figure 8-4 and Table 8-1 show that the range residual for the Garmin data is much worse, reaching almost around 8m at maximum and usually being around 2-4m. The standard deviation in this case is 1.978m.

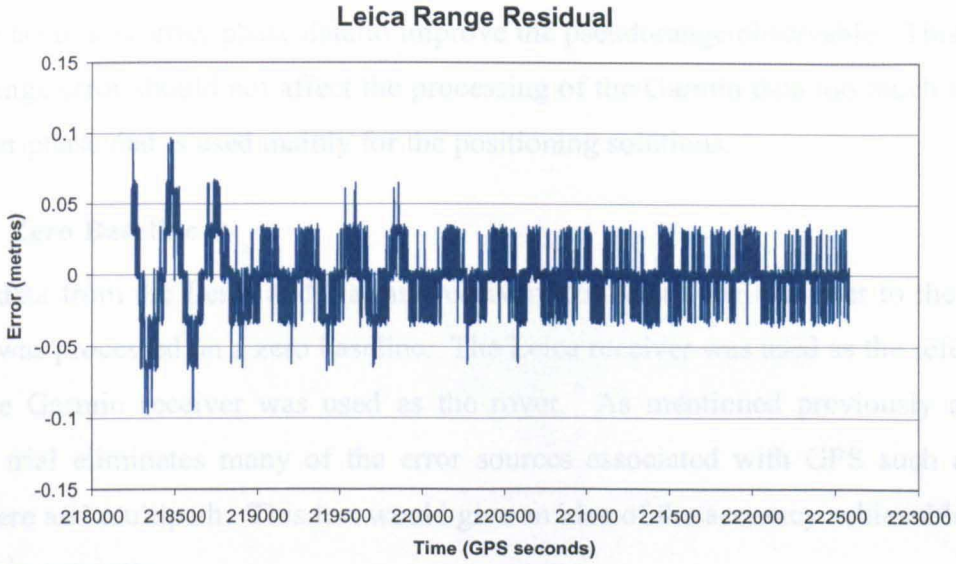

Figure 8-3 The range residual for the Leica data for satellite 16

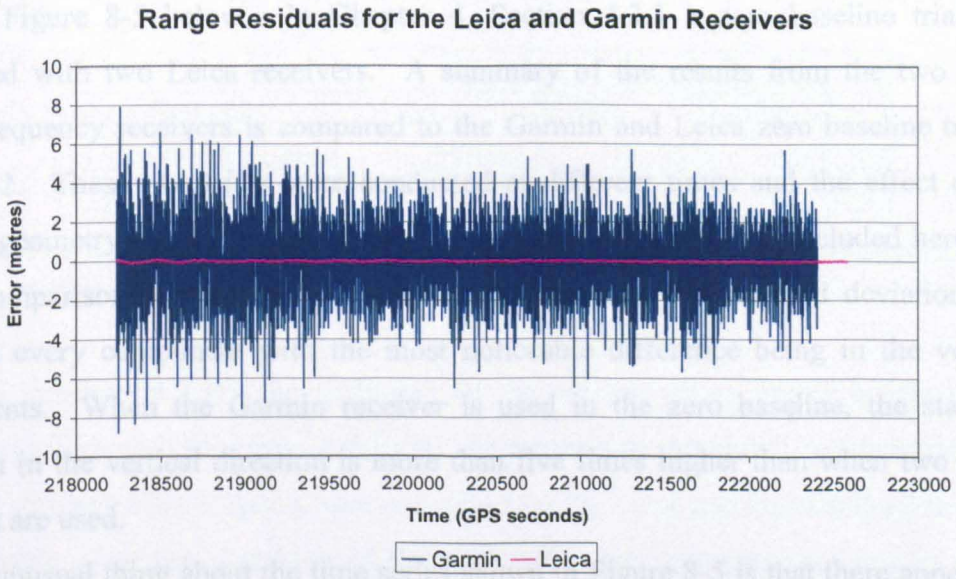

Figure 8-4 The range residual for the Garmin and Leica data for satellite 16

Range Residual	Maximum (m)	Minimum (m)	Standard Deviation (m)
Leica	0.096418	-0.096235	0.023375262
Garmin	7.895222	-8.650735	1.973210487

Table 8-1 Summary of results for the range residuals for the Leica and Garmin receivers

The reason for the huge differences in data quality is due to the accuracy and quality of the pseudorange data. For the Garmin receivers the pseudorange is not very precise at all. The quality of the Leica pseudorange data is improved by pseudorange

smoothing which occurs in the receiver itself. Pseudorange smoothing involves using the more accurate carrier phase data to improve the pseudorange observable. This large pseudorange error should not affect the processing of the Garmin data too much as it is the carrier phase that is used mainly for the positioning solutions.

8.4.1.2. Zero Baseline

The data from the Leica and Garmin receivers connected via a splitter to the same antenna was processed on a zero baseline. The Leica receiver was used as the reference while the Garmin receiver was used as the rover. As mentioned previously a zero baseline trial eliminates many of the error sources associated with GPS such as the atmosphere and multipath. This test would give an idea of the accuracy achievable with the Garmin receivers.

The results from the Garmin and Leica receivers processed as a zero baseline can be seen in Figure 8-5 below. In Chapter 4, Section 4.3.1 a zero baseline trial was conducted with two Leica receivers. A summary of the results from the two Leica single frequency receivers is compared to the Garmin and Leica zero baseline trial in Table 8-2. These two trials were conducted at different times and the effect of the satellite geometry has not be taken into account, but the results are included here as a rough comparison. When two Leica receivers are used the standard deviations are lower in every component with the most noticeable difference being in the vertical components. When the Garmin receiver is used in the zero baseline, the standard deviation in the vertical direction is more than five times higher than when two Leica receivers are used.

The unusual thing about the time series shown in Figure 8-5 is that there appears to be a slow pattern of movement within the data. The results from the zero baseline trials in Section 4.3.1 do not display this movement; the coordinates are evenly spread around the mean value.

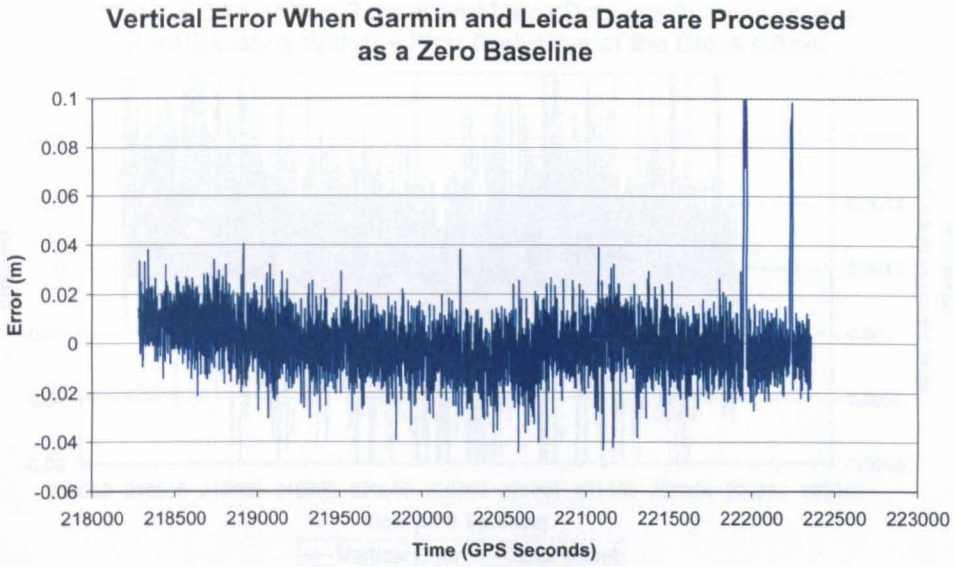

Figure 8-5 The vertical coordinate error shown when the Leica and Garmin data is processed as a zero baseline.

	Standard Deviations (m)		
Zero Baseline	East	North	Vertical
Garmin and Leica	0.0031	0.0040	0.0135
Two Leicas	0.0014	0.0030	0.0024

Table 8-2 The standard deviations of the Garmin and Leica receivers on a zero baseline compared to a zero baseline trial with two Leica receivers.

This movement could be attributed to the receiver clock errors in the Garmin receivers which are not removed fully by the processing software. To investigate this, the clock offsets at each epoch were calculated for the Leica and Garmin baseline, using P4 software. The first derivative of the clock offset was calculated and can be seen in Figure 8-6 overlaying the positioning solution. The first half of the positioning data has a downward trend which can also be seen in the clock offset. When the clock offset derivative starts to flatten out the positioning solution rises. The large jumps in the clock offset derivatives are due to missing epochs in the Garmin data. It does seem from the graph that there is a relationship between the clock offset and the slow pattern of movement within the positioning solution.

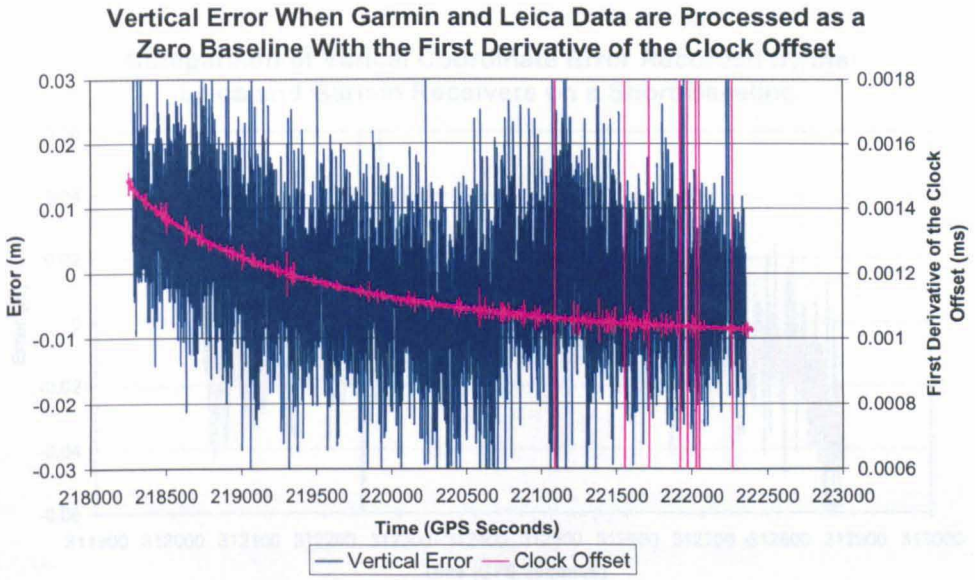

Figure 8-6 The vertical coordinate error shown when the Leica and Garmin data is processed as a zero baseline overlaid with the first derivative of the clock offset.

8.4.1.3. Short Baseline

In this trial, two different short baselines (around 20 metres) were processed, one between the reference Leica receiver and the rover Leica receiver and one between the reference Garmin receiver and the Garmin rover. These two baselines were identical, as the Leica and Garmin receivers were connected via a splitter to the same antenna at both ends of the baseline. So, these circumstances provide a means of directly comparing the results achieved by the Garmin and Leica receivers.

The vertical coordinates for the Leica and Garmin receivers can be seen in Figure 8-7. It can be seen from this Figure that the general pattern of the coordinates is the same for both receiver pairs, due to the multipath characteristics at the reference and rover sites. It is obvious however, that the Leica solutions are much less noisy than those provided by the Garmin receivers and this is further confirmed by the results shown in Table 8-3. For the short baseline trial the standard deviations of the Leica coordinates are half that of the Garmin coordinates for the east and vertical components, with a bigger difference in favour of the Leica receivers in the north component. This is a good result for the Garmin receivers considering the difference in quality of the Leica and Garmin raw data as seen in Section 8.4.1.1, and also considering the price difference between the receivers.

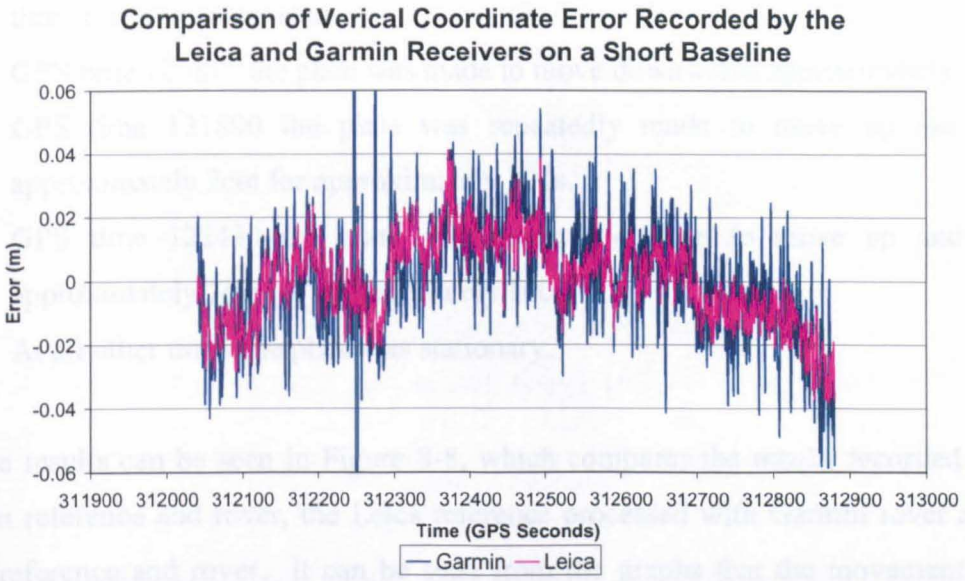

Figure 8-7 The vertical coordinate error produced by the Garmin and Leica receivers over a short baseline.

	Standard Deviations (m)		
	East	North	Vertical
Garmin	0.0048	0.0139	0.0282
Leica	0.0025	0.0056	0.0135
Ratio- Garmin/Leica	1.9472	2.4847	2.0793

Table 8-3 The standard deviations of the east, north and vertical components for the Leica and Garmin receivers over a static short baseline, plus the ratio of the standard deviations.

8.4.2. Kinematic Trials

A Leica single frequency SR510 GPS receiver and a Garmin 76 handheld GPS receiver were connected via a signal splitter to a Leica AT503 choke ring antenna at both the reference and rover locations. The reference location was on a known point on the tower of the IESSG building, while the rover was located on a monument outside the IESSG building, far enough away so that it had a clear view of the sky. The rover antenna was located on top of the monument which had a movable plate (this was the same monument that had been used for some initial total station trials described in Chapter 4, Sections 4.5.2 and 4.5.3 and is pictured in Figure 4–15). The plate on top of the monument was made to move up and down in the following ways:

1. GPS time 121352 the plate was made to move downwards approximately 15cm.
2. GPS time 121459 the plate was made to move upwards approximately 15cm.

3. GPS time 121578 the plate was made to move down and up approximately 15cm three times in succession.
4. GPS time 121817 the plate was made to move downwards approximately 15cm.
5. GPS time 121890 the plate was repeatedly made to move up and down approximately 2cm for approximately 100s.
6. GPS time 122430 the plate was repeatedly made to move up and down approximately 2cm for approximately 100s.
7. At all other times the plate was stationary.

The results can be seen in Figure 8-8, which compares the results recorded by the Garmin reference and rover, the Leica reference processed with Garmin rover and the Leica reference and rover. It can be seen from the graphs that the movement of the monument is recorded well by all the receiver combinations. The movements of 15cm at the beginning of the observation session are clearly visible as well as the small displacements of 2cm near the middle of the observation session.

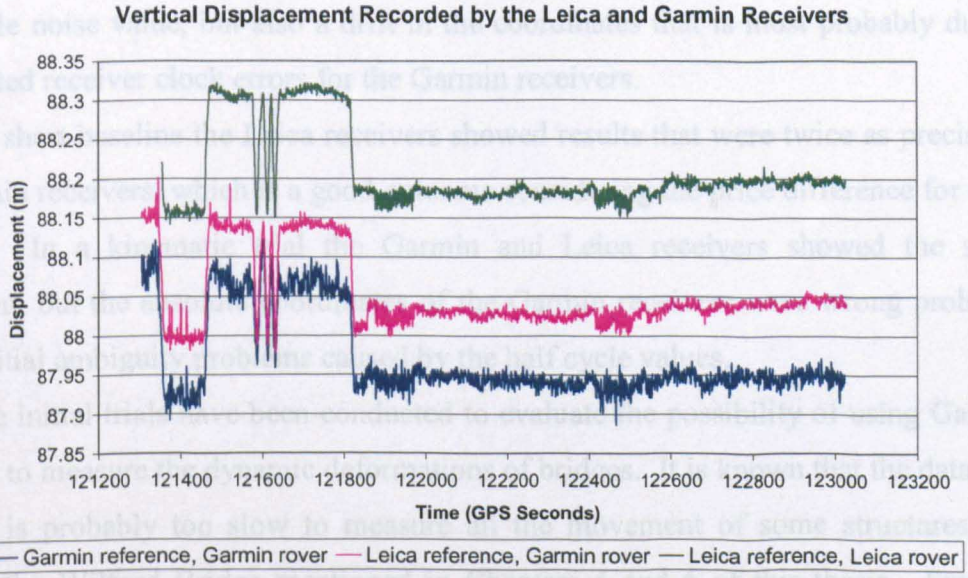

Figure 8-8 The vertical displacement recorded by the Garmin and Leica receivers for the kinematic trial.

The absolute coordinates for the different receivers, however, are not the same. Both for the Garmin reference and rover data and also for the Leica reference and Garmin rover, there is an offset in the absolute coordinates. This is caused by errors in the initial ambiguity values, probably because the ambiguities have to be solved to the

nearest half cycle whenever Garmin data is present. The interest of the author is to use Garmin receivers for the monitoring of the dynamic deformations of bridges and the relative movement of the receivers is of most importance. If the situation were truly dynamic this offset in coordinates would pose more of a problem. As long as this coordinate offset remains constant, as it has done in these trials, the solution can be corrected for this difference in coordinates.

When the receivers are static the noise in the Garmin data is about twice as bad as the Leica data in this experiment also. What is most interesting is that even with this high noise value, the Garmin receivers are still able to pick out all the movements of the monument.

8.5. Conclusions

The Garmin 76 handheld receivers have been tested and compared to the Leica survey grade geodetic receivers in a number of environments. The raw range residuals showed a very noisy Garmin pseudorange compared to the phase smoothed Leica pseudorange. A zero baseline trial with the Leica and Garmin receivers showed a reasonable noise value, but also a drift in the coordinates that is most probably due to uncorrected receiver clock errors for the Garmin receivers.

On a short baseline the Leica receivers showed results that were twice as precise as the Garmin receivers, which is a good outcome considering the price difference for each receiver. In a kinematic trial the Garmin and Leica receivers showed the same movement, but the absolute coordinates of the Garmin receivers were wrong probably due to initial ambiguity problems caused by the half cycle values.

These initial trials have been conducted to evaluate the possibility of using Garmin receivers to measure the dynamic deformations of bridges. It is known that the data rate of 1 Hz is probably too slow to measure all the movement of some structures, for example the Wilford Bridge mentioned in Chapters 4 and 6 of this thesis. For this bridge it may be possible to use the Garmin GPS receivers in conjunction with accelerometers to provide a higher data rate for measuring the dynamic displacements. Since the noise on the Garmin receivers is twice as bad as the Leica receivers, it may be difficult to pick out any movement of the Wilford Bridge, as only the largest movement could be detected by the Leica receivers. For larger bridges such as the Humber Bridge where the movement is relatively slow and the displacements are large, monitoring with

Garmin receivers could be a possibility. There is also the possibility that the Garmin receivers could be used to monitor slower natural processes, which do not need such high data rates.

9. JNS100 100 Hz GPS Receivers

9.1. Introduction

For all experiments conducted for this thesis so far and all trials carried out as part of The University of Nottingham's investigations into bridge deformation monitoring with GPS, the highest data rate used has been 10 Hz. This meant that only bridge dynamics of less than 5 Hz could be identified (using the Nyquist theorem (Hayes 1999)). However, it is known that the vibration frequencies of bridges could span from under 0.1 Hz for a long span suspension bridge, to over 50 Hz for a short span bridge of only a few metres long (Meng et al. 2003). The higher bridge dynamics cannot be identified by GPS receivers if they only measure at a 10 Hz data rate.

Until recently the highest frequency GPS receivers that could be purchased only measured up to 20 Hz. However, Javad Navigation Systems have newly developed JNS100 GPS OEM boards, which are able to output raw data and positions 100 times a second without interpolation (Javad Navigation Systems 2004a). Two JNS100 receivers were purchased for investigations of their applicability to bridge monitoring. One of the OEM boards is pictured in Figure 9-1. Using these receivers, it is hoped that GPS can be used to identify higher frequency bridge dynamics up to 50 Hz.

The raw code and carrier phase data are output from the receiver to a connected laptop and recorded using software called PCView (which was made available by Javad Navigation Systems). The raw data is automatically converted to Rinex format for post-processing. When the receiver output data at 100 Hz there were data overrun problems, first on the serial port and then on the USB port. Due to the large amount of data output at 100 Hz, the 115,200 bps baud rate of the serial port was too slow and large chunks of data were missing. USB to serial port converters were purchased. It was attempted to run the USB port at 430,800 bps, which would have allowed 100 Hz data collection.

Unfortunately PCView would only support the USB port running at 230,400 bps so only 50 Hz data collection was possible. Javad Navigation Systems are continuing to investigate this problem. It will be solved either by a higher baud rate being possible on the USB port, or a smaller amount of data being output from the receiver to the laptop.

Due to this problem, the data collected for this thesis was only recorded at a 50 Hz data rate, which is still fast enough to measure much higher frequency structural dynamics than has been possible with GPS before. Once the data overrun problems have been solved, using these receivers at 100 Hz data rate will be the subject of future investigations.

Figure 9-1 The JNS100 OEM board GPS receiver.

The JNS100 receivers record code and carrier phase data only on the L1 frequency. Chapter 5 has introduced the development of the single frequency processing software, Kinpos, which will also be used to process the data from the JNS100 receivers. Slight adjustments had to be made to Kinpos, so it could process data at this higher data rate.

This chapter outlines zero baseline (Section 9.2.1.1), short baseline (Section 9.2.1.2), test rig (Section 9.2.2) and bridge trials (Section 9.2.3) that have been conducted to analyse the precision attainable by the JNS100 receivers. The results from the JNS100 receivers are compared to those obtained from a Leica Geosystems System 500 receiver measuring at a 10 Hz data rate (the highest possible rate for these receivers) which was connected via a splitter to the same antenna. The Leica receivers have been used extensively for trials conducted for this thesis and also other bridge monitoring trials at The University of Nottingham, so their applicability to structural monitoring was known. Also, for the test rig and bridge trials the results from the JNS100 receiver are compared to a closely located accelerometer measuring at 50 Hz as well. Section 9.2.4 introduces some frequency identification carried out on the JNS100

and accelerometer data both measuring at 50 Hz. It is possible to identify much higher frequency bridge dynamics with the JNS100 receivers than has ever been possible with GPS before.

9.2. Results

The JNS100 receivers were always set to record at a 50 Hz data rate for all the trials outlined in this paper and the Leica receivers were always set to record at 10 Hz. In the Kinpos software the JNS100 data was processed at a 50 Hz data rate and then also resampled before processing to 10 Hz so that it could be easily compared to the Leica data.

9.2.1. Static Trials

9.2.1.1. Zero Baseline Trials

From Chapter 2, Section 2.3.2.2 it is known that a good way to assess the measurement noise of a GPS receiver is to conduct a zero baseline trial. Two receivers are connected by a signal splitter to the same antenna and processed as a baseline. Most error sources such as the atmosphere, clocks and multipath are differenced away and only the combined noise for the receiver pair is left.

Figure 9-2 The two JNS100 receivers connected to recording laptops, during the zero baseline trial.

Two separate zero baseline trials were conducted on consecutive days with the JNS100 receivers used on the first day and the Leica System 500 single frequency receivers on the next. The receivers recorded at the same time on the two consecutive days, but offset by 4 minutes, so that they would be recording with the same satellite

geometry. On both days the receivers were connected via a signal splitter to the same antenna, a Leica AT503 choke ring antenna, which was located on the roof of the IESSG building on The University of Nottingham campus. The two JNS100 receivers and the laptops recording data, during the zero baseline trial, can be seen in Figure 9-2. The aim of this trial was to compare the data from the JNS100 receivers and the Leica receivers under similar observation conditions.

The standard deviations of the east, north and vertical components for the Leica and JNS100 receivers can be seen in Table 9-1. For a fairer comparison the Leica data will be compared only with the JNS100 data resampled to 10 Hz. It can be seen that the Leica data has a lower standard deviation in every component when compared to the JNS100 data, with the largest difference being in the vertical direction. Figure 9-3 shows the vertical coordinate error of the Leica and JNS100 data at 10 Hz. It is clear from this graph and from Table 9-1 that the Leica receiver has a smaller spread of coordinates in the vertical direction. This implies that there is a better resolution of the carrier phase by the Leica receivers.

	Standard Deviations (m)		
Zero Baseline	East	North	Vertical
JNS100 (50 Hz)	0.0018	0.0023	0.0034
JNS100 (10 Hz)	0.0019	0.0021	0.0041
Leica (10 Hz)	0.0013	0.0017	0.0029

Table 9-1 The standard deviations of the east, north and vertical coordinates for the zero baseline trial for the Leica receivers and the JNS100 receivers. The results shown are for the JNS100 receiver are at 50 Hz and are resampled to 10 Hz.

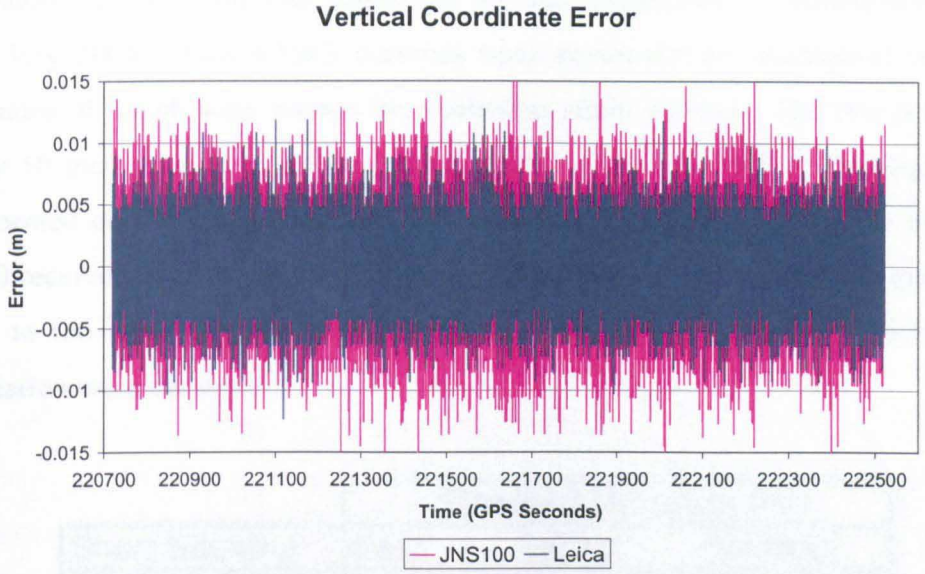

Figure 9-3 The vertical coordinate error for the zero baseline trial for the Leica receivers and the JNS100 receivers resampled to 10 Hz. The time of the Leica measurements have had 86160 seconds taken away from them (24 hours less 4 minutes), so that the measurements are compared during the same satellite constellation.

The double difference carrier phase residuals were calculated for the JNS100 data at 10 Hz and the Leica data and can be seen in Table 9-2. Satellite 13 was used as the base satellite for all the double difference calculations. It is clear from the table that for each satellite the residual is lower for the Leica receivers than for the JNS100 receivers, further confirming that the Leica receivers resolve the carrier phase with higher precision, or that there is lower internal noise within the Leica receivers. However, the precision of the JNS100 observations are still high and demonstrate the appropriateness of these receivers for high precision applications.

	Standard Deviation of the Satellite Residuals (m)					
Zero Baseline	PRN1	PRN4	PRN17	PRN20	PRN24	PRN27
JNS100 (10 Hz)	0.0021	0.0017	0.0009	0.0016	0.0016	0.0017
Leica (10 Hz)	0.0016	0.0013	0.0006	0.0012	0.0014	0.0012

Table 9-2 The standard deviations of the double difference carrier phase satellite residuals for the Leica data and the JNS100 data at 10 Hz for the zero baseline trial. The base satellite was 13 for all the calculations.

9.2.1.2. Short Baseline Trials

A short baseline static trial is a truer representation of survey conditions and so the performance of the receiver in practise can be better analysed. Atmospheric errors and clocks are still mitigated, but multipath is now present in the solution.

A short baseline trial was conducted on The University of Nottingham campus during July 2004. Two AT503 antennas were positioned on established points, the coordinates of which were known from previous static surveys. The two points were roughly 50 metres apart, with one located on the roof of the IESSG building, and the other located on a tripod outside the IESSG building. At each end of the baseline, a JNS100 receiver and a Leica system 500 single frequency receiver were connected by a splitter to the same antenna, meaning that the baselines measured by each receiver combination were the same.

	Standard Deviation (m)		
Short Baseline	East	North	Vertical
JNS100 (50 Hz)	0.0037	0.0056	0.0064
JNS100 (10 Hz)	0.0037	0.0056	0.0067
Leica (10 Hz)	0.0025	0.0050	0.0057

Table 9-3 The standard deviations for the east, north and vertical coordinates for the short baseline trial for the Leica and JNS100 receivers (at 50 Hz and resampled to 10 Hz).

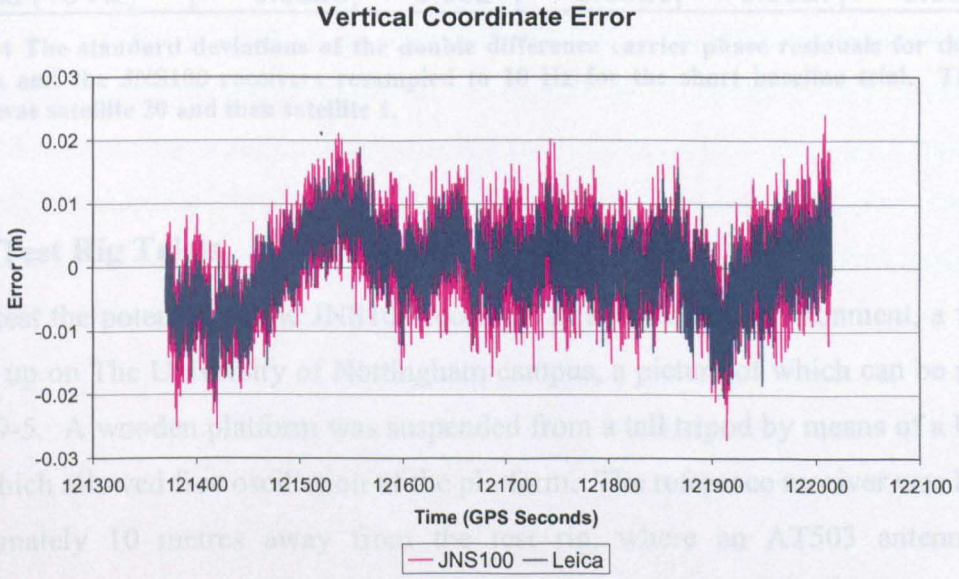

Figure 9-4 The vertical coordinate error for the short baseline trial for the Leica receivers and the JNS100 receivers resampled to 10 Hz.

The baselines for this trial were processed in Kinpos and the results can be seen in Table 9-3 and Figure 9-4. It can be seen from Table 9-3 that once again the standard deviations in all three components are lower for the Leica receivers, the largest difference being in the east component, at 1.2mm. Figure 9-4 shows the vertical coordinate error for the Leica receivers and the JNS100 receivers at 10 Hz. The

systematic bias of multipath is now visible within the data and follows the same pattern for both receiver pairs.

The double difference carrier phase residuals were calculated for each satellite used in the short baseline trial, the results of which can be seen in Table 9-4. Satellite 20 was the base satellite for the first part of the data, up to GPS time 121828.5 when the base satellite changed to satellite 1. The standard deviations of the carrier phase residuals are lower in every satellite pair for the Leica receivers, however the difference is very small for satellites 4, 11 and 25. The two satellites used as bases (1 and 20) seem to have the highest difference in standard deviations. Although the Leica receiver again seems to have performed better in the short baseline trial, the results for the JNS100 receivers are encouraging. The possibility of measuring at a 50 Hz data rate will offset the small loss of precision.

	Standard Deviations of the Satellite Residuals (m)				
Short Baseline	PRN1	PRN4	PRN11	PRN20	PRN25
JNS100 (10 Hz)	0.0030	0.0025	0.0022	0.0035	0.0029
Leica (10 Hz)	0.0026	0.0024	0.0020	0.0027	0.0028

Table 9-4 The standard deviations of the double difference carrier phase residuals for the Leica receivers and the JNS100 receivers resampled to 10 Hz for the short baseline trial. The base satellite was satellite 20 and then satellite 1.

9.2.2. Test Rig Trials

To test the potential of the JNS100 receivers in a kinematic environment, a test rig was set up on The University of Nottingham campus, a picture of which can be seen in Figure 9-5. A wooden platform was suspended from a tall tripod by means of a bungee cord, which allowed free oscillation of the platform. The reference receiver was located approximately 10 metres away from the test rig, where an AT503 antenna was connected via a splitter to the Leica and JNS100 receivers. An AT502 navigation antenna was mounted on the test rig, which was then, via a splitter, connected to the JNS100 and Leica receivers. A Kistler triaxial accelerometer was also strapped onto the test rig and located very close to the GPS antenna. The accelerometer data was logged to a laptop also at a 50 Hz data rate, meaning that the data from the JNS100 GPS receiver and the accelerometer could be compared at every epoch.

Using the test rig, two different trials were conducted. For the first test, the platform was in rotation either held still or disturbed from its resting position by someone forcing

the platform to move up and down. For the second trial, the platform was just left to swing.

Figure 9-5 Bungee test rig on which an accelerometer is located along with an AT502 GPS antenna attached by a splitter to a JNS100 and a Leica receiver.

The first bungee trial was conducted over a 10 minute time interval, where the bungee platform was held still for two minutes and then made to oscillate for 2 minutes and so on in rotation. The results for the first trial for the JNS100 receiver resampled to 10 Hz and the Leica receiver can be seen in Figure 9-6. The amplitude of the oscillation of the bungee platform was measured as between 15 and 20cm by both GPS receivers. The JNS receiver has a period within the last two minutes where there are a number of jumps within the time series. Apart from these jumps the measured displacements are very similar for both receivers. This demonstrates the capability of the JNS receivers to measure in a dynamic environment.

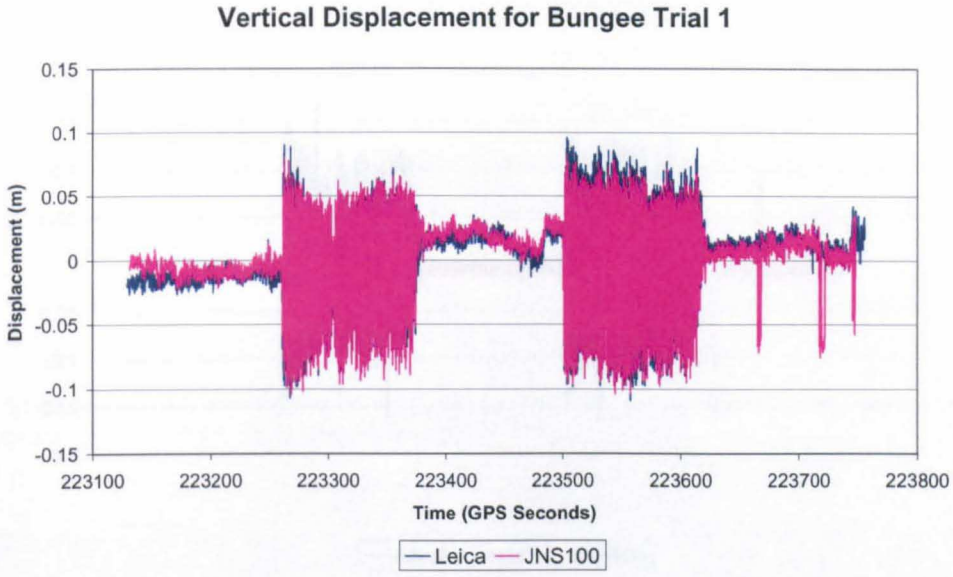

Figure 9-6 The vertical displacement shown by the JNS100 receivers resampled to 10 Hz and the Leica receivers for the first bungee trial.

The accelerometer data was recorded in volts, which was converted into accelerations and then integrated twice to obtain displacement values. For more information on the processing algorithms used on the accelerometer data the reader is referred to Meng (2002). The multipath signature that is obvious in Figure 9-6 was removed from the JNS100 data measured at 50 Hz, by a moving average filter of 50 samples before comparing the results to the accelerometer displacements.

The JNS100 displacements compared to those calculated from the accelerometer can be seen in Figure 9-7. It can be seen from this Figure, that the GPS and accelerometer disagree with regard to the amplitude of the displacement. While the GPS data has recorded an amplitude of 15 to 20cm, the accelerometer has recorded an amplitude of between 25 and 30cm.

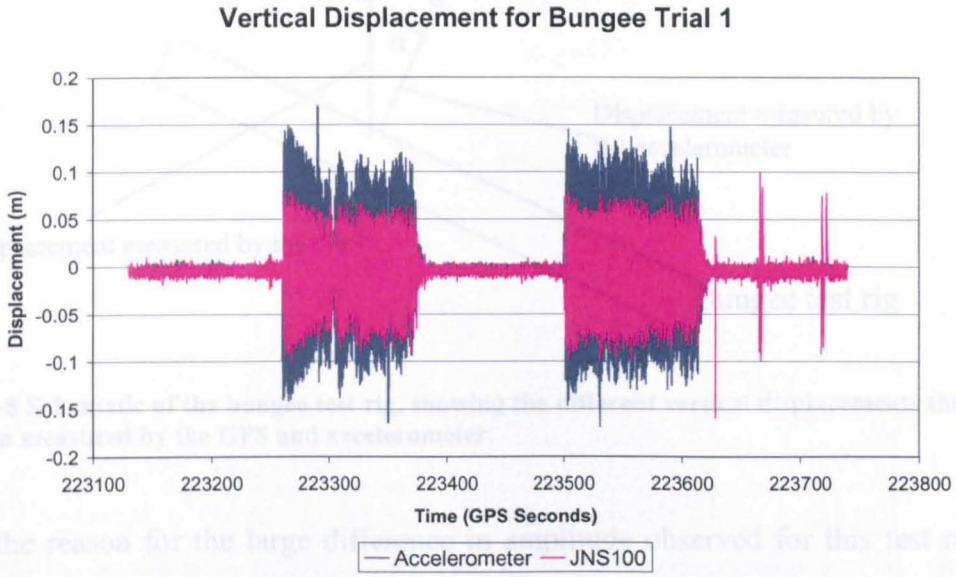

Figure 9-7 The vertical displacement shown by the accelerometer and JNS100 GPS receiver, both measuring at 50 Hz during the first bungee trial.

It was suggested that this discrepancy in amplitude could have been caused by the tilt of the bungee platform. The GPS data was converted from WGS84 into OSGB36, and so a local vertical was measured. If the bungee platform was slightly off vertical, the accelerometer would not measure the local vertical, but in its own measurements plane (perhaps better explained pictorially in Figure 9-8). Using equation (9-1), the average tilt of the bungee platform was calculated.

$$\alpha = a\cos\left(\frac{GPS\ displacement}{Accelerometer\ displacement}\right) \qquad (9\text{-}1)$$

The GPS displacement was calculated from an average of all the peaks of GPS displacement throughout the observation period and the accelerometer displacement was calculated in the same way from the accelerometer time series. Using equation (9-1) the tilt was calculated to be 57°, which is far too large to be plausible. It is not possible that the tilt of the platform could have reached 57°, since the operators were trying to keep it level and so only a slight misalignment would have gone unnoticed.

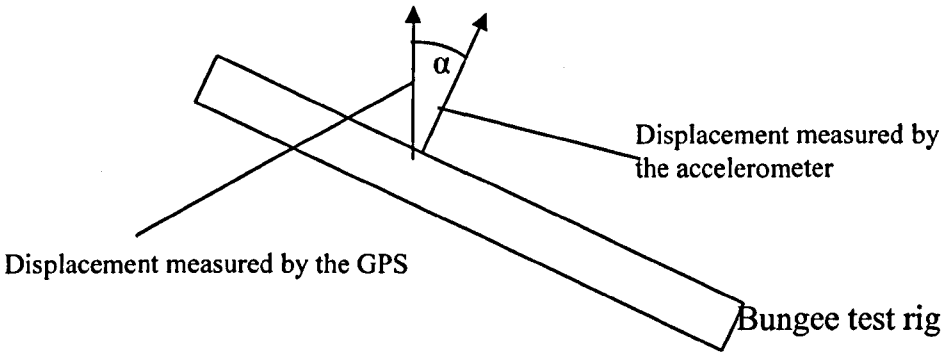

Figure 9-8 Schematic of the bungee test rig, showing the different vertical displacements that could have been measured by the GPS and accelerometer.

So the reason for the large difference in amplitude observed for this test remains unknown. It is thought that there could be a problem with the algorithm used to convert voltage to acceleration, specifically when a large amplitude is recorded. It will be seen in Section 9.2.3 that the accelerometer amplitudes recorded for the bridge trial are in line with GPS. It only appears to be when the movement is large that the discrepancies between GPS and accelerometers occur.

A further bungee trial was conducted using a different accelerometer. The bungee was kept in the vertical plane as much as possible during the trial by the use of the levelling bubble on a tribrach. The approximate movement of the bungee platform was measured using a levelling staff. Results from this test produced discrepancies in the amplitudes measured by the accelerometer and GPS also, with the GPS measuring the closest to the 'true' amplitude.

Investigations into the algorithms used in the accelerometer processing are still continuing. As mentioned previously this problem only seems to affect observations when there is a large amplitude displacement, and seems not to have affected the rest of the accelerometer results shown in this chapter. Since the subject of this thesis is not centrally focused around the use of accelerometers and they are only included here for a comparison to GPS, this difference in amplitude will not affect any conclusions drawn. It is the accelerometer and not the GPS that is measuring the wrong amplitude, which is confirmed by two independent GPS receivers measuring the same amplitude (Figure 9-6).

In the second test rig trial the bungee was just left to swing with the wind. The results for this trial for the east, north and vertical coordinates can be seen in Table 9-5. For this trial the results for both types of receiver match well, with the standard

deviations in the north and vertical components actually being slightly better for the JNS100 receiver. Figure 9-9 shows that the multipath characteristics displayed by both receiver solutions, in the vertical direction, are the same. This is an encouraging result for the JNS100 receivers, showing that in a dynamic environment they can measure to the same degree of precision as the Leica receivers.

	Standard Deviations (m)		
Bungee Trial 2	East	North	Height
JNS100 (50 Hz)	0.0074	0.0078	0.0113
JNS100 (10 Hz)	0.0074	0.0078	0.0115
Leica (10 Hz)	0.0074	0.0079	0.0118

Table 9-5 The standard deviations for the east, north and vertical coordinates for the second bungee trial for the Leica and JNS100 receivers.

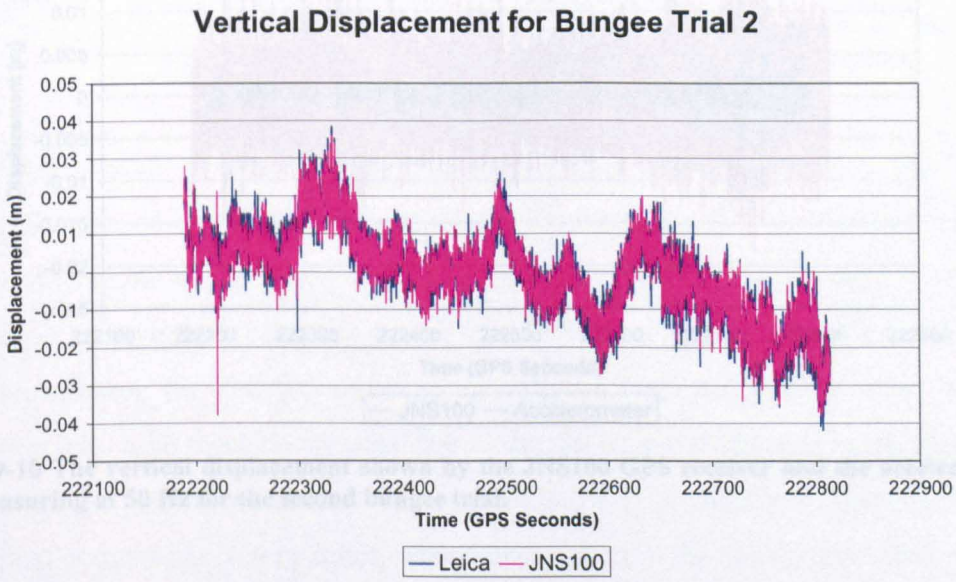

Figure 9-9 The vertical displacement of the bungee platform during the second trial where the platform was just left to swing, for the Leica data and the JNS100 data that was resampled to 10 Hz.

The JNS100 data had the multipath signature removed from the time series by using a moving average filter of 50 samples. The accelerometer data for the second bungee trial was also processed, converted to displacements and compared to the results achieved by the JNS100 data, which can be seen in Figure 9-10. It can be seen that again there is a discrepancy between the amplitudes shown by the GPS and accelerometers; however this time the GPS is showing a much higher amplitude than the accelerometer. The movement of the bungee platform during this particular trial

was so small that it cannot be distinguished from the background noise of the GPS measurements, which are at the ±1cm level.

When there is a larger amount of movement seen in the accelerometer time series towards the end of the observation period, it appears that the GPS data also shows this movement. Although overall the GPS observations are too noisy to be able to pick up the small amount of movement which occurred during this trial. This demonstrates the limiting amount of movement that must be present to allow detection with a GPS monitoring system.

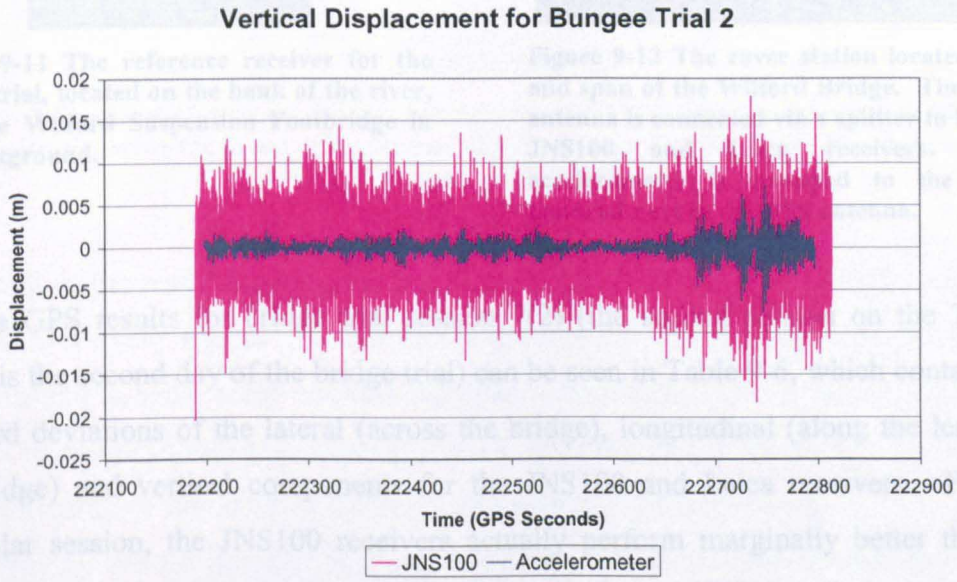

Figure 9-10 The vertical displacement shown by the JNS100 GPS receiver and the accelerometer, both measuring at 50 Hz for the second bungee trial.

9.2.3. Bridge Trials

A GPS and accelerometer bridge trial was conducted on the Wilford Suspension Footbridge in Nottingham, over two days in July 2004 (6th and 7th). This bridge has been the focus of many trials conducted by The University of Nottingham, including the trials discussed in Chapters 4 and 6 of this thesis. The purpose of this trial was to analyse the performance of the JNS100 receivers in a bridge environment.

The reference station was set up on the bank of the river, on a point whose coordinates were well established from previous trials (Figure 9-11). The rover receiver was located at the mid span of the bridge, where most of the movement was expected (Figure 9-12). At both locations an AT503 antenna was connected via a splitter to both the JNS100 and Leica receivers. The accelerometer was strapped to the handrail of the

bridge, very close to the GPS antenna. A number of sessions of data were collected on each day, a selection of which will be analysed.

Figure 9-11 The reference receiver for the bridge trial, located on the bank of the river, with the Wilford Suspension Footbridge in the background.

Figure 9-12 The rover station located at the mid span of the Wilford Bridge. The AT503 antenna is connected via a splitter to both the JNS100 and Leica receivers. The accelerometer is strapped to the bridge handrail next to the GPS antenna.

The GPS results for bridge trial session 7(2) (the second session on the 7th July which is the second day of the bridge trial) can be seen in Table 9-6, which contains the standard deviations of the lateral (across the bridge), longitudinal (along the length of the bridge) and vertical components for the JNS100 and Leica receivers. For this particular session, the JNS100 receivers actually perform marginally better than the Leica receivers in all three component directions, the largest difference being seen in the lateral direction. Both receivers are seeing exactly the same satellites. The difference in the vertical component is very small, which can be seen in the similar multipath patterns shown in Figure 9-13.

	Standard Deviations (m)		
Session 7(2)	Lateral	Longitudinal	Vertical
JNS100 (50 Hz)	0.0029	0.0026	0.0043
JNS100 (10 Hz)	0.0029	0.0026	0.0045
Leica (10 Hz)	0.0035	0.0028	0.0046

Table 9-6 The standard deviations of the lateral, longitudinal and vertical coordinates for the bridge trial, session 7(2).

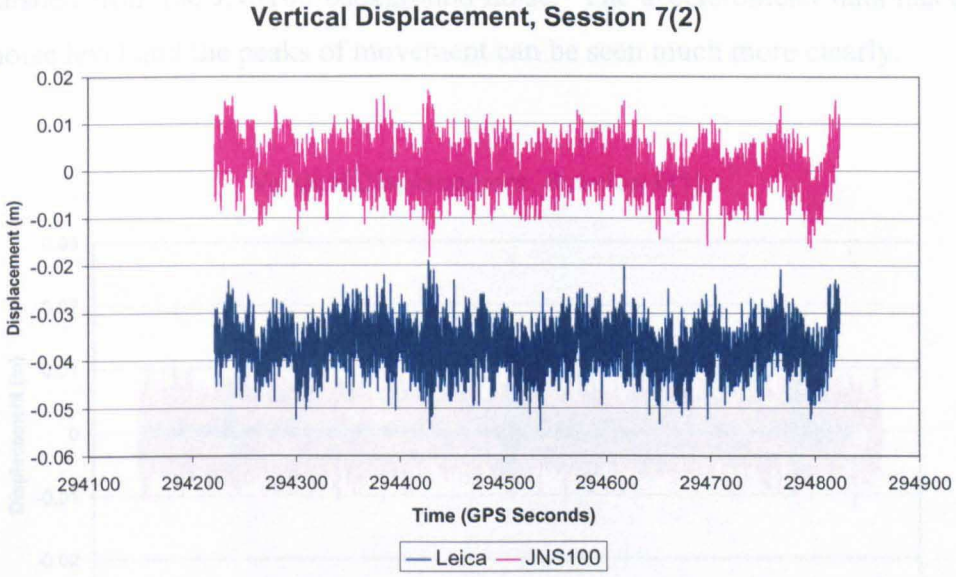

Figure 9-13 The vertical displacement recorded by the JNS100 receivers resampled to 10 Hz and Leica receivers during the bridge trial, session 7(2). The Leica data has been offset from zero by -0.04m.

For all of the sessions during the bridge trial, the results from the JNS100 and Leica receivers were very similar. In some cases the JNS100 was slightly more precise than the Leica and in some cases this was the other way around. The difference between n the two receivers in all cases was very small, showing that in the bridge environment the performance of the JNS100 is comparable with the Leica receivers.

A moving average filter of 50 samples was applied to the JNS100 data recorded at 50 Hz to remove the multipath signature from the time series. Applying a moving average filter to bridge data was discussed in Chapter 6, Section 6.3.3. A moving average filter of 50 samples will remove all signals present in this 50 Hz data that are less than 1 Hz. It is known from Chapter 6 and also from previous trials that the first natural frequency of the Wilford Bridge is around 1.73 Hz (Roberts et al. 2004a) and so important information about the bridge characteristics would not be removed by this filter. The accelerometer data was converted to displacements and compared with the displacements measured by the JNS100.

Results from four sessions can be seen in Figure 9-14 to Figure 9-17, comparing the accelerometer displacements to the JNS100 GPS measurements. It can be seen from these Figures that there is a large amount of noise on the GPS signal. The background noise level seems to be higher during session 6(2) (the second session on 6th July) compared to the other three sessions, so it is harder to distinguish movement from the noise. In all four figures, only the periods of largest bridge movement can be

distinguished from the JNS100 background noise. The accelerometer data has a much lower noise level and the peaks of movement can be seen much more clearly.

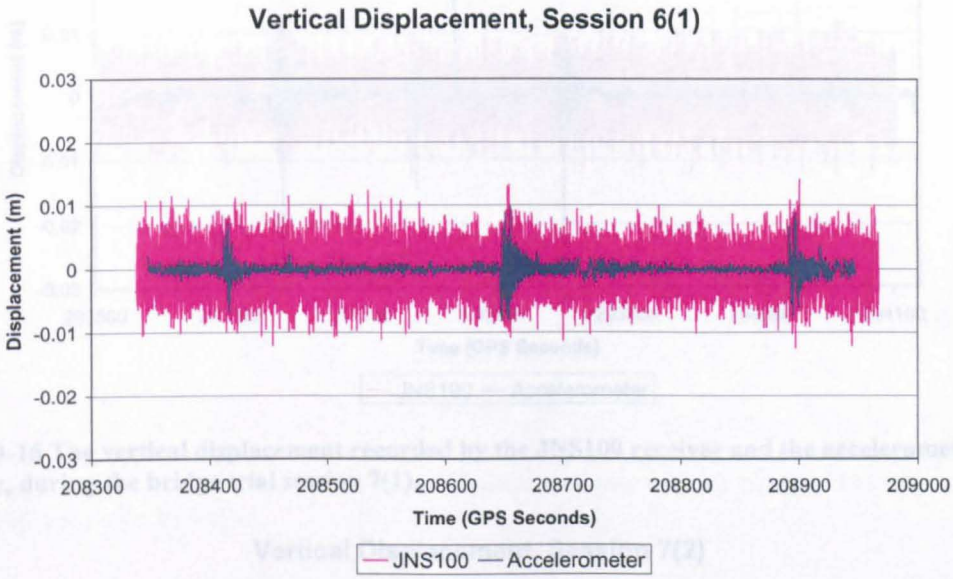

Figure 9-14 The vertical displacement recorded by the JNS100 receiver and the accelerometer, both at 50 Hz, during the bridge trial session 6(1).

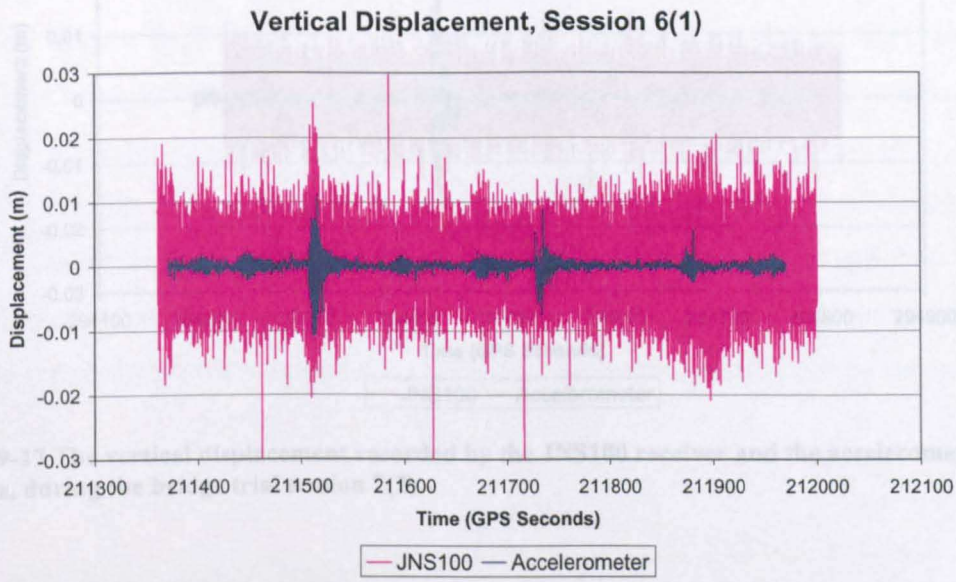

Figure 9-15 The vertical displacement recorded by the JNS100 receiver and the accelerometer, both at 50 Hz, during the bridge trial session 6(2).

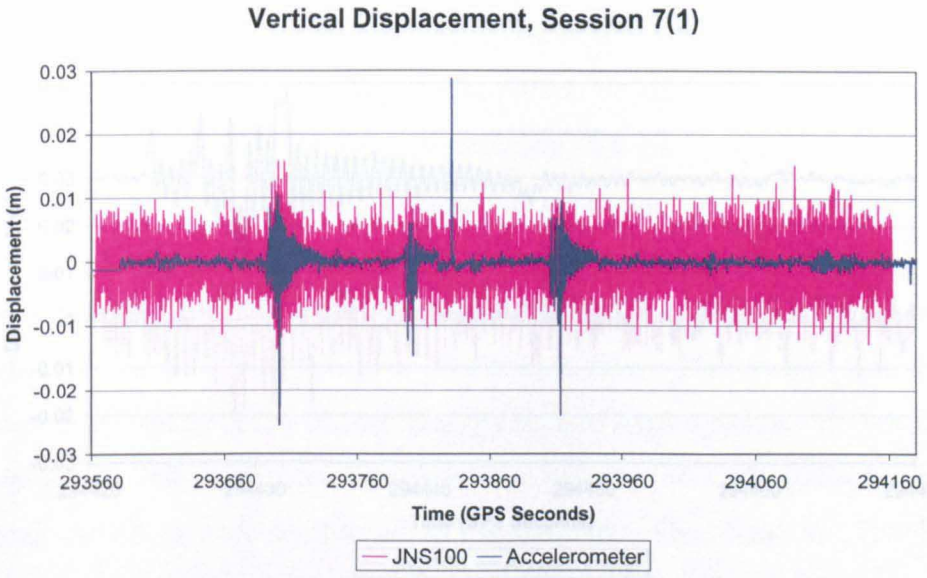

Figure 9-16 The vertical displacement recorded by the JNS100 receiver and the accelerometer, both at 50 Hz, during the bridge trial session 7(1).

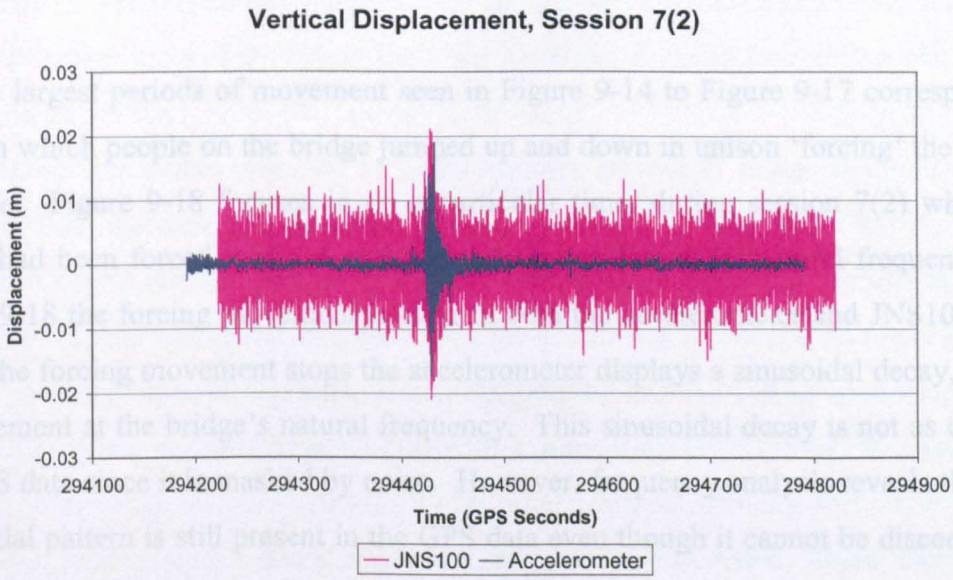

Figure 9-17 The vertical displacement recorded by the JNS100 receiver and the accelerometer, both at 50 Hz, during the bridge trial session 7(2).

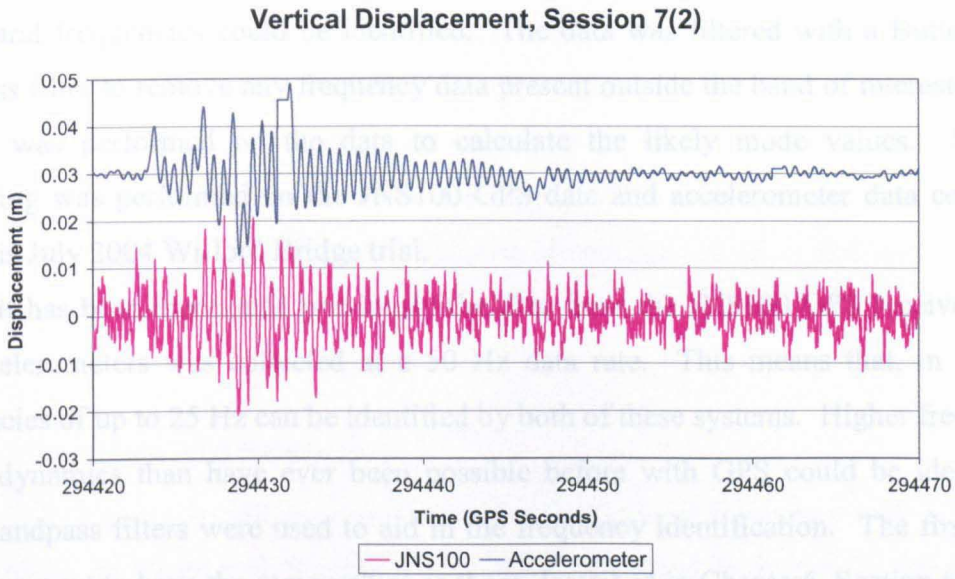

Figure 9-18 The JNS100 and accelerometer vertical displacement both recorded at 50 Hz. This graph focuses in on a time when there was the largest movement on the bridge. The accelerometer data offset from zero by 0.03m

The largest periods of movement seen in Figure 9-14 to Figure 9-17 correspond to times in which people on the bridge jumped up and down in unison 'forcing' the bridge to move. Figure 9-18 focuses in on a particular time, during session 7(2) when the bridge had been forced to move and then left to oscillate at its natural frequency. In Figure 9-18 the forcing movement is clear in both the accelerometer and JNS100 data. When the forcing movement stops the accelerometer displays a sinusoidal decay, which is movement at the bridge's natural frequency. This sinusoidal decay is not as clear in the GPS data since it is masked by noise. However, frequency analysis reveals that this sinusoidal pattern is still present in the GPS data even though it cannot be discerned by the eye.

9.2.4. Frequency Identification

In Chapter 6, Section 6.5 the Leica GPS data and accelerometer data was analysed to find the natural frequencies of the Wilford Bridge. Since the Leica GPS receivers have a maximum data rate of 10 Hz, only frequencies of 5 Hz or less can be identified (due to the Nyquist Theorem (Hayes 1999)). The first natural frequency of the bridge was found to be 1.73 Hz and two other possible frequencies were identified at 2.3 and 2.9 Hz.

Section 6.5.1 discusses how the GPS and accelerometer data was processed so that the natural frequencies could be identified. The data was filtered with a Butterworth bandpass filter to remove any frequency data present outside the band of interest. Then a DFT was performed on the data to calculate the likely mode values. Similar processing was performed on the JNS100 GPS data and accelerometer data collected from this July 2004 Wilford Bridge trial.

As it has been mentioned previously the data from the JNS100 GPS receivers and the accelerometers was collected at a 50 Hz data rate. This means that, in theory, frequencies of up to 25 Hz can be identified by both of these systems. Higher frequency bridge dynamics than have ever been possible before with GPS could be identified. Eight bandpass filters were used to aid in the frequency identification. The first three filters were set to have the same values as those described in Chapter6, Section 6.5.2, to see whether similar frequency values were identified. So, the first filter has its lower limit set to 1.5 Hz and its upper limit to 2.5 Hz, the second filter had a lower limit of 2 Hz and an upper limit of 3 Hz and the third filter had a lower limit of 2.5 Hz and an upper limit of 3.5 Hz.

The next five filters were set to enable higher frequency bridge dynamics to be identified from the data. The fourth filter was set with a lower limit of 4.5 Hz and an upper limit of 5.5 Hz; the fifth filter was set with a lower limit of 6 Hz and an upper limit of 10 Hz; the sixth filter was set with a lower limit of 10 Hz and an upper limit of 11.5 Hz; the seventh filter was set with a lower limit of 11.5 Hz and an upper limit of 13 Hz; and the eighth and final filter was set with a lower limit of 13 Hz and an upper limit of 16 Hz. Previous analysis using DFTs without bandpass filtering had occurred and these filter values were chosen since the analysis had revealed where there were possible modes present.

The frequency identification focussed on four specific time periods, one from each of the sessions shown in Figure 9-14 to Figure 9-17. Each peak will be referred to by its session name. Peak 6(1) started at GPS time 208657.1; peak 6(2) started at GPS time 211518.2; peak 7(1) started at GPS time 293702.1; and finally peak 7(2) started at GPS time 294432.6. As mentioned in Chapter 6, Section 6.5.2, it is important that only the periods where the bridge is left to swing are included in DFT and not the periods where there is a forcing occurring. So the times when people were jumping up and down on the bridge are left out of the DFT and only the natural oscillation afterwards is included.

As mentioned in Chapter 6, Section 6.5.2, the number of samples used in a DFT is very important and can affect the results that occur. Since the most useful results in Chapter 6 for the 10 Hz GPS data had occurred when 100, 200, 300 and 400 samples had been used, it was decided that for this data at 50 Hz data, samples sizes of 500, 1000, 1500 and 2000 samples would be used for both the GPS and accelerometer data. This corresponded to 10, 20, 30 and 40 seconds of data respectively. The results for the JNS100 and accelerometer data can be seen in Appendix E, Table E–1 to Table E–8.

9.2.4.1. First Natural Frequency

The initial analysis will concentrate on the first natural frequency of the Wilford Bridge only. In Chapter 6, Section 6.5.2.1 the first natural frequency of the Wilford Bridge was found to be 1.73 Hz by both the Leica GPS data and also the accelerometer. This trial was carried out in May 2003. It was expected that the first frequency would be the same for the data from the JNS100 Wilford Bridge trial, conducted in July 2004. However, the results presented below and in Appendix E seemed to suggest that the first frequency had changed.

As mentioned in Section 6.5.2.1 the DFT can only take a certain finite number of values. The possible values between 1.7 and 1.8 Hz that the DFT could take, for the different number of samples, are listed in Table 9-7 along with the corresponding number of samples which gave that result. It can be seen from the table that the most likely value of the mode of the Wilford Bridge is 1.77 Hz, shown by both the JNS100 GPS and accelerometer data. Due to the large amount of evidence from this table that 1.77 Hz is the correct frequency, it can only be concluded that there has been a change in the first natural frequency of the Wilford Bridge between the May 2003 and July 2004 trials. The increase in the first natural frequency is about 2%.

Time (seconds)	Possible Modes	GPS	Accelerometer
10	1.70	0	1
	1.80	4	3
20	1.70	0	0
	1.75	1	0
	1.80	3	4
30	1.70	0	0
	1.73	0	0
	1.77	4	4
	1.80	0	0
40	1.70	0	0
	1.73	0	0
	1.75	2	2
	1.78	2	2
	1.80	0	0

Table 9-7 Summary of the results for the first natural frequency for the GPS and accelerometer data for all four peaks of movement.

It is stated by Owen and Pearson (2004) that a reduction in stiffness will cause a reduction in the natural frequency. In this case there has been an increase in the frequency and so there must have been an increase in the stiffness. It is possible that some kind of strengthening of the bridge has occurred between the two trials, which has resulted in this frequency increase. It is know that the bridge is owned by Severn Trent Water Company, but attempts to contact them with regard to the bridge have always been unsuccessful.

An increase in the natural frequency could also have been caused by a reduction in the mass of the bridge. During the first trial introduced in Chapter 6 there were around thirty people on the bridge and their total combined weight was 2,353Kg. During the bridge trial introduced in this chapter there were only three people on the bridge at any one time. This reduction in mass on the bridge could have been the cause of the change in natural frequency. The fundamental frequency calculated from both the JNS100 GPS data and the accelerometer data for the Wilford Bridge is now 1.77 Hz.

9.2.4.2. Higher Frequency Mode Values

Higher frequency mode values other than the first fundamental frequency will be considered in the following section. The higher frequency modes will be split into two parts. The second, third and fourth mode will be considered together first and subsequently the fifth, sixth, seventh and eighth mode values will be considered.

Figure 9-19 to Figure 9-26 show the results of the eight bandpass filters for the four peaks of movement for both the accelerometer and JNS100 GPS data. All the graphs show the data when 1500 samples are used, which corresponds to 30 seconds. The scales of all the JNS100 GPS graphs are the same with a magnitude from 0 to 1.2. The scales of all the accelerometer graphs are the same as each other going from 0 to 0.1, but this is different from the scales of the GPS graphs. The first natural frequency for every graph shown is 1.77 Hz. It is obvious in this case that the magnitudes of all the JNS100 GPS graphs are considerably higher than the magnitudes of the accelerometer graphs. The results for the May 2003 trial showed the opposite was true (Section 6.5.2.2).

The reason that the analysis of the mode values has been split into two sections is because only the first four mode values are visible in the accelerometer data. The last four bandpass filtered pieces of data are completely flat and show no information about what frequencies are present. No frequency identification is possible with the accelerometer above 5 Hz in this case. The magnitudes of the GPS data are consistently high and this is true also for the last four pieces of filtered data for each graph. There are still peaks clearly visible within the last four pieces of filtered data for the GPS.

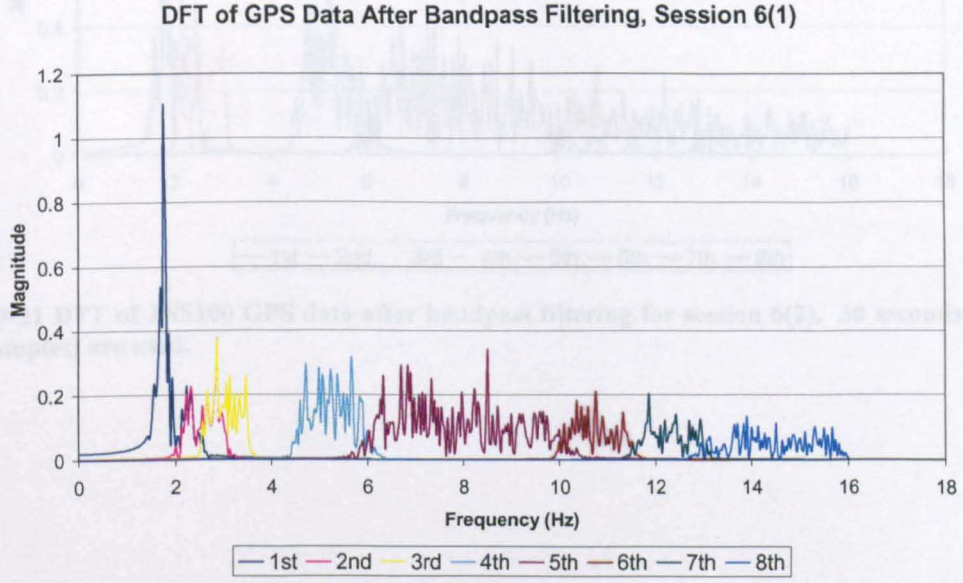

Figure 9-19 DFT of JNS100 GPS data after bandpass filtering for session 6(1). 30 seconds of data (1500 samples) are used.

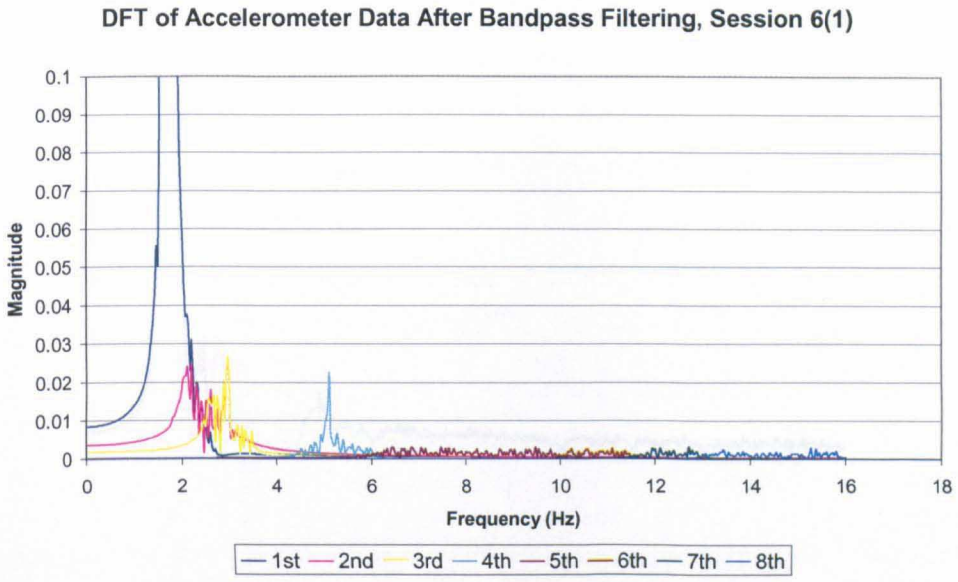

Figure 9-20 DFT of accelerometer data after bandpass filtering for session 6(1). 30 seconds of data (1500 samples) are used.

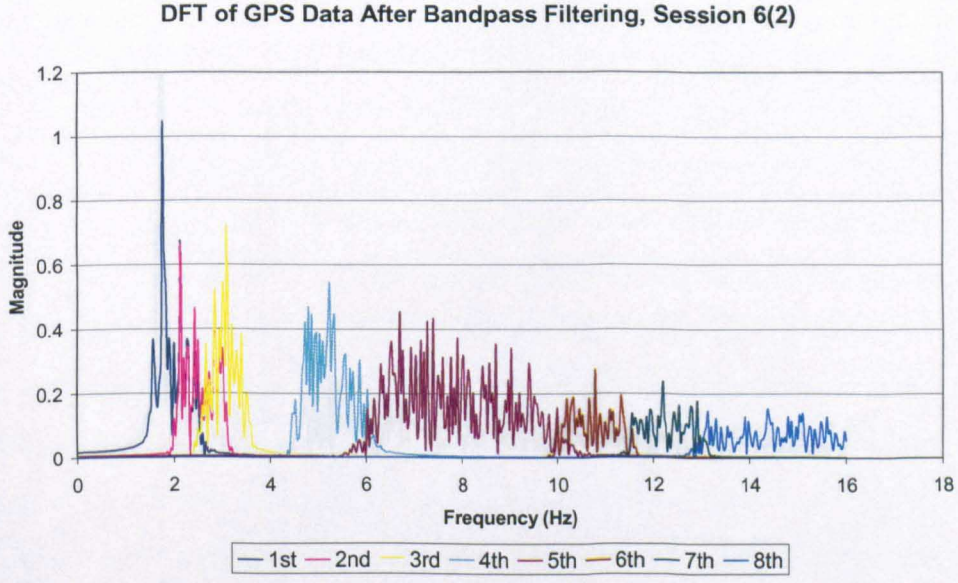

Figure 9-21 DFT of JNS100 GPS data after bandpass filtering for session 6(2). 30 seconds of data (1500 samples) are used.

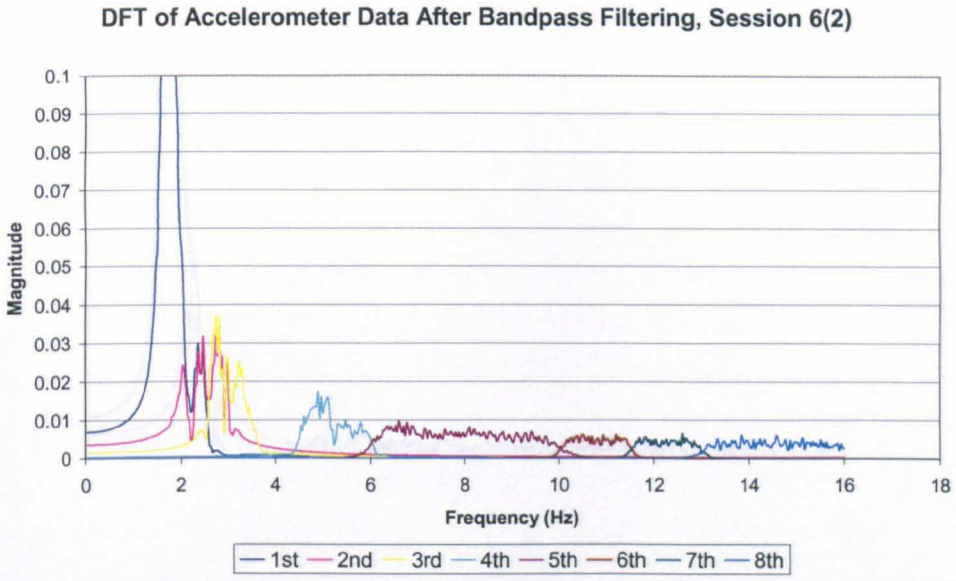

Figure 9-22 DFT of accelerometer data after bandpass filtering for session 6(2). 30 seconds of data (1500 samples) are used.

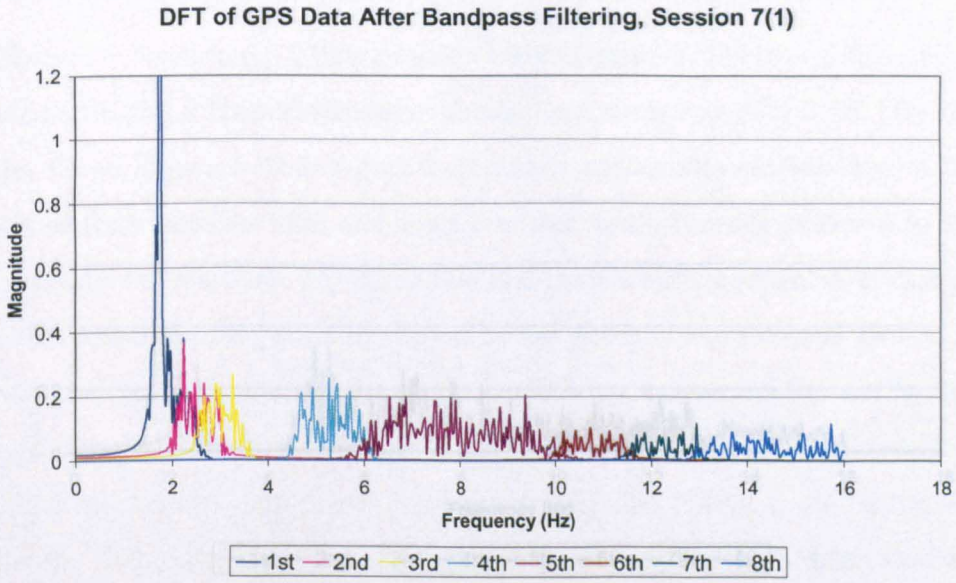

Figure 9-23 DFT of JNS100 GPS data after bandpass filtering for session 7(1). 30 seconds of data (1500 samples) are used.

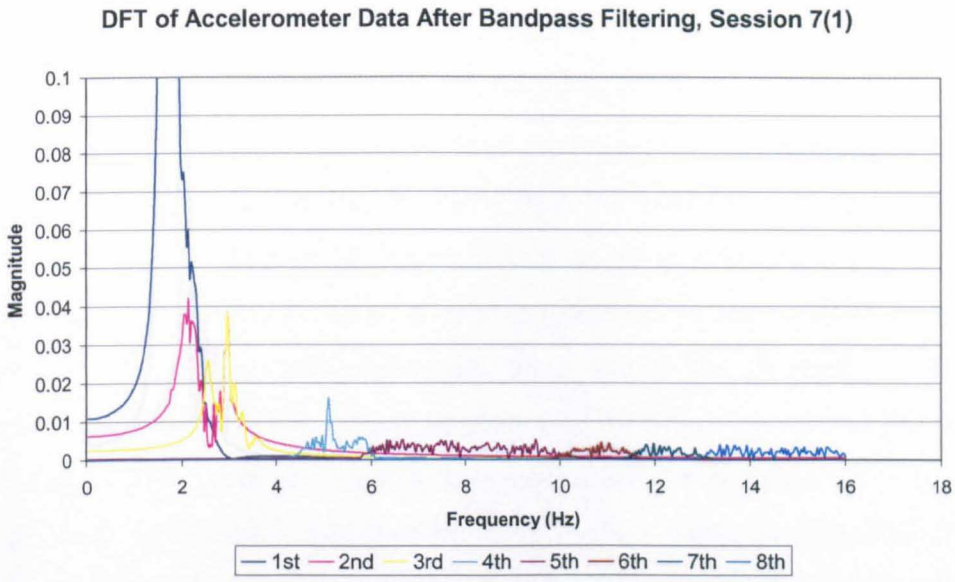

Figure 9-24 DFT of accelerometer data after bandpass filtering for session 7(1). 30 seconds of data (1500 samples) are used.

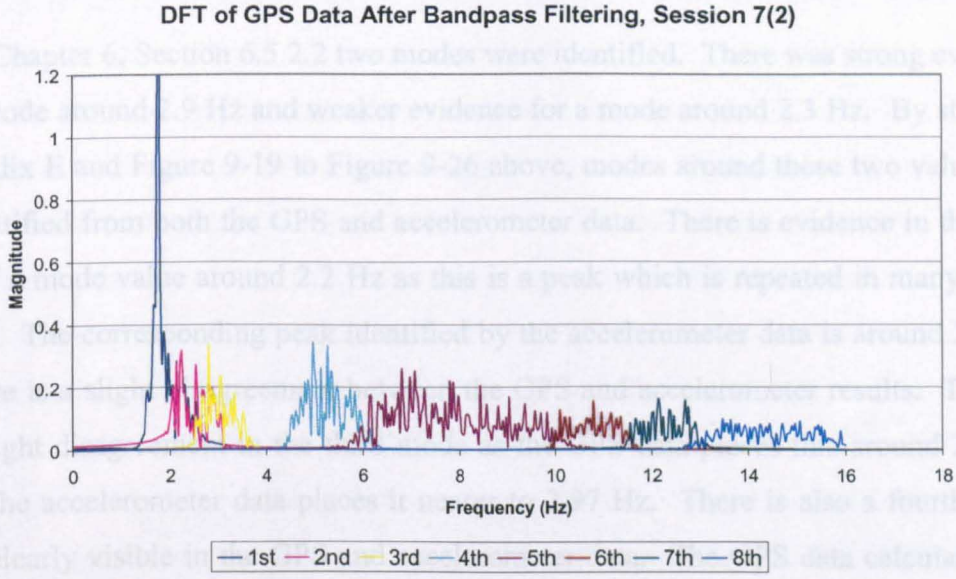

Figure 9-25 DFT of JNS100 GPS data after bandpass filtering for session 7(2). 30 seconds of data (1500 samples) are used.

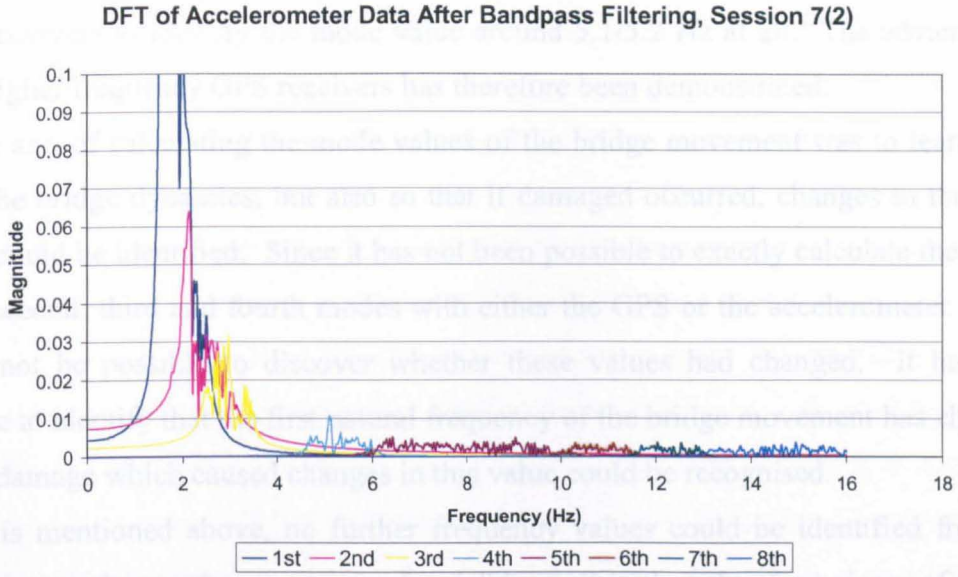

Figure 9-26 DFT of accelerometer data after bandpass filtering for session 7(2). 30 seconds of data (1500 samples) are used.

In Chapter 6, Section 6.5.2.2 two modes were identified. There was strong evidence for a mode around 2.9 Hz and weaker evidence for a mode around 2.3 Hz. By studying Appendix E and Figure 9-19 to Figure 9-26 above, modes around these two values can be identified from both the GPS and accelerometer data. There is evidence in the GPS data of a mode value around 2.2 Hz as this is a peak which is repeated in many of the graphs. The corresponding peak identified by the accelerometer data is around 2.1 Hz. So there is a slight disagreement between the GPS and accelerometer results. There is also slight disagreement in the third mode as the GPS data places this around 2.8 Hz, while the accelerometer data places it nearer to 2.97 Hz. There is also a fourth mode value clearly visible in the GPS and accelerometer data. The GPS data calculates this mode to be around 5.2 Hz and the accelerometer places it around 5.1 Hz.

In all the above cases where there is slight disagreement between the mode values identified by the GPS and accelerometer, it is the accelerometer data which appears more consistent and therefore more reliable. In the results for the accelerometer data shown in the graphs above (Figure 9-20, Figure 9-22, Figure 9-24 and Figure 9-26), the first four peaks are very clearly visible and well defined. The results for the GPS (Figure 9-19, Figure 9-21, Figure 9-23 and Figure 9-25), however, are much noisier and it is much harder to discern the exact mode values.

Although there is a slight disagreement between the GPS and accelerometer about the exact values of the modes identified, similar modes were discovered by both

systems. Before using JNS100 receivers, it would not have been possible with the Leica receivers to identify the mode value around 5.1/5.2 Hz at all. The advantage of using higher frequency GPS receivers has therefore been demonstrated.

The aim of calculating the mode values of the bridge movement was to learn more about the bridge dynamics; but also so that if damaged occurred, changes in the mode values could be identified. Since it has not been possible to exactly calculate the values of the second, third and fourth modes with either the GPS or the accelerometer data, it would not be possible to discover whether these values had changed. It has been possible to identify that the first natural frequency of the bridge movement has changed, and so damage which caused changes in this value could be recognised.

As is mentioned above, no further frequency values could be identified from the accelerometer data as there are no peaks visible at all in the other four pieces of filtered data. There are, however, peaks visible in the JNS100 GPS data. There are two mode values which appear often throughout the data shown in Appendix E and also the GPS graphs shown above. The first is a mode around 10.8 Hz. This peak is clearly visible in most of the JNS100 graphs and tables. The second mode is around 12.2 Hz. Both of these cannot be confirmed with the accelerometer results. There is clearly evidence for both of these mode values within the GPS data, but due to the subjective nature of identifying frequencies with DFT, these values can only be treated as possible modes.

Before the introduction of JNS100 receivers, the highest data rate possible with any GPS receiver was 20 Hz (Novatel Inc 2004) and so only frequencies of 10 Hz or less could be recognised. The identification of possible mode values at 10.8 and 12.2 Hz, are the highest frequency values that have ever been achievable with GPS before. It has also been possible, in this case, to identify higher frequencies with the GPS data than with the accelerometer data, even though they were recorded at the same data rate. The magnitudes of the high frequency DFT on the accelerometer data were so small that no useful information could be gained from them.

There are likely to be more mode values within both the GPS and accelerometer data, but it has not been possible to identify any more of them with any certainty from the data and analysis performed. Future work should include different methods of obtaining frequency information from GPS and accelerometer data. Various methods are available for this, including stochastic subspace identification (Peeters and De Roeck 1999) and statistical pattern recognition approaches (Owen and Pearson 2004), but were beyond the scope of this study.

9.3. Conclusions

This chapter has outlined the preliminary work conducted with the JNS100 receivers. Zero baseline and short baseline trials have been conducted to assess the precision of the receivers compared to known high quality survey grade receivers (Leica system 500 single frequency receivers). The results show that the Leica receivers performed slightly better than the JNS100 in the static trials, but the difference was small. The JNS100 receivers do have a high precision carrier phase observable.

Kinematic trials were conducted on a bungee test rig and also on a bridge. In a kinematic situation the JNS100 receivers performed as well as the Leica receivers. The JNS100 results measured at 50 Hz were also compared to those from a closely located triaxial accelerometer, measuring at the same data rate. When the bungee test rig was forced to move up and down by a considerable amount, the accelerometer measured an amplitude that was almost twice as large as the amplitude measured by GPS. The reason for this is still slightly unclear, but it could be caused by un-calibrated scale factor parameters.

JNS100 bridge trial results compared well to the accelerometer findings, when identifying periods of large movement. Most movement on the bridge was masked by the GPS noise, but periods where large displacements occurred could be discerned.

Frequency identification was conducted with the JNS100 GPS data and the accelerometer data. The accelerometer and GPS data agreed that the first fundamental frequency of the Wilford Bridge was 1.77 Hz. This is a change from the 1.73 Hz that was calculated during the Wilford Bridge trial in May 2003 (Chapter 6) of around 2%. The reason for this change was unknown, but it could have been caused by strengthening of the bridge by the owners.

Higher frequency bridge dynamics were also identified by the accelerometer and JNS100 GPS data. There were three further modes identified by both systems around 2.1/2.2 Hz, 2.8/3 Hz and 5.1/5.2 Hz. The GPS and accelerometer did disagree about the exact values of all three of these modes, with the accelerometer providing the most consistent and therefore most reliable results.

The JNS100 GPS data identified two other possible modes at 10.8 and 12.2 Hz. These were not confirmed by the accelerometer as it was not possible to discern any peaks or mode values in the accelerometer data above 5.1 Hz. The detection of these

possible mode values is the higher frequency identification that has ever been possible with GPS receivers. Further research is suggested to confirm these mode values and find others within both the GPS and accelerometer data.

10. Augmentation of GPS Monitoring Systems with Pseudolites

10.1.Introduction

Throughout this thesis, most of the analysis has been focussed on the vertical component of the GPS solution. In a bridge monitoring situation, this is the most important component. However, for a GPS solution this is the least accurate component. Due to the satellite geometry (all the satellites are above the receiver location), the precision of the vertical component is usually two to three times worse than the horizontal. One of the ways currently being researched, to improve the accuracy, availability and reliability of GPS, is the introduction of pseudolites.

Pseudo-satellites or pseudolites are ground based transmitters of the GPS code and carrier phase signals transmitting on either L1 or L2 (usually L1). They are not a new concept in GPS positioning. In fact, before the first GPS satellite was launched pseudolites were used to validate the concept and to test initial GPS user equipment (Wang 2002).

The author, along with researchers from The University of Nottingham and the University of New South Wales (UNSW), has been investigating the impact of introducing pseudolites into GPS positioning solutions, particularly in the context of bridge monitoring. The joint collaboration has led to many papers and the interested reader is referred to, for example, Barnes et al. (2003b), Cosser et al. (2004a) and Meng et al. (2004b).

This chapter explains the deficiencies of the current GPS constellation and the need for augmentation by pseudolites (Section 10.2). Section 10.3 introduces the extra errors sources and issues associated with using pseudolites, while Section 10.4 investigates

previous research conducted into using pseudolites for deformation monitoring. The results from a static trial conducted on The University of Nottingham campus are described in Section 10.5. Simulations of the improvement in positioning solutions in a bridge environment and actual bridge trial results can be found in Chapter 11.

10.2.The Need for Augmentation of GPS with Pseudolites

The geometry of the GPS constellation quantified by dilution of precision (DOP) values changes over time and GPS receiver location (Elrod and Van Dierendonck 1995). It is known that for a reliable solution the GDOP (geometric DOP) should not exceed 6 (Hofmann-Wellenhof et al. 2001). A low DOP is achieved with a scattered distribution of satellites at both high and low elevation angles and ideally with one satellite in each of the four quadrants (Hofmann-Wellenhof et al. 2001). However, a compromise must always be made between low DOP values and the selection of an appropriate cut-off angle, as the effects of a number of GPS error sources are larger at low elevation angles (e.g. multipath and propagation medium errors). For bridge monitoring trials as with other high precision engineering applications a cut-off angle between 10° and 15° is usually chosen.

Santerre (1991) demonstrated that due to the inclination of the GPS satellite constellation at 55°, the distribution of satellites will not be uniform in the sky. It will in fact be a function of the station latitude with the distribution at low latitudes being almost uniform; at mid latitudes (such as the UK) almost no observations will be possible in the north direction (between azimuths 315° and 45°); and at high latitudes observations can only be made between elevations of 0° and 45°. In mid latitude areas, where the Wilford and Humber Bridge experiments for this thesis have taken place, an hole in the GPS constellation is formed in the north direction, where no satellites are available. Figure 10-1 shows the satellite sky distribution for 24 hours at the Wilford Bridge in Nottingham, UK (52° 56′ North) on 19th June, 2002 with a 15° cut-off angle. The Figure clearly shows the hole in the north direction where no satellites can be observed throughout the whole 24 hour period.

Parsley Bridge is also in a mid-latitude area, but south of the equator. Figure 10-2 shows a sky plot of 24 hours at Parsley Bay Bridge in Sydney, Australia (33° 51′ South) on the 16th January, 2003 with a 15° cut off angle. It can be seen from this Figure that

the hole is now in the southern direction, which means that no satellites can be observed there. This will lead to a similar decrease in accuracy in the north-south component.

The uneven effect of the satellite geometry on the east, north and vertical components could lead to erroneous conclusions about the actual bridge dynamics. Meng, et al. (2002b) highlights the case of a bridge in London where the satellite geometry causes it to appear as though the longitudinal movement is larger than the lateral movement, even though the wind loading was high. This disagreed with the expected bridge dynamics and also with parallel observations recorded by an accelerometer.

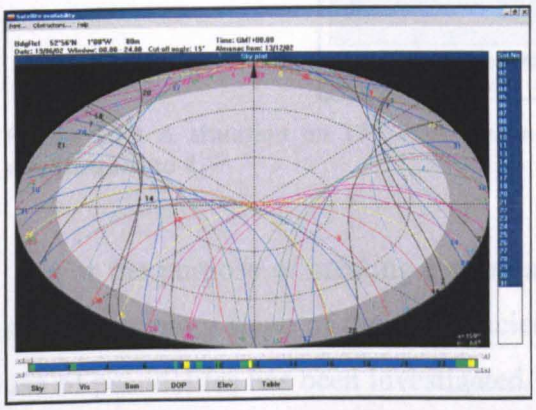

Figure 10-1 The satellite sky plot at the Wilford Bridge (52° 51′ N, 1° 8′ W) for 24 hours on the 19th June, 2002

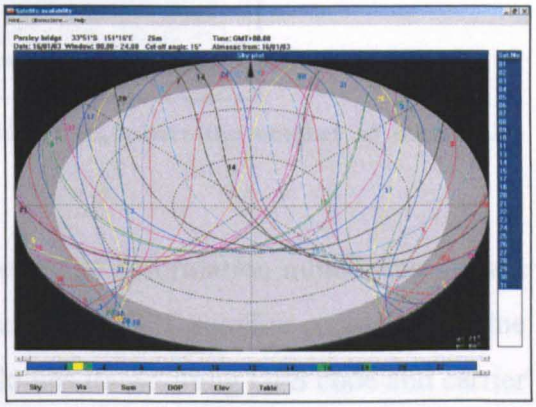

Figure 10-2 The satellite sky plot at the Parsley Bridge (33° 51′ S, 151° 16′ E) for 24 hours on the 16th January, 2003

As mentioned earlier in this chapter, it is known that the current GPS constellation usually causes the vertical positioning accuracy to be two to three times worse than the horizontal accuracy. This is due to all the satellites being located above the horizon. For bridge monitoring applications the vertical direction is the most important component and so improving the accuracy in this component is a research aim.

In certain areas such as urban or natural canyons and deep open pits, due to obstructions from the surrounding environment, the number of satellites can be insufficient for a reliable solution. Furthermore, the current satellite constellation provides instances when there are insufficient satellites to allow positioning to be carried out even in ideal circumstances. During the June, 2002 bridge trial on the Wilford Suspension Footbridge in Nottingham (see Chapter 4), there was a period of approximately 10 minutes each day where only 4 satellites were available above a cut-off of 15° (Figure 10-3). This caused the GDOP to rise to a maximum of 37 and meant

that the coordinates calculated by the GPS-only system were unreliable. This GPS outage causes degradation in the accuracy of the results and can affect the reliability of the whole deformation monitoring system.

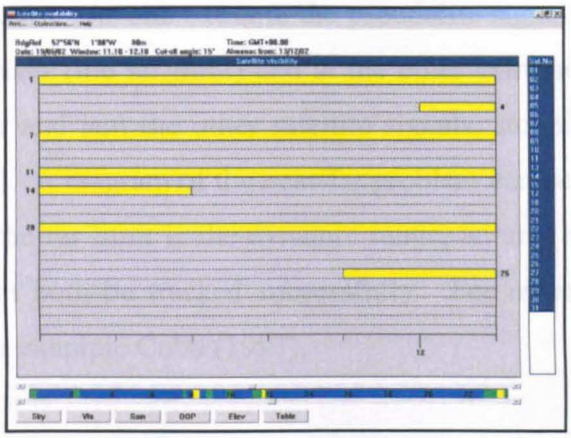

Figure 10-3 A situation on 19th June, during a bridge trial, where the number of measurable satellites fell to 4

For the purpose of creating a more accurate bridge deformation monitoring system and overcoming some of the deficiencies of the current GPS satellite constellation, the use of pseudolites has been investigated. Pseudolites transmitting GPS code and carrier phase signals, from known ground locations, can be used as another ranging source which can improve the DOP values and the overall quality of the solution. Through simulation (Chapter 11, Section 11.3.1) it can be seen that with augmentation from just one pseudolite the GDOP value in the above situation (Figure 10-3) can be reduced from 37 to less than 3 for the whole observation session (Daub 2002).

10.3.Additional Pseudolite Issues and Error Sources

When pseudolites are used to augment the GPS constellation there are additional error sources and issues that need to be taken into account due to the relatively close proximity of the GPS receivers to the stationary pseudolites. Some of these issues, the near-far problem, pseudolite location bias, multipath, atmospheric delays and ambiguity resolution, are described here. For more details see for example Dai, et al. (2001).

10.3.1.Near-Far Problem

GPS receivers are designed to receive relatively weak and constant signals from satellites approximately 20,000 kilometres away. Pseudolites operate outside this design assumption, since the distance between a pseudolite and receiver can vary from tens to thousands of metres. At one extreme the pseudolite signal may be too weak to be detected by the receiver (the far limit) and at the other extreme the pseudolite may overwhelm the receiver and jam the other satellite signals, stopping them from being received (the near limit). A diagram of the near-far problem can be seen in Figure 10-4. Between the near and the far limit is the dynamic range, an area where the pseudolite and satellite signals can both be tracked successfully. For more information on the near-far problem see for example Cobb (1997).

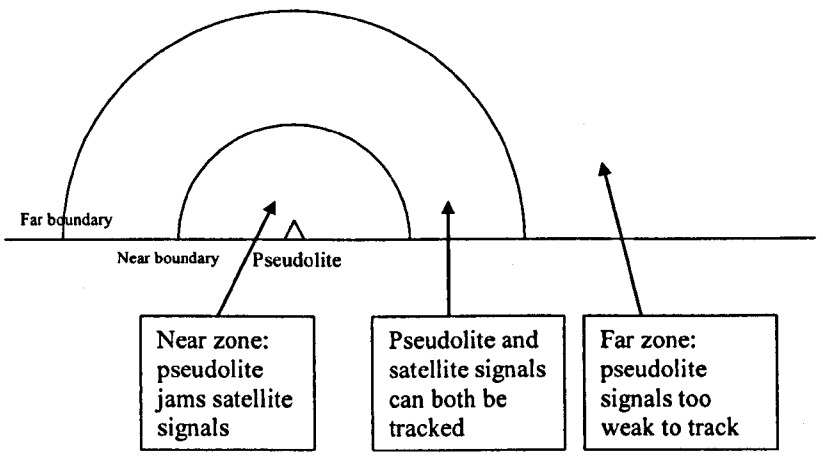

Figure 10-4 Zones of the Near-Far problem (Cobb 1997)

Elrod and Van Dierendonck (1995) suggest there are three solutions to the near-far problem. These are the use of a different carefully selected C/A code, a frequency offset from L1 and/or a pulsed pseudolite signal. As the first two require alterations to the GPS receiver before the pseudolite signal can be acquired, a pulsed signal is favoured. A pulsed signal means that the pseudolite will only, for example, transmit 10% of the time, which means it will only interfere with 10% of the satellite signals. The receiver treats the pseudolite signal as continuous so that there is still continuous tracking of the pseudolite carrier phase signal (Morley 1997). The Integrinautics pseudolites used in this thesis implement RTCM pulsing, which means they emit one pulse per epoch at a pseudo-random time, which repeats every 200 epochs

(Integrinautics 2002). RTCM is the standardized format for the transmission of GPS corrections, proposed by the Radio Technical Commission for Maritime Services (Hofmann-Wellenhof et al. 2001).

For the application of bridge monitoring the distances between the pseudolites and receivers are relatively constant over time, so the near-far problem can be solved by the use of attenuation. A pseudolite signal can be weakened, by adding attenuation, to approximately the same power level as a satellite when it reaches the receiver. Integrinautics (2002) suggests using 40 dB attenuation when the antenna and the pseudolite are 10 metres apart. During pseudolite trials conducted for this thesis the strength of the pseudolite signal was adjusted at the beginning of the observation session by trial and error, to give a pseudolite signal strength at the receiver that was in line with the satellite signals.

10.3.2.Pseudolite Location Bias

The pseudolite location bias has a different (and perhaps much larger) effect on the positioning solution than the satellite orbit error. For GPS receivers on a short baseline satellite orbit errors mainly cancel out in a double difference solution. This is not necessarily the case for the pseudolite location bias. Figure 10-5 shows the best and worst locations for pseudolite location bias. In the best location the pseudolite location bias cancels out completely in a double difference solution, but in the worst location this bias is doubled. So, this demonstrates that a good choice of pseudolite location can mean that this error is mitigated.

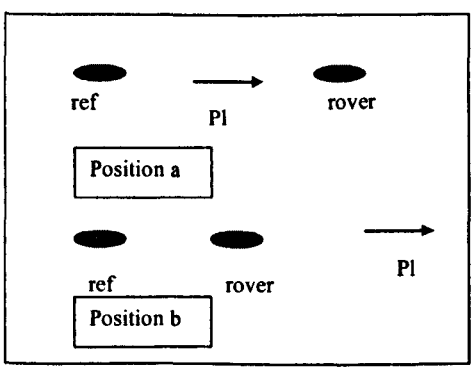

Figure 10-5 The best (position b) and worst (position a) locations for a pseudolite for the mitigation of the pseudolite location bias (Dai et al. 2000).

Measuring the coordinates of the pseudolites to a high degree of accuracy can also help to mitigate this error. However, the degree of accuracy that is needed may not be achievable. For the same location error as with a normal satellite, if the satellite orbit is known to within 5cm, the pseudolite location needs to be known to within 10^{-4}mm (for a pseudolite 40m away). It is obviously not possible for the coordinates of the pseudolite to be known to that degree of accuracy and so at least some location error will be present in the positioning solution. Since the receivers in a bridge monitoring environment are almost stationary the location bias will be present in the solution as a constant bias.

10.3.3.Multipath

Pseudolite multipath has different characteristics compared to GPS multipath (GPS multipath is introduced in Chapter 2, Section 2.3.3.3). The amount of 'transmitted' multipath from a GPS satellite is small, but the transmitted multipath from a pseudolite is significant (Ford et al. 1997). The elevation angle of a pseudolite is often lower than for a satellite and so multipath is more serious. However, if the receiver is stationary (or semi-static in the case of bridge monitoring) the multipath bias from a pseudolite is constant and so can be mitigated and reduced over time or calibrated in advance (Barnes et al. 2002). For a moving receiver, pseudolite multipath is harder to eliminate than GPS multipath as it is a stronger signal and is less likely to cancel in a differential system. The effects of multipath in a dynamic environment are discussed further in Ford, et al. (1997). Using multipath mitigating antennas at both the pseudolite and the receiver can greatly reduce the amount of multipath disturbance (Dai et al. 2000).

10.3.4.Atmospheric Delay

In GPS processing software, models are applied for atmospheric delays. The typical GPS processing tropospheric models (for example Saastamonienen and Hopfield) cannot be used for pseudolites as they are designed for GPS signals that travel from 20,000km away. A simple tropospheric model for pseudolites is derived by Dai, et al. (2000), which will mitigate the troposphere if there is a small distance between the pseudolites and the receivers. No correction is needed for the ionosphere for the ground-based pseudolites.

10.3.5.Pseudolite Clock Synchronisation

A pseudolite contains a cheap crystal oscillator and not an expensive atomic clock that can be found on a GPS satellite. This means that the pseudolite time is not synchronised to GPS time and so the magnitude of the pseudolite measurements are unpredictable. The measurements can be large or small, positive or negative. In a differential system the clock offset is cancelled out in the double difference solution. Pseudolites can be 'slaved' to GPS time if they can receive feedback from a GPS receiver (Ford et al. 1997). This would allow pseudolites to be used for stand-alone and real-time applications. Attempts to synchronise pseudolite constellations have so far resulted in positions that are up to six times worse than a double difference pseudolite solution (Yun and Kee 2002).

10.3.6.Ambiguity Resolution

Pseudolites can aid the resolution of carrier phase ambiguities making resolution quicker and more reliable in the case of a moving receiver, due to a well conditioned matrix of ambiguity parameters (Dai et al. 2001). In a static environment pseudolite ambiguities can only be resolved with the help of GPS observations because the geometry does not change. Since the pseudolites are at a low elevation angle and they are a high accuracy observable they contribute significantly to the solution accuracy.

10.4.Previous Research

During the last ten year pseudolites have been mostly used in aviation for precision approach and landing (Wang 2002). For a review of the historical development of pseudolites and more recent progress in pseudolite-based positioning, please refer to Wang (2002). Here, only the literature concerning the use of pseudolites for deformation monitoring will be discussed. Since 1999 the SNAP (Satellite Navigation and Positioning) group at UNSW have been investigating the use of pseudolites for deformation applications (Choi et al. 2000). Originally many technical problems were encountered with operation and data collection (similar problems were also encountered during initial experiments at The University of Nottingham). Three pseudolites were

installed on the roofs of high buildings, with two receivers collecting GPS and pseudolite data. The results showed a multipath bias in the pseudolite pseudorange measurements and also a less significant bias in the pseudolite carrier phase measurements. Due to these biases the positioning solutions were degraded when pseudolites were introduced.

Dai, et al. (2000) introduces some zero baseline pseudolite trials, which mean that the accuracy of the pseudolite pseudorange and carrier phase information can be assessed and compared to satellite data without errors such as multipath, pseudolite location and atmosphere influencing the result. The results indicate that the quality of the pseudolite pseudorange and carrier phase data are almost as good as those for a satellite. In an experiment with three pseudolites the accuracy of the height component was improved to almost the same level as the horizontal.

The feasibility of using pseudolites in industrial environments is investigated in Dai, et al. (2001). Also, the pseudolite-based inverted positioning concept for deformation monitoring is tested. Six GPS receivers are placed in a 'constellation', where they track a reference and mobile pseudolite. There was only a small difference in height between the six receivers which led to a bad geometry and high DOP, which affected the positioning solution. In Barnes, et al. (2002) the geometry for the inverted positioning is improved by having five receivers placed in an equally spaced circle with the last receiver placed directly below the roving pseudolite. As the inverted positioning method is not used in the study, it will not be discussed any further.

The constant multipath bias that affects the positions and double difference residuals, when pseudolites are used in the processing, is investigated by Barnes, et al. (2002). A procedure for the calculation and removal of this bias is discussed. After initial processing, plots of the carrier phase double difference residuals between a high elevation satellite and a pseudolite reveal a constant bias, the value of which is calculated and removed from the pseudolite raw carrier phase data. The pseudolite and satellite data is then reprocessed with this bias removed. The results show that the inclusion of pseudolites brings the accuracy of the height component to almost the same level as the horizontal. The effect of the antenna type (helical which have a more directional gain pattern versus a patch antenna) on the size of the pseudolite multipath bias is investigated. Results suggest that pseudolite multipath is reduced due to the directional beam of the helical antenna.

10.5.Static Trials

During October, 2002 two Integrinautics IN200C (IN200) pseudolites and two Canadian Marconi Corp Allstar (Allstar) receivers were loaned to The University of Nottingham by UNSW. Together with the IN200 pseudolite owned by The University of Nottingham a number of experiments were carried out.

To test the equipment before it was used in a bridge environment a static trial was carried out on 10th October, 2002 on The University of Nottingham campus. The three Integrinautics pseudolites were located on points downs1, downs2 and downsc, which were locations known to a high degree of accuracy from other trials. The pseudolites transmitted on PRN codes 12, 16 and 32, with their antennas mounted vertically so they were pointing towards the receiver locations. The two Allstar receivers were positioned on downsa and downsb. Figure 10-6 shows the location of the pseudolites and receivers, while Table 10-1 shows the elevations and azimuths of the three pseudolites from downsb. Approximately 30 minutes of data was collected for this trial.

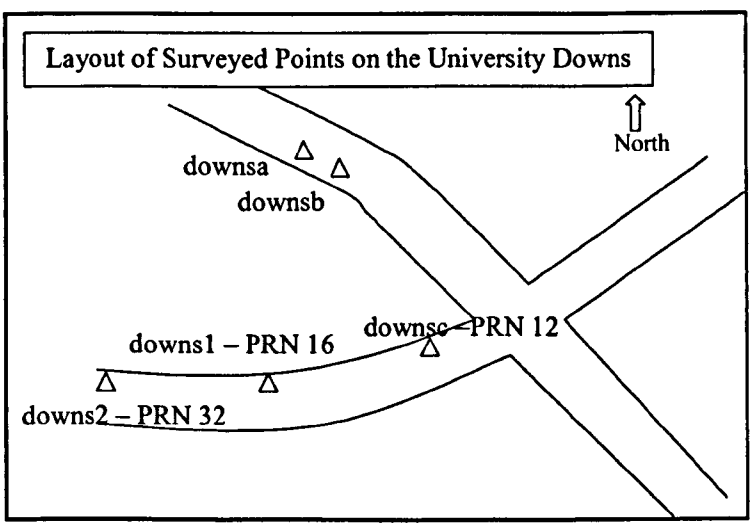

Figure 10-6 The layout of the points for the static trial on The University of Nottingham campus on 10th October, 2002.

	Elevation	Azimuth
downsc - PRN 12	1.66	142.98
downs1 - PRN 16	4.23	164.33
downs2 - PRN 32	1.85	196.91

Table 10-1 The elevation and azimuth of the pseudolite locations from downsb for the static trial.

Figure 10-7 to Figure 10-9 show the east, north and vertical coordinate scatters for the GPS only solution and GPS augmented by three pseudolites. Table 10-2 shows the

standard deviations of each of the three coordinates with and without the three pseudolites, and also the percentage improvement seen when pseudolites are introduced into the solution. The data was processed using software developed at UNSW called Baseline, with downsa as the reference receiver and downsb as the rover. For the GPS only solution it can be seen that the vertical component is considerably less accurate than the horizontal ones, and also that the north component is slightly worse than the east, confirming the need for augmentation with pseudolites. The introduction of three pseudolites improves the positioning solution in all three component directions, with the most significant improvement seen the vertical direction where the standard deviation falls from 5.7mm to 3.0mm, an improvement of 48%. This confirms that for static positioning pseudolites can improve the vertical accuracy to almost the same level as the horizontal.

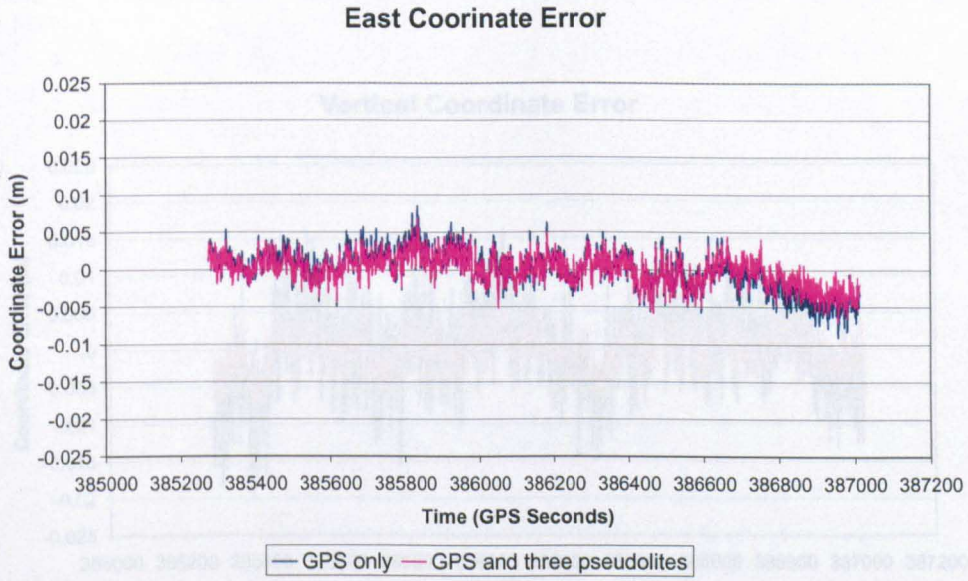

Figure 10-7 The east coordinate scatter for the GPS only solution and GPS augmented by three pseudolites

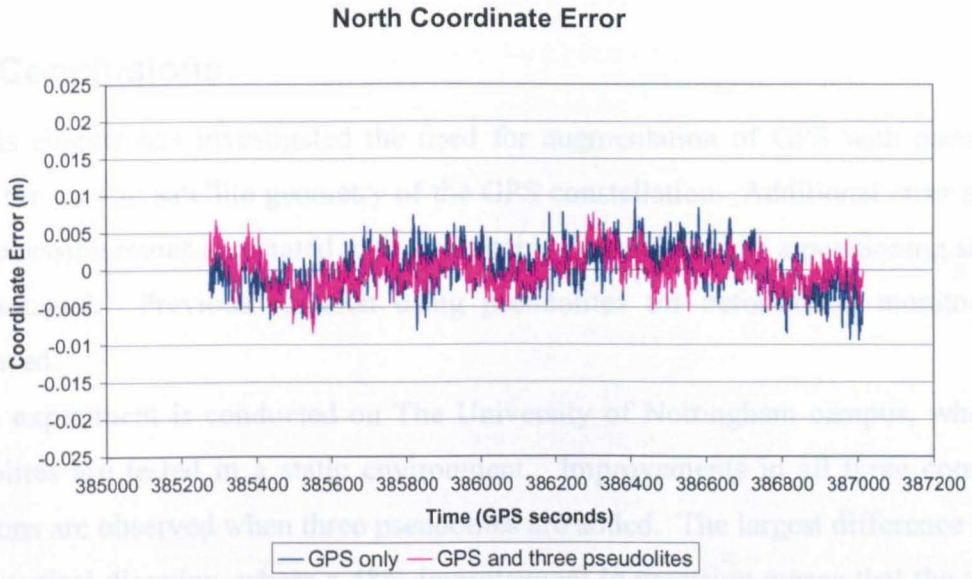

Figure 10-8 The north coordinate scatter for the GPS only solution and GPS augmented by three pseudolites

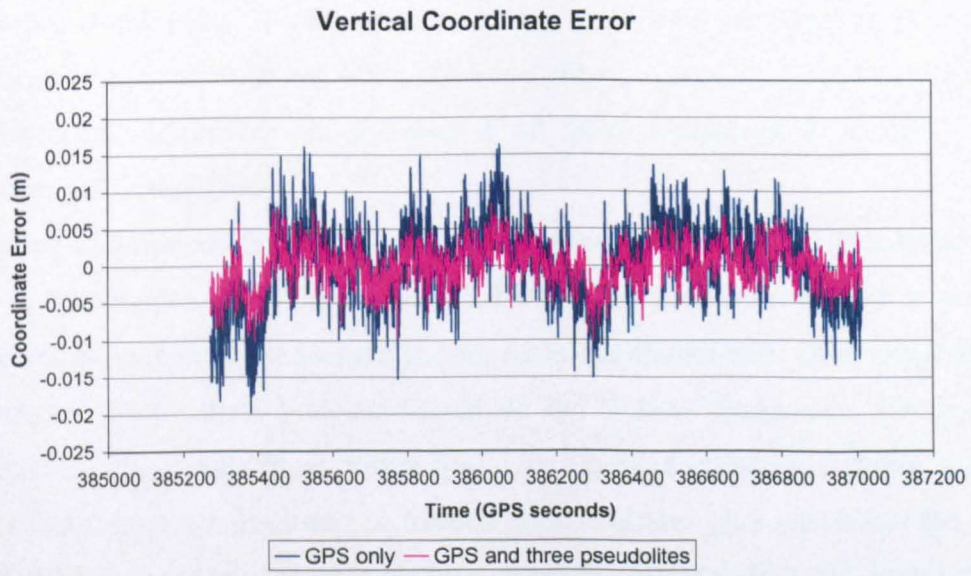

Figure 10-9 The vertical coordinate scatter for the GPS only solution and GPS augmented by three pseudolites

	Standard Deviations (m)		
Static Trial	East	North	Vertical
GPS only	0.0026	0.0028	0.0057
GPS and three pseudolites	0.0021	0.0023	0.0030
% improvement	19	17	48

Table 10-2 The standard deviations of the east, north and vertical components for GPS only and GPS augmented by three pseudolites, plus the percentage improvement seen with the introduction of pseudolites.

10.6.Conclusions

This chapter has investigated the need for augmentation of GPS with pseudolites due to the current satellite geometry of the GPS constellation. Additional error sources and processing issues associated with introducing pseudolites into a positioning solution are discussed. Previous research using pseudolites for deformation monitoring is introduced.

An experiment is conducted on The University of Nottingham campus, where the pseudolites are tested in a static environment. Improvements in all three coordinate directions are observed when three pseudolites are added. The largest difference is seen in the vertical direction, where a 48% improvement in precision means that the vertical component is almost at the same level as the horizontal.

11. Pseudolites for Bridge Deformation Monitoring

11.1.Introduction

The previous chapter introduced the concept of pseudolites as ground based GPS transmitters to augment the current GPS satellite constellation. This chapter looks at the inclusion of pseudolites in a GPS positioning solution for the application of bridge deformation monitoring. Two pseudolite bridge trials, one conducted in Nottingham, UK using three pseudolites and the second in Sydney, Australia using two pseudolites are introduced. Improvements are seen in all three component directions with the introduction of pseudolites.

Section 11.2 introduces the equipment layout and procedure for pseudolite bridge trial 1 in Nottingham, UK. In Section 11.3 the theoretical improvement in precision expected when one or three pseudolites are added, is shown with DOP simulations of two different bridge trials both conducted on the Wilford Suspension Footbridge in Nottingham. The results from bridge trial 1 in Nottingham and pseudolite multipath removal techniques are discussed in Section 11.4. Section 11.5 introduces the second pseudolite bridge trial conducted in Sydney, Australia. DOP values during this trial, on the Parsley Bay Bridge, are simulated in Section 11.6, which includes periods where the number of satellites falls to only 3. Section 11.7 contains the results from the second pseudolite bridge trial while Section 11.8 contains conclusions drawn from this chapter.

11.2.Pseudolite Bridge Trial 1- Nottingham, UK

A GPS and pseudolite bridge trial was conducted on the Wilford Suspension Footbridge in Nottingham on 16th October, 2002. The layout of the pseudolites and receivers can be seen in Figure 11-1. Three IN200 pseudolites were located at sites

PL12, PL16 and PL32 transmitting the respective PRN codes with their antennas mounted vertically so they are pointing towards the receiver locations (Figure 11-2). Table 11-1 shows the elevations and azimuths of the pseudolites from the roving receiver Bdg2.

The pseudolite locations were chosen for a number of reasons. The environment surrounding the bridge meant that the only viable locations had negative elevations. In Section 10.2 the deficiencies in the current satellite constellation that lead to the north-south component being less accurate than the east-west are explained. It is a research interest to find ways to improve the accuracy in the north-south direction and so all the pseudolites were located north of the bridge. However, the negative elevations of all the pseudolites actually caused more problems for the north-south accuracy which is explained later in Section 11.4. The coordinates chosen for the pseudolite locations were already known to a high degree of accuracy from previous trials that had been conducted at the bridge; this was another reason for the choice of locations.

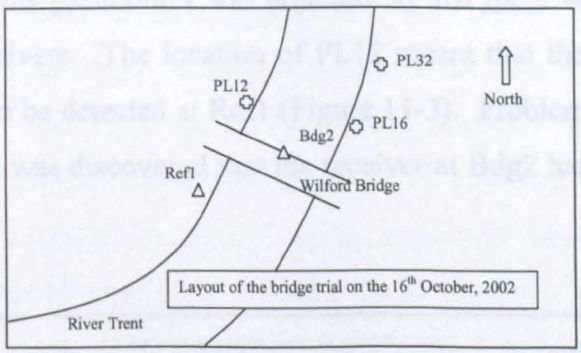

Figure 11-1 The layout of pseudolites and receivers on and around the Wilford Bridge trial on 16th October, 2002

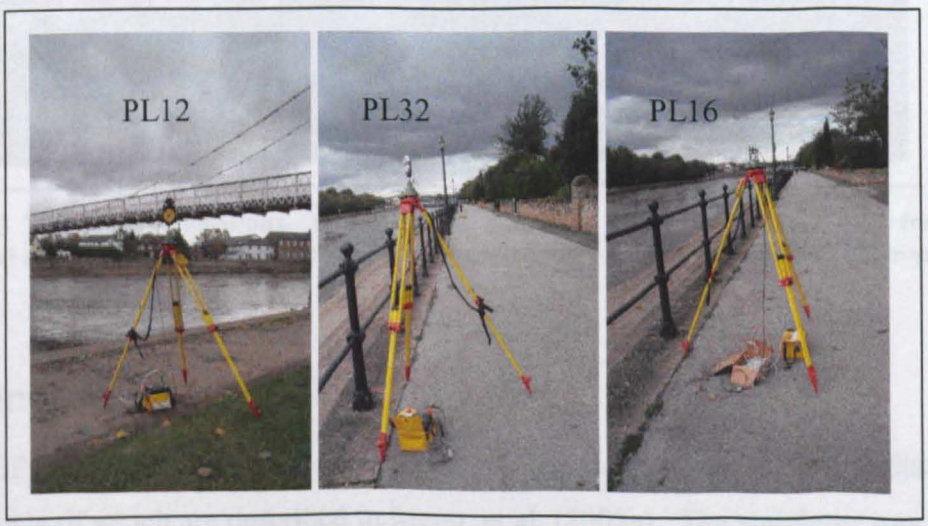

Figure 11-2 The location of the three pseudolites on the footpaths alongside the River Trent

	Elevation	Azimuth
PL12	-7.42	311.66
PL16	-4.12	70.60
PL32	-3.11	51.79

Table 11-1 The elevations and azimuths of the pseudolites from roving receiver site Bdg2

The reference receiver was also located on the bank of the river at point Ref1 and the rover was located at the mid-span of the bridge, point Bdg2. At both receiver locations there was a Leica dual frequency GPS receiver and an Allstar GPS/pseudolite receiver connected via a splitter to an AT502 antenna (Figure 11-3). The configuration was designed so that the data from the dual frequency Leica receivers could be compared directly to the results from the Allstar receivers. The comparison of the Leica data with the Allstar data is not undertaken here, but the interested reader is referred to Barnes et al. (2003b) for these results.

The attenuation of the pseudolites was adjusted so that there was a good signal to noise ratio at both receivers. The location of PL12 meant that the signal had to pass through a bridge arch to be detected at Ref1 (Figure 11-3). Problems were encountered during the trial when it was discovered that the receiver at Bdg2 had only logged about 40 minutes of data.

Figure 11-3 The receiver locations. At both Ref1 and Bdg2 there was a Leica dual frequency receiver and an Allstar GPS/pseudolite receiver connected via a splitter to an AT502 antenna.

11.3.Simulations 1

A DOP simulator has been developed at The University of Nottingham, the fundamentals of which are described in Meng, et al. (2002a). The simulator was further

developed for pseudolite applications by Daub (2002). Using this simulator the effect on DOP values, and therefore positioning accuracy, is researched when three pseudolites are added in the locations described in Section 11.2 above. In the simulator the actual bridge ephemeris is used and by inserting the locations of the pseudolites into this, a new ephemeris is formed. Using this new ephemeris, fresh DOP values are calculated for the situation with pseudolites.

In this section the DOP values for two separate bridge trials, both at the Wilford Suspension Footbridge, are investigated. Figure 10–3 shows a situation from the June bridge trial where the number of observable satellites fell to only 4. The effect of adding pseudolites to this situation is examined. Also a simulation of DOP values from the actual pseudolite bridge trial is conducted and compared to the real results.

11.3.1.June 2002 Bridge Trial

In a bridge trial on the Wilford Bridge that took place in June 2002 there was a period of ten minutes when the number of observable satellites fell to only four (Figure 10–3). Due to the bad geometry of these four satellites the GDOP value rose to 37 at maximum. It is known that when the GDOP value is above 6 the GPS positioning solution should not be trusted (Hofmann-Wellenhof et al. 2001). Table 11-2 shows the GDOP values for a GPS only solution and for GPS augmented with either one or three pseudolites. The location of each of the pseudolites corresponds to its position in the real pseudolite trial. It can be seen that with the inclusion of any one of the pseudolites the GDOP value falls to less than 6 for the whole of the observation session. When three pseudolites are included the GDOP value is always less than 3. The need for augmentation with pseudolites is demonstrated for this bridge trial, to guarantee reliable solutions for the whole of the observation session.

GDOP	Maximum	Minimum	Average	% Improvement on Average
GPS only	37.43	2.07	4.28	-
With pseudolite 12 only	4.42	1.70	2.16	50
With pseudolite 16 only	3.51	1.67	2.27	47
With pseudolite 32 only	4.68	1.68	2.38	44
With three pseudolites	2.73	1.38	1.78	58

Table 11-2 Summary of GDOP values for GPS only and with augmentation from one or three pseudolites for the June 2002 bridge trial

11.3.2.Pseudolite Bridge Trial, October 2002

Figure 11-4 shows the GDOP for a GPS only solution and for GPS augmented by three pseudolites for the pseudolite bridge trial conducted in October 2002. It can be seen from the graph that there is a period of approximately 19 minutes where the GDOP for the GPS only solution is above 7. This means that the coordinate produced are unreliable. When three pseudolites are added it brings the GDOP down to just over 3 for the 19 minutes of concern. This is well below the accepted value and is sure to provide a more accurate and consistent solution.

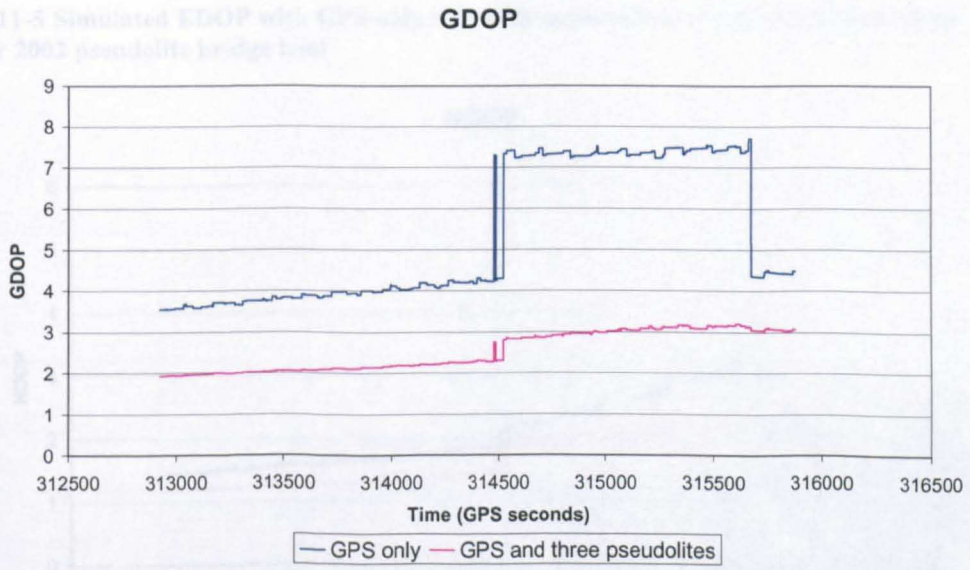

Figure 11-4 Simulated GDOP with GPS only and with augmentation from three pseudolites, for the October 2002 pseudolite trial on the Wilford Bridge

Figure 11-5 to Figure 11-7 show the EDOP (east DOP), NDOP (north DOP) and VDOP (vertical DOP) for the data from the October trial. A summary of these DOP values and GDOP can be seen in Table 11-3. Improvements in the DOP in all three directions can be observed when three pseudolites are added. There are large improvements of 47% and 59% in the east and vertical directions, whereas the improvement in the north direction is only 20%. Also the average DOP in the vertical direction is 1.5 when three pseudolites are added which is slightly better than the DOP in the north direction which is 1.6.

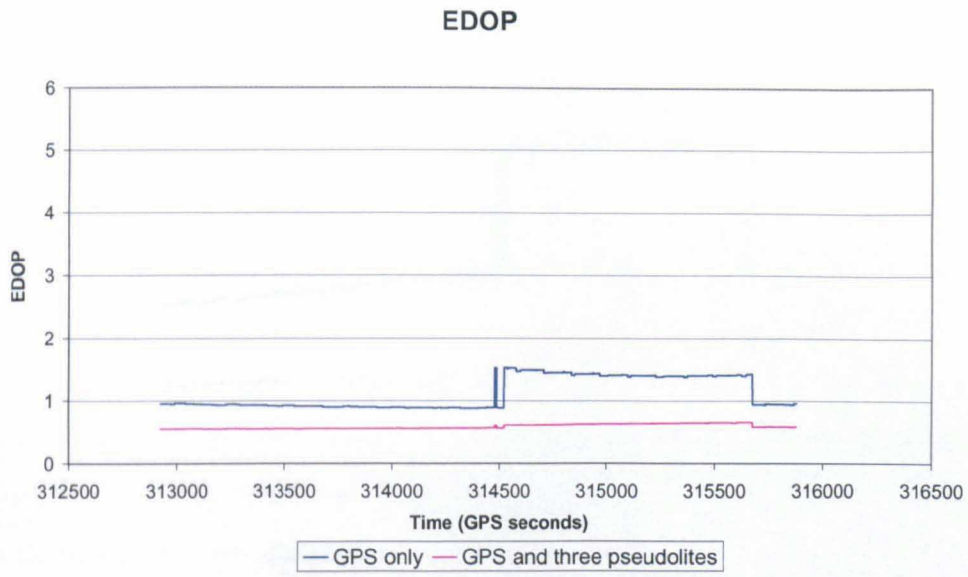

Figure 11-5 Simulated EDOP with GPS only and with augmentation from three pseudolites, for the October 2002 pseudolite bridge trial

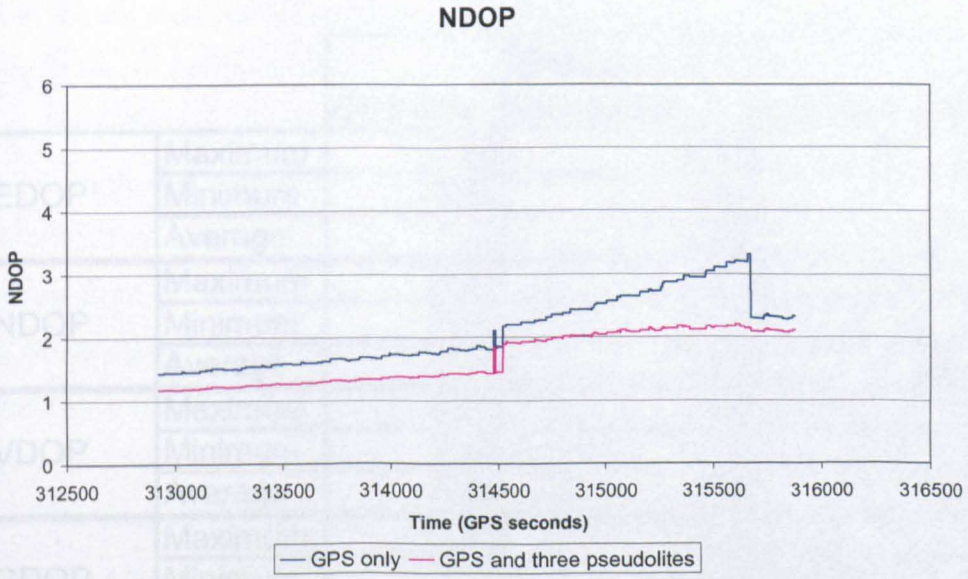

Figure 11-6 Simulated NDOP with GPS only and with augmentation from three pseudolites, for the October 2002 pseudolite bridge trial

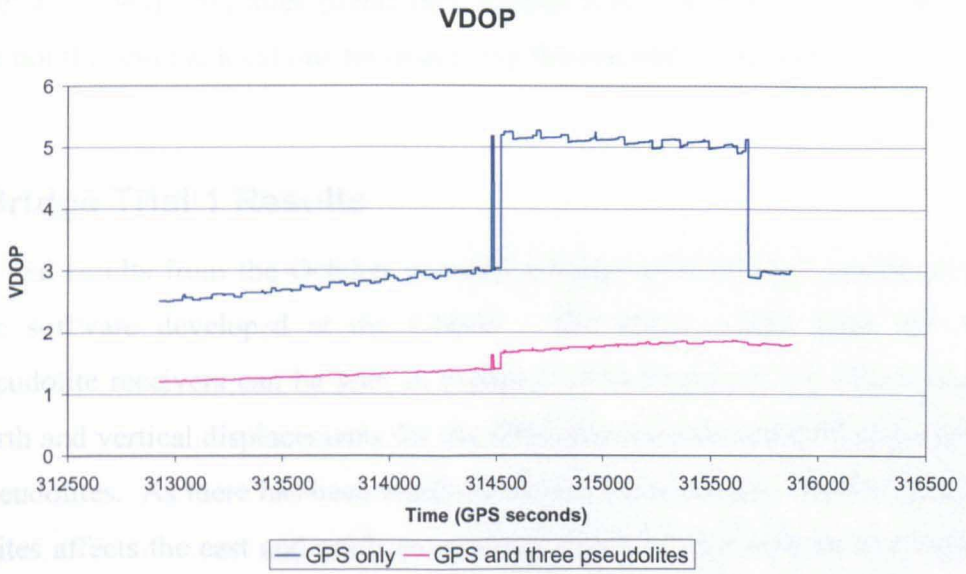

Figure 11-7 Simulated VDOP with GPS only and with augmentation from three pseudolites, for the October 2002 pseudolite bridge trial

		GPS only	GPS and three pseudolites	% Improvement
EDOP	Maximum	1.53	0.66	
	Minimum	0.89	0.56	
	Average	1.12	0.59	47
NDOP	Maximum	3.31	2.20	
	Minimum	1.43	1.18	
	Average	2.08	1.66	20
VDOP	Maximum	5.27	1.87	
	Minimum	2.50	1.20	
	Average	3.69	1.52	59
GDOP	Maximum	7.70	3.21	
	Minimum	3.54	1.93	
	Average	5.30	2.53	52

Table 11-3 Summary of DOP values for GPS only and GPS augmented by three pseudolites

This shows that the introduction of three pseudolites in the locations chosen has a greater effect on the vertical component than on the north component of the positioning solution. It also suggests that the northing component may provide a less accurate solution than the vertical component when the pseudolites are added. Previous simulations have shown that the best locations for improving the geometry in the vertical and east components, are three pseudolites below the horizon; whereas three pseudolites above the horizon are best for improving the north component (Meng 2002;

Cosser et al. 2004a). So, three pseudolites located below the horizon as in this bridge trial, are not the optimal locations for improving the northern component.

11.4.Bridge Trial 1 Results

The real results from the October pseudolite bridge trial were processed using the Baseline software developed at the UNSW. The initial results from the Allstar GPS/pseudolite receivers can be seen in Figure 11-8 to Figure 11-10, which show the east, north and vertical displacements for the GPS only solution and GPS augmented by three pseudolites. As there has been much discussion about the way that the addition of pseudolites affects the east and north component, it is these that will be analysed here, rather than the lateral and longitudinal directions in a bridge coordinate system.

All the graphs show an offset between the coordinates when pseudolites are included in the solution and when there is a GPS only solution. Due to the nature of the processing software the instantaneous coordinate of the rover needs to be known and input into the software for ambiguity resolution to be possible. This coordinate is calculated from the Leica receiver that was connected via a splitter to the Allstar. When the pseudolites are used in the processing, the positions in each component become further away from the 'truth'. The largest coordinate shift is evident in the vertical direction which can be seen in Figure 11-10.

As well as this offset in the coordinates, Table 11-4 shows that the addition of pseudolites also makes the standard deviation of the north component worse; an increase of 9% from 9.0mm to 9.8mm. There is a large improvement of 37% in the east component and a smaller improvement of 20% in the vertical component.

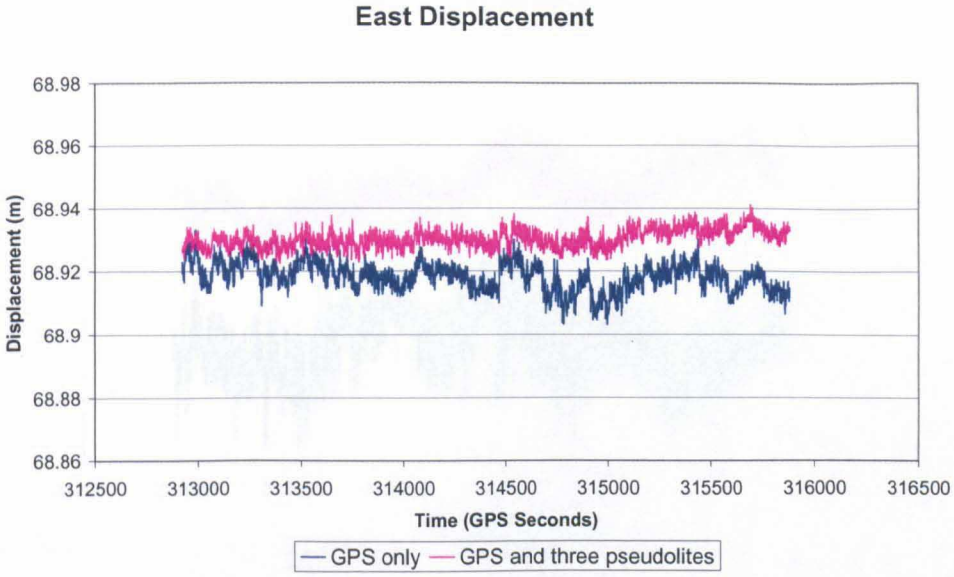

Figure 11-8 The east displacement with GPS only and GPS augmented by three pseudolites

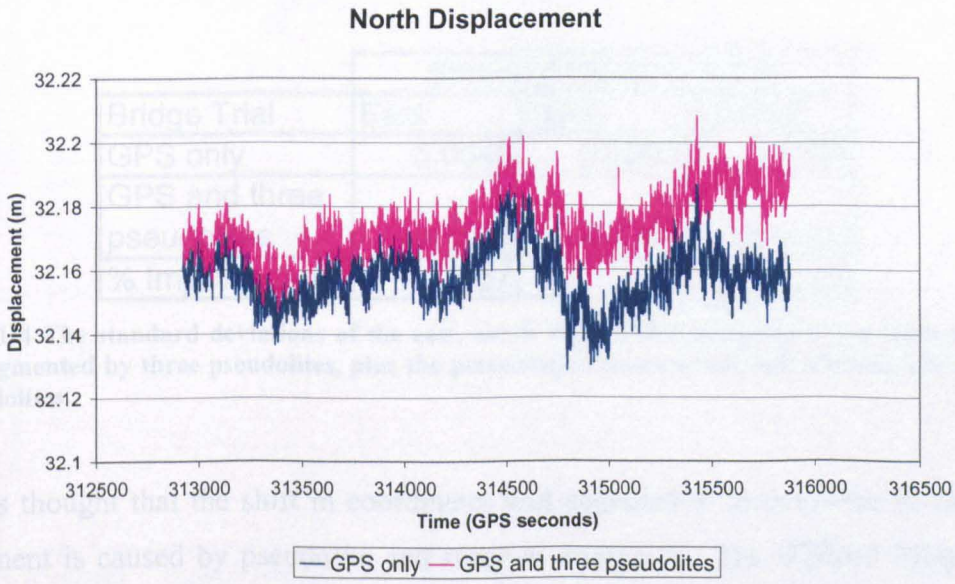

Figure 11-9 The north displacement with GPS only and GPS augmented by three pseudolites

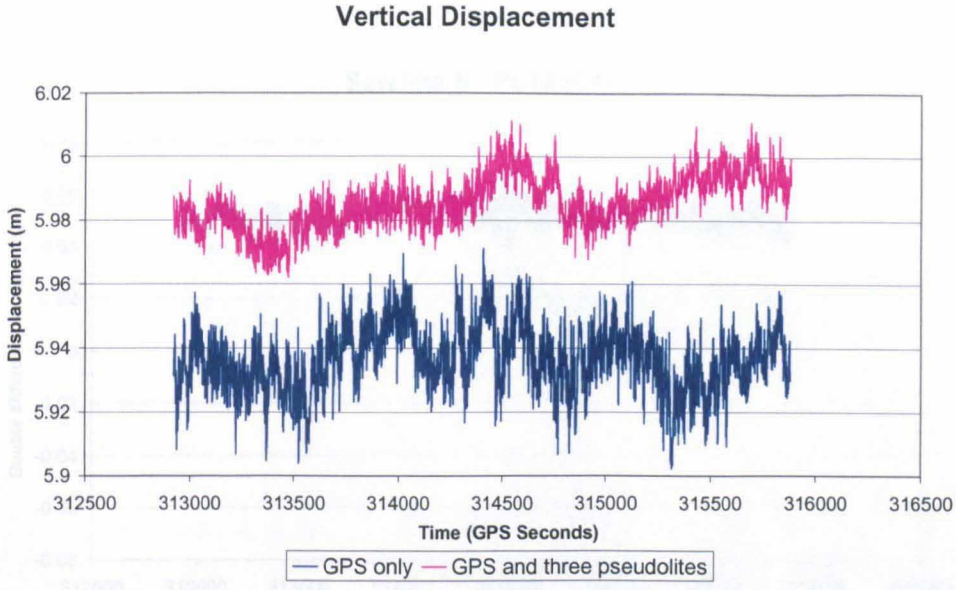

Figure 11-10 The vertical displacement with GPS only and GPS augmented by three pseudolites

	Standard Deviations (m)		
Bridge Trial	East	North	Vertical
GPS only	0.0045	0.0090	0.0104
GPS and three pseudolites	0.0029	0.0098	0.0084
% Improvement	37	-9	20

Table 11-4 The standard deviations of the east, north and vertical components for GPS only and GPS augmented by three pseudolites, plus the percentage improvement seen with the introduction of pseudolites.

It is thought that the shift in coordinates and degradation in precision in the north component is caused by pseudolite and receiver multipath. The Wilford Bridge does not have a very large amplitude movement and so for multipath mitigation purposes it can be considered static. Therefore the multipath will display itself as a constant bias in the positioning solution. Figure 11-11 to Figure 11-13 show the double difference residuals between satellite 5 (the base satellite) and each of the three pseudolites. It can be seen from the graphs that PL12 and PL16 have significant biases which offset them from zero. A typical satellite residual can be seen in Figure 11-14 for satellite 9, which exhibits a mean of approximately zero and the residual values are scattered about this. PL32 does not appear to have a significant bias. The average offset of the residuals is 51.4mm for PL12 and 38.8mm for PL16. The large offset for PL12 could be due to the signal having to travel through the bridge arch to the reference receiver, as mentioned previously.

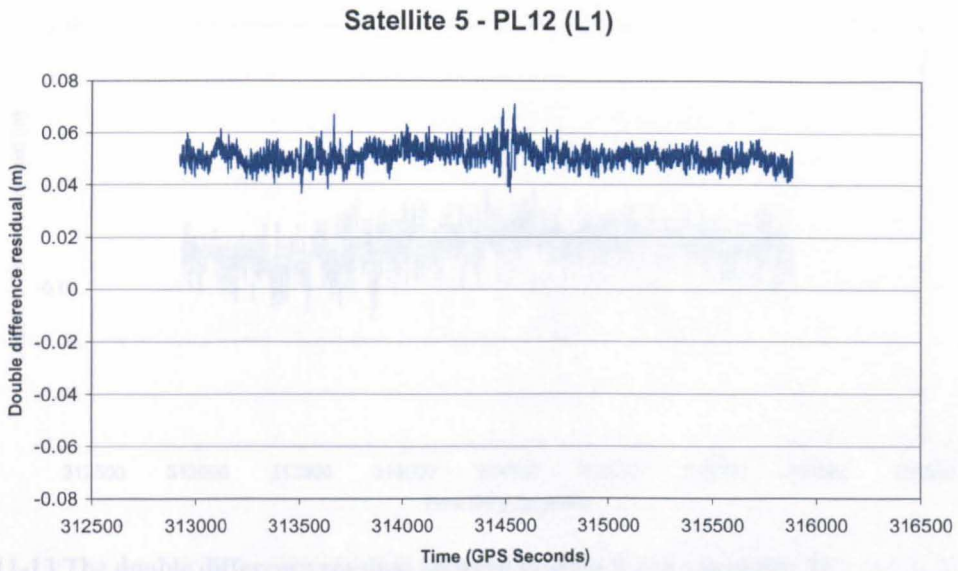

Figure 11-11 The double difference residual between satellite 5 and pseudolite 12

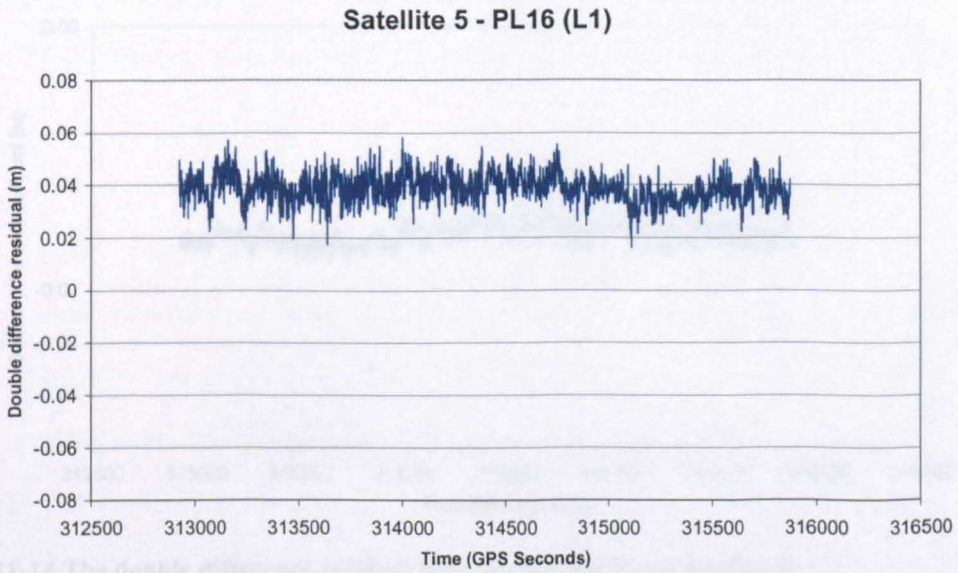

Figure 11-12 The double difference residual between satellite 5 and pseudolite 16

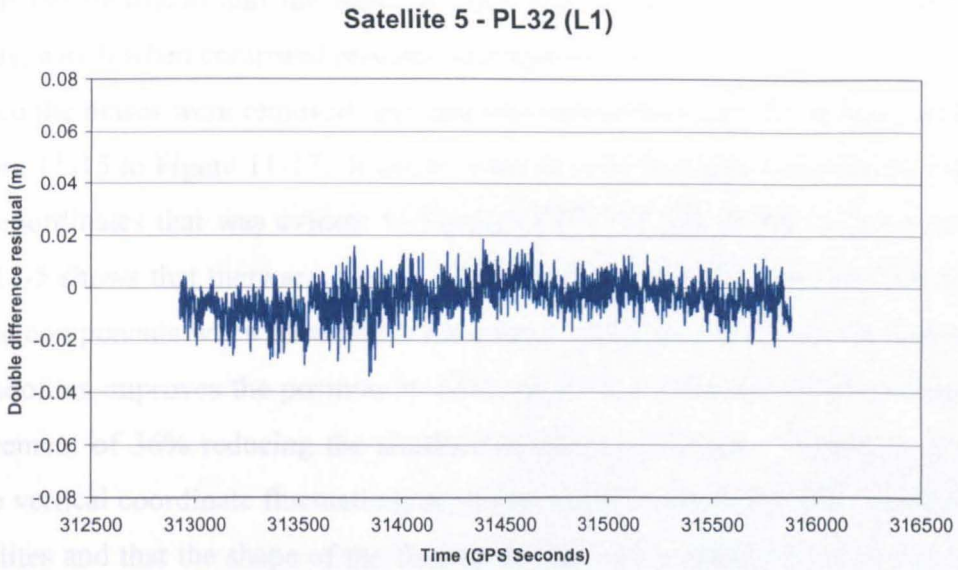

Figure 11-13 The double difference residual between satellite 5 and pseudolite 32

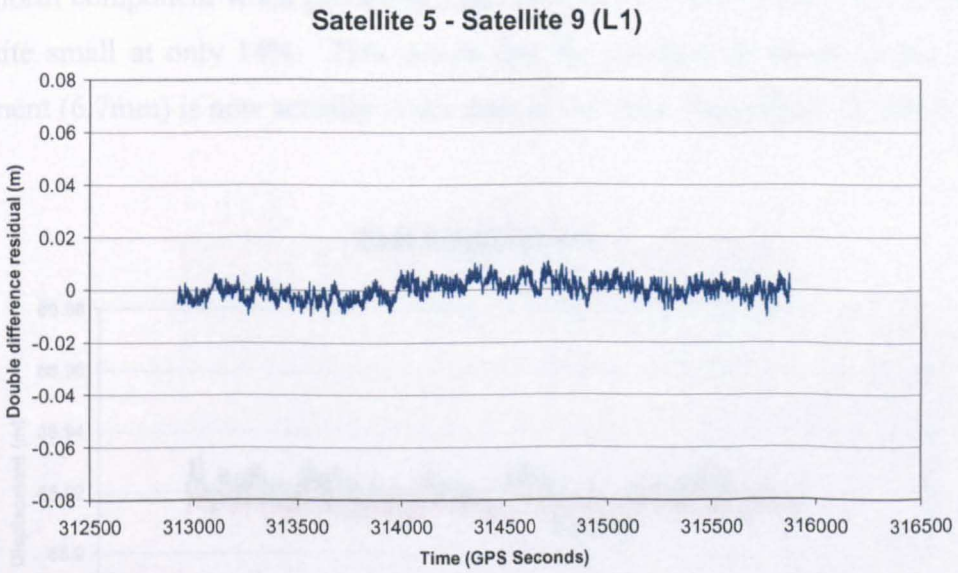

Figure 11-14 The double difference residual between satellite 5 and satellite 9

Barnes, et al. (2002) calculate the magnitude of the pseudolite multipath bias from the double difference residuals and then remove this value from the raw carrier phase of the pseudolite data. Then the data is reprocessed with the multipath bias and coordinate offset removed. The author investigated another method of multipath removal. The multipath bias was calculated in the same way from the double difference carrier phase residuals and then this bias was removed from the height component of the pseudolite coordinate, changing its location. It is likely that a component of the bias was caused by pseudolite location error and so modifying the pseudolite coordinate will help

mitigate the multipath and the location error also. The bias is removed using both methods, which when compared produce identical results.

Once the biases were removed, the data was reprocessed and the results can be seen in Figure 11-15 to Figure 11-17. It can be seen from these Figures that most of the bias in the coordinates that was evident in Figure 11-8 to Figure 11-10 has been removed. Table 11-5 shows that there are also further improvements in the standard deviations in all three components when pseudolites are added. In the east direction the introduction of pseudolites improves the position by 45%, while in the vertical direction there is an improvement of 36% reducing the standard deviation to 6.7mm. Figure 11-17 shows that the vertical coordinate fluctuations have been greatly reduced by the introduction of pseudolites and that the shape of the fluctuations are now actually very similar to those in the north component. The removal of the multipath bias has led to an improvement in the north component when pseudolites are introduced; however this improvement is still quite small at only 14%. This means that the standard deviation in the vertical component (6.7mm) is now actually lower than in the north component (7.7mm).

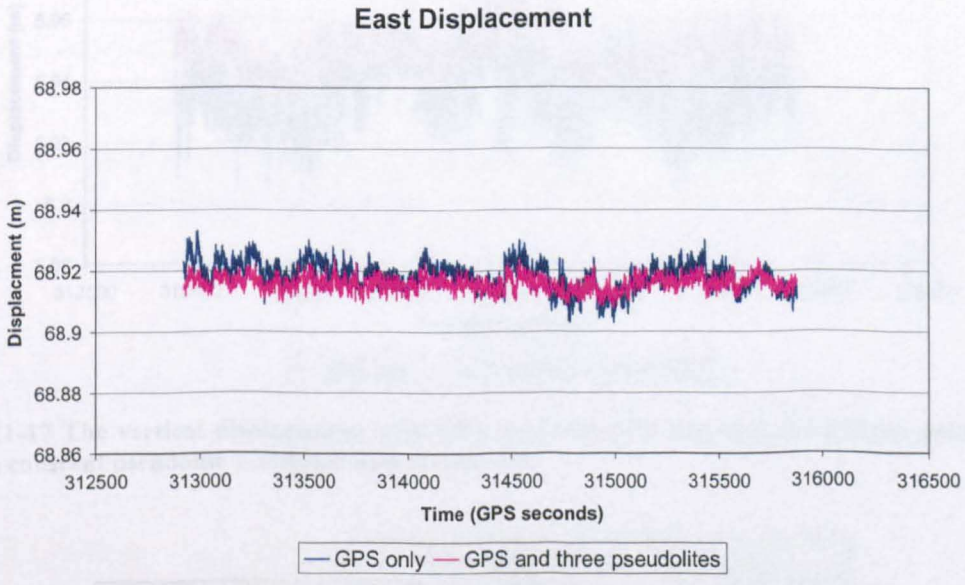

Figure 11-15 The east displacement with GPS only and GPS augmented by three pseudolites after the constant pseudolite multipath bias is removed

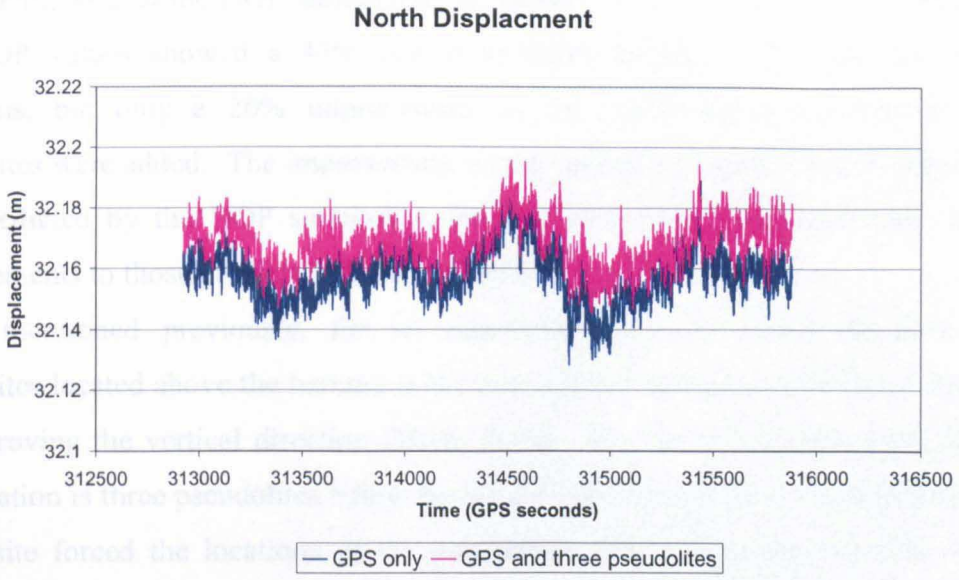

Figure 11-16 The north displacement with GPS only and GPS augmented by three pseudolites after the constant pseudolite multipath bias is removed

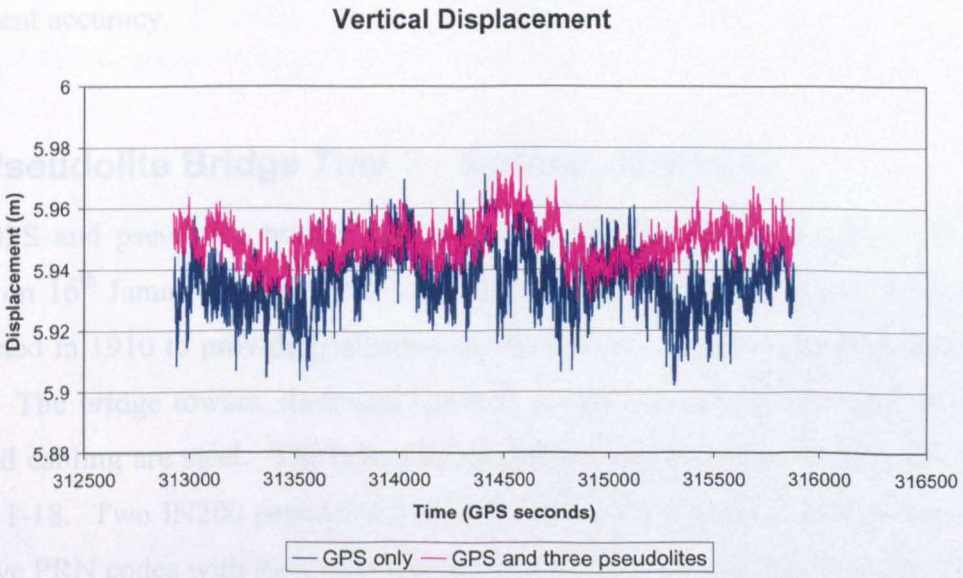

Figure 11-17 The vertical displacement with GPS only and GPS augmented by three pseudolites after the constant pseudolite multipath bias is removed.

	Standard Deviations (m)		
Bridge Trial	East	North	Vertical
GPS only	0.0045	0.0090	0.0104
GPS and three pseudolites	0.0025	0.0077	0.0067
% Improvement	45	14	36

Table 11-5 The standard deviations of the east, north and vertical components for GPS only and GPS augmented by three pseudolites, plus the percentage improvement seen with the introduction of pseudolites.

Looking back at the DOP simulations in Section 11.3.2 the results are as expected. The DOP values showed a 47% and 59% improvement in the east and vertical directions, but only a 20% improvement in the north direction when the three pseudolites were added. The improvement in the vertical direction is not as large as the 59% predicted by the DOP simulation, but the other two components have similar improvements to those predicted by the simulation.

As mentioned previously, for an improvement in the north direction three pseudolites located above the horizon is the best constellation; however this is not good for improving the vertical direction (Meng 2002). For vertical improvement the best constellation is three pseudolites below the horizon as in this trial. The geometry of the bridge site forced the locations of the pseudolites to be below the horizon. Future pseudolite locations could be on the towers of the bridge or further away on one of the surrounding buildings to investigate the effect of different constellations on the north component accuracy.

11.5.Pseudolite Bridge Trial 2 - Sydney, Australia

A GPS and pseudolite bridge trial was conducted on the Parsley Bay Bridge in Sydney on 16th January, 2003. The cable stayed footbridge, Parsley Bay Bridge, was constructed in 1910 to provide pedestrian access between the two shores (Barnes et al. 2003a). The bridge towers, deck and handrail are all constructed of wood, while the sides and cabling are steel. The layout of the pseudolites and receivers can be seen in Figure 11-18. Two IN200 pseudolites were located at PL12 and PL32 transmitting the respective PRN codes with their antennas pointed towards the receiver locations (Figure 11-19). Table 11-6 shows the elevations and azimuths for the pseudolites from the rover receiver Bridge. It should be pointed out that the environment surrounding the Parsley Bay Bridge also meant that both the pseudolites had to be located at negative elevation angles as had been the case in the Nottingham trial. The locations of the pseudolites were chosen so that the distance to the reference receiver (Base) and the roving receiver (Bridge) were approximately the same and also so that the locations had a clear view of the sky for surveying the positions with GPS (Figure 11-19).

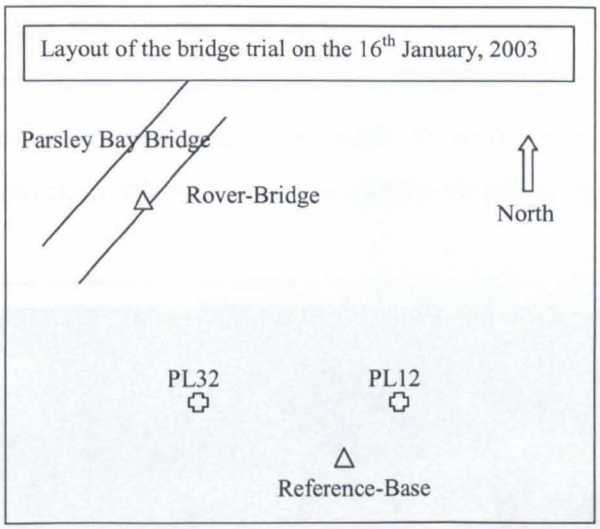

Figure 11-18 The layout of the pseudolites and receivers on and around the Parsley Bay Bridge trial on 16th January, 2003

	Elevation	Azimuth
PL12	-6.61	134.51
PL32	-9.61	174.36

Table 11-6 The elevations and azimuths of the pseudolites from roving receiver Bridge

Figure 11-19 The locations of the two pseudolites around Parsley Bay

The rover was located at the mid span of the bridge (Bridge) and the reference station was located on a stable point in the bay (Base). At both receiver locations there was a Leica dual frequency GPS receiver and a NovAtel Millennium (OEM3) GPS/pseudolite receiver connected via a splitter to a NovAtel 600 antenna (Figure 11-20). The pseudolite attenuation was adjusted so that there was a good signal to noise ratio at both receivers. Approximately two and three quarter hours worth of data were

collected at a 2 Hz data rate during this trial. On six occasions during the trial the bridge was made to move by four people located on the bridge rocking it from side to side. Five of the occasions the bridge was made to move were between GPS times 347750 and 349250 and the sixth occasion was approximately at time 353550.

Figure 11-20 The receiver locations. At both Base and Bridge there was a Leica dual frequency GPS receiver and a NovAtel Millennium (OEM3) GPS/pseudolite receiver connected via a splitter to a NovAtel 600 antenna.

11.6.Simulations 2

The DOP simulator described in Section 11.3 was used to simulate the expected results for the Parsley Bay Bridge trial also. The actual satellite ephemeris was used to simulate the DOP values without pseudolites and with the two pseudolites in the locations described in Table 11-6. The real GPS GDOP values and the simulated GPS and pseudolites values can be seen in Figure 11-21. For the simulations satellite 9 was removed because this satellite had to also be removed from the actual processing due to poor residual values. There were occasions during the trial where due to obstructions the number of satellites fell briefly to only four or in some circumstances to only three satellites. At GPS time 352670 the number of satellites fell to only four with a bad geometry and after this point the GDOP values are very high for the rest of the observation session (actually so high that you cannot see the values in Figure 11-21). At some points the GDOP rose to values considerably greater than 800 and so the GPS only solution cannot be trusted.

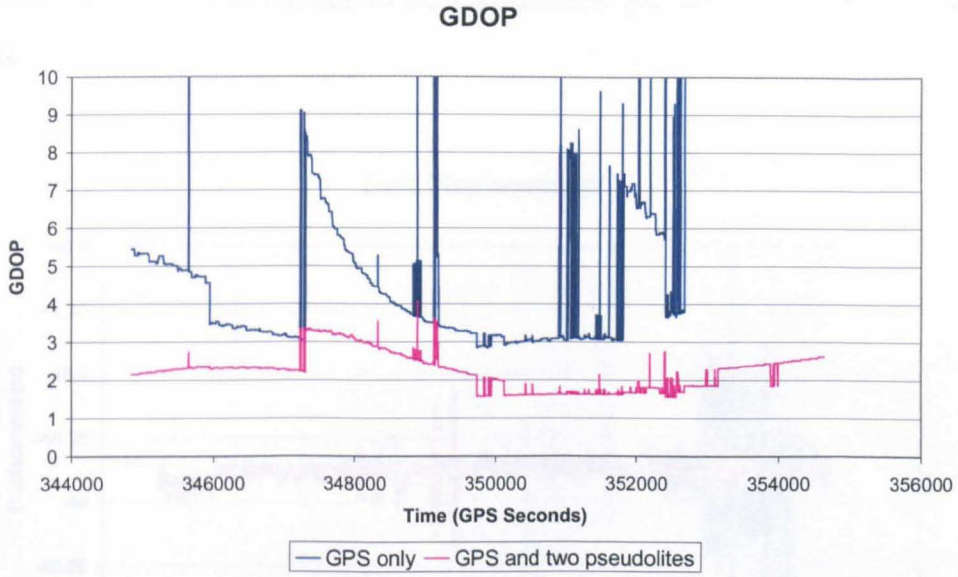

Figure 11-21 Simulated GDOP with GPS only and GPS augmented by two pseudolites, for the January 2003 pseudolite bridge trial

When the two pseudolites in positions described in Table 11-6 are introduced into the solution there is a great improvement in the GDOP values. The highest GDOP value observed is just above 4. After GPS time 352670 when the GPS only solution is completely unusable due to the high DOP values, the GPS and pseudolite GDOP does not rise above 3. Since the GPS only GDOP values are so high it is hard to actually quantify the improvement when pseudolites are introduced, but it can be seen that the improvement is considerable in a situation like this where the GPS geometry is so bad. High GDOP values are observed for a considerable amount of this observation session with GPS only and so without the pseudolites the integrity of the bridge monitoring system would be compromised.

11.7.Bridge Trial 2 Results

The results from the pseudolite bridge trial in Sydney, Australia were also processed using the Baseline software. The combination of pseudolite multipath and location error was removed from the pseudolite data by the method described in Section 11.4. The results shown in Figure 11-22 to Figure 11-24 are the positioning solutions with the pseudolite multipath and location bias removed. It is evident, particularly from Figure 11-24 that the introduction of pseudolites improves the positioning solution especially

after GPS time 352670 when, due to the bad satellite geometry, the GPS only solution worsens.

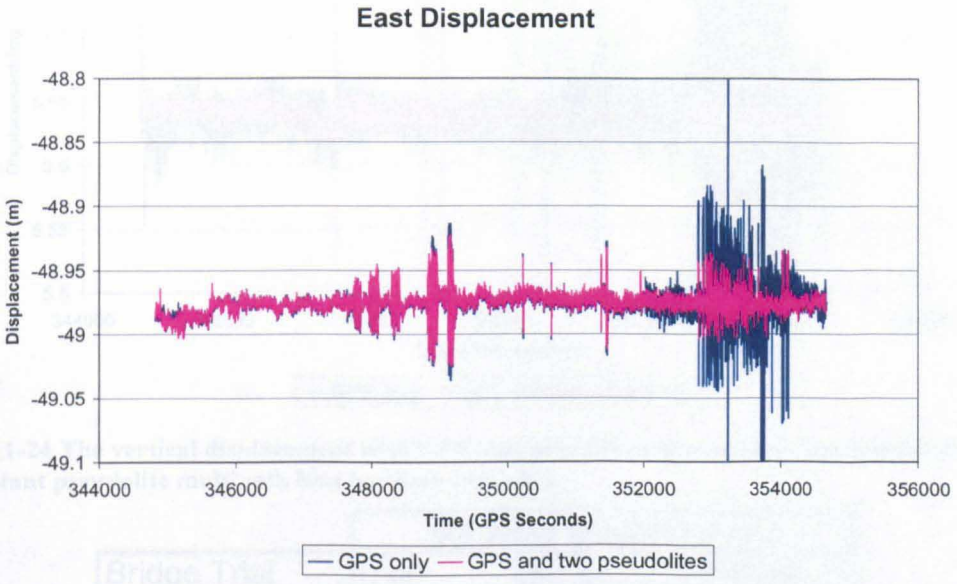

Figure 11-22 The east displacement with GPS only and GPS augmented by two pseudolites after the constant pseudolite multipath bias has been removed

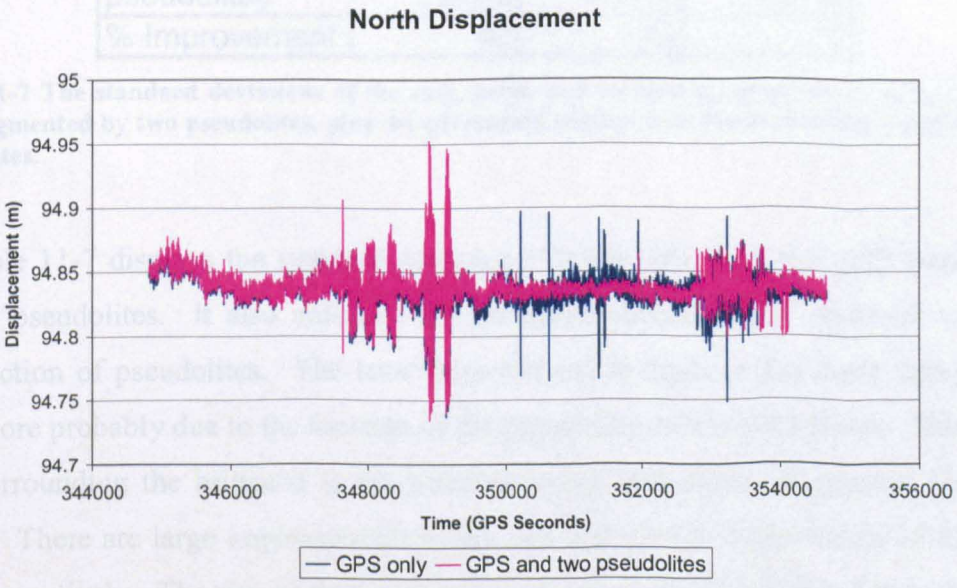

Figure 11-23 The north displacement with GPS only and GPS augmented by two pseudolites after the constant pseudolite multipath bias has been removed

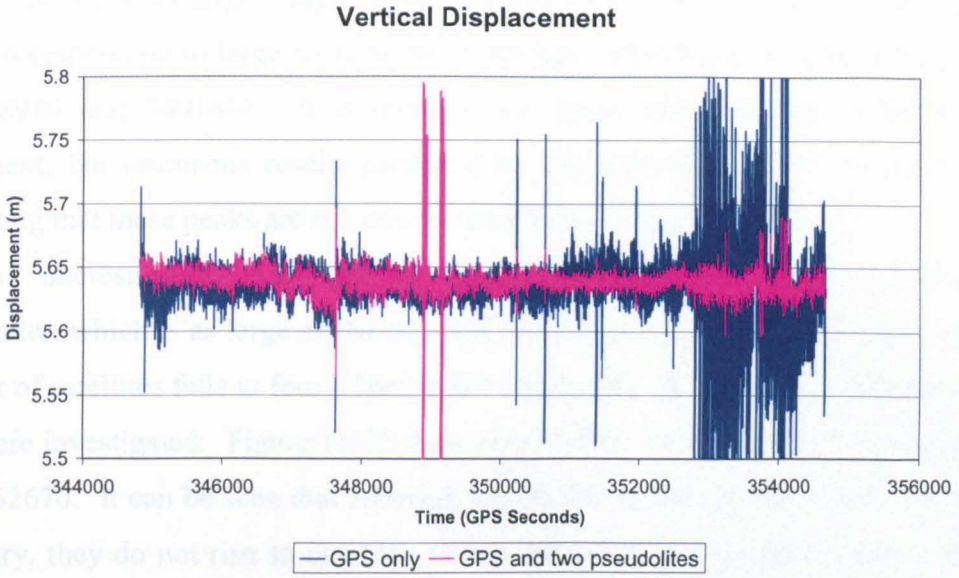

Figure 11-24 The vertical displacement with GPS only and GPS augmented by two pseudolites after the constant pseudolite multipath bias has been removed.

	Standard Deviations (m)		
Bridge Trial	East	North	Vertical
GPS only	0.0135	0.0124	0.0340
GPS and two pseudolites	0.0078	0.0112	0.0102
% Improvement	42	10	70

Table 11-7 The standard deviations of the east, north and vertical components for GPS only and GPS augmented by two pseudolites, plus the percentage improvement seen with the introduction of pseudolites.

Table 11-7 displays the standard deviations for the GPS only and GPS augmented by two pseudolites. It also indicates the percentage improvement observed with the introduction of pseudolites. The least improvement is again in the north component, once more probably due to the location of the pseudolites below the horizon. Due to the area surrounding the bridge it is not possible to put pseudolites at positive elevation angles. There are large improvements in the east and vertical components of 42% and 70% respectively. The size of these improvements is mainly due to the deterioration of the GPS only solution seen after time 352670.

It was mentioned above that there were six occasions when horizontal bridge movement was induced by people on the bridge. The five occasions between 347750 and 349250 are clear in Figure 11-22 and Figure 11-23, but the movement at 353550 is masked by the noise in the solution. As the induced movement was only in the horizontal component it should not be evident in the vertical component. However,

Figure 11-24 shows large 'displacement' in the GPS and pseudolite solution at two times corresponding to large movements in the horizontal direction (approximate times are 348940 and 349180). It is thought that these peaks are not actually bridge movement, but erroneous results produced by the large horizontal movement. It is interesting that these peaks are not seen in the GPS only solution.

It is interesting to note that the north displacement does not experience a degradation which is as large as the east and vertical components experience, when the number of satellites falls to four. The NDOP values after the number of satellites fell to four were investigated. Figure 11-25 shows the EDOP, NDOP and VDOP values after time 352670. It can be seen that although the NDOP values do rise due to the satellite geometry, they do not rise so quickly. When the number of satellites falls to four the geometry for the northern component is slower to be affected. However, the geometry of the northern component does worsen eventually, along with the east and vertical, so it is strange that only a very small amount of deterioration is seen in the north component.

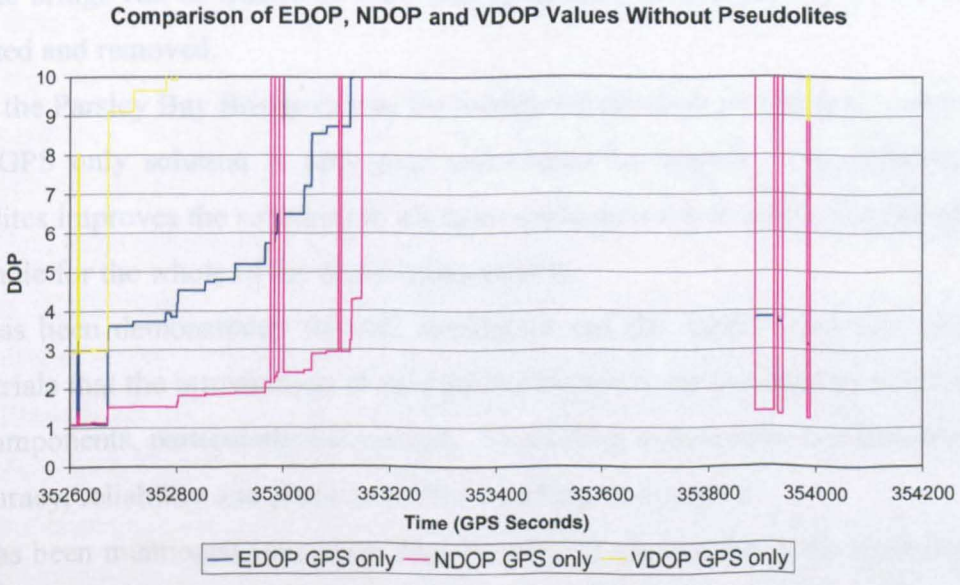

Figure 11-25 Comparison of the EDOP, NDOP and VDOP values without pseudolites from GPS time 352670

11.8.Conclusions

Simulations were conducted to assess the improvement in coordinate accuracy when one, two or three pseudolites were introduced for different bridge trials. For the Wilford

it was seen that during a period when only four satellites were available and the GDOP for a GPS only solution had risen to 37, the introduction of just one pseudolite reduced the GDOP to below 5, which meant that the positioning solution could be trusted for the whole of the observation window. For the Parsley Bay Bridge, in a situation where the GDOP rose to above 800, the introduction of two pseudolites meant that the GDOP value was always around 4 or less.

For the Wilford Bridge the simulation for the pseudolite bridge trial was compared to the results from the actual observations. It was seen from the simulation that the pseudolite constellation was not ideal for improving the north component. The actual results showed that the vertical component was improved to better than the north component with the introduction of three pseudolites. For a larger improvement in the north component a constellation with three pseudolites above the horizon is ideal, however the area surrounding the bridge makes positioning pseudolites at positive elevation angles difficult (Meng et al. 2004b).

Problems with pseudolite multipath and pseudolite location error were encountered in the bridge environment. The double difference pseudolite residuals show a bias, and since the bridge can be treated as static due to its small amplitude, these biases can be calculated and removed.

For the Parsley Bay Bridge due to the number of satellites dropping to 4 and then to 3, the GPS only solution is very poor and cannot be trusted. The introduction of pseudolites improves the solutions in all three components and means that the solutions are reliable for the whole of the observation session.

It has been demonstrated through simulation and the results from two pseudolite bridge trials that the introduction of pseudolites improves the positioning solution in all three components, particularly the vertical. Pseudolites enhance the solution improving the accuracy, reliability and precision of the resulting coordinates.

It has been mentioned previously that the vertical component is the most important for bridge deformation monitoring and so improving the accuracy of this component has been a research aim. This chapter and Chapter 11 have demonstrated the feasibility of using pseudolites in a bridge environment to improve the results in all three coordinate directions. This would results in a more accurate and reliable bridge monitoring system.

11.9.Corollary, Locatalites- A Replacement for Pseudolites in the Future?

11.9.1.Disadvantages of Pseudolites

Although pseudolites have been around since the design stages of the GPS system their use is not very widespread. There are a number of reasons for this.

- Constellation- The operational issues and errors that are discussed in Section 10.3 all act as barriers to the widespread use of pseudolites. Special processing software must be developed for integrating pseudolites into a positioning solution.
- Hardware- Pseudolites are not manufactured by very many companies. In fact the company that manufactured the pseudolites used for experiments in this thesis has now stopped making them, further reducing the number of manufacturers. The pseudolites that are available are expensive (usually more than $10,000 (US)) and very few GPS receivers can track their signal. To be able to track the signal the GPS receiver must allow manual assigning of channels. Two of the receivers that allow this are used in this thesis. They are Allstar and NovAtel Millennium. These receivers will only allow the pseudolite data to be recorded for post-processing; the results are not available in real time.
- Synchronisation- The pseudolites contain a cheap oscillator much like those found in the GPS receivers, not expensive atomic clocks found on satellites. Pseudolites are not synchronised with each other or to GPS time. This means that single point positioning is not possible due to huge clock errors. A solution containing pseudolites must be processed in differential mode which requires a second receiver on a known location. For real-time positioning the corrections from the reference receiver must be transmitted to the rover via a communication link. This adds greatly to the cost of the system. Attempts to synchronise pseudolite constellation have so far resulted in positions that are up to six times worse than a double difference pseudolite solution (Yun and Kee 2002).

Despite these problems pseudolites have been used by the author with good results for the application of bridge deformation monitoring. However, there is new technology being developed to overcome the deficiencies of the GPS and pseudolites approach. LocataNet technology is being developed by Locata Corporation Pty Ltd, Australia in collaboration with UNSW. The basics of this technology will be introduced in the following section as an extension to the author's work on pseudolites.

11.9.2.LocataNet Fundamentals

11.9.2.1. Core Components

The LocataLite is an intelligent pseudolites transceiver. The receiver part can receive signals from the GPS constellation and other LocataLites, while the transmitter pulses its own unique code. The Locata is a stand-alone low cost receiver which is capable of picking up GPS and LocataLite signals. When four or more LocataLite signals are tracked, the Locata will produce cm-level positioning solutions.

11.9.2.2. Time-Loc

LocataLites work on a system of synchronised clocks. The process of clock synchronisation is called Time-Loc and is the principle behind the Locata technology. From Barnes, et al. (2003d) the procedure for Time-loc of two LocataLites is described by the following steps:

1. LocataLite A is set up and it begins to transmit its own unique code and carrier phase signal.
2. LocataLite B is set up and with its receiver section it acquires, tracks and measures the signal from LocataLite A.
3. LocataLite B then starts to generate its own unique signal.
4. LocataLite B calculates the difference between the received signal from A and a locally generated signal. Ignoring propagation effects the difference between the two signals are the time difference and the geometric distance between them.
5. B adjusts its local oscillator so the difference between its signal and the signal of A is 0 using Direct Digital Synthesis (DDS). Signal differences are

continually monitored so that they stay at 0. The oscillator of B is following directly the oscillator of A.

6. Finally the geometric distance between the two LocataLites (which is known due to the coordinates of each LocataLite being known) is corrected for and Time-Loc is achieved.

Experiments have shown that the LocataLites achieve Time-Loc with accuracies of better than 33 pico-seconds.

11.9.2.3. Cascaded or Master System?

The LocataNet is the established system of LocataLites all having achieved Time-Loc. This can be accomplished in two ways. The first is called a master system where all LocataLites achieve Time-Loc relative to a master LocataLite. The second is a cascaded system where Time-Loc is achieved in steps where each LocataLite attains Time-Loc relative to each preceding LocataLite (ie B achieves Time-Loc to A, C achieves Time-Loc to B and so on). The accuracies of both systems are tested by Barnes, et al. (2003e). In both cases Time-Loc is achieved in less than ten minutes. The LocataLites in the cascaded system do have larger standard deviations than in the master system, but this does not seem to be related to the distance over which the Time-Loc is carried out.

11.9.3. Advantages of LocataNet

There are many advantages of LocataLites over currently available technology.

1. There is no base station and so no data links are required.
2. For real time differential GPS the rover station must wait to receive corrections from the reference. This latency is avoided by the Locata system.
3. Pseudolites pulse their signals to reduce signal jamming of GPS. Since the pseudolite clocks are not synchronised it is possible for pseudolites to transmit at the same time and so interfere with each other. Since LocataLite clocks are synchronised they will never pulse at the same time.
4. Since a double difference solution is avoided and only the raw carrier phase is used for positioning, theoretically the precision achievable is greater.

11.9.4. Preliminary Experiments Conducted

Barnes, et al. (2003c) introduce outdoor static and kinematic tests of the LocataNet. Static tests produced a mean error of less than 2mm, with a standard deviation of less 6mm and 93% of the east and north errors less than ±1cm. A kinematic test was conducted with an old record turntable making the Locata repeat a circular path. In this case 82% of the values are less then 2cm away from the best-fit circle. This demonstrates that sub-cm accuracy is clearly achievable with the Locata technology.

Indoor Locata test are conducted by Barnes, et al. (2003d) where five LocataLites were located on the roof of a building with their signal power at such a level that it could be received inside. The signal to noise values of the received LocataLite signals varied depending on the material that the signal was penetrating and the elevation angle. The Locata tracked all the LocataLite signals without any difficulty even though some of the signals were travelling through metal and several double brick walls. In this case a static test produced a mean error of less than 2.1mm, a standard deviation of less than 4mm and 99% of the east and north errors less than ±1cm. A kinematic test was conducted where the Locata was moved around the inside of the building finally returning to the start point. The final coordinate of the rover agreed with the known coordinate to less than 20cm. This level of precision is at least ten to one hundred times better than GPS can currently achieve indoors, even with high sensitivity receivers.

Indoor kinematic tests were conducted at a basketball court in Canberra, Australia on 23rd April, 2004 for which the author was present. A screen shot of the Locata can be seen in Figure 11-26, while the Locata receiver with the specially designed multipath mitigating antenna can be seen in Figure 11-27. Accuracies of around 2cm from the true position were achieved in the horizontal direction, in this high multipath environment. Due to a bad vertical DOP this component was not considered in the test. Results were in the order of 4m when a normal patch antenna was used for the same experiment, demonstrating that multipath is the biggest limitation to any indoor positioning.

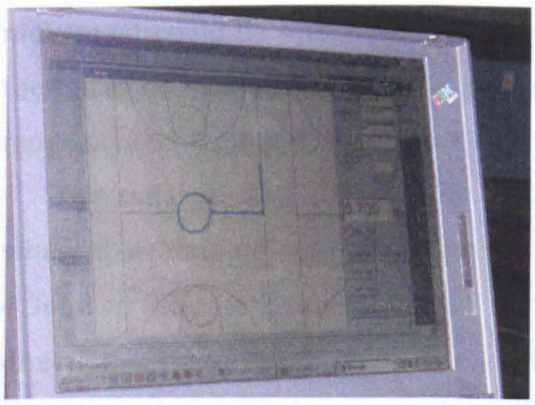

Figure 11-26 Screen shot of the Locata showing positioning accuracy in relation to a map of the basketball court

Figure 11-27 The Locata rover with specially designed multipath mitigating antenna

11.9.5.Parsley Bay Bridge Trial- Comparison with Pseudolite Results

Barnes et al. (2004) conducted a LocataLite trial at the Parsley Bay Bridge in Sydney, Australia on 5th May 2004. The main aim of the trial was to test the LocataLites in a bridge environment and also to compare the results to those achieved at the Parsley Bridge with GPS and pseudolites in the January 2003 trial.

Four LocataLites were positioned around the bridge, in positions where each LocataLite could see at least one other LocataLite and also so they had a good geometry. The location of the LocataLites was severely restricted by the natural features of the area surrounding the bridge and also by time constraints affecting the trial. This meant that all the LocataLites were installed below the bridge at low angles. Some LocataLite positions were surveyed with GPS, but due to limited views of the sky some had to be surveyed with a total station.

The Locata receiver was mounted on a pole which was secured to hang below the bridge deck, to increase visibility of the LocataLites and also to stop obstructions due to people walking on the bridge. The DOP values were 0.9 in the east direction, 0.7 in the north direction and 5.4 in the vertical direction. For a future trial, more effort would be made to improve the vertical component geometry.

Time-loc of all the LocataLites took a few minutes and was conducted using one LocataLite as the master. Ambiguity resolution was achieved at the Locata, by a static initialisation upon a known point. There were no positions computed independently by GPS due to the current interoperability issues with the two systems.

The bridge was rocked four times during the trial in the horizontal plane, to see if the Locata would be able to pick out this movement. The four periods of induced

movement could be seen clearly in the east and north component directions, however there was no movement visible in the vertical direction. It was thought that not much movement took place in the vertical direction anyway.

The standard deviations of the components were calculated only during periods where there was no induced movement on the bridge. The standard deviations were 4.3mm in the east direction, 3.0mm in the north direction and 23.5mm in the vertical direction. These results were as expected when the DOP values in each component were taken into consideration. The DOP value of 5.4 in the vertical direction was five and a half times worse than the horizontal DOP, which is why the standard deviation in this component is so much worse.

The results for the LocataLite trial were compared to those from the pseudolite and GPS trial on the Parsley Bridge described in Sections 11.5, 11.6 and 11.7 of this thesis. The results shown below in Table 11-8 and Table 11-9 from Barnes et al. (2004), are different from the results for the GPS only and GPS and pseudolites shown in Section 11.7. This is because Barnes et al. (2004) only include results when the number of available satellites is above five. Therefore the results for the GPS only and GPS and pseudolites are slightly more optimistic than those calculated for this thesis.

It can be seen from Table 11-8 that the Locata geometry is pretty near constant since the bridge does not move very much. For the GPS only and GPS and two pseudolites solutions, the DOP values vary widely over time and so the precision of the solution varies too.

		Locata	GPS only	GPS and two pseudolites
EDOP	Maximum		3.51	0.83
	Minimum		0.60	0.56
	Average	0.9	0.77	0.64
NDOP	Maximum		2.89	1.93
	Minimum		0.74	0.54
	Average	0.7	1.29	1.02
VDOP	Maximum		8.46	2.30
	Minimum		1.99	1.19
	Average	5.4	2.69	1.54

Table 11-8 Summary of the DOP values for Locata, GPS only and GPS augmented by two pseudolites (Barnes et al. 2004).

		Locata	GPS only	GPS and two pseudolites
Standard Deviations (m)	East	0.0430	0.0053	0.0039
	North	0.0030	0.0069	0.0050
	Vertical	0.0235	0.0131	0.0054

Table 11-9 The standard deviations of the east, north and vertical components for Locata, GPS only and GPS augmented by two pseudolites (Barnes et al. 2004).

The coordinate which has the closest geometry when comparing the Locata and GPS solutions is the east component. In this component the standard deviations are similar for all the systems. In the vertical direction the Locata precision is much worse than either the GPS only or the GPS and two pseudolites, but the VDOP explains why this is the case.

Based on these results, it can be concluded that the basic measurement precision of the Locata is as good as the GPS and pseudolite solution. This is a good result for the Locata as there are a number of advantages of using Locata over pseudolites as mentioned in Section 11.9.3. However, it also shows that the measurement precision of the Locata is no better than the GPS and pseudolite combined solution, and so once operating errors are overcome pseudolites are still a viable alternative for deformation monitoring.

11.9.6.The Next Generation

The Locata Corp in conjunction with UNSW is currently working on the next generation of LocataLites which will not transmit on a GPS frequency. The prototype used a GPS frequency for speed and ease as receiver technology was already established. It is hoped that LocataLites will work in conjunction with GPS, but by moving away from the GPS band they remove the problem of jamming the GPS signal with the high power LocataLite signals.

The LocataNet will be established by an autonomous process in which outdoor LocataLites will self-survey their position using the current GPS constellation and any established LocataLites. A fifth LocataLite can self-survey using the LocataLite constellation only and so can be placed indoors if needed. This process allows a theoretically infinite number of LocataLites to be added to a LocataNet.

12. Summary and Conclusions

This chapter gives an overview of the research conducted for this thesis and the conclusions that can be drawn. The final section gives recommendations for further work in the area of structural monitoring with single frequency GPS and pseudolites.

12.1. Summary

The main objective of this thesis was to investigate the use of single frequency GPS for bridge deformation monitoring. The main achievements of this research which help to satisfy this aim are summarised below.

- Initial comparisons were made between the accuracies achievable with single and dual frequency receivers in the first Wilford Bridge trial. The accuracies achievable with single frequency receivers, once the integer ambiguities had been resolved, were comparable with those achieved by dual frequency receivers. SKi-Pro was used to process both the single and dual frequency results for this trial. The 'stop and go' method used to resolve the single frequency integer ambiguities resulted in coordinate outages and would not have been appropriate for longer span bridges. The need to develop single frequency processing software for bridge deformation monitoring applications was highlighted by this trial.

- The first Wilford Bridge trial was also used to test the feasibility of using a total station for dynamic bridge monitoring. Initial trials showed that the total station may have problems measuring fast moving objects and this was confirmed by the results from the bridge trial. It was concluded that for

small bridges with high frequency vibrations the total station is not fast enough to pick out all the movement. For longer bridge with slower movements and lower natural frequencies, the use of the total station for dynamic monitoring is a possibility.

- Kinpos dual frequency processing software was modified by the author to process single frequency data. The main challenges were the cycle slip detection and ambiguity resolution routines. A triple order time difference of the carrier phase was used to detect and repair cycle slip. Three different methods of integer ambiguity resolution were used in Kinpos. The first accumulated the reduced normal equations using the Helmert-Wolf method to calculate the float values. These values were passed to the LAMBDA subroutine to fix to the true integer ambiguity values. This method would take around 20 minutes to resolve the ambiguities and sometimes the ambiguities were not resolved at all. Two other methods to accelerate the integer ambiguity resolution were added, one for small bridges and one for larger bridges.

- A second short bridge trial on the Wilford Bridge was conducted. The results produced by the new single frequency version of Kinpos were compared to the dual frequency results produced by SKi-Pro. SKi-Pro performed slightly better in all cases, which was probably due to the post-processing nature of the software which takes advantage of backwards and forwards processing algorithms. Kinpos can work in real-time. The latest version of dual frequency Kinpos, which had been developed in parallel, was compared to the single frequency version Kinpos. The single frequency version of Kinpos performed much better in a bridge situation, as the correct ambiguities were always resolved. When there were five satellites or less the dual frequency version of Kinpos was prone to fixing the wrong ambiguities so erroneous coordinates resulted. These results demonstrated the ability of the single frequency Kinpos to resolve the integer ambiguities instantly and correctly when used on a short bridge.

- The time series from two consecutive days were compared for the Wilford Bridge trial and it was discovered that some bridge sites had very low day to

day correlations. Adaptive filtering could not be used on these bridge sites and had problems removing all the noise even on the bridge sites with a high day to day correlation. So moving average filters were used to remove the multipath noise.

- Frequency identification was conducted using Bandpass filtering and DFT of the accelerometer and GPS data located at bridge site Bg09. The first natural frequency of the Wilford Bridge was identified as 1.73 Hz. Two other possible frequencies were also identified at 2.3 and 2.9 Hz.

- Two long bridge trials both on the Humber Bridge in Hull were analysed. One took place in February 1998 and the other in March 2004. Two of the methods of ambiguity resolution implemented in Kinpos, LAMBDA^{orig} and LAMBDA^{def} were compared to see what improvement was provided by LAMBDA^{def}. For the first trial an improvement was seen in every bridge location when LAMBDA^{def} was used. However, there were still long integer ambiguity outages for the single frequency data. The output from the dual frequency data processed in SKi-Pro produced much better results in this case.

- For the second trial (March 2004), there was a great improvement when the LAMBDA^{def} method of ambiguity resolution was implemented. The average time for ambiguities to be resolved with LAMBDA^{orig} was 7 minutes and 24.1 seconds, compared to 8.4 seconds for LAMBDA^{def}. The longest time to ambiguity resolution was 28 minutes 4.7 seconds for LAMBDA^{orig} and in some cases the ambiguities were not resolved at all. All ambiguities were resolved for LAMBDA^{def}, the longest taking only 41.7 seconds. The results from the single frequency data performed well compared to the dual frequency data processed in SKi-Pro. There was a great improvement in single frequency ambiguity resolution times; meaning that the possibility of monitoring the movement of large suspension bridges with single frequency GPS has been demonstrated. The long term movement of the bridge deck over an eight hour period was investigated and compared to changes in air temperature.

- The use of Garmin handheld GPS receivers for structural deformation applications was investigated and compared to results from high quality Leica system 500 survey grade GPS receivers. On a short baseline the Leica receivers showed results that were twice as precise as the Garmin receivers, which is a great outcome considering the difference in price for each receiver. In a kinematic environment the Garmin and Leica receivers showed the same movement, but the absolute coordinates of the Garmin receivers were wrong, probably due to initial ambiguity problems caused by the half cycle values. The possibility of measuring displacements with Garmin GPS receivers has been demonstrated, but it would only be possible to measure the displacements of structures which move a considerable amount due to the higher noise on the Garmin signal.

- Most of the research conducted in this thesis uses receivers measuring at a 10 Hz data rate. The use of JNS100 receivers measuring at 50 Hz has also been investigated. Zero baseline and short baseline trials were conducted to assess the accuracy of the JNS100 receivers compared to Leica system 500 receivers. The Leica receivers performed slightly better than the JNS100 in these static trials, but the difference was very small. Kinematic trials were conducted on a bungee test rig and the Wilford Bridge. The JNS100 receivers were again compared to the Leica receivers, and to a closely located accelerometer also measuring at 50 Hz. The accelerometer amplitudes did not compared well to the GPS in the bungee test rig trials, but the results for the bridge trial were good.

- Frequency identification took place with the JNS100 data measuring at 50 Hz and also on the accelerometer data measuring at the same data rate. The GPS and accelerometer data agreed that the first natural frequency of the Wilford Bridge was 1.77 Hz. This is a 2% increase compared to the frequency identified (1.73 Hz) by the data from the May 2003 trial. It is possible that some strengthening of the bridge might have occurred between the two trials or that extra weight on the bridge during the first trial caused the change in frequency. The GPS and accelerometer identified frequencies around 2.1/2.2 Hz, 2.8/3 Hz and 5.1/5.2 Hz. Since the exact values of these

modes were very unclear, it would be difficult to identify any changes in the modes. The JNS100 data recognised two modes at 10.8 and 12.2 Hz. Since these modes could not be discerned in the accelerometer data, it was not possible to confirm them.

- The use of pseudolites to augment the current GPS constellation for bridge deformation monitoring was also investigated. Static trials were conducted to analyse the improvement seen when pseudolites are added into a GPS solution. Improvements in the positioning precision was seen in all coordinate directions with the largest improvement seen in the vertical direction; the standard deviation fell from 5.7mm to 3.0mm, an improvement of 48%.

- Two different pseudolite and GPS bridge trials are introduced, one on the Wilford Bridge in Nottingham UK and one on the Parsley Bay Bridge in Sydney Australia. DOP simulations of the satellite constellation and results expected with and without pseudolites are conducted. Due to the location of the pseudolites below the horizon in both trials, large improvements are expected in the east and vertical coordinates, but lower improvements are expected in the north coordinates. For the Wilford Bridge trial, the accuracy of all three components is improved when pseudolites are added into the solution; with the biggest improvement seen in the vertical direction, making it more accurate than the north component. For the Parsley Bridge, the number of satellites drops to four and then to three meaning that the GPS only solution is very poor and cannot be trusted. The introduction of pseudolites improves the solution in all component directions meaning that the solutions are reliable for the whole of the observation session.

- Problems with pseudolite multipath and location error were encountered in the bridge environment. The double difference pseudolite carrier phase residuals show a bias which, since the bridge can be considered static, can be calculated and removed.

- The use of LocataLites as an extension to the pseudolite work is introduced. Literature reviews of the LocataLite work show that the measurement

precision of the LocataLite stand-alone solution is similar to the precision achieved by the GPS and pseudolites in a double difference solution for a trial on the Parsley Bay Bridge.

12.2. Conclusions

The work conducted for this thesis has resulted in the development of single frequency processing software, Kinpos. This software enables the use of single frequency GPS in a bridge environment. Before undertaking this research the use of single frequency GPS was impeded by the long integer ambiguity resolution times. There is no commercially available software that enables single frequency integer ambiguities to be resolved quickly on the fly. With Kinpos it is now possible to resolve integer ambiguities instantly for short bridges and in greatly reduced times for longer bridges. This thesis outlined the development of Kinpos as well as demonstrating the results with real bridge trials.

As an extension to the use of single frequency receivers, the possibility of using Garmin receivers for deformation monitoring has been investigated. Kinpos has enabled Garmin data to be processed in a kinematic mode and the possibility for monitoring has been demonstrated.

Kinpos has also been modified to facilitate processing of high frequency GPS observations from JNS100 single frequency receivers. This is the first study in which receivers of such high frequency have been used to monitor the movement of bridges, enabling the identification of high frequency bridge dynamics.

The final contribution made by this thesis has been the demonstration of the improvements in the precision of positioning solutions with the introduction of pseudolites. Bridge trials have shown that the vertical component can be improved to the same level as the horizontal when pseudolites are used.

The study has demonstrated that with the correct procedures and tools single frequency receivers can provide useful information for the application of bridge deformation monitoring.

12.3. Further Work

The research in this thesis has concentrated on the use of single frequency GPS to monitor the movement of bridges. Initial findings have been presented and it is recognised that there are many areas that future work could take. Some of these areas are mentioned below.

- Initial trials were conducted to assess the use of a total station for dynamic bridge deformation monitoring. The 1 Hz data rate of the total station was found to be too slow to measure all the movement of the Wilford Bridge. Experiments could be performed with two total stations measuring angles only. Angle measurements can be taken faster than distances at four times per second. The main error sources with the total station are concerned with the distance measurements and so faster and more reliable observations could be made.

- All the scripts written for Kinpos single frequency processing software could be implemented in real-time. However, this real-time implementation is not currently achievable and a small amount of research needs to be conducted to enable real-time data to be collected. Meng et al. (2004a) investigate the use of the internet to transmit GPS corrections and results. Currently this method can only be used for dual frequency receivers, but it could be further extended to include single frequency GPS data.

- The original dual frequency version of Kinpos allows the use of multiple reference station data (Pattinson 2002). This is a further extension that could be implemented for the single frequency data and would be particularly useful for trials on long bridges. Data from two reference stations can be used to check ambiguity values, which would mean more reliable and possibly quicker ambiguity resolution for long bridges.

- Initial trials to test the possibility of using Garmin handheld receivers for deformation monitoring were conducted in this thesis. However, no bridge trials were actually carried out. Trials could be carried out on the Wilford Bridge; however the noise on the Garmin receivers' signal would probably mean that the movement could not be detected. Trials on a longer bridge

with larger movements could be conducted to analyse the use of Garmin receivers in this situation.

- Further experiments should be conducted with the JNS100 receiver. The problems with data logging to a laptop need to be considered to enable data to be collected at 100 Hz. The possibility of measuring higher frequency bridge dynamics with this 100 Hz data could be examined. Frequency identification methods such as stochastic subspace identification (Peeters and De Roeck 1999), statistical pattern recognition approaches (Owen and Pearson 2004) and wavelet analysis (Ogaja et al. 2001) should be investigated to enable more reliable mode detection.

- The development of in-house pseudolite processing software should be a research aim to further the initial investigations into pseudolite augmented GPS for bridge deformation monitoring.

- The location of the pseudolites for bridge monitoring in this thesis has always resulted in a smaller improvement in the north direction compared to the east and vertical components. Location of pseudolites for improvement of the north direction should be further investigated.

References

Aktan, E., Chase, S., Inman, D. and Pines, D., 2001. "Monitoring and Managing the Health of Infrastructure Systems". Proceedings of the 2001 SPIE Conference on Health Monitoring of Highway Transportation Infrastructure, 6-8 March.

Anon, 2002. "Koror-Babeldaob Bridge." [online]. Wow Palau Newsletter, Available at: <http://www.geocities.com/SouthBeach/Palms/6757/bridge.html> [Accessed 23 September 2002].

Ashkenazi, V., Dodson, A. H., Moore, T. and Roberts, G. W., 1996. "Real Time OTF GPS Monitoring of the Humber Bridge." Surveying World, 4(4), May/June: 26-28.

Barnes, J., Wang, J., Rizos, C. and Tsujii, T., 2002. "The Performance of a Pseudolite-Based Positioning System for Deformation Monitoring". 2nd Symposium on Geodesy for Geotechnical and Structural Engineering, 21-24 May, Berlin, Germany. 326-337.

Barnes, J., Rizos, C., Lee, H.-K., Roberts, G. W., Meng, X., Cosser, E. and Dodson, A. H., 2003a. "The Integration of GPS and Pseudolites for Bridge Monitoring". XXIIIth General Assembly of the IUGG, 30 June- 11 July, Sapporo, Japan.

Barnes, J., Rizos, C., Wang, J., Meng, X., Cosser, E., Dodson, A. H. and Roberts, G. W., 2003b. "The Monitoring of Bridge Movements using GPS and Pseudolites". 11th International Symposium on Deformation Measurements, International Federation Surveyors (FIG), Commission 6 - Engineering Surveys, Working Group 6.1, 25-28 May, Santorini, Greece. 563-571.

Barnes, J., Rizos, C., Wang, J., Small, D., Voigt, G. and Gambale, N., 2003c. "Locata: the Positioning Technology of the Future?" SatNav 2003. The 6th International Symposium on Satellite Navigation Technology Including Mobile Positioning and Location Services, 22-25 July, Melbourne, Australia.

Barnes, J., Rizos, C., Wang, J., Small, D., Voigt, G. and Gambale, N., 2003d. "Locata: A New Positioning Technology for High Precision Indoor and Outdoor

Positioning". ION GPS 2003, The 16th Technical Meeting of the Satellite Division of the Institute of Navigation, 9-12 September, Portland, Oregon.

Barnes, J., Rizos, C., Wang, J., Small, D., Voigt, G. and Gambale, N., 2003e. "High Precision Indoor and Outdoor Positioning using LocataNet". International Symposium on GPS/GNSS, 15-18 November, Tokyo, Japan. 9-18.

Barnes, J., Rizos, C., Kanli, M., Small, D., Voigt, G., Gambale, N. and Lamance, J., 2004. "Structural Deformation Monitoring Using Locata". 1st FIG International Symposium on Engineering Surveys for Construction Works and Structural Engineering, 28 June-1 July, Nottingham, England.

BBC, 1999. "Bridging the Kingston Gap." [online]. BBC, Available at: <http://news.bbc.co.uk/1/hi/uk/scotland/471337.stm> [Accessed 23 September 2002].

Bell, B., <Brian.BELL@networkrail.co.uk>, 2004. "Visual Inspection of Railway Bridges." 24 February. Email to: E. Cosser, <isxec@nottingham.ac.uk>.

Bingley, R. M. and Roberts, G. W., 1998. Global Positioning System. Technical Report. IESSG, University of Nottingham.

Bona, P. and Tiberius, C., 2000. "An Experimental Comparison of Noise Characteristics of Seven High-End Dual Frequency GPS Receiver-Sets". IEEE Position Location and Navigation Symposium, March, San Diego, California.

Bourke, P., 1993. "Discrete Fourier Tranforms." [online]. Available at: <http://astronomy.swin.edu.au/~pbourke/analysis/dft/> [Accessed 18 November 2004].

Brown, C. J., Karuna, R., Ashkenazi, V., Roberts, G. W. and Evans, R. A., 1999. "Monitoring of Structures Using the Global Positioning System." Proc. Institute Civil Engineers, Structures and Buildings, 134, February.

Choi, I. K., Wang, J., Han, S. and Rizos, C., 2000. "Pseudolites- A New Tool For Surveyors?" The 2nd TransTasmen Surveyors Conference, 20-26 August, Queenstown, New Zealand.

Clark, R. A., 2003. "Tropospheric Effect on GPS Deformation Monitoring of Tall Buildings." MSc thesis, Univesity of Nottingham, Nottingham.

Cobb, H. S., 1997. "GPS Pseudolites: Theory, Design and Applications." PhD thesis, Stanford University.

Cooper, J. D., 1998. "World's Longest Suspension Bridge Opens in Japan." Public Roads, 62(1), July/August.

Cosser, E., Roberts, G. W., Meng, X. and Dodson, A. H., 2003. "The Comparison of Single and Dual Frequency GPS for Bridge Deflection and Vibration Monitoring". 11th International Symposium on Deformation Measurements, International Federation Surveyors (FIG), Commission 6 - Engineering Surveys, Working Group 6.1, 25-28 May, Santorini, Greece. 613-620.

Cosser, E., 2004. "Bridge Deflection Monitoring and Frequency Identification with Single Frequency GPS Receivers". ION GNSS 2004, The 17th Technical Meeting of the Satellite Division of the Institute of Navigation, 21-24 September, Long Beach, California.

Cosser, E., Meng, X., Roberts, G. W., Dodson, A. H., Barnes, J. and Rizos, C., 2004a. "Precise Engineering Applications of Pseudolite Augmented GNSS". 1st FIG International Symposium on Engineering Surveys for Construction Works and Structural Engineering, 28 June-1 July, Nottingham, England.

Cosser, E., Roberts, G. W., Meng, X. and Dodson, A. H., 2004b. "Single Frequency GPS for Bridge Deflection Monitoring: Progress and Results". 1st FIG International Symposium on Engineering Surveys for Construction Works and Structural Engineering, 28 June-1 July, Nottingham, England.

Cross, P. A., 1983. Advanced Least Squares Applied to Position Fixing. North East London Polytechnic, London.

Czepiel, E., 1995. "Bridge Management System Literature Review and Search." [online]. Northwestern University BIRL Research Laboratory, Available at: <http://www.iti.northwestern.edu/publications/technical_reports/tr11.html#introduction> [Accessed 17 February 2004].

Dai, L., Zhang, J., Rizos, C., Han, S. and Wang, J., 2000. "GPS and Pseudolite Integration for Deformation Monitoring Applications". ION GPS 2000, The 13th Technical Meeting of the Satellite Division of the Institute of Navigation, 19-22 September, Salt Lake City, Utah. 1-8.

Dai, L., Wang, J., Rizos, C. and Han, S., 2001. "Applications of Pseudolites in Deformation Monitoring Systems". 10th FIG Symposium on Deformation Measurements, 19-22 September, Orange, California, USA. 11-22.

Dallard, P., Fitzpatrick, T., Flint, A., Low, A., Ridsdill Smith, R., Willford, M. and Roche, M., 2001. "London Millenium Bridge: Pedestrian-Induced Lateral Vibration." Journal of Bridge Engineering, 6(6), November/December: 412-417.

Das, P. C., 1996. Bridge Management Objectives and Methodologies. In: Bridge Management 3. J. E. Harding, G. A. R. Parke and M. J. Ryall. E & F Spon, London.

Daub, C., 2002. "Pseudolite for Deformation Monitoring." MSc thesis, The University of Nottingham, Nottingham, UK.

De Jonge, P. and Tiberius, C., 1996. The LAMBDA method for Integer Ambiguity Estimation: Implementation Aspects. Delft Computing Centre.

Dodson, A. H., Meng, X. and Roberts, G. W., 2001. "Adaptive Methods for Multipath Mitigation and Its Applications for Structural Deflection Monitoring". International Symposium on Kinematic Systems in Geodesy, Geomatics and Navigation (KIS 2001), 5-8 June, Banff, Canada.

Duff, K., Hyzak, M., McDonald, H., McGown, A. and Innes, J., 1997. "Deformation Monitoring with GPS, Part 1: System Design and Performance". FIG, Symposium of Large Bridges and Tunnel Projects, 2-5 June, Copenhagen, Denmark. 239-251.

Duff, K. and Nelson, S., 1997. "Deformation Monitoring with GPS, Part 2: Performance, Affordability and Technology Developement". FIG, Symposium of Large Bridges and Tunnel Projects, 2-5 June, Copenhagen, Denmark. 253-267.

Elrod, B. D. and Van Dierendonck, A. J., 1995. Pseudolites. In: Global Positioning System: Theory and Applications Volume II. B. W. Parkinson, J. J. Spilker Jr, P. Axelrad and P. Enge. American Institute of Aeronautics and Astronautics Inc, USA. 2: 51-79.

EPSRC, 2001. A Remote Heath Monitoring System Using Computational Simulation and GPS Sensors: EPRSC Research Proposal.

Farah, A., 2003. "A Light On: GPS/Galileo Data Simulation". 2003 International Symposium on GPS/GNSS, 15-18 November, Tokyo, Japan. 395-399.

Ford, T., Neumann, J., Toso, N., Petersen, W., Anderson, C., Fenton, P., Holden, T. and Barltrop, K., 1997. "HAPPI- a High Accuracy Pseudolite/GPS Positioning Integration". ION GPS 1997, The 10th Technical Meeting of the Satellite Division of the Institute of Navigation, September, Kansas City, Montana, USA. 1719-1728.

Forward, T., Stewart, M. P. and Tsakiri, M., 2003. "GPS Data Stacking for Small Scale GPS Deformation Monitoring Applications". 11th International Symposium on Deformation Measurements, International Federation Surveyors (FIG), Commission 6 - Engineering Surveys, Working Group 6.1, 25-28 May, Santorini, Greece. 233-239.

Fosburgh, B. and Peetz, B., 2004. "GPS Modernization." [online]. Available at: <http://www.profsurv.com/ps_scripts/article.idc?id=1191> [Accessed 5 November 2004].

Fujino, Y., Murata, M., Okano, S. and Takeguchi, M., 2000. "Monitoring System of the Akashi Kaikyo Bridge and Displacement Measurement Using GPS." Nondestructive Evaluation of Highways, Utilities and Pipelines, IV, Proceedings of SPIE, 3995: 229-236.

GPS Warehouse, 2004. "Garmin GPS." [online]. Available at: <http://www.gpsw.co.uk> [Accessed 12 August 2004].

Hayes, M. H., 1999. Digital Signal Processing. The McGraw-Hill Companies Inc., USA.

Haynes, L., 1997. Introduction. In: Safety of Bridges. P. C. Das. Thomas Telford Publishing, London: 3-6.

Hein, G. W. and Riedl, B., 1995. "First Results Using the New DGPS Real-Time Deformation Monitoring System "DREAMS"". ION GPS 95, 12-15 September, Palm Springs, California.

Hein, G. W. and Riedl, B., 2003. "Real-Time Monitoring of Highway Bridges Using "DREAMS"". 11th FIG Symposium on Deformation Measurements, 25-28 May, Santorini, Greece. 201-208.

Hide, C., 2003. "Integration of GPS and Low Cost INS Measurements." PhD thesis, University of Nottingham, Nottingham.

Hill, C. D. and Sippel, K. D., 2002. "Modern Deformation Monitoring: A Multi Sensor Approach". FIG XXII International Congress, April 19-26, Washington DC, USA.

Hill, C. J., Moore, T. and Dumville, M., 2000. "Carrier Phase Surveying with Garmin Handheld GPS Receivers". ION GPS 2000, The 13th Technical Meeting of the Satellite Division of the Institute of Navigation, 19-22 September, Salt Lake City, Utah. 178-182.

Hill, C. J. and Moore, T., 2002. "Gringo Software; Online User Manual." [online]. IESSG, University of Nottingham, Available at: <http://www.nottingham.ac.uk/iessg/gringo> [Accessed 12 September 2003].

Hoffman, F., 2004. "An Introduction to Fourier Theory." [online]. Available at: <http://aurora.phys.utk.edu/~forrest/papers/fourier/> [Accessed 18 November 2004].

Hofmann-Wellenhof, B., Lichenegger, H. and Collins, J., 2001. GPS, Theory and Practice. Springer-Verlag, Austria.

Hyzak, M. D. and Leach, M. P., 1995. "Bridge Monitoring with GPS." Surveying World, March: 8-11.

IGS, 2004. "International GPS Service." [online]. Available at: <http://igscb.jpl.nasa.gov/> [Accessed 4 August 2004].

Institute of Engineering Surveying and Space Geodesy, 2004. Kinpos Kinematic GPS Software, User Guide v1.1. The University of Nottingham, Nottingham, England.

Integrinautics, 2002. IN200D General Purpose Pseudolite Signal Generator: User's Manual.

Javad Navigation Systems, 2004a. "OEM boards." [online]. Available at: <http://www.javad.com/> [Accessed 12 August 2004].

Javad Navigation Systems, 2004b. "Product Price List." [online]. Available at: <http://www.javad.com/> [Accessed 12 August 2004].

Johns, B., 2000. "Bridge Monitoring Developmental Support." [online]. University NAVSTAR Consortium (UNAVCO), Available at: <http://www.unavco.ucar.edu/project_support/permanent/reports/bridge_report.pdf> [Accessed 6 February 2002].

Klobuchar, J. A., 1996. Ionospheric Effects on GPS. In: Global Positioning System; Theory and Applications. B. W. Parkinson, J. J. Spilker Jr, P. Axelrad and P. Enge. American Institute of Aeronautics and Astronautics, Inc, USA. Volume One: 485-515.

Kotthoff, H., Hilker, C. and Ziegler, C., 2004. "Strategy of Reliable Ambiguity Resolution for Static and Kinematic Applications." [online]. Leica Geosystems, Available at: <http://www.leicaatl.com/support/gps/Technical_papers/AmbiguityStrategy.pdf > [Accessed 16th January 2004].

Kouba, J. and Heroux, P., 2000. "GPS Precise Point Positioning Using IGS Products." [online]. Available at: <http://www.geod.nrcan.gc.ca/index_e/products_e/publications_e/papers_e/final.pdf> [Accessed 3 May 2005].

Kuhlmann, H. and Glaser, A., 2002. "Investigation of New Measurement Techniques for Bridge Monitoring". 2nd Symposium on Geodesy for Geotechnical and Structural Engineering, 21-24 May, Berlin, Germany.

Langley, R., 1997. "GPS Receiver System Noise." GPS World, 8(6), June: 40-45.

Leica Geosystems, 1999. GPS Equipment User Manual. Leica Geosystems.

Leica Geosystems, 2000. TPS-System 100: Electronic Theodolites and Total Stations, User Manual. Leica Geosystems, Heerbrugg, Switzerland.

Leica Geosystems, 2002a. "Bridge Surveys." [online]. Available at: <http://www.leica-geosystems.com/civil/application/bridge.htm> [Accessed 1st October 2002].

Leica Geosystems, 2002b. "Tunnel Surveys." [online]. Available at: <http://www.leica-geosystems.com/civil/application/tunnel.htm> [Accessed 1st October 2002].

Leick, A., 1995. GPS Satellite Surveying. John Wiley & Sons, Inc, USA.

Lennartz-Johansen, H. and Ellegaard, S., 2002. "Analyzing Europe's Largest Suspension Bridge". FIG XXII International Congress, 19-26 April, Washington DC, USA.

Li, X., Ge, L., Tamura, Y., Yoshida, A., Rizos, C. and Peng, G.-D., 2004. "Seismic Response of a Tower as Measured by an Integrated RTK-GPS System". 1st FIG International Symposium on Engineering Surveys for Construction Works and Structural Engineering, 28 June-1 July, Nottingham, England.

Lovse, J. W., Teskey, W. F., Lachapelle, G. and Cannon, M. E., 1995. "Dynamic Deformation Monitoring of Tall Structures Using GPS Technology." ASCE Journal of Surveying Engineering, 121(1): 35-40.

Maaskant, R., Alavie, T., Measures, R. M., Tadros, G., Rizkalla, S. H. and Guha-Thakurta, A., 1997. "Fiber-optic Bragg Grating Sensors for Bridge Monitoring." Cement and Concrete Composites, 19: 21-33.

MATLAB®, 2004. Documentation, Release 13. The Mathworks Inc., Natick, Massachusetts.

Meng, X., 2002. "Real-time Deformation Monitoring of Bridges Using GPS/Accelerometers." PhD thesis, The University of Nottingham, Nottingham, UK.

Meng, X., Roberts, G. W., Dodson, A. H. and Cosser, E., 2002a. "The Use of Pseudolites to Augment GPS Data for Bridge Deflection Measurements". ION GPS 2002, The 15th Technical Meeting of the Satellite Division of the Institute of Navigation, Portland, Oregon, USA. 851-862.

Meng, X., Roberts, G. W., Dodson, A. H., Cosser, E. and Noakes, C., 2002b. "Simulation of the Effects of Introducing Pseudolite Data into Bridge Deflection Monitoring Data". 2nd Symposium on Geodesy for Geotechnical and Structural Engineering, 21-24 May, Berlin, Germany.

Meng, X., Meo, M., Roberts, G. W., Dodson, A. H., Cosser, E., Iuliano, E. and Morris, A., 2003. "Validating GPS Based Bridge Deformation Monitoring with Finite Element Model". GNSS 2003, 22-25 April, Graz, Austria.

Meng, X., Dodson, A. H., Andreotti, M., Roberts, G. W., Cosser, E. and Moore, T., 2004a. "Prototype of a Remote Bridge Health Monitoring System (RBHMS) using Wired/Internet Based RTK GPS". GNSS 2004, 17-19 May, Rotterdam, Netherlands.

Meng, X., Roberts, G. W., Dodson, A. H., Cosser, E., Barnes, J. and Rizos, C., 2004b. "Impact of GPS satellite and pseudolite geometry on structural deformation monitoring: analytical and empirical studies." Journal of Geodesy, 77(12), June: 809 - 822.

Moore, T., Hill, C. J. and Napier, M. E., 2002. "Rapid Mapping with Post-Processed Data from Garmin Handheld Receivers". ION GPS 2002, The 15th Technical Meeting of the Satellite Division of the Institute of Navigation, 24-27 September, Portland, Oregon. 1414-1422.

Morley, T. G., 1997. "Augmentation of GPS with Pseudolites in a Marine Environment." MSc thesis, The University of Calgary, Calgary, Canada.

Mulgrew, B., Grant, P. and Thompson, J., 2003. Digital Signal Processing; Concepts and Applications. Palgrave Macmillian, Basingstoke, UK.

National Geodetic Survey, 2000. "Removal of GPS Selective Availability (SA)." [online]. Available at: <http://www.ngs.noaa.gov/FGCS/info/sans_SA/> [Accessed 5 November 2004].

Nova Scotia Department of Transportation and Public Works, 2003. "Province Moves Forward on $50-Million Steel Bridge Program." [online]. Available at: <http://www.gov.ns.ca/news/details.asp?id=20030616004> [Accessed 24 Febuary 2004].

Novatel Inc, 2004. "Product Guide." [online]. Available at: <http://www.novatel.com/Documents/Papers/novatel_productguide_web.pdf> [Accessed 8 December 2004].

O'Connor, C. and Shaw, P. A., 2000. Bridge Loads. Spon Press, London.

Ogaja, C., Rizos, C., Wang, J. and Brownjohn, J. M. W., 2001. "Towards the Implementation of On-line Structural Monitoring Using RTK-GPS and Analysis of Results Using the Wavelet Transform". 10th FIG International Symposium on Deformation Measurements, 19-22 March, Orange, California. 284-293.

Omar, S. and Rizos, C., 2003. "Incorporating GPS into Wireless Networks: Issues and Challenges". The 6th International Symposium on Satellite Navigation Technology Including Mobile Positioning and Location Servies, 22-25 July, Melbourne, Australia.

Ordnance Survey, 2004. "National GPS Network Information." [online]. Available at: <http://www.gps.gov.uk/guidecontents.asp> [Accessed 4 May 2005].

Owen, J. S. and Pearson, S. R., 2004. "The Use of Dynamic Data for the Structural Health Monitoring of Bridges". 1st FIG International Symposium on Engineering Surveys for Construction Works and Structural Engineering, 28 June- 1 July, Nottingham, England.

Parkinson, B. W., Spilker Jr, J. J., Axelrad, P. and Enge, P., eds., 1995. Global Positioning System: Theory and Applications Volume I and II. American Institute of Aeronautics and Astronautics Inc, USA.

Pattinson, M., 2000. Kinpos User Manual. University of Nottingham.

Pattinson, M., 2002. "Estimation of Tropospheric Delay from a Moving GPS Receiver." PhD thesis, The University of Nottingham, Nottingham.

Peeters, B., De Roeck, G., Hermans, L., Wauters, T., Kramer, C. and de Smet, C., 1998. "Comparison of System Identification Methods using Operational Data of a Bridge Test". ISMA 23, The International Conference On Noise and Vibration, September, KU Leuven, Belgium. 923-930.

Peeters, B. and De Roeck, G., 1999. "Reference Based Stochastic Subspace Identification In Civil Engineering." Inverse Problems in Engineering, 00: 1-28.

Pratt, M., Burke, B. and Misra, P., 1997. "Single-Epoch Integer Ambiguity Resolution with GPS-GLONASS L1-L2 Data." [online]. Available at: <http://www.tc.faa.gov/logistics/grants/pdf/97-g-010a.pdf> [Accessed 17 November 2004].

Radovanovic, R. S. and Teskey, W. F., 2001. "Dynamic Monitoring of Deforming Structures: GPS verses Robotic Tacheometry Systems". The 10th FIG International Symposium on Deformation Measurements, 19-22 March, Orange, California, USA.

Railtrack, 2001. Railtrack Line Code of Practice; The Structural Assessment of Underbridges: 18.

Rizos, C., 1999a. "GPS Enhancements. Techincal Report." [online]. University of New South Wales, Available at: <http://www.gmat.unsw.edu.au/snap/gps/gps_notes2.pdf> [Accessed 4 August 2004].

Rizos, C., 1999b. "How Good is GPS?" [online]. Available at: <http://www.gmat.unsw.edu.au/snap/gps/gps_survey/chap2/243saas.htm> [Accessed 5 November 2004].

Roberts, G. W., 1997a. "Real Time On-The-Fly Kinematic GPS." PhD thesis, University of Nottingham, Nottingham.

Roberts, G. W., 1997b. OTF Integer Ambiguity Resolution. Satellite Positioning Module Lecture Notes. Nottingham, University of Nottingham.

Roberts, G. W., Dodson, A. H. and Ashkenazi, V., 1999. "Twist and Deflect, Monitoring Motion of the Humber Suspension Bridge." GPS World, October: 24-34.

Roberts, G. W., Meng, X. and Dodson, A. H., 2000. "Structural Dynamic and Deflection Monitoring Using Integrated GPS and Triaxial Accelerometers". ION GPS 2000, The 13th Technical Meeting of the Satellite Division of the Institute of Navigation, 19-22 September, Salt Lake City, Utah. 59-67.

Roberts, G. W., Meng, X. and Dodson, A. H., 2001a. "The Use of Kinematic GPS and Triaxial Accelerometers to Monitor the Deflections of Large Bridges". 10th International Symposium on Deformation Measurement, FIG, 19-22 March, California, USA. (CD-ROM).

Roberts, G. W., Meng, X. and Dodson, A. H., 2001b. "Data Processing and Multipath Mitigation for GPS/Accelerometer Based Hybrid Structural Deflection Monitoring System". ION GPS 2001, The 14th Technical Meeting of the Satellite Division of the Institute of Navigation, 11-14 September, Salt Lake City, USA.

Roberts, G. W., Meng, X. and Dodson, A. H., 2002. "Using Adaptive Filtering to Detect Multipath and Cycle Slips in GPS/Accelerometer Bridge Deflection Monitoring Data". FIG XXII International Congress, 19-26 April, Washington DC.

Roberts, G. W., Cosser, E., Meng, X. and Dodson, A. H., 2004a. "Monitoring the Deflection of Suspension Bridges Using 100 Hz GPS Receivers". ION GNSS

2004, The 17th Technical Meeting of the Satellite Division of the Institute of Navigation, 21-24 September, Long Beach, California.

Roberts, G. W., Meng, X. and Brown, C. J., 2004b. "From St Pauls to the Tate Modern; Overcoming Problems in Monitoring Bridge Deflections Using GPS". 1st FIG International Symposium on Engineering Surveys for Construction Works and Structural Engineering, 28 June-1 July, Nottingham, England.

Santerre, R., 1991. "Impact of GPS Satellite Sky Distribution." Manuscripa Geodaetica, 16: 28-53.

Satalich, J., 2004. "Multipath Effects on Ellipsoid Height Positioning Using Kinematic GPS Techniques." [online]. Available at: <http://www.ascm.net/gpsvertical.pdf> [Accessed 7 October 2004].

Satellite Positioning and Navigation Group, 2001. "A Glossary of Terms." [online]. Available at: <http://www.gmat.unsw.edu.au/snap/gps/glossary_a-c.htm> [Accessed 17 November 2004].

Sharpe, 1999. Sharpe XR6 GPS Receiver User Manual. Symmetricom Ltd.

Smith, D., 1974. "Tacoma Narrows Bridge Failure." [online]. Available at: <http://www.civeng.carleton.ca/Exhibits/Tacoma_Narrows/DSmith/photos.html > [Accessed 20th February 2004].

Spilker Jr, J. J., 1994. Tropospheric Effects on GPS. In: Global Positioning System: Theory and Application. B. W. Parkinson, J. J. Spilker Jr, P. Axelrad and P. Enge. American Institute of Aeronautics and Astronautics, Inc, USA. Volume One: 517-546.

Teunissen, P. J. G. and Kleusberg, A., 1998. GPS for Geodesy. Springer-Verlag, Germany.

The Humber Bridge Board, 2001. "The Humber Bridge." [online]. The Humber Bridge Board, Available at: <http://www.humberbridge.co.uk> [Accessed 17 February 2004].

Townsend, B. R. and Fenton, P. C., 1994. "A Practical Approach to the Reduction of Pseudorange Multipath Errors in a L1 GPS Receiver". ION GPS 94, The 7th Technical Meeting of the Satellite Division of the Institute of Navigation, 20-23 September, Salt Lake City, Utah.

Tsakiri, M., Lekidis, V., Stewart, M. P. and Karabelas, J., 2003. "Testing Procedures for the Monitoring of Seismic Induced Vibrations on a Cable-Stayed Highway Bridge". 11th International Symposium on Deformation Measurements, International Federation Surveyors (FIG), Commission 6 - Engineering Surveys, Working Group 6.1, 25-28 May, Santorini, Greece. 621-628.

Unknown source, "Cycle Slip Detection and Repair Algorithm."

US Department of Transportation, 2001. Reliability of Visual Inspection for Highway Bridges. Virginia, Federal Highways Administration.

Virola, J., 2003. "World's Longest Bridge Spans." [online]. Available at: <http://www.hut.fi/Units/Departments/R/Bridge/longspan.html> [Accessed 11 March 2004].

Wagner, B. and Barr, M., 2002. "Introduction to Digital Filtering." Embedded Systems Programming, December: 47-48.

Wang, J., 2002. "Pseudolite Applications in Positioning and Navigation: Progress and Problems." Journal of Global Positioning Systems, 1(1): 48-56.

Weill, L. R., 1997. "Conquering Multipath: The GPS Accuracy Battle." GPS World, 8(4), April: 59-66.

Weisstein, E. W., 2004. "Fourier Transform." [online]. From Mathworld- a Wolfram Web Resource, Available at: <http://mathworld.wolfram.com/FourierTransform.html> [Accessed 18 November 2004].

Wieser, A. and Brunner, F. K., 2002. "Analysis of Bridge Deformations using Continuous GPS Measurements". INGEO2002, November, Bratislava.

Wong, K. Y., Man, K. L. and Chan, W. Y., 2001. "Monitoring Hong Kong's Bridges: Real-Time Kinematic Spans the Gap." GPS World, 12(7): 8-10.

Young, C., 1998. "Single Frequency OTF Kinematic GPS Bridge Deflection Monitoring." MSc thesis, University of Nottingham, Nottingham.

Yun, D. and Kee, C., 2002. "Centimeter Accuracy Stand-Alone Indoor Navigation System by Synchronised Pseudolite Constellation". ION GPS 2002, The 15th Technical Meeting of the Satellite Division of the Institute of Navigation, Portland, Oregon. 213-225.

Author Publications

Barnes, J., Rizos, C., Lee, H.-K., Roberts, G. W., Meng, X., Cosser, E. and Dodson, A. H., 2003a. "The Integration of GPS and Pseudolites for Bridge Monitoring". XXIIIth General Assembly of the IUGG, 30 June- 11 July, Sapporo, Japan.

Barnes, J., Rizos, C., Wang, J., Meng, X., Cosser, E., Dodson, A. H. and Roberts, G. W., 2003b. "The Monitoring of Bridge Movements using GPS and Pseudolites". 11th International Symposium on Deformation Measurements, International Federation Surveyors (FIG), Commission 6 - Engineering Surveys, Working Group 6.1, 25-28 May, Santorini, Greece. 563-571.

Cosser, E., Roberts, G. W., Meng, X. and Dodson, A. H., 2003a. "Measuring the Dynamic Deformation of Bridges Using a Total Station". 11th International Symposium on Deformation Measurements, International Federation Surveyors (FIG), Commission 6 - Engineering Surveys, Working Group 6.1, 25-28 May, Santorini, Greece. 605-612.

Cosser, E., Roberts, G. W., Meng, X. and Dodson, A. H., 2003b. "The Comparison of Single and Dual Frequency GPS for Bridge Deflection and Vibration Monitoring". 11th International Symposium on Deformation Measurements, International Federation Surveyors (FIG), Commission 6 - Engineering Surveys, Working Group 6.1, 25-28 May, Santorini, Greece. 613-620.

Cosser, E., Roberts, G. W., Dodson, A. H. and Meng, X., 2003c. "Bridge Monitoring." Civil Engineering Surveyor, Autumn.

Cosser, E., 2004. "Bridge Deflection Monitoring and Frequency Identification with Single Frequency GPS Receivers". ION GNSS 2004, The 17th Technical Meeting of the Satellite Division of the Institute of Navigation, 21-24 September, Long Beach, California.

Cosser, E., Meng, X., Roberts, G. W., Dodson, A. H., Barnes, J. and Rizos, C., 2004a. "Precise Engineering Applications of Pseudolite Augmented GNSS". 1st FIG

International Symposium on Engineering Surveys for Construction Works and Structural Engineering, 28 June-1 July, Nottingham, England.

Cosser, E., Roberts, G. W., Meng, X. and Dodson, A. H., 2004b. "Single Frequency GPS for Bridge Deflection Monitoring: Progress and Results". 1st FIG International Symposium on Engineering Surveys for Construction Works and Structural Engineering, 28 June-1 July, Nottingham, England.

Cosser, E., Hill, C. J., Roberts, G. W., Meng, X., Moore, T. and Dodson, A. H., 2004c. "Bridge Monitoring With Garmin Handheld Receivers". 1st FIG International Symposium on Engineering Surveys for Construction Works and Structural Engineering, 28 June-1 July, Nottingham, England.

Dodson, A. H., Meng, X., Roberts, G. W., Cosser, E., Barnes, J. and Rizos, C., 2003. "Integrated Approach of GPS and Pseudolites for Bridge Deformation Monitoring". GNSS 2003, 22-25 April, Graz, Austria.

Meng, X., Roberts, G. W., Dodson, A. H. and Cosser, E., 2002a. "The Use of Pseudolites to Augment GPS Data for Bridge Deflection Measurements". ION GPS 2002, The 15th Technical Meeting of the Satellite Division of the Institute of Navigation, Portland, Oregon, USA. 851-862.

Meng, X., Roberts, G. W., Dodson, A. H., Cosser, E. and Noakes, C., 2002b. "Simulation of the Effects of Introducing Pseudolite Data into Bridge Deflection Monitoring Data". 2nd Symposium on Geodesy for Geotechnical and Structural Engineering, 21-24 May, Berlin, Germany.

Meng, X., Dodson, A. H., Roberts, G. W. and Cosser, E., 2003a. "Hybrid Sensor System for Bridge Deformation Monitoring: Interfacing With Structural Engineers". IUGG 2003, July, Japan.

Meng, X., Meo, M., Roberts, G. W., Dodson, A. H., Cosser, E., Iuliano, E. and Morris, A., 2003b. "Validating GPS Based Bridge Deformation Monitoring with Finite Element Model". GNSS 2003, 22-25 April, Graz, Austria.

Meng, X., Roberts, G. W., Cosser, E. and Dodson, A. H., 2003c. "Real-time Bridge Deflection and Vibration Monitoring Using an Integrated

GPS/Accelerometer/Pseudolite System". 11th International Symposium on Deformation Measurements, International Federation Surveyors (FIG), Commission 6 - Engineering Surveys, Working Group 6.1, 25-28 May, Santorini, Greece. 573-581.

Meng, X., Dodson, A. H., Andreotti, M., Roberts, G. W., Cosser, E. and Moore, T., 2004a. "Prototype of a Remote Bridge Health Monitoring System (RBHMS) using Wired/Internet Based RTK GPS". GNSS 2004, 17-19 May, Rotterdam, Netherlands.

Meng, X., Roberts, G. W., Dodson, A. H., Cosser, E., Barnes, J. and Rizos, C., 2004b. "Impact of GPS satellite and pseudolite geometry on structural deformation monitoring: analytical and empirical studies." Journal of Geodesy, 77(12), June: 809 - 822.

Meng, X., Roberts, G. W., Dodson, A. H., Andreotti, M., Cosser, E. and Meo, M., 2004c. "Development of a Prototype Remote Structural Health Monitoring System (RSHMS)". 1st FIG International Symposium on Engineering Surveys for Construction Works and Structural Engineering, 28 June-1 July, Nottingham, England.

Roberts, G. W., Cosser, E., Meng, X. and Dodson, A. H., 2002a. "Creating Virtual L2 GPS Data Using a Combination of L1 Receivers and L1/L2 Reference Receivers". ION GPS 2002, The 15th Technical Meeting of the Satellite Division of the Institute of Navigation, Portland, Oregon, USA.

Roberts, G. W., Meng, X., Dodson, A. H. and Cosser, E., 2002b. "Geodetic Signal Diagnosis and Its Application to Structural Deformation". 2nd Symposium on Geodesy for Geotechnical and Structural Engineering, 21-24 May, Berlin, Germany.

Roberts, G. W., Meng, X., Dodson, A. H. and Cosser, E., 2002c. "Multipath Mitigation for Bridge Deflection Monitoring." Journal of Global Positioning Systems, 1(1): 25-33.

Roberts, G. W., Cosser, E., Meng, X., Dodson, A. H., Morris, A. and Meo, M., 2003a. "A Remote Bridge Health Monitoring System Using Computational Simulation

and Single Frequency GPS". ION GPS 2003, The 16th Technical Meeting of the Satellite Division of the Institute of Navigation, 9-12 September, Portland, Oregon.

Roberts, G. W., Meng, X., Meo, M., Dodson, A. H., Cosser, E., Iuliano, E. and Morris, A., 2003b. "A Remote Health Monitoring System Using Computational Simulation and GPS Sensor Data". 11th International Symposium on Deformation Measurements, International Federation Surveyors (FIG), Commission 6 - Engineering Surveys, Working Group 6.1, 25-28 May, Santorini, Greece. 547-553.

Roberts, G. W., Cosser, E., Meng, X. and Dodson, A. H., 2004a. "Monitoring the Deflection of Suspension Bridges Using 100 Hz GPS Receivers". ION GNSS 2004, The 17th Technical Meeting of the Satellite Division of the Institute of Navigation, 21-24 September, Long Beach, California.

Roberts, G. W., Meng, X., Cosser, E. and Dodson, A. H., 2004c. "The Use of Single Frequency GPS to Measure the Deformations and Deflections of Structures." Civil Engineering Surveyor, September (GIS/GPS Supplement): 6-12.

Appendix A

Kinpos Control File Example

```
FILES
 INPUT
  REFREC RINEX base c:\Kinpos\ref20640.04o CHOKE XYZ SING LEIC KNOWN
     3782346.9045  -29764.3635  5118418.5846   1.491
  KINREC RINEX b001 c:\Kinpos\bdg50640.04o CHOKE XYZ SING LEIC SEMI
     3784175.0991  -29664.0169  5117063.5142   0.000
  EPH RNX c:\Kinpos\ref20640.04n
 END
 OUTPUT
   POS  bdg5_4b.pos
   POA  bdg5_4b.amb
   REP  bdg5_4b.rep
   RES  bdg5_4bres.out
 END
END

OPTIONS
  MODE 4  (1:standalone,2:diff_pse,3:diff_car, 4 diff_car&pse, 5:WL)
  DOPPLER  NO
  WL     NO
  SMOOTHPSE  YES  1
  FREQUENCY  1
  PSEUDERR 1.0d0
  DPSEUDERR 0.50d0
  CARRERR  0.010d0
  SDOPERR  0.1d0
  DDOPERR  0.002d0
  PROCNOISE   1.0d0
  INTERVAL    0.1d0
  CONSTRAINT  NO  5.0
  START   YMDHMS 2004  3  4 11 57 57.00
  STOP    YMDHMS 2004  3  4 12 30 0.00
  TROP    1
  ELEVMIN  10.0
  NOACC   0
  KINSMOOTH NO
  AZIM YES
```

```
  POSITIONMODEL  CONSTACC
  TILT    NO c:\GSTB\cycleslip\bu109458.02t
  PHASECENTRES NO
END

ATMOSPHERE
 BASE
  DRYMD NONE     NEILL
  WETMD NONE     NEILL
  SOLVE NONE     DIRECT
  METDAT STD
  DELAY NO
 END

 ROVER
  DRYMD NONE     NEILL
  WETMD NONE     NEILL
  SOLVE NONE     DIRECT   2.36
  METDAT STD
 END
END
```

Appendix B

IESSG Simulated Slip File

GPS week	GPS Second	Receiver	Satellite	Slip Value
1120	388846.00	1	14	-271.0
1120	388853.00	1	14	272.0
1120	388857.00	1	25	277.0
1120	388875.00	1	20	306.0
1120	388877.00	1	1	269.0
1120	388879.00	1	14	382.0
1120	388887.00	1	11	278.0
1120	388896.00	1	20	261.0
1120	388899.00	1	1	302.0
1120	388900.00	1	11	267.0
1120	388940.00	1	14	261.0
1120	388944.00	1	14	268.0
1120	388972.00	1	11	279.0
1120	388987.00	1	4	-260.0
1120	388988.00	1	20	-311.0
1120	388992.00	1	4	-327.0
1120	389006.00	1	20	265.0
1120	389014.00	1	11	-270.0
1120	389044.00	1	29	-316.0
1120	389046.00	1	11	-319.0
1120	389054.00	1	14	306.0
1120	389061.00	1	20	329.0
1120	389121.00	1	14	310.0
1120	389188.00	1	29	264.0
1120	389211.00	1	29	-272.0
1120	389226.00	1	14	323.0
1120	389260.00	1	4	-275.0
1120	389373.00	1	11	322.0
1120	389397.00	1	25	271.0
1120	389416.00	1	7	310.0
1120	389428.00	1	29	310.0
1120	389433.00	1	29	-265.0

1120	389436.00	1	29	266.0
1120	389491.00	1	14	-261.0
1120	389494.00	1	14	-347.0
1120	389525.00	1	14	271.0
1120	389543.00	1	7	271.0
1120	389544.00	1	1	264.0
1120	389577.00	1	25	277.0
1120	389608.00	1	29	323.0
1120	389621.00	1	7	261.0
1120	389675.00	1	25	-260.0
1120	389677.00	1	4	-270.0
1120	389697.00	1	14	-271.0
1120	389716.00	1	1	-342.0
1120	389782.00	1	7	312.0
1120	389791.00	1	7	-300.0

Kinpos Cycle Slip File

The slip file below was output by Kinpos when the Rinex file produced by the IESSG simulator was processed.

Kinpos Slip Detection File

Time	Satellite	Receiver	Corrected?	Epoch	Slip Value	Accumulated Slip Value	Variance
388846.00	14	1	corr	46	-271.00	-271.00	0.0563
388853.00	14	1	var>- nocorr	53	272.00		7.3558
388857.00	25	1	corr	57	277.00	277.00	0.0551
388875.00	20	1	corr	75	306.00	306.00	0.0560
388877.00	1	1	corr	77	269.00	269.00	0.0553
388879.00	14	1	corr	26	382.00	382.00	0.0540
388887.00	11	1	corr	87	278.00	278.00	0.0550
388896.00	20	1	var>- nocorr	96	261.00		6.0734
388899.00	1	1	var>- nocorr	99	302.00		5.2455
388900.00	11	1	var>- nocorr	100	267.00		5.4007
388940.00	14	1	var>- nocorr	87	261.00		7.9788
388944.00	14	1	carr-nocorr	4			
388972.00	11	1	corr	72	279.00	279.00	0.0491
388987.00	4	1	corr	184	-260.00	-260.00	0.0523
388988.00	20	1	corr	92	-311.00	-311.00	0.0499
388992.00	4	1	var>- nocorr	189	-327.00		3.6322
389006.00	20	1	var>- nocorr	110	265.00		5.7545
389014.00	11	1	var>- nocorr	114	-270.00		5.0568
389044.00	29	1	corr	244	-316.00	-316.00	0.0532
389046.00	11	1	corr	32	-319.00	-319.00	0.0555
389054.00	14	1	corr	110	306.00	306.00	0.0562
389061.00	20	1	corr	55	329.00	329.00	0.0593
389121.00	14	1	var>- nocorr	177	310.00		4.4331
389188.00	29	1	var>- nocorr	388	264.00		3.0739
389211.00	29	1	corr	23	-272.00	-272.00	0.0562
389226.00	14	1	corr	102	323.00	323.00	0.0554
389260.00	4	1	corr	268	-275.00	-275.00	0.0549

389373.00	11	1	var>-	nocorr	359	322.00		3.2192
389397.00	25	1	var>-	nocorr	597	271.00		2.1683
389416.00	7	1		corr	614	310.00	310.00	0.0541
389428.00	29	1	var>-	nocorr	240	310.00		3.3644
389433.00	29	1	RR-	nocorr	2	-260.89		
389436.00	29	1	RR-	nocorr	3	270.46		
389491.00	14	1	var>-	nocorr	367	-261.00		3.2308
389494.00	14	1	RR-	nocorr	3	-345.90		
389525.00	14	1		corr	31	271.00	271.00	0.0579
389543.00	7	1	var>-	nocorr	741	271.00		2.1761
389544.00	1	1		corr	645	264.00	264.00	0.0542
389577.00	25	1		corr	177	277.00	277.00	0.0541
389608.00	29	1		corr	172	323.00	323.00	0.0543
389621.00	7	1		corr	78	261.00	261.00	0.0570
389675.00	25	1	var>-	nocorr	275	-260.00		3.2035
389677.00	4	1	var>-	nocorr	685	-270.00		2.0029
389697.00	14	1	var>-	nocorr	203	-271.00		3.6601
389716.00	1	1	var>-	nocorr	817	-342.00		1.7634
389782.00	7	1	var>-	nocorr	239	312.00		3.2351
389791.00	7	1		corr	9	-300.00	-300.00	0.0589

Appendix C

Simulated Slip File- Java Cycle Slip Simulator

Time	GPS Seconds	Receiver	Satellite	Slip Value
10 45 45.6	384345.6	1	sat 20	2
10 46 30.3	384390.3	2	sat 7	1
10 47 40.4	384460.4	2	sat 7	-1
10 50 17.0	384617.0	2	sat 11	2
10 50 30.1	384630.1	1	sat 14	-2
10 52 33.2	384753.2	2	sat 28	-2
10 53 15.0	384795.0	1	sat 25	1
10 55 59.2	384959.2	1	sat 7	-1

Receiver 1 is the reference receiver Ref1 and receiver 2 is the rover receiver Bdg2.

Kinpos Cycle Slip File

The slip file below was output by Kinpos when the Rinex file with cycle slips added by the Java simulator was processed.

Kinpos Slip Detection File

Time	Satellite	Receiver	Corrected?	Epoch	Slip Value	Accumulated Slip Value	Variance
384345.60	20	1	corr	656	2.00	2.00	0.0034
384345.70	20	1	corr	657	-2.00	0.00	0.0153
384390.30	7	2	corr	1141	1.00	1.00	0.0049
384390.40	7	2	corr	1142	-1.00	0.00	0.0075
384460.40	7	2	corr	1842	-1.00	-1.00	0.0081
384460.50	7	2	corr	1843	1.00	0.00	0.0092
384617.00	11	2	corr	3408	2.00	2.00	0.0034
384617.10	11	2	corr	3409	-2.00	0.00	0.0073
384630.10	14	1	corr	3501	-2.00	-2.00	0.0065
384630.20	14	1	corr	3502	2.00	0.00	0.0092
384753.20	28	2	corr	4770	-2.00	-2.00	0.0079
384753.30	28	2	corr	4771	2.00	0.00	0.0098
384795.00	25	1	corr	298	1.00	1.00	0.0120

384795.10	25	1	corr	299	-1.00	0.00	0.0167
384959.20	7	1	corr	6792	-1.00	-1.00	0.0049
384959.30	7	1	corr	6793	1.00	0.00	0.0055

Appendix D

Fourier Transform Results - Wilford Bridge Trial 2

These graphs show the results of the Discrete Fourier Transforms (DFT) of the GPS and accelerometer data. Table D-1 to Table D-16Table D-16 show results from peak 1 to peak 4. Peak 1 starts at GPS time 388261.2, peak 2 starts at GPS time 388358.2, peak 3 starts at 389169.5 and peak 4 starts at 389254.1. Table D-17 and Table D-18 show results from point 5 and point 6 respectively and their start times can be seen in the tables.

		Frequency (Hz)		
GPS	Peak 1	1	2	3
Number of Sample Points	128	1.80	2.50	2.66
	256	1.72	2.54	3.20
	384	1.72	2.47	2.58
	512	1.70	2.46	2.81

Table D-1 Discrete Fourier Transform results for the GPS data after peak 1.

		Frequency (Hz)		
Accelerometer	Peak 1	1	2	3
Number of Sample Points	1024	1.72	2.97	2.97
	2048	1.72	2.93	2.93
	3072	1.72	2.92	2.92
	4096	1.70	2.27	2.93

Table D-2 Discrete Fourier Transform results for the accelerometer data after peak 1.

		Frequency (Hz)		
GPS	Peak 2	1	2	3
Number of Sample Points	128	1.80	2.97	3.13
	256	1.72	2.58	3.09
	384	1.72	2.53	3.02
	512	1.78	2.56	3.09

Table D-3 Discrete Fourier Transform results for the GPS data after peak 2.

		Frequency (Hz)		
Accelerometer	Peak 2	1	2	3
Number of Sample Points	1024	1.72	2.34	2.97
	2048	1.72	2.30	2.93
	3072	1.72	2.29	2.92
	4096	1.72	2.27	2.91

Table D-4 Discrete Fourier Transform results for the accelerometer data after peak 2.

		Frequency (Hz)		
GPS	Peak 3	1	2	3
Number of Sample Points	128	1.80	2.97	2.97
	256	1.76	2.34	2.93
	384	1.74	2.34	2.89
	512	1.74	2.89	2.89

Table D-5 Discrete Fourier Transform results for the GPS data after peak 3.

		Frequency (Hz)		
Accelerometer	Peak 3	1	2	3
Number of Sample Points	1024	1.80	2.97	2.97
	2048	1.76	2.93	2.93
	3072	1.74	2.92	2.92
	4096	1.74	2.91	2.91

Table D-6 Discrete Fourier Transform results for the accelerometer data after peak 3

		Frequency (Hz)		
GPS	Peak 4	1	2	3
Number of	128	1.80	2.34	2.81
Sample	256	1.76	2.93	2.93
Points	384	1.72	2.92	3.31
	512	1.72	2.91	2.91

Table D-7 Discrete Fourier Transform results for the GPS data after peak 4.

		Frequency (Hz)		
Accelerometer	Peak 4	1	2	3
Number of	1024	1.80	2.11	2.66
Sample	2048	1.76	2.23	2.62
Points	3072	1.72	2.14	2.60
	4096	1.72	2.05	2.93

Table D-8 Discrete Fourier Transform results for the accelerometer data after peak 4.

		Frequency (Hz)		
GPS	Peak 1	1	2	3
Number of	100	1.80	2.50	2.70
Sample	200	1.75	2.50	2.95
Points	300	1.73	2.47	3.23
	400	1.70	2.45	3.23

Table D-9 Discrete Fourier Transform results for the GPS data after peak 1.

		Frequency (Hz)		
Accelerometer	Peak 1	1	2	3
Number of	800	1.80	3.00	3.00
Sample	1600	1.75	2.95	2.95
Points	2400	1.73	2.93	2.93
	3200	1.70	2.28	2.93

Table D-10 Discrete Fourier Transform results for the accelerometer data after peak 1.

		Frequency (Hz)		
GPS	Peak 2	1	2	3
Number of	100	1.80	2.60	3.00
Sample	200	1.70	2.60	3.10
Points	300	1.70	2.90	3.10
	400	1.78	2.90	2.90

Table D-11 Discrete Fourier Transform results for the GPS data after peak 2.

		Frequency (Hz)		
Accelerometer	Peak 2	1	2	3
Number of	800	1.80	2.30	3.00
Sample	1600	1.75	2.30	2.95
Points	2400	1.73	2.30	2.93
	3200	1.73	2.28	2.93

Table D-12 Discrete Fourier Transform results for the accelerometer data after peak 2.

		Frequency (Hz)		
GPS	Peak 3	1	2	3
Number of	100	1.80	2.40	3.00
Sample	200	1.75	2.95	2.95
Points	300	1.73	2.90	2.90
	400	1.75	2.90	2.90

Table D-13 Discrete Fourier Transform results for the GPS data after peak 3.

		Frequency (Hz)		
Accelerometer	Peak 3	1	2	3
Number of	800	1.80	3.00	3.00
Sample	1600	1.75	2.95	2.95
Points	2400	1.73	2.93	2.93
	3200	1.73	2.93	2.93

Table D-14 Discrete Fourier Transform results for the accelerometer data after peak 3.

		Frequency (Hz)		
GPS	Peak 4	1	2	3
Number of	100	1.80	2.40	2.90
Sample	200	1.75	2.55	2.85
Points	300	1.73	2.30	2.90
	400	1.73	2.30	3.30

Table D-15 Discrete Fourier Transform results for the GPS data after peak 4.

		Frequency (Hz)		
Accelerometer	Peak 4	1	2	3
Number of	800	1.80	2.10	2.70
Sample	1600	1.75	2.10	2.65
Points	2400	1.73	2.13	2.63
	3200	1.73	2.13	2.63

Table D-16 Discrete Fourier Transform results for the accelerometer data after peak 4.

		Frequency (Hz)		
GPS	Point 5 (388424.5)	1	2	3
Number of	100	1.90	2.80	3.10
Sample	200	1.85	2.75	2.75
Points	300	1.83	2.93	3.40
	400	1.83	2.70	3.25

Table D-17 Discrete Fourier Transform results for the GPS data at point 5.

		Frequency (Hz)		
GPS	Point 6 (388580.5)	1	2	3
Number of	100	2.50	2.80	2.80
Sample	200	2.45	2.90	2.90
Points	300	2.03	2.73	3.03
	400	2.05	2.78	3.03

Table D-18 Discrete Fourier Transform results for the GPS data at point 6.

Appendix E

Fourier Transform Results – JNS100 Wilford Bridge Trial

These graphs show the results of the DFT of the JNS100 GPS data and the accelerometer data, both measured at a 50 Hz data rate. The data from session 6(1) starts at GPS time 208657.1; the data from session 6(2) starts at GPS time 211518.2; the data from session 7(1) starts at GPS time 293702.1; and the data from session 7(2) starts at GPS time 294432.6.

JNS100 GPS	6(1)	1	2	3	4	5	6	7	8
Number of	500	1.80	2.40	3.20	5.60	6.90	10.50	11.90	15.40
Sample	1000	1.80	2.85	2.85	5.10	6.90	10.45	11.85	13.65
Points	1500	1.77	2.87	2.87	5.67	8.50	10.77	11.87	13.90
	2000	1.78	2.85	2.85	5.70	6.88	10.45	11.85	15.30

Table E-1 Discrete Fourier Transform results for the JNS100 GPS data during session 6(1).

Accelerometer	6(1)	1	2	3	4	5	6	7	8
Number of	500	1.80	2.10	3.00	5.20	6.70	10.30	12.60	14.60
Sample	1000	1.80	2.05	2.95	5.10	6.70	11.15	12.60	15.25
Points	1500	1.77	2.97	2.97	5.10	9.47	11.10	12.70	15.27
	2000	1.78	2.05	2.93	5.10	6.68	11.10	11.98	15.25

Table E-2 Discrete Fourier Transform results for the accelerometer data during session 6(1).

JNS100 GPS	6(2)	1	2	3	4	5	6	7	8
Number of	500	1.80	2.50	3.30	5.30	7.30	10.40	12.90	14.90
Sample	1000	1.80	2.15	3.00	5.20	9.05	10.35	12.20	14.45
Points	1500	1.77	2.13	3.10	5.23	6.70	10.80	12.20	14.37
	2000	1.78	2.13	2.83	5.30	6.70	10.68	12.18	14.38

Table E-3 Discrete Fourier Transform results for the JNS100 GPS data during session 6(2).

Accelerometer	6(2)	1	2	3	4	5	6	7	8
Number of	500	1.80	2.80	2.80	5.00	6.70	10.60	11.90	14.70
Sample	1000	1.80	2.75	2.75	5.10	6.80	10.95	11.85	14.65
Points	1500	1.77	2.80	2.73	4.90	6.60	10.50	12.60	13.83
	2000	1.78	2.45	2.73	4.95	6.43	10.40	11.83	13.83

Table E-4 Discrete Fourier Transform results for the accelerometer data during session 6(2).

JNS100 GPS	7(1)	1	2	3	4	5	6	7	8
Number of	500	1.80	2.70	3.30	5.50	6.90	11.20	12.70	14.10
Sample	1000	1.75	2.25	3.00	5.45	7.50	11.10	12.60	14.05
Points	1500	1.77	2.23	3.27	5.27	9.37	10.73	12.93	15.73
	2000	1.75	2.23	2.90	5.63	7.48	11.25	12.93	13.68

Table E-5Discrete Fourier Transform results for the JNS100 GPS data during session 7(1).

Accelerometer	7(1)	1	2	3	4	5	6	7	8
Number of	500	1.70	3.00	3.00	4.80	6.10	10.60	12.00	13.70
Sample	1000	1.80	2.05	3.00	5.10	6.40	10.70	12.85	13.40
Points	1500	1.77	2.13	2.97	5.10	9.47	10.87	11.97	13.37
	2000	1.75	2.05	2.95	5.10	6.38	11.03	12.10	13.38

Table E-6 Discrete Fourier Transform results for the accelerometer data during session 7(1).

JNS100 GPS	7(2)	1	2	3	4	5	6	7	8
Number of	500	1.80	2.30	2.80	5.40	7.20	11.20	12.40	13.60
Sample	1000	1.80	2.25	3.05	5.35	6.75	10.80	12.15	13.65
Points	1500	1.77	2.23	2.80	4.97	6.80	10.80	12.13	13.47
	2000	1.75	2.23	3.35	5.25	7.43	11.28	12.35	13.68

Table E-7 Discrete Fourier Transform results for the JNS100 GPS data during session 7(2).

Accelerometer	7(2)	1	2	3	4	5	6	7	8
Number of	500	1.80	2.10	3.10	5.20	6.90	10.70	12.70	15.00
Sample	1000	1.80	2.05	3.00	5.10	6.45	10.70	12.35	15.45
Points	1500	1.77	2.13	2.97	5.10	6.43	10.30	12.03	14.93
	2000	1.75	2.13	2.98	5.10	6.30	10.78	12.53	15.18

Table E-8 Discrete Fourier Transform results for the accelerometer data during session 7(2).